The Pennsylvania State University
The Graduate School
College of Agricultural Sciences

PREDICTING THE CONSEQUENCES OF DIVERSE LIFE HISTORY IN MALARIA PARASITES: SYNCHRONY AND TRANSMISSION INVESTMENT

A Dissertation in
Entomology
by
Megan A. Greischar

Submitted in Partial Fulfillment
of the Requirements
for the Degree of

Doctor of Philosophy

August 2014

The dissertation of Megan A. Greischar was reviewed and approved* by the following:

Ottar N. Bjørnstad
Professor of Entomology & Biology, Adjunct Professor of Statistics
Dissertation Co-Adviser, Co-Chair of Committee

Andrew F. Read
Alumni Professor in the Biological Sciences & Professor of Entomology, Eberly College of Science Distinguished Senior Scholar
Dissertation Co-Adviser, Co-Chair of Committee

Robert F. Paulson
Professor of Veterinary & Biomedical Sciences

Jason L. Rasgon
Associate Professor of Entomology & Disease Epidemiology

Gary W. Felton
Professor of Entomology
Head of the Department of Entomology

*Signatures are on file in the Graduate School.

Abstract

Malaria parasites have evolved astonishingly varied means of solving the same basic problem of converting host resources—red blood cells—into parasite biomass that can be transmitted to vectors and ultimately, new hosts. This diversity is challenging to explain, because if a life history trait improved transmission, parasites with that trait would be expected to displace others. How can such divergent strategies all lead to sustained transmission success? I focus on two aspects of the malaria life cycle, synchronization of blood stage infection and allocation to transmission, to examine how within-host ecology can maintain diverse parasite strategies. The models I develop to address that question are also used to identify robust methods for inferring parasite traits from time series data.

The models show that the advantages of synchrony depend on the interplay between competition for host resources, immune clearance, and the odds of transmitting to a vector, all of which vary with parasite densities. Using data from lab-cultured parasites, I examine the intra-strain competitive interactions in more detail, finding preliminary support for a form of density-dependent competition that, counterintuitively, may benefit synchronous parasites. The model demonstrates that traditional inference methods can give misleading estimates of parasites' life cycle length. Within the host, the model suggests that competition between coinfecting strains should reduce allocation to transmission stage production. Allowing transmission investment to vary through time, the model indicates that transmission investment is especially costly early in infection. Inspired by the controversy in the literature concerning how best to infer transmission investment, I use the model to show that current methods are likely incapable of ruling out the null hypothesis that transmission investment is fixed through time rather than plastic, and develop improved methods for inferring transmission investment. The theory developed here can inform efforts to describe the rich diversity in parasite life history as well as the adaptive significance of that diversity.

Table of Contents

List of Figures viii

List of Tables xx

Acknowledgments xxi

Chapter 1
Introduction 1

Chapter 2
Synchrony in malaria infections: How intensifying within-host competition can be adaptive 11

2.1 Abstract . . . 11
2.2 Introduction . . . 12
2.3 Methods . . . 15
2.3.1 Delayed differential model . . . 15
2.4 Results . . . 22
2.4.1 Low gametocyte investment favors synchrony . . . 22
2.4.2 Interference among merozoites can benefit synchronous parasites . . . 24
2.4.3 Synchronous strains can transmit better from single infections 25
2.4.4 Synchronous strains perform poorly in coinfections . . . 27
2.4.5 Sensitivity to model assumptions . . . 27
2.5 Discussion . . . 30
2.5.1 Model assumptions . . . 31
2.5.2 Synchrony as an adaptation to improve transmission . . . 31
2.5.3 Merozoite interference and virulence . . . 33

2.5.4 Synchrony as a means of overwhelming natural enemies . . . 34
2.5.5 Synchrony and drug treatment . . . 35
2.5.6 Broader implications . . . 36
2.6 Acknowledgements . . . 36
2.7 Notes . . . 37

Chapter 3
Characterizing malaria dynamics *in vitro*: developmental plasticity and interference 38
3.1 Abstract . . . 38
3.2 Introduction . . . 39
3.3 Methods . . . 43
3.3.1 Distributed-delay model framework . . . 43
3.3.2 Model fitting . . . 46
3.3.3 Invasion assays: experimental setup & analysis of blood smear images . . . 48
3.4 Results . . . 50
3.4.1 Stage percentage data biases the estimated cycle length . . . 50
3.4.2 Model fits to detailed time series data . . . 53
3.4.3 Invasion assays: interference . . . 54
3.5 Discussion . . . 57
3.6 Acknowledgements . . . 64
3.7 Notes . . . 64

Chapter 4
Predicting optimal transmission investment in malaria parasites 66
4.1 Abstract . . . 66
4.2 Introduction . . . 67
4.3 Model . . . 70
4.3.1 Single infections . . . 71
4.3.2 Coinfections . . . 74
4.4 Results . . . 78
4.4.1 Gametocyte investment delays infectivity . . . 78
4.4.2 Saturating immunity selects for reduced gametocyte investment . . . 81
4.4.3 Coinfection favors in-host replication . . . 82
4.4.4 Optimal cues: how can parasites tell time? . . . 84
4.4.5 Sensitivity to burst size, red blood cell replenishment, and synchrony . . . 86
4.5 Discussion . . . 87

4.6 Acknowledgements . . . 92
4.7 Notes . . . 92

Chapter 5
Challenges in estimating transmission investment in malaria parasites **93**
5.1 Abstract . . . 93
5.2 Quantifying transmission investment . . . 94
5.3 Transmission investment in malaria . . . 96
5.4 How well can we estimate transmission investment from simulated data? . . . 99
5.5 Early markers for sexual differentiation . . . 102
5.6 Interpreting plastic conversion rates *in vivo* . . . 106
5.7 Alternative approach . . . 108
5.8 Concluding remarks . . . 113
5.9 Acknowledgments . . . 115
5.10 Notes . . . 115

Chapter 6
Discussion **116**

Appendix A
Chapter 2 Supplemental Information **122**
A.1 Description of Modeling Framework . . . 122
A.1.1 Age-structured model . . . 122
A.1.2 Two strain model . . . 123
A.1.3 Annotated code for basic fixed delay model . . . 124
A.2 Supplemental figures . . . 132

Appendix B
Chapter 3 Supplemental Information **140**
B.1 Annotated code for distributed delay model . . . 140
B.2 Image processing . . . 145
B.3 Supplementary figures and tables . . . 147

Appendix C
Chapter 4 Supplemental Information **154**
C.1 Supplemental methods: simulations and free spline investment . . . 154
C.2 Supplemental figures . . . 156

Appendix D

Chapter 5 Supplemental Information **170**

D.1 Supplemental methods: Age-structured gametocyte development . . 170

D.2 Description of spline method 172

D.3 Description of modified spline method, assuming early markers for gametocyte differentiation 176

D.4 Supplementary figures 177

Bibliography **184**

List of Figures

1.1 Key events in the asexual life cycle. Sources: 1, Boyle *et al.* (2010); 2, ter Kuile *et al.* (1993); 3, Elliott *et al.* (2008); 4, Arnot & Gull (1998); 5, McMorran *et al.* (2009); 6, Costa *et al.* (2011). 3

2.1 When fitness is a convex function of density (e.g., the a values in the accelerating part of the curve), oscillations in density can increase mean fitness as a consequence of Jensen's inequality (reviewed in Ruel & Ayres 1999). A strain that alternates between densities a_1 and a_2 has higher mean fitness (red point) than a strain that maintains a constant density a_{mean} (black point). If fitness is a concave or decelerating function of density (d values), oscillations in numbers decrease mean fitness compared to a strain that maintains a constant density (red versus black point). Cumulative fitness is altered in an identical manner. 14

2.2 Synchronous versus asynchronous infections are initialized using a beta distribution with large or small shape parameter, s_P, to specify the bursting of the initial inoculum (synchronous in black, $s_P = 100$; and asynchronous in red $s_P = 1$). 21

2.3 Synchronous infections transmit better at low gametocyte investment—without any qualitative change in dynamics—due to the sigmoidal shape of the relationship between gametocyte numbers and probability of transmission. Single-strain infections were simulated in the absence of merozoite interference ($q = 0$) and immune clearance ($a = 0$), with solid curves indicating synchronous infections and dashed lines referring to asynchronous dynamics. Abundance of uninfected and infected red blood cells (RBCs) in the asexual cycle are shown with gametocyte (transmission stage) numbers (A & B, logarithmic scale), with total transmission potential—the cumulative transmission probability—shown below (C & D). Simulations in panels A & C assume low gametocyte investment ($c = 0.001$), while panels B & D show dynamics with relatively high gametocyte investment ($c = 0.05$). 23

2.4 Merozoite interference reduces anemia (A) and gametocyte abundance (B), but increases transmission potential (cumulative probability of transmission, C). Synchronized and asynchronous dynamics (solid and dashed lines, respectively) when merozoite interference is present (orange curve, $q = 10$) or absent (blue curve, $q = 0$). Gametocyte investment is set relatively high ($c = 0.05$) and immunity is absent ($a = 0$). The blue curves are identical to the red blood cell and gametocyte abundance shown in Fig. 3B, save that here they are plotted on a conventional rather than logarithmic scale. 25

2.5 Synchronous parasites frequently transmit better from single infections. Smoothed relative fitness (ratio of cumulative probability transmission for synchronous:asynchronous strain) with increasing competition among merozoites (x axis) and investment in producing transmission stages (y axis). Synchronous infections transmit better in the white/gray areas. Immunity is set to zero (A, $a = 0$), to target infected red blood cells (B, $a = 150$, $b = 100$) or to remove merozoites (C, $a = 7200$, $b = 100$). Immunity targeting short-lived merozoites increases the parameter space favorable to synchronous infections. 26

2.6 Coinfections. Smoothed relative fitness of synchronous:asynchronous strain, with increasing levels of merozoite competition and gametocyte investment. As in Fig 2.5, values greater than 1 (white areas) indicate superior transmission of the synchronous strain. Immunity is absent (A, $a = 0$), immunity acts on the total number of red blood cells infected by asexual parasites of both strains (B, $a = 150$, $b = 100$) or on merozoites of both strains (C, $a = 7200$, $b = 100$). Again, synchronous strains perform better when immunity targets short-lived parasite stage. 28

3.1 *P. falciparum* parasites (called "merozoites", purple dots) that have failed to invade a red blood cell (pink circles), along with three parasites that have invaded successfully but clustered within the same red blood cell (right). The three successful invaders have developed into the so-called ring stage forms. These parasites are in the Dd2 strain. 41

3.2 The period between peaks in the percentage of parasites in the mature schizont stage gives a biased estimate of the real cycle length, depending on whether the infection is declining (A,C) or growing (B,D). Simulations were run assuming hyperbolic interference ($q = 10$), a burst size of 16, and large variability in cycle length ($n = 30$, $CV = 0.18$). In each case, the true cycle length was set at 42 hours (dashed vertical line). In the left panels (A,C), the maximum invasion rate was set to 2×10^{-9}, while in the right panels, the maximum invasion rate was 2×10^{-8}, leading to growth. 51

3.3 The maximum invasion rate can bias the apparent length of the life cycle, as estimated by the proportion of parasites in the schizont stage. The true cycle length (42 hours) is indicated by a dashed black line, while the red curve refers to simulations run with a high degree of developmental plasticity ($n = 30$) and the blue curve to simulations with little variability in life cycle length ($n = 300$). Other parameters as in Fig. 3.2. 52

3.4 Model fits assuming hyperbolic interference (black solid curve, Eq. 3.2) or parasitoid-like interference (black broken curve, Eq. 3.3), with data is shown in colored lines. The black curves for each strain indicate a single best model fit to both the proportion of sampled red blood cells in the immature parasite stages (A-C) and in the schizont stage (D-F). Weighted least squares errors corresponding to each fit can be found in Table 3.1, along with the coefficient of variation in cycle length, cycle duration, and schizont stage length. The associated invasion parameters are listed in Table B.1. 54

3.5 The number of merozoites successfully invading red blood cells as a function of the expected number of schizonts in the initial sample according to Eqn. 3.12 for Dd2 (A) and HB3 (B). Each blue dot represents a single replicate, with the blue lines indicated 95% confidence intervals obtained by bootstrapping the counts for individual fields. The dashed black line represents the expected number of invasions if each schizont contained the mean number of merozoites and each merozoite invaded, with dotted lines indicating the expectation if every schizont contained the maximum versus minimum number of merozoites reported (Reilly *et al.*, 2007). The orange triangles indicate counts done on a subset of the replicates by microscopy; thus these are not independent data points but are included here to allow comparison between estimates obtained from automated red blood cell counts and those derived from standard microscopy. 55

3.6 The excess number of merozoites invading (that is, the number of merozoites invading already-occupied red blood cells) as a function of the expected number of schizonts in the initial sample according to Eqn. 3.12 for Dd2 (A) and HB3 (B). Each blue dot represents a single replicate, with the blue lines indicated 95% confidence intervals obtained by bootstrapping the counts for individual fields. Two samples had too few invasions to construct reliable confidence intervals (B, black circles). As before, the orange triangles indicate counts done on a subset of the replicates by microscopy for comparison, and are not independent data points. The dashed line refers to the mean burst size for each strain. . . 56

4.1 Reproductive investment limits asexual growth (A) and delays gametocyte production (B) and infectivity to mosquitoes (C). Infection was simulated assuming a fixed conversion rate and no immunity. Optimal investment (42.1%) gives the highest cumulative transmission potential (1078), while sub-optimal (35.1%) and super-optimal (48.1%) investment yield similar transmission potentials (1028). 79

4.2 Optimal fixed (red) and free spline (gray/black) reproductive investment strategies (A) balance growth and transmission to maximize cumulative transmission potential over the course of the infection (B). The dark red and black lines ending at 20 days indicate outcomes for 20 day infections, with lighter curves and lightest curves showing the corresponding strategies and payoff for 30 and 50 days, respectively. Infection was simulated in the absence of host immunity, and the parameters defining each spline can be found in Table C.1. 80

4.3 Saturating immunity favors reduced reproductive investment (A) despite the cost to cumulative transmission potential (B). If conversion rates are fixed (broken lines), the optimum gametocyte investment drops from 42.1% to 22.1%. When reproductive investment is allowed to vary through time (solid lines), immunity is predicted to select for delayed gametocyte investment early in infection. The parameters for the best spline strategies are in Table C.1. 82

4.4 Coinfection reduces optimal reproductive investment. Relative fitness (transmission potential of focal/competing strain) is shown as both strains modify their conversion rates, either without immunity (A) or with saturating immunity removing infected red blood cells (B; $a = 150$, $b = 100$, $\sigma = 0$). Red regions indicate where the competing strain has higher relative fitness, while the gray area denotes where the focal strain has higher relative fitness. White boxes indicate that both strains have the same transmission potential (relative fitness of one). An open circle indicates the evolutionarily stable conversion rate. 83

4.5 Dueling splines in successive optimizations: When two parasite strains infect the same host and differ only in their allocation to transmission, they should converge on an optimal strategy. In the first case (A), we assume the competitor uses the evolutionarily stable constant conversion rate identified in Fig. 4.4A (black line) and find the optimal free spline strategy. In B-E, we retain the optimal free spline strategy from the previous simulation and find the best free spline response. In each case the winning strategy is marked with an asterisk (fitness of each strategy in each iteration shown in Fig. C.4). For simplicity, we assume infection lasts 20 days, and that host immunity is absent. Spline parameters are given in Table C.1. 85

5.1 Longer gametocyte lifespan leads to spurious oscillations in the estimated conversion rate. Dynamics of uninfected and infected red blood cells (dark blue and red, respectively) and mature gametocytes (green) for short and long gametocyte lifespans (A and B, respectively). Estimates of conversion rate are shown below (C, D), with the actual conversion rate (5%) shown as a dashed line. We try an unrealistically short gametocyte lifespan (about 3 hours, A & C), and a more realistic longer lifespan as found by Reece *et al.* (2003) (half-life of 14 hours, equivalent to a mean lifespan of about 20 hours, B & D). 101

5.2 Hypothetical early markers for sexual differentiation can improve conversion rate estimates. The expression profile of the hypothetical marker is shown in red (A, B), the corresponding dynamics of the total abundance of cells (asexual and early sexual stage, gray) and early sexual parasites (red) is shown on a log scale with sampling given as dots (C, D), and the resulting estimates for conversion rate in the bottom panels (E, F). The actual conversion rate (5%) is shown as a dashed line, with conversion rates estimated as the fraction of early sexual stages divided by the total number of cells (asexual and early sexual). Mid- and late-stage sexual parasites, as well as mature gametocytes, were excluded from the calculations. We assume daily samples were taken six hours after peak-bursting and invasion. 104
5.3 Conversion rates estimated from a spline fit to simulated data (purple dots and black lines, respectively) using two parameters (a slope and an intercept). This fitted conversion rate represents the best fit according to AIC values (AIC = −135), with the exception of a more complicated estimated conversion rate that gave a similar AIC value (AIC = −137). The other fitted conversion rates and AIC values can be found in Fig. D.4. 111
5.4 Conversion rates estimated from spline fits to simulated data (purple dots), with the real conversion rate shown in black. The time-varying conversion rate used to simulate the data was the predicted optimum strategy for single infections lasting 20 days in the absence of immunity (from Greischar *et al.*, manuscript). From those simulated data, the conversion rate was either estimated assuming that developing gametocytes cannot be distinguished from asexual parasites (A), or using a modified method assuming that the effective propagation number could be estimated from the abundance of asexual parasites only (B). Modified method replaces Eqn. 5.7 with details in appendix. 112
5.5 Conversion rates estimated from spline fits to real data for six mice. Solid lines indicate the fit giving the lowest AIC values. When other fits gave similar AIC values (i.e., within two units of the lowest AIC), those are also shown as broken black or gray lines. 114

A.1 Extremes in transmission biology: the probability of transmission is shown as a function of gametocyte abundance for drug-sensitive *P. chabaudi* (red, Eqn. 2.13), drug-resistant *P. chabaudi* (black, *probability of transmission* $= \exp(-6.37+1.42\log_{10}G(t))/(1+\exp(-6.37+1.42\log_{10}G(t)))$, and *P. falciparum* (blue, *probability of transmission* $= 1\times10^{-5}G(t)^2/(1+1\times10^{-5}G(t)^2)$). Equations and parameter values from curves fit to data by Huijben *et al.* 2010a and Bell *et al.* 2012. Red and blue dots represent the inflection points for *P. chabaudi* (drug-sensitive) and *P. falciparum*, respectively, i.e., where the curve switches from accelerating to saturating. The drug-sensitive *P. chabaudi* curve was used for all simulations in the main text. Its inflection point falls below a 50% probability of infection—even though it is derived from a logistic regression—because it is a function of the $\log_{10}$ abundance of gametocytes and the chain rule applies. Note the absence of an inflection point on the drug-resistant *P. chabaudi* curve. Despite its appearance on a log scale, the black curve is saturating over the entire range. 132

A.2 Smoothed relative fitness of synchronous:asynchronous infections either for no immunity (A, $a = 0$) or for immunity targeting infected red blood cells in the last hour before bursting (B, $a = 1800$, $b = 100$). Younger infected red blood cells are not subject to immune clearance. Panel A is identical to Fig. 2.5A, and is placed here for comparison. 133

A.3 Smoothed relative fitness in single infections (ratio of cumulative transmission for synchronous:asynchronous strain) calculated using the drug-resistant *P. chabaudi* transmission function (black curve in Fig. A.1). Otherwise, dynamics are identical to Fig. 2.5. Since the transmission function is entirely saturating, the relative fitness does not vary much with changes in gametocyte investment. 134

A.4 Smoothed relative fitness in single infections (ratio of cumulative transmission for synchronous:asynchronous strain) calculated using the *P. falciparum* transmission function (blue curve in Fig. A.1). Save for the calculation of relative fitness, dynamics are identical to Fig. 2.5. Since the transmission function saturates earlier, a smaller region of the parameter space is favorable to synchronous parasites in the absence of immunity. 135

A.5 Smoothed relative fitness in single infections (ratio of mean transmission for synchronous:asynchronous strain) using an alternate form of merozoite interference ($z(t)$, Eqn. 2.3). Parameters otherwise identical to Fig. 2.5 (i.e., relative fitness calculated with Eqn. 2.13). 136

A.6 Red blood cell abundance (A), gametocyte abundance (B), and transmission potential (C, cumulative probability of transmission) simulated for parasitoid-like merozoite interference (Eqn. 2.3), with $m = 0.05$ for orange curves. Synchronous dynamics are again shown in solid lines while asynchronous infections are denoted with dashed lines. Gametocyte investment was set low ($c = 0.002$), and immunity was absent ($a = 0$). Transmission potential was calculated using Eqn. 2.13. Synchronous strains can benefit from merozoite competition (C, orange lines), while the asynchronous infection would have transmitted better in the absence of competition (C, blue lines). 137

A.7 Smoothed relative fitness of synchronous:asynchronous infections as shown in Fig. 2.5A, except that gametocytes have a mean infectious lifespan of approximately 20 hours (based on data in Reece *et al.* 2003) instead of six hours (from data in Gautret *et al.* 1996). 138

A.8 Gametocyte abundance (A) and the transmission potential (i.e., the cumulative probability of transmission) (B) as gametocyte longevity increases. Asynchronous dynamics are given by dashed lines, and synchronized infections are shown with solid lines. Merozoite interference is absent ($q = 0$), and there is relatively high investment in gametocytes ($c = 0.05$). Increasing gametocyte longevity to 20 hours give synchronous strains an advantage, but increasing longevity still further—such that gametocytes outlive asexual forms—sharply reduces transmission differences between synchronous and asynchronous parasites. 139

B.1 Image processing. The original image (A) is converted to black and white (B, Process → Binary → Make Binary). The background must be set to be black prior to this step (with the dialog box in Process → Binary → Options...). The holes are filled in (C, Process → Binary → Fill Holes. The watershed command (Process → Binary → Watershed) subdivides shapes into individual red blood cells (or at least, ImageJ's best guess as to how many red blood cells comprise a clump of dots, D). ImageJ can now be directed to count to number of particles of a particular size and circularity (Analyze → Analyze Particles, with the size range set from 2000 to ∞ and the circularity range set from 0.2 to 1). ImageJ can be directed to show the outlines of the counted particles by selecting "Outlines" from the Show drop down menu in the Analyze Particles dialog box (E). The Fill Holes and Watershed commands run into errors at the edges of images (F), so ImageJ is directed omit particles touching the edges of the image by selecting the "Exclude on edges" option in the Analyze Particles dialog box. 147

B.2 Manual versus digital counts for Dd2 and HB3. Dashed line indicates the 1-to-1 line. 148
B.3 Image J counts for HB3 as a function of area covered on the original image. The red points refer images that were excluded either because the count was improbably low, or because the maximum area of the particle detected was too high, indicating that the algorithm could not separate a large clump of red blood cells. 149
B.4 Figure 3A from Reilly *et al.* (2007), reproduced here for illustrative purposes. The caption reads "Magnetically purified schizonts are viewed by light microscopy to determine the number of merozoites produced per schizont. Five replicates consisting of a minimum of 50 schizonts are counted. Error bars represent the SEM. Unpaired t-tests comparing merozoite numbers between Dd2 and HB3 give a $P < 0.05$ for 18, 20 and 22 merozoites per schizont." 150
B.5 Model fits assuming hyperbolic interference (black solid curve, Eq. 3.2) or parasitoid-like interference (black broken curve, Eq. 3.3), with data is shown in colored lines. The black curves for each strain indicate a single best model fit to both the proportion of sampled red blood cells in the immature parasite stages (A) and in the schizont stage (B). Weighted least squares errors are 0.03995 for hyperbolic interference, and 0.09685 for parasitoid-like interference. 151
B.6 Data collected by Nestor Agbayani (red) compared with data collected by Heather Reilly (gray and black curves). Initial parasitemia was 0.5% for the red curve, and 1% for the gray and black curves. 152
B.7 Data collected by Nestor Agbayani (blue curves) compared with data collected by Heather Reilly (gray and black curves). Initial parasitemia was 0.5% for the red curve, and 1% for the gray and black curves. . . . 153

C.1 The adaptive landscape shifts as infections last longer, with a single optimal conversion rate splitting into two optima (A). One optimum corresponds to relatively low conversion, generating rapid growth of the infection and allowing two peaks in transmission probability (green curves in B and C). The other optimum is a high conversion rate (purple curves), resulting in slow growth of the infection, and one drawn-out peak in the probability of transmission. The relative fitness of these two optima (i.e., which one is local and which one is global), depends on the length of the infection. As infections become longer, the fitness differences are less pronounced between intermediate conversion rates. 156

C.2 In single, asynchronous infections, saturating immunity constrains the optimal fixed conversion rate (solid points). In the absence of immunity (black), the optimum transmission investment is 42.1% when infections last 20 days. With saturating immunity acting against infected red blood cells (blue, $a = 150$, $b = 100$) or merozoites (purple, $a = 7200$, $b = 100$), the optimal conversion rate is reduced to 22.1% and 24.4%, respectively. Except for the difference in x-axis range, the black curve shown here is identical to the black 20-day curve shown in Fig. C.1A. 157
C.3 Best free spline response to the gray strategy shown as the solid dark red line. For comparison, the best free spline response to fixed reproductive investment is shown as the red broken line (identical to the winning strategy shown in Fig. 4.5A). 158
C.4 Fitness of dueling splines in successive optimizations. X-axis labels correspond to panel letters in Fig. 4.5, with the colors and line styles chosen to match the dueling spline strategies in that figure. 159
C.5 Asexual abundance is a poor cue for the optimal conversion rate in single infections, because the same number of parasites corresponds to diverse conversion rates over nearly the entire range. The start of infection is indicated by a dot, and the end is marked with an 'x'. 160
C.6 Asexual abundance of the focal parasite strain is a poor cue for optimal conversion in coinfections. The start and end of infection are indicated by a dot or an 'x', respectively. 161
C.7 Red blood cell abundance could help parasites determine when to begin investing in transmission, but not when to increase investment towards the end of infection. The start of infection is indicated by a dot, and the end is marked with an 'x'. 162
C.8 Red blood cell abundance could serve as an effective cue in coinfections, at least until infection draws to a close. The start of infection is indicated by a dot, and the end is marked with an 'x'. 163
C.9 In single infections, parasite growth in the last 24 hours is a poor indicator of when to turn on transmission investment, but could help parasites decide to increase investment towards the end of infection. The start of infection is indicated by a dot, and the end is marked with an 'x'. 164
C.10 In coinfections, growth of the focal strain in the last 24 hours is a poor proxy for time. The start of infection is indicated by a dot, and the end is marked with an 'x'. 165
C.11 The optimal conversion rate increases with the burst size (β) in single infections in the absence of immunity. Infections were simulated for 20 days for burst sizes of 8 (dotted), 10 (solid), and 12 (dashed). 166

C.12 The optimal conversion rate decreases slightly with the maximum rate of erythropoiesis (λ) in single infections in the absence of immunity. Infections were simulated for 20 days for $\lambda = 1.85 \times 10^5$ (dotted), $\lambda = 3.7 \times 10^5$ (solid), and $\lambda = 5.55 \times 10^5$ (dashed). 167
C.13 Synchronous infections: the optimal conversion rate for single infections is still reduced in the presence of saturating immunity (blue), more so if immunity targets long-lived infected red blood cells. If immunity targets short-lived merozoites (purple), the optimal conversion rate is reduced to a lesser degree. In the absence of immunity, the optimal conversion rate is identical to that of asynchronous infections (black). 168

D.1 Early detection *per se* does not ensure that conversion rates will be correctly estimated. Here we assume that sexual differentiation can be detected as soon as a red blood cell is invaded, and the resulting abundance of infected red blood cells undergoing sexual differentiation (red) is compared with the total number of infected red blood cells (gray, A). Sampled time points are indicated by dots. The inferred conversion rate is shown below (B), taken as the fraction of the total number of infected red blood cells that are undergoing sexual differentiation. The true conversion rate (5%) is shown as a dashed black line. 177
D.2 Immune-mediated mortality of asexual parasites causes overestimation of the conversion rate early in infection. Dynamics of infected red blood cells (red) and mature gametocytes (green) assuming that immunity targets (and saturates as a function of) red blood cells infected with asexual parasites (A, maximum per capita clearance, $a = 150$, half-saturation constant, $b = 100$). The corresponding estimates of conversion rate are shown below (B), again with the actual conversion rate (5%) shown as a dashed line. 178
D.3 All three methods for inferring transmission investment are capable of detecting a wholesale decrease in conversion rates. Here the proportion of parasites differentiating into sexual forms was set at 5% (solid lines) or 1%, for single infections assuming no immunity. 179
D.4 Conversion rates estimated from spline fits to simulated data (purple dots), with the true conversion rate shown in black. The estimated conversion rate was assumed to be a curve of increasing complexity, with each panel showing the AIC value corresponding to the predicted versus observed gametocyte abundance, as well as the number of parameters fit to obtain the spline. Note that even as the fitted conversion rates assume more degrees of freedom, the predicted conversion rate stays approximately fixed, close to the true conversion rate. 180

D.5 The estimated conversion rate is closer to the true value when we correct for gametocyte mortality by dividing gametocyte abundance by $exp(-\mu_g * 0.3$, where μ_g is the mortality rate for gametocytes, and 0.3 represents the time lag between synchronous bursting events and sampling. Conversion rates estimated from spline fits to simulated data (purple dots), with the true conversion rate shown in black. We fit splines of increasing complexity as in Figures 5.3 and D.4. Fitting a constant conversion (one parameter) rate gave a less negative AIC and is not shown here. 181
D.6 Estimated conversion rate in the presence of immunity (purple dots), with the true conversion rate shown in black. As before, conversion rates of increasing complexity were fit to the data, with the number of parameters for the conversion rate and the corresponding AIC shown in each panel. The fit with two parameters had the largest AIC value (-120) and is not shown here. The "data" at each time point were simulated assuming that asexual parasites infecting red blood cells were cleared more efficiently at lower densities ($a = 150$, $b = 100$). 182
D.7 Abundance of red blood cells, infected red blood cells and gametocytes for the six mice used to estimate conversion rates. Data from infections with drug-resistant *P. chabaudi* parasites (Huijben *et al.*, 2010a,b). . . . 183

List of Tables

2.1 Parameter values, units, and sources 20

3.1 Fit parameters 53

B.1 Fit invasion parameters 148

C.1 Parameters for optimal time-varying strategies 169

Acknowledgments

I would like to thank my parents, Dave and Maggie Greischar, for encouraging my love of math and science. My family has been tremendously supportive, especially my uncle, Larry Greischar, my aunts, Jane Greischar and Barb Brown, and my cousin, Nathan Greischar. I appreciate my friends Rebecca Horne, Hanne Nørgaard, Lucie Salvaudon, Britt Koskella, Mandy Gibson, Daniela Vergara, Daniela Fuentes, Alisha Fernandez, Cheri Lee, Salil Siriwat, Muchu Zhou and Nina Stanczyk, not least for patiently listening to me speculate about parasite biology. I have been extremely fortunate in my lab mates, including Nicole Mideo, Jessi Waite, Laura Pollitt, Elsa Hansen, Dave Kennedy, Silvie Huijben, Katey Glunt, Becky Heinig, Monica Acosta, Nina Wale, and the other members of the Read, Thomas, and Bjørnstad groups for incredibly intelligent discussion and useful feedback. In particular, I would also like to thank my lab mates Lindsay Beck-Johnson and Jennie Lavine along with Bill Nelson for the help in delayed differential equation techniques. I greatly appreciate the help of Lindsey Turnbull, Michael Ferdig, Nestor Agbayani, and other members of the Ferdig group for being so generous with their data and their resources, without which my dissertation work would have been entirely theoretical. My committee members, Jason Rasgon and Robert Paulson, as well as Tim Reluga, have provided invaluable discussion. My undergraduate research advisor, Curt Lively, was most generous with lab space and resources when I needed to work remotely from Bloomington. Finally, I would like to thank Andrew Read and Ottar Bjørnstad for their kindness and support.

Chapter 1

Introduction

Malaria life history is enormously variable (Garnham, 1966), but the patterns of diversity are likely driven more by selection than by phylogenetic relationships (Perkins & Schall, 2010). This group of parasites has evolved an impressive range of strategies to cope with the challenges posed by immune defenses, resource competition, and uncertain chances of transmission. Within the vertebrate host, two life history traits have proven especially challenging to put into an adaptive context: synchronized cycles of blood-stage infection, and low investment into transmission. Parasites exhibit great diversity in their degree of synchronization (e.g., Kitchen, 1949; Garnham, 1966) and their investment in transmission (reviewed in Taylor & Read, 1997) both within and across species, suggesting that these curious life history traits may represent not a fundamental constraint on the biology but rather strategies whose adaptive benefits have yet to be characterized.

Synchronized dynamics

Periodic fevers are the classic malaria symptom, thought to be an outward manifestation of highly synchronized parasite dynamics (reviewed in Mideo *et al.*, 2013b). Cycles of fever are thought to be triggered when waves of parasites burst out of red blood cells in unison following tightly synchronized intra-erythrocytic development (Kitchen, 1949; Kwiatkowski & Nowak, 1991). These fevers are debilitating, and synchrony was once viewed as a host adaptation to minimize the ill-effects by confining them to a relatively short period (Kitchen, 1949). Accordingly, observations

of human infections suggest that asynchronous parasite development may cause more severe symptoms (Touré-Ndouo *et al.*, 2009). Once established, synchronous dynamics might be sustained through fever, which is especially devastating to late-stage parasites (Kwiatkowski, 1989). As waves of parasites burst out of red blood cells, they may provoke a fever that kills any mature parasites that have lagged behind, and models demonstrate that a density-dependent feedback loop of that sort could maintain synchrony (Kwiatkowski & Nowak, 1991). Some form of host-mediated intervention is needed to explain sustained synchrony, because cultured parasites cannot maintain synchrony for long without artificial stimulation (Trager & Jensen, 1976; Lambros & Vanderberg, 1979). However, fever cannot be the cause of synchrony, since highly synchronized infections have been observed in asymptomatic humans (Färnert *et al.*, 1997).

The ability of the host to enforce synchrony may depend in part on how the infection begins: Mosquitoes inoculate the host with parasite stages called sporozoites that migrate to the liver, where they multiply before detaching from the liver and releasing asexual merozoites that initiate blood-stage infection (Nardin & Nussenzweig, 1993). Presumably, parasites could be released in a pulse or gradually over many hours, though only gradual release has been documented so far (Sturm *et al.*, 2006), in a rodent malaria species that tends towards asynchronous growth (*P. berghei*, Deharo *et al.*, 1996). Thus the first round of infected red blood cells could consist of either parasites at nearly the same point in development or scattered across a broad range of life stages, reflecting either a synchronous or asynchronous start to infection. While fever may not be required, other host defenses could regulate synchrony in the parasite population, especially if their efficacy varies with parasite numbers. Early host defenses may saturate at high parasite density (Haydon *et al.*, 2003; Elliott *et al.*, 2007; McMorran *et al.*, 2009; Costa *et al.*, 2011; Metcalf *et al.*, 2011). Any parasites that fall out of sync would be present in small numbers by definition, and immunity could effectively clear those parasites away with only minimal effects on the large well-synchronized portion of the population, thereby maintaining synchrony through time. In contrast, specific immune measures are thought to scale up with parasite numbers (Antia & Koella, 1994), but theory suggest that negative feedbacks on growth could maintain synchrony if their action is delayed, allowing a synchronized cohort to trigger

strong immune defenses and escape by developing into a less vulnerable life stage by the time immunity has been upregulated (Kwiatkowski & Nowak, 1991). Recent theory suggests that synchrony could then benefit the host by allowing better immune control of parasite numbers (McQueen & McKenzie, 2008).

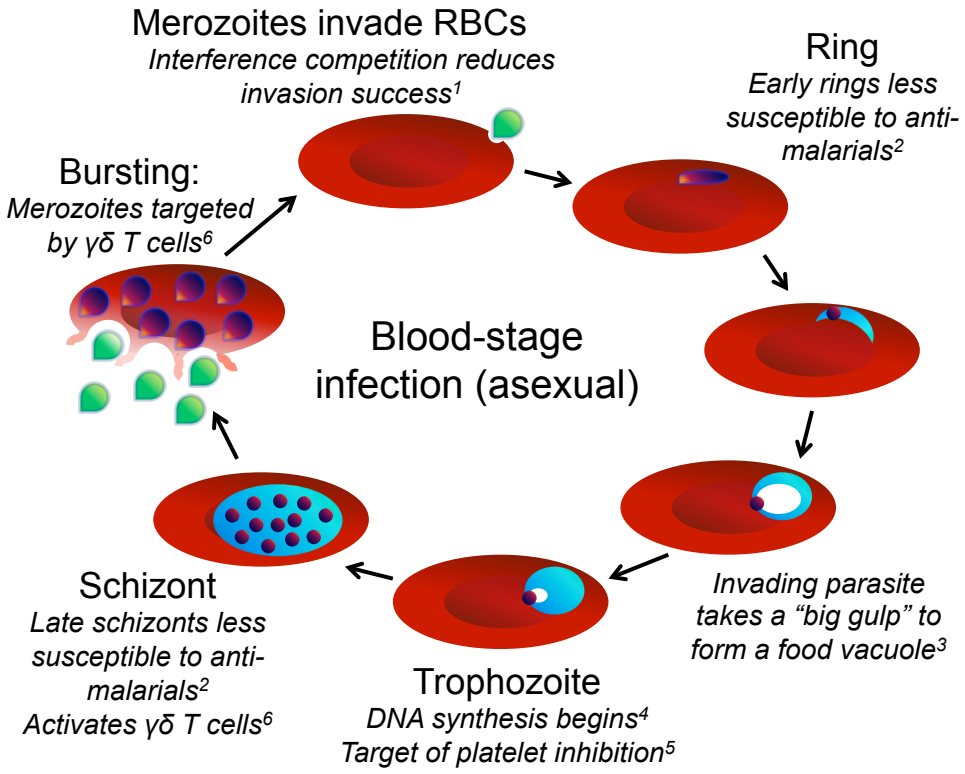

Figure 1.1. Key events in the asexual life cycle. Sources: 1, Boyle *et al.* (2010); 2, ter Kuile *et al.* (1993); 3, Elliott *et al.* (2008); 4, Arnot & Gull (1998); 5, McMorran *et al.* (2009); 6, Costa *et al.* (2011).

Yet whatever the benefits for the host, synchrony should come at a cost to parasites. Red blood cell-invasive forms (merozoites) have only minutes to invade red blood cells, and their chances of success decline when greater numbers of merozoites are present (Boyle *et al.*, 2010). This competition should be most costly to synchronous parasite populations, where huge numbers of merozoites burst out simultaneously. Consistent with this competitive cost, analysis of malaria infections in humans suggests that 'oscillatory' (i.e., synchronous) infections may have lower intrinsic growth rates than 'non-oscillatory' ones (Simpson *et al.*, 2002). Such a

growth disadvantage could be devastating in coinfections, which are common in malaria (e.g., Jafari-Guemouri *et al.*, 2006). Interestingly, synchronous dynamics are associated with less diverse infections (Touré-Ndouo *et al.*, 2009). The competitive cost of synchrony will be balanced against its potential advantages in the face of host defenses, with the fitness consequences playing out in the dynamics of transmission to new hosts.

Generating new infections requires the production of sexual stages (gametocytes) capable of infecting mosquitoes, which develop from a small fraction of infected red blood cells (reviewed in Taylor & Read, 1997). At least two gametocytes—a male and a female—must be present in a blood meal to successfully infect a mosquito (reviewed in Bousema & Drakeley, 2011). Synchronized waves of red blood cell invasion produce pulses of gametocytes later on, and it was thought that synchronization was required to produce a large population of gametocytes that would mature at the right time of day to be passed onto mosquitoes (Hawking *et al.*, 1968; Hawking, 1970). This hypothesis has since been discarded because the gametocytes of the human malaria parasite *P. falciparum* remain viable for days (Hogh *et al.*, 1995), and there is no clear correlation between peak mosquito activity and peaks in either human infectivity or gametocyte densities (Bray *et al.*, 1976; Githeko *et al.*, 1993; Magesa *et al.*, 2000). The hypothesis was further undercut by diversity in temporal dynamics of *P. falciparum* (Färnert *et al.*, 1997; Simpson *et al.*, 2002; Dobaño *et al.*, 2007; Touré-Ndouo *et al.*, 2009) which could not persist for long if synchronization were required for transmission.

Even though synchrony is not required to infect mosquitoes, it is still likely to alter the dynamics of gametocyte production and hence transmission success. The probability of infecting mosquitoes increases with greater gametocyte abundance (Huijben *et al.* 2010a; Bell *et al.* 2012, reviewed in Taylor & Read 1997), but in a nonlinear way. When gametocytes increase from low abundance, there is a disproportionately large increase in the probability of infecting mosquitoes, attributed to the difficulty of finding mates when gametocytes are rare (Bell *et al.*, 2012), while transmission success saturates with large numbers of gametocytes (Paul *et al.*, 2007; Huijben *et al.*, 2010a; Bell *et al.*, 2012). The challenge of finding mates when population density is low (i.e., mate-finding Allee effects, Courchamp *et al.*, 2008) can be overcome by synchronized reproduction (Kelly & Sork, 2002), and analo-

gously, the pulse of gametocyte production that would follow synchronized rounds of blood-stage infection might be expected to greatly enhance transmission success, at least when gametocyte populations are small. We would therefore expect that the advantages of synchrony would be tied to the level of transmission investment.

Understanding how synchrony might be maintained over evolutionary time requires accounting for the transmission consequences, as well as characterizing the variation across parasite strains. That variation is nearly impossible to discern *in vivo*, where the pattern of synchrony might be attributed to parasite, host, or, most likely, some combination of the two. By sidestepping this complexity, *in vitro* experiments provide the best evidence that parasites influence synchrony, since different strains lose synchrony at different rates (Reilly *et al.*, 2007), attributable to the degree of variation in developmental rates. This developmental plasticity is likely to influence the efficacy of anti-malarial drugs, which preferentially remove parasites at particular stages of development (Yayon *et al.*, 1983; Geary *et al.*, 1989; Delves *et al.*, 2012). Even the present frontline drug artemisinin, which has a broad range of action, does not efficiently remove parasites that have just invaded red blood cells (early rings) or parasites that are nearly ready to burst out (mature schizonts), most likely because those stages are not as metabolically active (ter Kuile *et al.*, 1993). The variability in life cycle length must be characterized separately from other strain-specific traits likely to influence dynamics—including burst sizes, invasion rates and frequency of multiple invasions—in order to understand how host and parasite interact to generate the diverse temporal dynamics we see in natural infections.

Transmission investment

Although greater numbers of gametocytes improve the odds of transmission, investing in gametocyte production comes at a clear cost to within-host growth because sexual stages cannot infect further red blood cells. Commitment to sexual differentiation occurs during the late schizont stage (Eksi *et al.*, 2012), when sexually-committed schizonts burst to release merozoites that infect red blood cells and subsequently develop into gametocytes (Bruce *et al.*, 1990). After invasion, gametocytes require a developmental period considerably longer than the asex-

ual cycle length before they are capable of infecting mosquitoes (two days for the murine species *P. chabaudi*, a week or more for *P. falciparum* Gautret *et al.*, 1996; Lensen *et al.*, 1999, respectively). Complicating the problem of balancing growth and transmission, malaria parasites must also cope with a time delay between allocation to transmission and the potential fitness gains associated with a mature gametocyte population. Such a time lag could erode the advantages of plastic strategies (Padilla & Adolph, 1996), but *in vitro* assays show that parasites can respond to crowded conditions by increasing their transmission investment, with allocation ranging from less than a percent to over 70% (Bruce *et al.*, 1990). The variability hints at impressive potential for adaptive plasticity. Despite the possibility of considerable transmission investment, many species—including *P. falciparum*—respond to the tradeoff by investing surprisingly little into gametocyte production (referred to as reproductive restraint, reviewed in Taylor & Read, 1997).

Reproductive restraint is predicted to be adaptive when parasites are competing with other strains within the same host (McKenzie & Bossert, 1998; Mideo & Day, 2008), because parasites need to invest in population expansion in order to gain a substantial share of the host resources. This hypothesis is especially appealing because malaria parasites commonly find themselves in coinfections with other strains (e.g., Jafari-Guemouri *et al.*, 2006), and it has found support in experimental rodent infections with *P. chabaudi* (Pollitt *et al.*, 2011b). While inter-strain competition can explain reduced transmission investment in coinfections, it cannot explain reproductive restraint *per se*. Single-strain infections of mice are estimated to have transmission investment of less than 10% at most (Buckling *et al.*, 1999; Pollitt *et al.*, 2011b), but realistic within-host models predict a level closer to 25% (Crooks, 2008), indicating a gap in our understanding. Additionally, the optimal balance between replication and transmission is expected to change through time, especially given that both within-host success and between-host transmission are strongly dependent on parasite numbers. Reproductive restraint might therefore be selected for more strongly at certain points in infection (for example, early in infection, Koella & Antia, 1995).

Aside from the difficulty of predicting the optimal level of transmission, testing those predictions represents a further challenge. For example, parasites are ex-

pected to alter their transmission investment in response to host condition (Pollitt *et al.*, 2011a), and red blood cell availability is one sensible proxy for host quality. Yet researchers examining the same data set came to opposite conclusions about how transmission investment should vary with red blood cell numbers (Pollitt *et al.*, 2011b; Cameron *et al.*, 2012). Since it is only possible to directly observe transmission investment under tightly controlled conditions *in vitro* (Bruce *et al.*, 1990), any efforts to quantify transmission investment under more realistic conditions must rely on inference, and the inference methods used change the conclusion. More work is needed both to generate predictions about transmission investment strategies and to ensure that those predictions can be tested by robust methods.

Modeling malaria life history

Since malaria parasites interact with their environment in a fundamentally stage-dependent manner, it makes sense to use compartmental models to describe the dynamics. A straightforward approach is to assign a compartment to each of the major players (e.g., uninfected red blood cells, infected red blood cells, merozoites, gametocytes, immune effectors) and describe the transitions in and out of each compartment with ordinary differential equations (ODEs), using numerical methods to observe the transient dynamics that are likely to be most relevant to acute infections(Hellriegel, 1992; Hetzel & Anderson, 1996). This type of model is heuristically useful for understanding how parasite populations may be regulated by resource availability and immunity. Hetzel & Anderson (1996) show that different *Plasmodium* species have life history traits that ensure initial expansion in the host, that immunity is required for clearance of the parasite population, and that immunity must act more intensely against merozoites versus infected red blood cells to generate the same change in dynamics, since the background mortality rate of merozoites is so high. Hellriegel (1992) use the ODE framework to demonstrate that immunity may regulate the interactions between coinfecting malaria strains (Hellriegel, 1992), lending context to the later finding that parasites inoculated into an already-infected mouse face much harsher competition than parasites injected into naïve mice (de Roode *et al.*, 2005).

Though appealing in their simplicity, these ODE models have serious flaws

relating to the constant rates of transition between compartments and resulting exponentially-distributed stage durations (Saul, 1998; Gravenor & Lloyd, 1998; Crooks, 2008). While the mean stage duration is sensible (e.g., 48 hours for *P. falciparum*), the variation around that mean is much too large, so that a large fraction of parasites may burst out of red blood cells immediately following invasion, leading to improbably large growth rates (Saul, 1998). Correspondingly, a substantial fraction of invaded red blood cells immediately mature into gametocytes, rather than taking required time for maturation, leading to major errors in estimating the impact of different levels of transmission investment (Crooks, 2008).

The flaws in simpler ODE models have been represented as a limitation of continuous time models (Crooks, 2008), and many subsequent efforts have instead employed discrete time models. In particular, a discrete time framework been used to good effect by fitting models to detailed time series data from *P. chabaudi* infections to characterize the impact of immunity and erythropoiesis on parasite dynamics (Miller *et al.*, 2010), as well as strain-specific differences in preference for immature red blood cells (reticulocytes), burst size, and invasion rates (Mideo *et al.*, 2008, 2011). Such models have also helped identify the timing and efficacy of immune clearance, and characterized density-dependent growth within parasite populations (Metcalf *et al.*, 2011). As Crooks (2008) notes, these models are entirely appropriate for highly synchronized infections (such as those observed in *P. chabaudi*, O'Donnell *et al.* 2011, and sometimes observed in *P. falciparum*, White *et al.* 1992), because bursting and invasion occur at discrete intervals. However, many *P. falciparum* infections appear poorly synchronized (Färnert *et al.*, 1997; Magesa *et al.*, 2000; Simpson *et al.*, 2002; Touré-Ndouo *et al.*, 2009). For an asynchronous parasite population, bursting and invasion could occur at any point in time, as evidenced by the continuous rather than discrete growth in asynchronous *P. falciparum* infections (Färnert *et al.*, 1997), dynamics that are difficult to describe with discrete time models. Splitting a discrete time model into two parasite age compartments can allow dynamics beyond highly synchronized (Kwiatkowski & Nowak, 1991), but incorporating immune defenses that are expected to occur in continuous time can require a more complicated framework (Crooks, 2008).

An alternative approach is to keep the continuous time differential equation framework, but constrain the distribution of stage durations to a reasonable range

(Gravenor & Kwiatkowski, 1998; Gravenor & Lloyd, 1998; Hoshen *et al.*, 2000). While these types of models are more computationally intensive to analyze, they do allow density-dependent processes, such as immune clearance, to occur in continuous time, which would otherwise necessitate a complicated arrangement mixing discrete and continuous time (Haydon *et al.*, 2003). They have the benefit of being readily able to describe a range of temporal dynamics, from asynchronous to highly synchronized. Equally important for mapping the fitness consequences of plastic transmission investment, we need to incorporate realistic time delays between the decision to invest in gametocyte production and the fitness consequences of that decision (Crooks, 2008). Models for other systems have shown that the benefits of plasticity can disappear entirely depending on the time lag between sensing an environmental changes and the ability to respond (Padilla & Adolph, 1996).

These continuous time models fall into the broad categories of fixed delay models, in which stage duration is constant with no variation (a Dirac-Delta distribution, e.g., Hoshen *et al.*, 2000), and distributed delay models, which allow the stage duration to vary, but not to the unrealistic extremes seen in simpler ODE models. These two formulations of time delays—fixed versus distributed—have slightly different biological implications. It is clear that life cycle duration varies, because synchrony decays rapidly *in vitro* (Trager & Jensen, 1976). However, synchrony can be maintained within the host (e.g., Färnert *et al.*, 1997), suggesting that not all of the variation apparent in culture is expressed *in vivo*. Fixed time delays might therefore be a good approximation of parasite development. A distributed delay model might be more realistic, at least for describing within-host dynamics, but it also comes at the cost of an additional parameter to describe the variability in the delay, which is not yet well-characterized. Further, variability in life cycle length means that synchrony will be lost over time, which makes it difficult to assess the fitness consequences of synchrony. Thus, fixed delays represent a good starting point for understanding complex within-host dynamics, but describing how synchrony changes through time requires a distribution of delays.

Objectives

To understand the fitness consequences of two curious aspects of malaria life history—synchrony and reproductive restraint—I make use of delay models to encapsulate the life stage- and density-dependent ways in which parasites interact with their environment. In Chapter 2, I develop a fixed delay model to describe the transmission consequences of synchronized infection dynamics within the host. Model simulations are used to examine the influence of parasite density-dependent transmission success, competition for red blood cells (interference), immune clearance, in addition to the impact of a coinfecting malaria strain. In Chapter 3, I develop a distributed delay model to examine the loss of synchrony *in vitro*, and explore the extent to which times series can be used to quantify life cycle duration, developmental plasticity, as well as intrinsic growth rates. Using two candidate forms of density-dependent interference developed in Chapter 2, I fit the model to detailed time series data to determine which form better describes dynamics while simultaneously quantifying differences in cycle length and developmental plasticity across strains. By analyzing invasion assays performed in collaboration with Lindsey Turnbull, I assess whether interference is likely to alter invasion rates or successful maturation within red blood cells. In Chapter 4, I return to the fixed delay model developed in Chapter 2 to identify optimal fixed and time-varying transmission investment strategies *in vivo*. I then simulate data from the fixed delay model in Chapter 5 to show why existing inference methods are unable to accurately describe transmission investment, and I develop a novel statistical approach to better characterize transmission investment strategies from existing data. Finally, in Chapter 6, I discuss the implications of this work and identify future directions.

Chapter 2

Synchrony in malaria infections: How intensifying within-host competition can be adaptive

2.1 Abstract

Malaria parasites exhibit great diversity in the coordination of their asexual life cycle within the host, ranging from asynchronous growth to tightly synchronized cycles of invasion and emergence from red blood cells. Synchronized reproduction should come at a high cost—intensifying competition among offspring—so why would some *Plasmodium* species engage in such behavior and others not? We use a delayed differential equation model to show that synchronized infections can be favored when: (1) there is limited interference among parasites competing for red blood cells; (2) transmission success is an accelerating function of sexual parasite abundance; (3) the target of saturating immunity is short-lived; and (4) coinfections with asynchronous parasites are rare. As a consequence, synchrony may be beneficial or costly, in line with the diverse patterns of synchronization observed in natural and lab infections. By allowing us to characterize diverse temporal dynamics, the model framework provides a basis for making predictions about disease severity and for projecting evolutionary responses to interventions.

2.2 Introduction

Synchronized reproduction represents a significant challenge to evolutionary theory: what benefits outweigh the costs of escalating competition among offspring? Despite the costs, many organisms do coordinate their reproductive efforts. Extreme examples are mass emergence of periodical cicadas (Williams *et al.* 1993) and mast-seeding of bamboos (Janzen 1976), but more subtle examples are common throughout the natural world (reviewed in Ims 1990, Kelly & Sork 2002). Yet even among organisms sharing similar life-histories, some synchronize their reproduction while others do not. Theory suggests that synchronized reproduction can be an adaptation to expedite mate-finding and overwhelm natural enemies (Ims 1990, Kelly & Sork 2002). These obstacles are not confined to free-living organisms, however; parasites likewise vary in how closely they coordinate their life cycles, with malaria species provide a striking example (Mideo *et al.* 2013b). We apply an ecological approach to identify plausible mechanisms that could favor synchronized infection cycles in malaria parasites even at the cost of intensifying within-host competition.

Synchronized cycles of blood stage infection are a fascinating aspect of malaria biology, with parasites invading red blood cells, reproducing asexually, and bursting out in unison (e.g., Garnham 1966, Hawking *et al.* 1968, Hawking 1970). Even considering a single malaria species, some human infections appear synchronous and some do not (Färnert *et al.* 1997, Bruce *et al.* 2000b, Simpson *et al.* 2002, Dobaño *et al.* 2007, Touré-Ndouo *et al.* 2009); these observations highlight variability in a fundamental aspect of within-host ecology, with critical implications for human health. Synchrony should limit host exploitation by intensifying competition for resources. The degree of synchronization should also influence parasites' susceptibility to anti-malarial drugs, which act against a subset of life stages (e.g., Yayon *et al.* 1983, Slater & Cerami 1992, ter Kuile *et al.* 1993, Dhar *et al.* 1998, Delves *et al.* 2012). The synchrony inherent to parasite dynamics thus represents a source of variation that could influence the course of evolution within the host, modulating the degree of virulence and drug susceptibility.

All else equal, synchrony should be costly. Malaria parasites face intense competition for red blood cells *in vitro* (Reilly *et al.* 2007, Boyle *et al.* 2010), and

parasites have only minutes to invade red blood cells before their viability is lost (Boyle *et al.* 2010). By bursting out of red blood cells in unison, synchronous parasites should pay a vastly increased cost of competition. Whether synchrony is ultimately beneficial or costly to the parasite will be determined by its effects on the transmission to the mosquito vector. Accordingly, synchrony was first thought to be an adaptation to enhance transmission (Hawking *et al.* 1968, Hawking 1970). Infecting mosquitoes requires sexual gametocytes that spawn from a small fraction of the asexual, blood-stage parasites (reviewed in Drakeley *et al.* 2006, Bousema & Drakeley 2011). Coordinated waves of red blood cell invasion generate periodic oscillations in gametocyte numbers that could be advantageous if peak gametocyte numbers occur when mosquitoes are most likely to feed (Hawking *et al.* 1968, Hawking 1970). However, neither peak infectivity (Bray *et al.* 1976, Githeko *et al.* 1993) nor peak gametocyte density (Magesa *et al.* 2000) have been shown to correspond with peak vector activity time for human cases.

More recent theory has focused on the success of the asexual parasites that ultimately produce transmission stages. Synchrony has been hypothesized to be a consequence of host defenses that intensify with parasite numbers (Kwiatkowski & Nowak 1991, Rouzine & McKenzie 2003). The reasoning is that if a particular parasite stage is immunogenic, and a later stage is vulnerable to immune clearance, then a large cohort of parasites may trigger an intense immune response that would effectively clear away other cohorts of parasites, leaving a synchronized group of parasites behind. While escalation might be characteristic of an adaptive immune response (Antia & Koella 1994), innate host defenses may instead saturate as parasite numbers increase. These early immune responses may be most effective against small numbers of parasites, as suggested by data from rodent infections (Haydon *et al.* 2003, Metcalf *et al.* 2011) and malaria parasites *in vitro* (*P. falciparum* cultured with platelets, McMorran *et al.* 2009; and $\gamma\delta$ T cells, Costa *et al.* 2011).

If immunity can saturate, pulses in parasite numbers may overwhelm host defenses, analogous to the way many organisms use synchronized reproduction as a way to satiate predators. If immunity targets a transient part of the parasite life cycle, synchronization would allow parasites in the vulnerable life stage to disappear between brief periods of overwhelming numbers, analogous to the way

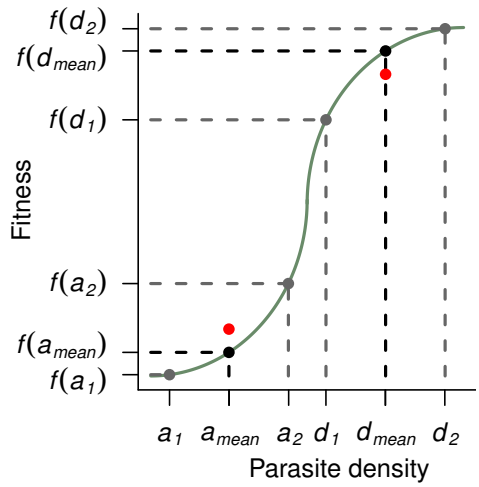

Figure 2.1. When fitness is a convex function of density (e.g., the a values in the accelerating part of the curve), oscillations in density can increase mean fitness as a consequence of Jensen's inequality (reviewed in Ruel & Ayres 1999). A strain that alternates between densities a_1 and a_2 has higher mean fitness (red point) than a strain that maintains a constant density a_{mean} (black point). If fitness is a concave or decelerating function of density (d values), oscillations in numbers decrease mean fitness compared to a strain that maintains a constant density (red versus black point). Cumulative fitness is altered in an identical manner.

periodical cicadas emerge synchronously—and briefly—to satiate predators. If immunity targets a long-lived part of the parasite life cycle, then even small variation in timing would result in vulnerable parasites persisting between peaks in abundance. As parasite numbers increase, their survival saturates, and this saturating fitness curve renders oscillations between high and low abundance costly (Fig. 2.1). For synchrony to be advantageous, vulnerable parasites need to oscillate between high and zero abundance, a scenario most likely with a short period of vulnerability. The brevity of the life-stage vulnerable to immunity may help determine whether synchronous parasites perform better in spite of increased competition for host resources.

Distinct from the success of blood-stage infection, synchrony may improve transmission by allowing the parasites to overcome Allee effects—where fitness declines as a result of dwindling numbers (Courchamp *et al.* 2008)—that would jeopardize the success of the small numbers of gametocytes present in a mosquito bloodmeal. Sexual organisms may experience sharp increases in fitness as population sizes increase and mates become easier to find (Courchamp *et al.* 2008).

Consequently, malaria transmission is a sigmoidal function of gametocyte density, with the probability of mosquito infection first accelerating as gametocytes increase and then saturating with large numbers of gametocytes (Paul *et al.* 2007, Huijben *et al.* 2010a, Bell *et al.* 2012). In the accelerating part of the transmission curve when gametocyte numbers are low, oscillations may improve mean fitness (through Jensen's inequality, Fig. 2.1). In contrast, fluctuating densities may become a liability in the saturating part of the curve where gametocytes are abundant (Fig. 2.1).

Here we develop a within-host model to estimate the probability of transmission from synchronous versus asynchronous malaria infections while accounting for the possibility of competition for red blood cells and saturating immunity. Treating the intra-erythrocytic part of the life cycle as a fixed delay, the model predicts that synchronous parasites have higher fitness when gametocyte investment is low, both in single and coinfections. Competition for red blood cells may subtly favor synchronous parasites in single infections by damping extreme changes in parasite density, but in coinfections, competition strongly disfavors synchronous strains. Saturating immunity favors synchrony, but only if the target is a brief life stage. These model results lay out a framework for explaining the varied patterns of synchronization observed in natural infections.

2.3 Methods

2.3.1 Delayed differential model

We model infection using a system of delayed differential equations, parameterized for the rodent malaria *Plasmodium chabaudi*. The model framework assumes that a fixed period of time is required for parasite development within red blood cells. Any infected red blood cells that persist through the delay will burst to release the parasite stages capable of invading new red blood cells (merozoites) or will develop into mature transmission stages (gametocytes). This time delay before bursting is essential for capturing synchronous infection dynamics (Hoshen *et al.* 2000). The delayed system also solves many of the problems associated with continuous time malaria models (reviewed in Crooks 2008), namely the implicit assumption that

merozoite release and gametocyte production can occur at any time, even if a red blood cell was only just infected. With a conventional compartmental model, infected cells would burst at a fixed rate (i.e., exponentially-distributed developmental periods). In the present model, we assume that the developmental period is fixed (i.e., Dirac-Delta distributed), with all surviving infected cells bursting exactly one day post-infection. We address the implications of assuming a fixed delay in the discussion.

Single infections

The model tracks five life stages critical to the dynamics of malaria infection: uninfected red blood cells (R), infected red blood cells, either committed to the asexual life cycle and bound to produce more merozoites (I) or committed to the sexual life cycle and destined to produce transmissible gametocytes (I_G), merozoites (M), and gametocytes (G). The dynamics of uninfected red blood cells are governed by the influx of new red blood cells via erythropoiesis and the outflux of red blood cells due to intrinsic mortality (μ) or infection ($p(t)$):

$$\frac{dR(t)}{dt} = \lambda\left(1 - \frac{R(t)}{K_{start}}\right) - \mu R(t) - p(t)R(t)M(t) \tag{2.1}$$

where $K_{start} = \lambda R^*/(\lambda - \mu R^*)$ so that in the absence of infection red blood cells remain at a homeostatic equilibrium (R^*). The rate of erythropoiesis following malaria infection in mice has been approximated as a linear function of red blood cell numbers, with erythropoiesis responding to the loss of red blood cells after a time lag of one or three days, depending on the immune status of the mice (Metcalf *et al.* 2011). A time lag in the erythropoietic response might select for parasites with a corresponding life cycle length, but it need not alter the fitness of synchronous versus asynchronous parasites. We therefore keep erythropoiesis as a linear function of red blood cell numbers and omit the time lag for simplicity. Red blood cells are infected by merozoites at a rate of $p(t)$. Invasion success declines in an approximately hyperbolic fashion as the ratio of merozoites to red blood cells increases, according to *in vitro* assays of *P. falciparum* (Reilly *et al.* 2007, Boyle *et al.* 2010), although the biological mechanisms underlying this pattern have not yet been worked out. We introduce the q parameter to specify the degree

of merozoite interference:

$$p(t) = \frac{p_{max}}{1 + q(M(t)/R(t))} \tag{2.2}$$

When $q = 0$, $p(t)$ reduces to the maximum invasion rate, p_{max}, and for $q > 0$, the invasion rate declines hyperbolically as the ratio of merozoites to red blood cells increases. We hence refer to this form of intereference as "hyperbolic". We also examine dynamics with an alternate invasion rate, $z(t)$, analogous to functional forms used to describe parasitoid inteference (Hassell 2000):

$$z(t) = \frac{p_{max}}{(M(t) + 1)^m} \tag{2.3}$$

Unless otherwise specified, we assumed hyperbolic merozoite inteference (Eqn. 2.2). Whenever red blood cells become infected, a small fraction c are assumed to be committed to the sexual cycle, while the rest continue to propagate blood-stage infection through the production of merozoites:

$$\begin{aligned} \frac{dI(t)}{dt} &= (1-c)p(t)R(t)M(t) - \mu I(t) - \frac{a}{b + I(t)}I(t) \\ &\quad -(1-c)p(t-\alpha)R(t-\alpha)M(t-\alpha)S \end{aligned} \tag{2.4}$$

Infected red blood cells are lost to intrinsic mortality (assumed to be equal to mortality rate of uninfected red blood cells, μ) and to immune clearance, with a proportion S surviving the length of the erythrocytic cycle (α) to burst and release merozoites. Immune clearance is assumed to be a saturating function of infected red blood cell density (type II functional responses in ecological terminology, Metcalf *et al.* 2011), with a per capita clearance of $\frac{a}{b+I(t)}$. The proportion, S, of infected red blood cells that survive background mortality and immune clearance to produce merozoites is found by integrating the mortality rates over the developmental period, α.

$$S = \exp\left(-\int_{t-\alpha}^{t} \mu + \frac{a}{b + I(\omega)} d\omega\right) \tag{2.5}$$

Each infected red blood cell that survives for α days bursts to release β merozoites:

$$\frac{dM(t)}{dt} = \beta(1-c)p(t-\alpha)R(t-\alpha)M(t-\alpha)S - p(t)R(t)M(t) - \mu_Z M(t) \quad (2.6)$$

Merozoites can infect red blood cells at the time-varying rate, $p(t)$, but are subject to intense background mortality (μ_Z).

We also consider the case where merozoites are the sole target of saturating immunity, to determine how abbreviating the vulnerable life stage can affect the benefit synchrony. If saturating immunity targets merozoites instead of infected red blood cells, Eqns. D.2-D.4 become:

$$\begin{aligned} \frac{dI(t)}{dt} &= (1-c)p(t)R(t)M(t) - \mu I(t) \quad (2.7) \\ &\quad -(1-c)p(t-\alpha)R(t-\alpha)M(t-\alpha)S \\ S &= \exp\left(-\int_{t-\alpha}^{t} \mu d\omega\right) = \exp(-\mu\alpha) \quad (2.8) \\ \frac{dM(t)}{dt} &= \beta(1-c)p(t-\alpha)R(t-\alpha)M(t-\alpha)S - p(t)R(t)M(t) \\ &\quad -\mu_Z M(t) - \frac{a}{b+M(t)}M(t) \quad (2.9) \end{aligned}$$

No complicated survival functions are needed for merozoites (Eq. 2.9), because their waiting times are assumed to be exponentially distributed (i.e., having fixed hazard rates). To generalize the results from this modified model, we also consider the case where immunity targets a brief portion of the intra-erythrocytic cycle (details of age-structured model in appendix A.1.1). The rate of immune removal competes with the rate of background mortality, so immunity was set to be stronger when acting against a brief portion of the life cycle. To simplify our model, we omit adaptive immunity, which is not likely to alter dynamics until later in the infection (Metcalf *et al.* 2011).

For infected red blood cells committed to making gametocytes, the dynamics are similar to Eq. D.2 save that there is a longer delay, α_G, before an infected red blood cell can develop into a gametocyte (Gautret *et al.* 1996).

$$\frac{dI_G(t)}{dt} = cp(t)R(t)M(t) - \mu I_G(t) - cp(t-\alpha_G)R(t-\alpha_G)M(t-\alpha_G)S_G \quad (2.10)$$

We simulate a range of c values suggested by studies of *P. chabaudi* infections (0.1% to 5%, Pollitt *et al.* 2011b). We assume that the innate immune response ignores parasites developing into gametocytes (I_G) because immune measures most effective against sexual blood stages have so far been reported as antibody-dependent rather than innate (reviewed in Bousema & Drakeley 2011, Riley & Stewart 2013). Given the low proportion of parasites developing into gametocytes, innate immune measures that act against sexual and asexual blood stages are unlikely to qualitatively alter the benefits of synchrony. At peak infection immune measures are already saturated, and this peak generates the bulk of gametocytes.

The proportion surviving to become gametocytes, S_G, is

$$S_G = \exp\left(-\mu\alpha_G\right) \tag{2.11}$$

Unlike the asexual cycle, where one infected cell becomes several merozoites (according to the burst size, β), each infected cell committed to the sexual cycle develops into a single gametocyte.

$$\frac{dG(t)}{dt} = cp(t-\alpha)G)R(t-\alpha_G)M(t-\alpha_G)S_G - \mu_G G(t) \tag{2.12}$$

Gametocytes are assumed to have an average lifespan of $1/\mu_G$. Gametocytes are maximally infectious for six hours (Gautret *et al.* 1996), so the infective lifespan of a *P. chabaudi* gametocyte is shorter than the length of the asexual life cycle (24 hours, Landau & Boulard 1978). We also extend gametocyte lifespan, a scenario more relevant to *P. falciparum* infections, where it is longer than the length of the asexual life cycle (reviewed in Bousema & Drakeley 2011).

The probability of transmission to the mosquito is assumed to be a sigmoidal function of gametocyte density, as has been shown for both *P. falciparum* (Huijben *et al.* 2010a) and *P. chabaudi* (Bell *et al.* 2012). We sum transmission probability over the first 20 days of infection, which encompasses the first and largest peak in parasite numbers, as our fitness measure. We use a sigmoidal curve parameterized for drug-sensitive *P. chabaudi* infections (Bell *et al.* 2012) to calculate the cumulative the probability of transmission for synchronous versus asynchronous

strains.

$$\textit{Probability of transmission to mosquito} = \frac{\exp(-12.69 + 3.6\log_{10}(G(t)))}{1 + \exp(-12.69 + 3.6\log_{10}(G(t)))} \tag{2.13}$$

Due to the extreme stiffness of this delayed system, the interpolating algorithm occasionally returned abundances slightly below zero (most negative result on the order of -10^{-19}). Since negative values cannot be evaluated by Eqn. 2.13, we set gametocyte abundance to zero whenever it became negative. We also calculate the cumulative probability of transmission using two other sigmoidal curves representing the extreme curves reported in the literature (Fig. A.1, equations and parameter values from Huijben *et al.* 2010a, Bell *et al.* 2012). Parameter values are shown in Table 3.1, and all simulations were run in **R** version 2.15.2 (R development team 2013), using the *PBSddesolve* package.

Table 2.1. Parameter values, units, and sources

Parameter	Value	Source
R^* (red blood cell count at homeostasis)	8.5×10^6 cells/μL	Savill *et al.* 2009
λ (maximum new red blood cells)	3.7×10^5 RBCs/μL/day	Savill *et al.* 2009
μ (red blood cell mortality rate)	0.025/day	Miller *et al.* 2010
p (max. per merozoite invasion rate)	4×10^{-6}/day	Mideo *et al.* 2008*
α (blood-stage delay)	1 day	Landau & Boulard 1978
α_G (gametocyte delay)	2 days	Gautret *et al.* 1996
β (burst size)	10 merozoites	Mideo *et al.* 2008*
μ_Z (merozoite mortality rate)	48/day	used in Hetzel & Anderson 1996, Mideo *et al.* 2008
μ_G (gametocyte mortality rate)	4/day	Gautret *et al.* 1996†
		*within realistic range
		†length of most infectious stage

Initial conditions

Infection is initialized with infected red blood cells to mimic the parasites being released from the liver over a short or long time period, initiating a synchronous or asynchronous infection respectively. Simulated synchronous versus asynchronous

infections differ only in the age structure of the initial inoculum, specified by a beta distribution. The initially infected red blood cells (I_0) are all committed to producing merozoites. For $t \leq \alpha$, Eqns D.2, 2.5, & D.4 are

$$\begin{aligned} \frac{dI(t)}{dt} &= (1-c)p(t)R(t)M(t) - \mu I(t) - \frac{a}{b+I(t)}I(t) \qquad (2.14) \\ &\quad -I(0)\text{Beta}(s_P, s_P)(t)S \\ S &= \exp\left(-\int_0^t \mu + \frac{a}{b+I(\omega)}d\omega\right) \qquad (2.15) \\ \frac{dM(t)}{dt} &= \beta I(0)\text{Beta}(s_P, s_P)(t)S - p(t)R(t)M(t) - \mu_Z M(t) \qquad (2.16) \end{aligned}$$

The beta distribution takes two shape parameters, both of which are set equal to s_P. With $s_P = 1$, the starting population bursts uniformly over the first delay, while $s_P = 100$ yields a narrow bell curve centered around 0.5 (Fig. 2.2). The underlying assumption is that the degree of synchronization is determined by the genetics (or epigenetics) of the parasite strain at the start of infection.

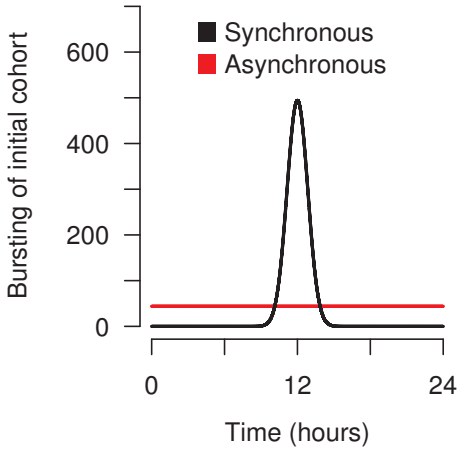

Figure 2.2. Synchronous versus asynchronous infections are initialized using a beta distribution with large or small shape parameter, s_P, to specify the bursting of the initial inoculum (synchronous in black, $s_P = 100$; and asynchronous in red $s_P = 1$).

Coinfection model.

Synchronous infections of humans seem to be more highly related than asynchronous infections, which tend to show more diversity (Touré-Ndouo *et al.* 2009). The advantages of synchrony may then depend on the presence of a competing strain. We therefore expand the single strain model into a coinfection model (details in appendix A.1.2). In short, two strains are assumed to be released from the liver on the same day, with the two strains differing only in the degree of synchronization. The invasion rate per merozoite declines based on the ratio of total merozoites to uninfected red blood cells, with both strains equally sensitive to competition for resources. The immune response is assumed to be non-specific, dependent on the total density of vulnerable parasites as has been suggested by data from human infections (Bruce *et al.* 2000a). Since we are modeling early infection, we again neglect adaptive immunity.

2.4 Results

2.4.1 Low gametocyte investment favors synchrony

In the absence of immunity or interference competition among merozoites, simulated infections peak near day 10 (Fig. 2.3), with subsequent damped oscillations towards an equilibrium. Infections peak due to resource limitation: parasite numbers begin to drop when there are more merozoites than uninfected red blood cells to infect. In this simulation, immunity and merozoites interference are set to zero, resulting in greater numbers of infected than uninfected red blood cells at peak infection. In addition to the multi-day oscillations, synchronous strains showed pronounced daily oscillations in abundance due to the 24 hour cycle length of the parasite *P. chabaudi* (Landau & Boulard 1978).

With low gametocyte investment, synchronous strains have higher fitness (i.e., greater cumulative transmission potential). As a smaller proportion of infected cells are committed to the sexual part of the life cycle, gametocyte abundance decreases, but dynamics are qualitatively similar (Fig. 2.3A & B). The critical difference is that the probability of transmission is an accelerating function of gametocyte density at low gametocyte investment, so that oscillations in gametocyte

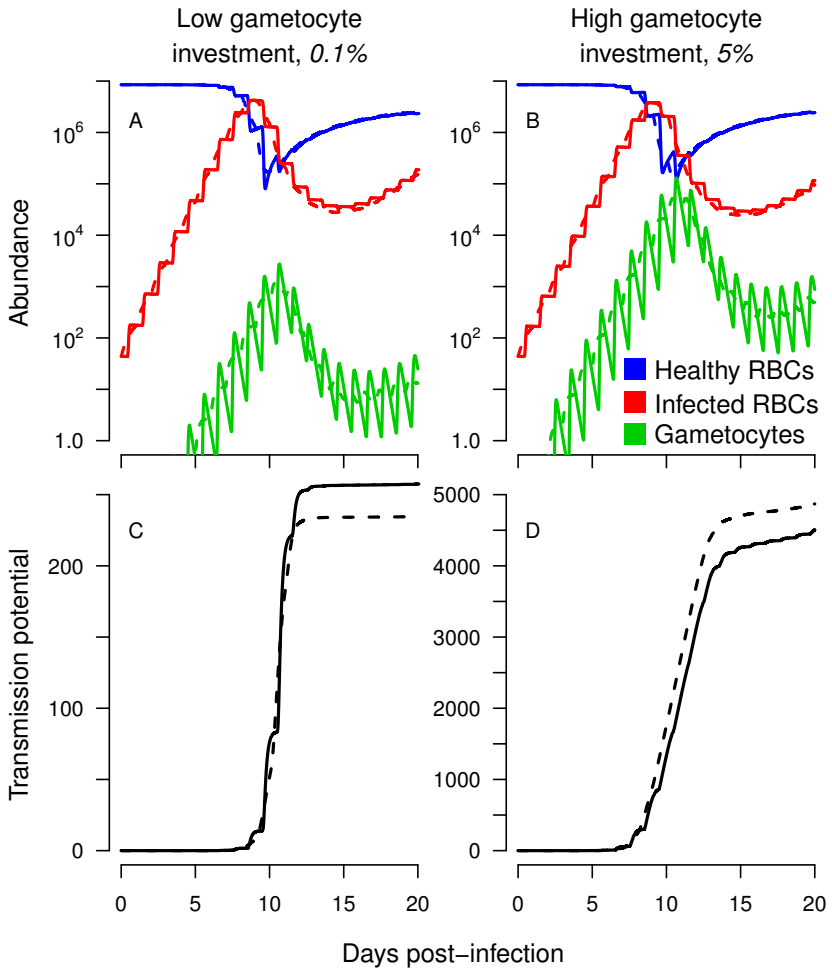

Figure 2.3. Synchronous infections transmit better at low gametocyte investment—without any qualitative change in dynamics—due to the sigmoidal shape of the relationship between gametocyte numbers and probability of transmission. Single-strain infections were simulated in the absence of merozoite interference ($q = 0$) and immune clearance ($a = 0$), with solid curves indicating synchronous infections and dashed lines referring to asynchronous dynamics. Abundance of uninfected and infected red blood cells (RBCs) in the asexual cycle are shown with gametocyte (transmission stage) numbers (A & B, logarithmic scale), with total transmission potential—the cumulative transmission probability—shown below (C & D). Simulations in panels A & C assume low gametocyte investment ($c = 0.001$), while panels B & D show dynamics with relatively high gametocyte investment ($c = 0.05$).

density increase fitness (Fig. 2.3C). At high gametocyte investment, transmission probability saturates (at day 10 in Fig. 2.3D) and oscillations reduce the transmission potential. From Fig. 2.1, it can be seen that when numbers fluctuate

in the accelerating part of the curve, mean and cumulative fitness are increased compared to when numbers hold steady. Fluctuations in the saturating part of the curve reduce fitness—the parasite strain would have done better to maintain steady numbers.

2.4.2 Interference among merozoites can benefit synchronous parasites

Interference competition increases uninfected red blood cell density and reduces gametocyte abundance by limiting merozoite invasion success (Fig. 2.4). In the absence of interference competition, gametocyte numbers are predicted to rise to a high peak due to efficient depletion of uninfected red blood cells (Fig. 2.4A, B, blue curves). Once red blood cells become limiting, there is a precipitous drop in gametocyte numbers. When merozoites interfere with each other, red blood cells cannot be depleted to the same degree (Fig. 2.4A), resulting in a lower peak gametocyte density and subsequent shallower trough especially for synchronous infections (Fig. 2.4B, orange curves). For certain parameter values, synchronous infections can catch up and sometimes even exceed the transmission potential of asynchronous infections (Fig. 2.4C).

Though asynchronous infections have superior gametocyte production in the face of interference, greater gametocyte production does not always result in greater transmission because of the sigmoidal relationship between gametocyte density and probability of infecting a mosquito. Despite large differences in peak gametocyte density, the corresponding probabilities of transmission saturate to similar values (Fig. 2.4C). In the absence of interference competition, the synchronous strain exhibits lower cumulative transmission potential than the asynchronous infection (high transmission investment, Fig. 2.4C). Merozoite interference gives the synchronous strain a larger pool of uninfected red blood cells post-peak, allowing gains in gametocyte production and increasing transmission potential above that of the asynchronous infection (Fig. 2.4C).

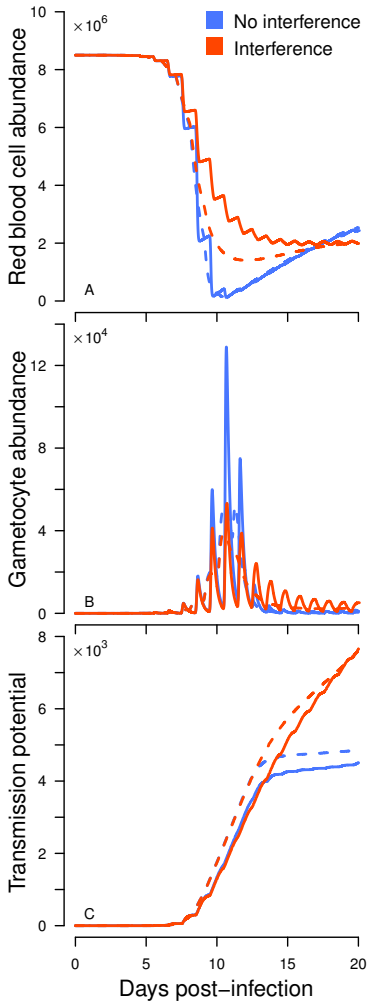

Figure 2.4. Merozoite interference reduces anemia (A) and gametocyte abundance (B), but increases transmission potential (cumulative probability of transmission, C). Synchronized and asynchronous dynamics (solid and dashed lines, respectively) when merozoite interference is present (orange curve, $q = 10$) or absent (blue curve, $q = 0$). Gametocyte investment is set relatively high ($c = 0.05$) and immunity is absent ($a = 0$). The blue curves are identical to the red blood cell and gametocyte abundance shown in Fig. 3B, save that here they are plotted on a conventional rather than logarithmic scale.

2.4.3 Synchronous strains can transmit better from single infections

We simulate single infections as a function of interference among merozoites and gametocyte investment for three different immunity scenarios: (1) no immune response; (2) saturating immunity targeting infected red blood cells in the asexual

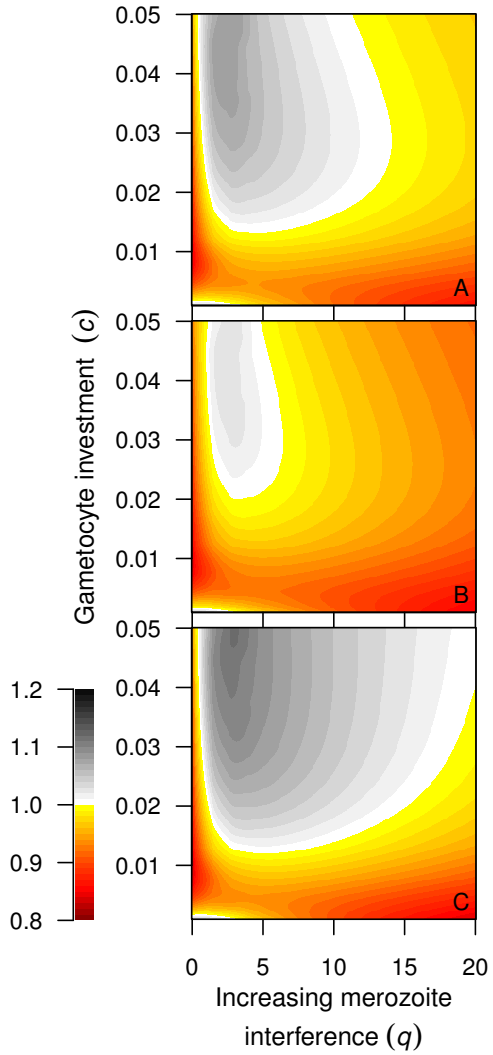

Figure 2.5. Synchronous parasites frequently transmit better from single infections. Smoothed relative fitness (ratio of cumulative probability transmission for synchronous:asynchronous strain) with increasing competition among merozoites (x axis) and investment in producing transmission stages (y axis). Synchronous infections transmit better in the white/gray areas. Immunity is set to zero (A, $a = 0$), to target infected red blood cells (B, $a = 150$, $b = 100$) or to remove merozoites (C, $a = 7200$, $b = 100$). Immunity targeting short-lived merozoites increases the parameter space favorable to synchronous infections.

cycle; (3) saturating immunity targeting merozoites. In simulations without immunity, synchrony is only advantageous with minimal merozoite interference and low gametocyte investment, and at intermediate levels of merozoite interference with greater investment in gametocytes (Fig. 2.5A). When immunity removes infected

red blood cells, it reduces the region of the parameter space where synchronous strains have a relative fitness advantage (Fig. 2.5B versus A). When immunity targets merozoites, synchronous strains transmit better over a wide range of parameter values because of efficient saturation of the immune response (Fig. 2.5C). The parameter space favorable to synchronous strains is similarly increased when immunity targets only a brief part of the intra-erythrocytic cycle (Fig. A.2). In both cases, synchrony is advantageous because the vulnerable life-stage is either present in overwhelming numbers or absent altogether.

2.4.4 Synchronous strains perform poorly in coinfections

When immunity is absent or when immunity acts on infected red blood cells, asynchronous strains out-transmit synchronous strains in the same host for all parameter values simulated (Fig. 2.6A & B). The success of asynchronous strains suggests that interference competition among merozoites is much more devastating to synchronous strains in coinfections. Synchronous strains do not deplete red blood cells as efficiently in single infections (Fig. 2.4), and in coinfections, synchronous parasites face more severe resource limitation as asynchronous strains efficiently remove uninfected red blood cells. For these substantial costs, synchronous strains are only predicted to out-transmit their asynchronous counterparts when immunity targets the short-lived merozoite stage (Fig. 2.6C).

2.4.5 Sensitivity to model assumptions

Choice of transmission function. We find that the benefits of synchrony vary with the transmission function used to calculate relative fitness, but two generalities emerge: (1) synchronous strains have higher relative fitness over a greater portion of the parameter space when immunity targets a short-lived life stage (Figs. 2.5C, A.3C, A.4C); (2) the relative fitness of synchronous strains can be broadly understood in terms of Jensen's inequality (Fig. 2.1). The three different transmission curves vary in the exact location of their inflection points—that is, the point where the curve switches from accelerating to saturating (Fig. A.1). The inflection point for the *P. falciparum* curve occurs at a lower gametocyte abundance than the drug-sensitive *P. chabaudi* curve; thus there is a smaller range of gametocyte numbers

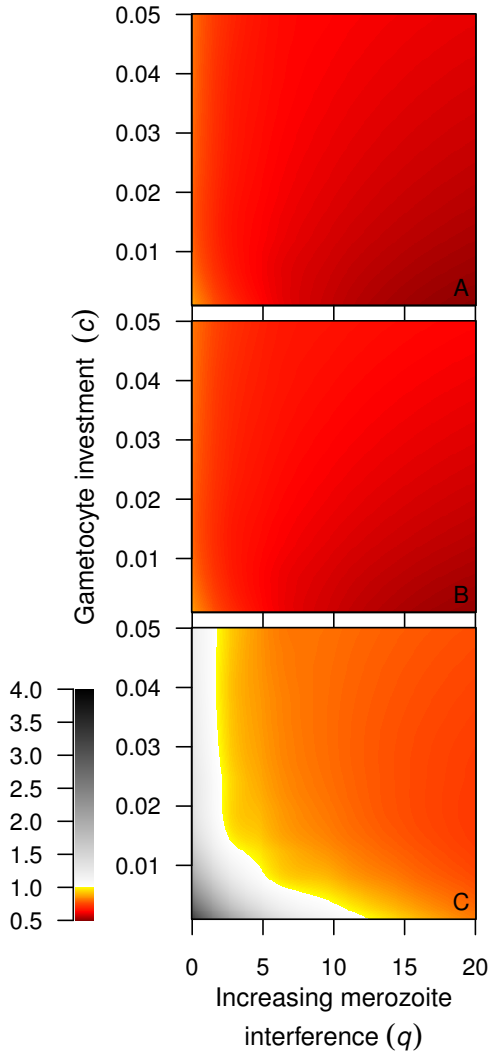

Figure 2.6. Coinfections. Smoothed relative fitness of synchronous:asynchronous strain, with increasing levels of merozoite competition and gametocyte investment. As in Fig 2.5, values greater than 1 (white areas) indicate superior transmission of the synchronous strain. Immunity is absent (A, $a = 0$), immunity acts on the total number of red blood cells infected by asexual parasites of both strains (B, $a = 150$, $b = 100$) or on merozoites of both strains (C, $a = 7200$, $b = 100$). Again, synchronous strains perform better when immunity targets short-lived parasite stage.

where transmission is an accelerating function, and the region of the parameter space where synchronous strains transmit better is accordingly reduced (compare Fig. A.4A to Fig. 2.5A). The drug-resistant *P. chabaudi* transmission curve is always saturating; thus the transmission of synchronous infections suffers and is

relatively insensitive to changes in gametocyte investment (compare Fig. A.3A to Fig. 2.5A).

Functional form of merozoite inteference. We also examine infection dynamics for parasitoid-like merozoite interference (Eqn. 2.3). We observe damped oscillations in parasite abundance—qualitatively similar to early infections of rodents, e.g., Metcalf *et al.* (2011)—for only a small range of m values (approx. $0 \leq m \leq 0.35$). Larger m values cause infection to saturate at an equilibrium with minimal oscillations. For $m = 0.05$, peak infection is substantially delayed (Fig. A.5A, B) and transmission potential is reduced for synchronous and asynchronous strains (Fig. A.5C). In contrast, hyperbolic interference (Eqn. 2.2) yields damped oscillations for a much wider range of q values with only minimal shifts in the timing of peak infection (Fig. 2.4). This form of competition increases transmission potential even while depressing gametocyte abundance (Figs. 2.4B and C). Using parasitoid-like merozoite interference therefore dramatically alters the relative fitness landscape (Fig. A.5), but there are still portions of the parameter space where synchronous strains have greater relative fitness because of merozoite inteference (Fig. A.6). As with hyperbolic interference (Fig. 2.4), parasitoid-like interference can preferentially increase the transmission potential of synchronous infections. Gametocyte production is reduced by interference (Fig. A.6B), so the improved transmission potential results from alterations to the timing of gametocyte production.

Impact of gametocyte lifespan. Synchrony was initially viewed as an adaptation to ensure that short-lived gametocytes would be present in the blood when mosquitoes were feeding (Hawking *et al.* 1968). However *P. falciparum* gametocytes are infectious for about a week in culture (Lensen *et al.* 1999) and circulate for days in hosts (reviewed in Bousema & Drakeley 2011). Thus the parasites' asexual cycle need not be precisely timed to ensure that infectious gametocytes are present when mosquitoes are feeding (e.g., Bray *et al.* 1976). Although we do not assume any particular vector feeding behavior, lengthening the infectious period of gametocytes could still change the advantages of synchrony by damping the otherwise sharp oscillations in gametocyte density. We therefore simulate infections relaxing the assumption that gametocytes have a short infectious lifespan. When gametocytes' infectious lifespan is extended from a mean of six hours to

approximately 20 hours, the net effect is to substantially increase the parameter space where synchrony is advantageous (Fig. A.7). Individual simulations at high gametocyte investment (5%) and no merozoite interference show that lengthening gametocyte longevity has two effects: damping the extreme daily oscillations of synchronous strains and increasing gametocyte abundance (Fig. A.8A). Longer gametocyte lifespan can improve the mean transmission probability of synchronous strains by damping otherwise costly oscillations in gametocyte density late in infection (as in Fig. A.8B, 20 hour lifespan). When gametocyte lifespan is increased to 36 hours (longer than the length of the asexual cycle), mean transmission probability is similar between synchronous and asynchronous infections (Fig. A.8B).

2.5 Discussion

Synchronized reproduction increases the cost of competition for resources among offspring while simultaneously easing the burden of natural enemies and mate-finding. The optimal degree of synchronization strikes a balance between these constraints; thus synchrony may shift from beneficial to costly with changes in ecology. We apply these principles to malaria parasites to predict the fitness consequences of synchronization across different within-host environments. Modeling the malaria life cycle using our delayed differential equation framework, we find that synchronized infection cycles may help malaria parasites (1) transmit efficiently by ensuring successful mate-finding in the mosquito midgut; (2) overwhelm host defenses; and (3) avoid over-exploiting host resources. Notably, these properties are sometimes but not always advantageous. The first two situations are analogous to the evolution of synchronized reproduction in plants, which is most likely for wind-pollinated species—that is, species at low risk of overwhelming their means of dispersing sexual stages—and for species contending with predators capable of being satiated (Kelly & Sork 2002). The present modeling framework builds on previous theory for malaria dynamics (e.g., Kwiatkowski & Nowak 1991, Hoshen *et al.* 2000) to provide a more comprehensive explanation of diverse temporal behavior.

2.5.1 Model assumptions

Malaria life history is enormously complicated, and we make simplifying assumptions—most notably a fixed life cycle length—to illustrate the key fitness consequences of synchrony. The fixed delay framework allows us to compare transmission from synchronous versus asynchronous infections by varying only the initial age-structure of the parasites. Synchrony breaks down if the simulation is run long enough due to the variability in life cycle length added by modest differences in how long merozoites take to invade red blood cells, but this minimal variability allows strongly synchronized dynamics to be maintained over the 20 days simulated so that we can compare the costs and benefits of synchrony early in infection. Whether a fixed life cycle length is a good approximation of within-host dynamics remains an open question. There is some evidence for within-strain variation in the life cycle length *in vitro* in that some strains maintain synchrony much more readily than others (Reilly *et al.* 2007), but that variability could be lost as host circadian rhythms constrict the timing of parasite development. Detailed data on the loss of synchrony in *in vivo* infections may justify the use of distributed delay models (e.g., Lloyd 2001) that can account for within-strain variability in life cycle length and explore how selection may act on that variability.

2.5.2 Synchrony as an adaptation to improve transmission

Past theory suggested that synchrony should carry a transmission advantage by ensuring that gametocytes will be mature when mosquito vectors are most active (Hawking *et al.* 1968, Hawking 1970). Synchrony has since been discounted as an adaptation to improve transmission by this mechanism, because daily peaks in gametocyte density and infectivity do not align with peak mosquito activity times (Bray *et al.* 1976, Githeko *et al.* 1993, Magesa *et al.* 2000). It has also been argued that since *P. falciparum* gametocytes maintain their infectiousness for weeks (Smalley & Sinden 1977), there is no need to produce gametocytes on a circadian schedule (Bray *et al.* 1976). With such a long lifespan, mature gametocytes will be present when mosquitoes are biting, regardless of what time of day red blood cells are infected.

Independent of any circadian rhythm in mosquito feeding behavior, Jensen's

inequality suggests that oscillations in gametocyte numbers will improve transmission, even if the period of those oscillations is several days. The present model shows a 24-hour periodicity in transmissibility due to the length of the blood-stage life cycle in *P. chabaudi*, but the periodicity need not be on that time scale for other malaria species. Since *P. falciparum* has an asexual life cycle lasting approximately 48 hours (Garnham 1966), any periodicity in transmission should be on that time scale (Gautret *et al.* 2001). Two-day oscillations could still substantially improve transmission over the long infectious periods sustained by human malaria parasites, where strains can persist for weeks in coinfections (Daubersies *et al.* 1996) or hundreds of days in single infections (Miller *et al.* 1994). Any periodicity in transmission success would be most easily detected where infectivity is an accelerating function of gametocyte density, such that small changes in gametocyte numbers translate into large changes in infectivity to mosquitoes.

Human infections often contain extremely small numbers of gametocytes (reviewed in Bousema & Drakeley 2011), suggesting that synchronized dynamics could frequently enhance transmission. Minimal investment in gametocytes may be selected for if large numbers of gametocytes increase mosquito mortality or trigger transmission-blocking immunity (Taylor & Read 1997). Low transmission investment may also be favored when strains find themselves in competition with other strains, as has been predicted by theory (McKenzie & Bossert 1998, Mideo & Day 2008) and shown for rodent malaria infections (Pollitt *et al.* 2011b). Modest gametocyte investment may often be selected for, and synchronous dynamics along with it.

Even at low gametocyte densities, periodic changes in infectivity may begin to disappear if gametocytes persist for a long time. Discrete oscillations in gametocyte numbers would then blur together as the infection progressed, making it difficult to tell synchronous from asynchronous gametocyte dynamics. Nevertheless, synchronized fluctuations could still benefit strains early in infection, and, incidentally, that is when gametocyte populations are small and finding mates in the mosquito midgut presents the greatest challenge. Synchrony may become costly later on, when gametocyte populations have grown large enough to render periodic fluctuations costly (Fig. 2.1), but simulations suggest that long gametocyte persistence may help by smoothing away the oscillations later in infection (Fig. A.7). Fur-

ther, any transmission benefits garnered by synchronous strains early on could be amplified by superior survival against saturating immune measures, which should be most severe for the small parasite numbers present early in infection (Metcalf *et al.* 2011). Whether synchrony can be maintained through chronic infection—and whether the fitness advantages carry over—will depend on the functional form and target of immune clearance.

2.5.3 Merozoite interference and virulence

Synchronized dynamics have the potential to improve transmission, but may also limit the exploitation of host resources and hence the virulence of infection. Theory has suggested that synchronous infections should cause less severe anemia than asynchronous infections as periodic spikes above the host's detection threshold trigger a more effective immune response (McQueen & McKenzie 2008). The present model also shows that synchronous infections result in less severe anemia, but without making any assumptions about the immune response. The reduced anemia of synchronous infections emerges as a consequence of interference among merozoites as they compete for red blood cells. Consistent with this idea, synchronous infections are frequently encounted in asymptomatic children (Färnert *et al.* 1997, Bruce *et al.* 2000b) and less frequently encountered in symptomatic or fatal cases (Touré-Ndouo *et al.* 2009 and Dobaño *et al.* 2007, respectively). Among symptomatic individuals, there are some indications that asynchronous infections are associated with more severe symptoms (Touré-Ndouo *et al.* 2009), a trend that warrants further examination. While a correlation is all that can be assessed from human infections, rodent malaria systems could be used to test whether synchronous growth limits virulence by synchronizing parasites in the initial inoculum as has been done in previous experiments (Deharo *et al.* 1994, Deharo *et al.* 1996).

Asynchronous parasites are less susceptible to interference among merozoites, simply by virtue of their dynamics, and can exploit red blood cell populations to a greater degree. More intense host exploitation leads to a sharper drop-off in parasite numbers that synchronous parasites are able to avoid. Synchrony may then represent a prudent or risk-averse way of utilizing host resources. Surprisingly, we find that interference among merozoites can improve transmission potential, but

that result depends critically on the functional form of competition, and further *in vitro* work is needed to elucidate the underlying biology. The present model suggests that any benefits of interference competition for synchronous parasites disappear in the presence of an asynchronous competitor. As the asynchronous strain severely depletes the red blood cell population, the synchronous strain bears the cost of overexploitation without receiving any of the benefits. In more diverse infections, there is a greater chance that a synchronized strain would suffer from competition with a less synchronized strain. Correspondingly, asynchronous infections of humans are likely to be more diverse than synchronous ones (Touré-Ndouo *et al.* 2009). If synchronization is fixed, the model simulations suggest that synchronous parasites would often be outcompeted when coinfection is frequent. If synchrony is instead a facultative response, selection should tend to favor parasites that de-synchronize in response to competitors. However, both reproductive restraint and relatedness could mitigate the predicted costs of synchrony in coinfections. Selection may act to reduce gametocyte investment when parasites have to compete with other strains (Pollitt *et al.* 2011b), driving dynamics into a parameter space favorable to synchrony. Though multiple strain infections are extremely common, recent data from *P. falciparum*-infected patients shows much higher relatedness than expected (Nkhoma *et al.* 2012), meaning that synchronous parasites might often share their hosts with parasites that exhibit similar temporal dynamics.

2.5.4 Synchrony as a means of overwhelming natural enemies

Even in the absence of benefits to transmission and host exploitation, theory suggests that synchrony may arise due to the nature of host defenses (Kwiatkowski & Nowak 1991). Theory so far has focused on synchronous infections faced with host defenses that intensify with density (such as fever), but our model shows that saturating immunity could selectively benefit synchronous parasites in the same way that predator satiation favors synchronized reproduction in free-living organisms (Ims 1990, Williams *et al.* 1993, Kelly & Sork 2002). It has been speculated that synchronization might allow merozoites to overwhelm immune measures (Hoshen

et al. 2000), and we use simulations to expand on that idea. The model suggests that saturating immunity should benefit synchronous strains only when the target of defenses is a transient stage, for example either short-lived merozoites or late-stage schizonts. Thus immunity against brief portions of the parasite life cycle could select for synchronous strains. Recent experiments show that components of the human immune system may behave in a way that should maximize the benefit of synchrony: *P. falciparum* merozoites are cleared by $\gamma\delta$ T cells—while intracellular life-stages are relatively protected—and merozoite clearance declines with increasing numbers of parasites per $\gamma\delta$ T cells (Costa *et al.* 2011). Malaria parasites may therefore have a lengthy, relatively protected life stage followed by a transient, vulnerable stage, analogous to the life cycle of the periodical cicadas. In this way, synchrony may be a strategy to overwhelm natural enemies.

2.5.5 Synchrony and drug treatment

Plasmodium falciparum infections exhibit both synchronous and asynchronous dynamics (e.g., Färnert *et al.* 1997, Simpson *et al.* 2002), and these diverse temporal dynamics may correspond to critically different patterns of drug susceptibility. A variety of anti-malarials, including the front-line drug artemisinin, disrupt particular portions of the life cycle, while leaving other stages relatively unscathed (e.g., ter Kuile *et al.* 1993). With a short half-life (reviewed in Meshnick *et al.* 1996), artemisinin will be largely metabolized by the time drug-insensitive life stages have matured into drug-sensitive ones, making it fundamentally different from other drugs in its ability to select for particular temporal dynamics in malaria parasites. If artemisinin were administered at the wrong time, a synchronous infection might not be cleared effectively, hence the advocacy for monitoring the synchronization of infections and treating accordingly (chronotherapy, Landau *et al.* 1991, White *et al.* 1992, ter Kuile *et al.* 1993). If the timing of drug administration varies greatly from person to person and clinic to clinic, asynchronous parasites may fare better on average, since there are likely to be life stages able to survive drugs no matter what time of day the anti-malarial is administered. Asynchronous growth could therefore function as a form of non-classical resistance. Predicting the evolutionary consequences of intervention requires putting the synchronization and timing of the

malaria life cycle into the context of host and parasite fitness (outlined in Mideo *et al.* 2013b). Efforts to disrupt disease transmission may incidentally shift the balance to favor or disfavor synchrony, with the potential to select for within-host dynamics inherently more devastating to human health.

2.5.6 Broader implications

Using a set of models, we have studied the costs and benefits of synchrony in the within-host dynamics of malaria. Our conclusions are broadly similar to those used to explain synchrony in free-living organisms (e.g., Kelly & Sork 2002, Rees *et al.* 2002): synchrony is favored when competition is limited, when mate-finding is difficult at low abundance, and when top-down controls can be saturated. However, we show that the fitness associated with synchrony versus asynchrony is a surprisingly complex function of the dynamics within the vertebrate host as well as nonlinearities in vector transmission. Relatively small changes in interference competition among asexual stages, frequency of coinfections and allocation to sexual versus asexual reproduction can shift a synchronous parasites from having a robust fitness advantage to a severe disadvantage. The interplay between these density-dependent relationships could explain the range of synchronization patterns observed both within and among malaria species. The case study of malaria further suggests that the transmission biology of the system could generate strong selection for or against synchrony, with synchrony unlikely to evolve where parasites are close to saturating their means of transmission. For instance, if lengthy blood meals allow efficient transmission of small numbers of parasites to vectors, then we might expect the probability of transmission to rapidly saturate with increasing parasite abundance, favoring asynchronous dynamics. The question remains whether similar factors can shed light on the enormous variation in developmental synchrony across diverse parasites.

2.6 Acknowledgements

I thank L. Beck-Johnson and W.A. Nelson for their assistance with delay-differential equation techniques, S. Huijben for helpful discussion, and N. Mideo and F. Ellis

McKenzie for invaluable comments on earlier drafts of this manuscript.

2.7 Notes

This chapter is published in *The American Naturalist* (Greischar *et al.*, 2014), with Andrew F. Read and Ottar N. Bjørnstad as co-authors.

Chapter 3

Characterizing malaria dynamics in vitro: developmental plasticity and interference

3.1 Abstract

Malaria infections exhibit surprisingly complex dynamics *in vitro*, and analysis of those dynamics can be used to make inferences about key life history traits. Cultures that begin with tightly synchronized development—culminating in discrete bursts of population expansion—subside into asynchronous dynamics, with parasites distributed evenly throughout developmental stages. This loss of synchrony suggests intra-strain variation in developmental rates, and the fact that different strains lose synchrony at different rates suggests that strains may vary in their distribution of developmental rates. As synchrony decays, the competition among parasites at similar developmental stages may likewise fade, but the functional form of that interference still needs to be characterized. We develop a mechanistic model of *in vitro* growth and show that conventional methods yield biased estimates of life cycle duration and may hence be incapable of assessing within-strain variation in developmental rates. We fit the model to detailed time series data to distinguish between two ways of describing interference competition for red blood cells, while simultaneously inferring the life cycle length and variability in developmental rates.

We find that strains are likely to differ in their life cycle duration, as well as the range of variability in developmental rates. Interference competition is more likely to vary according to the ratio of parasites to red blood cells, rather than taking a form analogous to that used in host-parasitoid models. We use *in vitro* assays and develop an image processing algorithm to count red blood cells, finding no evidence that parasites are less likely to invade red blood cells as parasite numbers increase. We instead find greater numbers of excess invasions—parasites invading red blood cells that have already been infected—when greater numbers of parasites are present. Infected red blood cells have been reported to produce a characteristic number of new parasites, and while that number varies with strain, there is no evidence that multiply-infected red blood cells produce a greater number of new parasites. We therefore conclude that the cost of interference is likely to appear as parasites waste their efforts invading cells that have already been infected.

3.2 Introduction

Malaria infections can be highly synchronized, with periodic spikes in parasitemia as waves of parasites burst out of red blood cells and trigger a new cycle of infection (e.g., Kitchen, 1949; Färnert *et al.*, 1997). These synchronized dynamics are lost when parasites are cultivated *in vitro* (Trager & Jensen, 1976), but can be artificially-induced by removing parasites of a certain age through chemical or mechanical means (e.g., Lambros & Vanderberg, 1979; Mata-Cantero *et al.*, 2014). Cultured parasites cannot maintain synchrony without intervention, but they lose synchrony at strain-specific rates (Reilly *et al.*, 2007). Therefore, whatever host factors may be acting to enforce synchronized dynamics, different parasite strains likely vary in their response. Theory suggests that highly synchronized populations should experience more intense competition, since parasites will be competing for the same resources at the same time (Greischar *et al.*, 2014). In order to understand and manipulate parasite dynamics *in vivo*, we need to characterize the competitive interactions that regulate parasite abundance: during which life stages is competition most intense and how does the distribution of life stages change through time? *In vitro* cultures provide a unique opportunity to observe parasite dynamics in the absence of host influence, and the resulting decay in synchrony can help us

identify the fundamental processes that regulate malaria infections.

Though the human malaria *Plasmodium falciparum* is typically said to require 48 hours to develop and replicate within red blood cells (Kitchen 1949; Garnham 1966, reviewed in Mideo *et al.* 2013b), cultured strains exhibit different cycle lengths—ranging from 43 to 51 hours on average—and that variation is largely heritable (Reilly Ayala *et al.*, 2010). In addition to inter-strain variation, we expect variability within a strain because if life cycle length were fixed, parasites would be expected to maintain synchrony through time (Hoshen *et al.*, 2000; Greischar *et al.*, 2014). The decay of synchrony *in vitro* suggests instead that there is variation in the time required for parasites to progress through the asexual life cycle, in addition to inter-strain differences in developmental rates. Artificial synchronization leaves only parasites in a subset of developmental stages, but variation in the rate of development will subsequently increase the diversity of parasite life stages. Critically, greater developmental plasticity should lead to more rapid loss of synchrony, and a more rapid increase in the diversity of parasite life stages present at any one time. It should therefore be possible to characterize parasites' developmental heterogeneity by tracking the diversity of parasite life stages through time following artificial synchronization, using the type of data that are collected to measure life cycle length in different malaria strains (e.g., Deharo *et al.*, 1994, 1996; Reilly *et al.*, 2007; Reilly Ayala *et al.*, 2010).

Yet the distribution of malaria life stages also varies depending on whether the population is expanding or contracting (Khoury *et al.*, 2014). The intrinsic growth rate of the parasite population will interact with variability in developmental rates to influence parasite dynamics. Classic models of disease spread can be modified to include realistic variation in latent periods (e.g., Wearing *et al.*, 2005; Feng *et al.*, 2007), analogous to the period of time a red blood cell is infected before parasites burst. The classic assumption that hosts become infectious at a constant rate—an exponential distribution of waiting times—generates far too much variation in incubation periods, leading to systematic underestimates of the rate of spread along with other unrealistic dynamics (Wearing *et al.*, 2005). Applied to the case of malaria infection within the host, exponentially-distributed developmental periods would mean that parasites could replicate at any time, with a proportion of parasites completing development immediately after invasion (Saul,

1998; Crooks, 2008). Incorporating realistic individual variation into simple compartmental models has dramatically improved our ability to predict disease spread (Wearing *et al.*, 2005), explain time series data on disease incidence (Lavine *et al.*, 2011), and—for malaria infections—describe the progression through the life cycle in a biologically-sensible way (Gravenor & Lloyd, 1998).

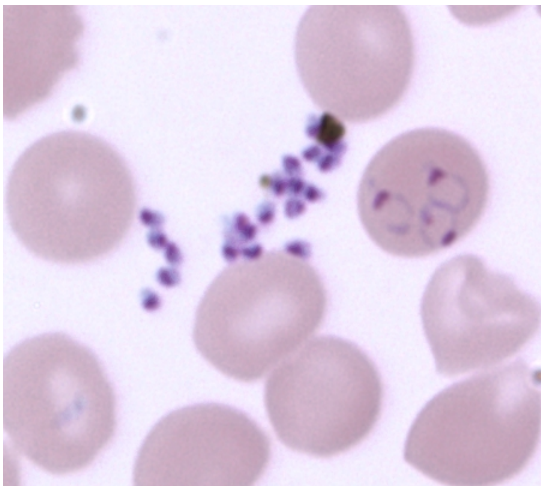

Figure 3.1. *P. falciparum* parasites (called "merozoites", purple dots) that have failed to invade a red blood cell (pink circles), along with three parasites that have invaded successfully but clustered within the same red blood cell (right). The three successful invaders have developed into the so-called ring stage forms. These parasites are in the Dd2 strain.

Distinct from the impact of developmental rates, competition for resources will strongly influence dynamics. Even in culture, not all parasites that burst out of red blood cells will find another red blood cell to infect (Fig. 3.1). *In vitro* assays suggest that red blood invasive parasites (merozoites) have only minutes to infect a red blood cell before losing viability, and that as merozoites become more abundant, their success rate declines (Boyle *et al.*, 2010). Other experiments also indicate that merozoite success declines with increasing parasite abundance (Reilly *et al.*, 2007). Similarly, analysis of rodent infections suggests that early parasite population growth saturates as the initial inoculum size increases (Metcalf *et al.*, 2011). These intra-stage competitive interactions are likely to interact with variability in life cycle length, with competitive interactions potentially becoming less important as synchrony decays: in a poorly synchronized infection, competition for red blood cells may be weaker since only a subset of the parasite population

will be capable of invading (Greischar *et al.*, 2014). The rate of successful invasion varies with the starting densities of parasites and red blood cells, so that percentage data of the sort commonly reported (percent parasitemia, percent parasites in a particular life stage, e.g., Deharo *et al.*, 1994, 1996; Chimanuka *et al.*, 1997; Reilly *et al.*, 2007; Reilly Ayala *et al.*, 2010; Allen & Kirk, 2010) may be inadequate to reconstruct infection dynamics without data on the total number of red blood cells.

Interference is common among consumers, including parasitoid-host and predator-prey systems. By analyzing rates of prey-consumption, it is often possible to rule out the null hypothesis that no interference is occurring and the per capita rate of success saturates with host numbers (Holling Type II functional response, Skalski & Gilliam, 2001). This null hypothesis may not be appropriate for malaria parasites *in vitro*—at least for the starting conditions that have been tested so far—because the per merozoite rate of successful invasion increases with red blood cell abundance, even when red blood cells are not limiting (Boyle *et al.*, 2010). The mechanism responsible has not yet been identified, making it difficult to determine the appropriate formation of that density-dependent competition. Previous theory described two candidate forms of interference, each giving dramatically different infection dynamics (Greischar *et al.*, 2014). The extreme differences in dynamics suggest that it may be possible to distinguish between different forms of density-dependence through analysis of time series data.

It is also unclear when in the life cycle interference occurs, whether it be at the point of invasion, or as multiple parasites attempt to develop within a single red blood cell, or both. Successful parasite invasion is typically defined as the rate at which uninfected red blood cells are invaded (e.g., Boyle *et al.*, 2010), but researchers have also examined the rate at which parasites invade any red blood cell, infected or not, and found differences between strains (Reilly *et al.*, 2007). The timing of such intra-stage competition is likely to be important for predicting how external forces such as the immune system or antimalarial drugs can most efficiently control parasite numbers, analogous to the efficiency of natural enemies in controlling insect pest populations (Bjørnstad *et al.*, 2001).

Even in the relatively simple environment of artificial culture, the interplay between competition for resources and variability in developmental rates may alter dynamics in unexpected ways. To tease apart these processes, we model malaria

dynamics in culture, incorporating interference competition for red blood cells along with gamma-distributed variability in life cycle duration. Initial model simulations show that standard methods of assessing the life cycle length can confound cycle duration, developmental synchrony and invasion rates. To characterize differences in these parasite life history traits, we fit two candidate functional forms described previously (Greischar *et al.*, 2014) to detailed time series data for three strains, identifying which form of density-dependence, cycle length, and distribution of developmental rates best fit the data. We then perform *in vitro* assays on two of those strains to identify which points in the parasite life cycle are subject to interference: the invasion process itself, development within a red blood cell, or both.

3.3 Methods

3.3.1 Distributed-delay model framework

We model the asexual, blood-stage life cycle of *P. falciparum* parasites, tracking numbers of uninfected red blood cells along with parasite life stages. The model framework mirrors *in vitro* experiments (Reilly *et al.* 2007) in which infected red blood cells are added to a pool of unparasitized red blood cells and no new cells are added once the experiment begins, at least until parasitemia increases enough to put the population in danger of crashing. The model could be modified to incorporate subsequent additions of red blood cells, but since we lack data on the timing and size of red blood cell additions, we instead focus on the simpler dynamics that occur prior to any additions of red blood cells. Thus, uninfected red blood cells (R) are subject to a low background mortality rate ($\mu = 1/120$ days, Koury & Ponka 2004) or infection by red blood cell-invasive merozoites (M) at a rate $x(t)$:

$$\frac{dR(t)}{dt} = -\mu R(t) - x(t)R(t)M(t) \tag{3.1}$$

where $x(t)$ is the merozoite invasion rate, which may decline as conditions become more crowded. Since the mechanism of merozoite interference is unknown, we consider two candidate functional forms described previously (Greischar *et al.*, 2014). Interference reduces invasion success as the ratio of merozoites to uninfected

red blood cells increases (Boyle *et al.*, 2010), so we first consider a functional form in which invasion success declines hyperbolically with the ratio of merozoites to red blood cells:

$$p(t) = \frac{p_{max}}{1 + q(M(t)/R(t))}. \tag{3.2}$$

Alternatively, interference could take a form analogous to the saturating responses used in host-parasitoid models (Hassell, 2000):

$$z(t) = \frac{p_{max}}{(M(t) + 1)^m}. \tag{3.3}$$

Previous simulations used Eqns. 3.2 and 3.3 in a fixed delay model of rodent malaria infections, finding surprisingly different dynamics between the two functional forms (Greischar *et al.*, 2014). Therefore it is important to distinguish which functional form is more likely based on time series data.

Upon infection, a red blood cell will progress through infection. At the end of the parasites' developmental period (α days on average), a surviving red blood cell will burst open to release merozoites. We assume that the waiting times from invasion until bursting are Gamma-distributed with an integer shape parameter n (i.e., an Erlang distribution). Constraining n to be a positive integer allows the infected red blood cell class to be modeled as n ordinary differential equations, each with an exponential distribution of waiting times. With a single infected compartment ($n = 1$), the waiting time until bursting would be exponentially-distributed, leading to rapid desynchronization of development. As n increases, the distribution of waiting times becomes narrow, limiting the variance around the mean, and leading to more sustained developmental synchrony. The coefficient of variation in life cycle length decreases as n increases according to $1/\sqrt{n}$.

We split the developmental period between the immature stages (rings and trophozoites, $I(t)$) and parasites in the mature schizont stage ($S(t)$). Thus we assume it takes an average of α_1 days for invaded red blood cells to mature into schizonts, and another α_2 days on average for those schizonts to burst and release merozoites. The resulting chained ordinary differential equation model for early and late development takes the form:

Immature forms

(rings and trophozoites)

$$\frac{dI_1(t)}{dt} = x(t)R(t)M(t) - \mu I_1(t) - \frac{n_1}{\alpha_1}I_1(t) \tag{3.4}$$

$$\frac{dI_2(t)}{dt} = \frac{n_1}{\alpha_1}I_1(t) - \mu I_2(t) - \frac{n_1}{\alpha_1}I_2(t) \tag{3.5}$$

$$\vdots \quad \vdots$$

$$\frac{dI_{n_1}(t)}{dt} = \frac{n_1}{\alpha_1}I_{n_1-1}(t) - \mu I_{n_1}(t) - \frac{n_1}{\alpha_1}I_{n_1}(t) \tag{3.6}$$

Schizonts

$$\frac{dS_1(t)}{dt} = \frac{n_1}{\alpha_1}I_{n_1}(t) - \mu S_1(t) - \frac{n_2}{\alpha_2}S_1(t) \tag{3.7}$$

$$\frac{dS_2(t)}{dt} = \frac{n_2}{\alpha_2}S_1(t) - \mu S_2(t) - \frac{n_2}{\alpha_2}S_2(t) \tag{3.8}$$

$$\vdots \quad \vdots$$

$$\frac{dS_{n_2}(t)}{dt} = \frac{n_2}{\alpha_2}S_{n_2-1}(t) - \mu S_{n_2}(t) - \frac{n_2}{\alpha_2}S_{n_2}(t) \tag{3.9}$$

where $n = n_1 + n_2$. We constrain $n_1/\alpha_1 = n_2/\alpha_2$ so that the transitions through compartments will occur at the same rate regardless of the life stage (immature or schizont), thereby constraining the immature and schizont stages to have the same variance to mean ratio. We make this simplifying assumption since we are interested in the cycle length and the distribution of developmental rates over the full length of the intraerythrocytic cycle. The split between immature and schizont classes allows comparisons with commonly gathered experimental data.

Schizonts that survive through the n_2 compartments are assumed to burst to release β merozoites according to:

$$\frac{dM(t)}{dt} = \beta\frac{n_2}{\alpha_2}S_{n_2}(t) - \mu_z M(t) - x(t)R(t)M(t) \tag{3.10}$$

We assume that merozoites die at rate μ_z, corresponding to an exponential half-life of five minutes (in line with *in vitro* assays, Boyle *et al.*, 2010). We do not explicitly model multiply-invaded red blood cells. While multiple infections are

common, especially in static cultures (Allen & Kirk, 2010), there is no evidence that these multiply-infected red blood cells would have dynamics different from what we describe in Eqns. 3.4-3.10. Previous *in vitro* experiments counted the number of merozoites within mature segmenting schizonts, finding a unimodal distribution (Fig. B.4 reproduced in the supplement Reilly *et al.*, 2007). If a twice-invaded cell burst to release twice the number of merozoites, we would expect a bimodal distribution, which would necessitate a more complex model than the one presented here. However, the unimodal distribution of burst sizes suggest three possibilities: (1) multiply-infected red blood cells are inviable, producing no merozoites, and those failures can be absorbed by the interference function; (2) each parasite in a multiply-infected red blood cell produces a fraction of the usual number of merozoites (for example, two parasites each producing half the usual number of merozoites); (3) within a multiply-invaded red blood cell, only one parasite successfully produces the usual number of merozoites, while the others fail to develop. All three possibilities can be described with the current model framework.

3.3.2 Model fitting

We fit the distributed delay model to detailed time series data taken from cultures kept in 5mL flasks at 5% hematocrit. Red blood cell counts are not typically made prior to setting up experiments; rather the stock is assumed to be at 50% hematocrit and diluted down to the appropriate hematocrit (5%). A previous study estimated red blood cell counts from human volunteers, finding 4.84×10^6 and 4.64×10^6 red blood cells per mL in two control groups, with hematocrits of 42.9% and 41.9%, respectively (Gonzalez-Alonso *et al.*, 2006). Averaging those estimates, we obtain 2.37 million red blood cells in the culture flask. Since the starting number of red blood cells is likely to influence the fits, we also re-fit the model for one strain assuming a larger number of red blood cells (an estimated 5×10^9 red blood cells per mL used in a clinical trial, Etablissement Français du Sang, 2012), which would yield a starting abundance of 2.5 billion red blood cells. A synchronized inoculum of parasites was introduced at 0.5% parasitemia. Parasite cultures were synchronized three times via sorbitol, which kills off mature stages

leaving mainly rings (Lambros & Vanderberg, 1979), and allowed to progress to the schizont stage before inoculating them into cultures with washed red blood cells and culture medium (details of solution in Reilly *et al.*, 2007). Synchronization was not perfect, but the initial distribution of parasite life stages was observed from a blood smear, which we use as the initial conditions for the model. We assume no red blood cells are added after the start of the experiment, and truncate the time series before red blood cells would have been added. Researchers usually aim to keep the parasitemia from exceeding 5%, so red blood cell additions can be detected by noting when the parasitemia exceeds 5% and is reduced by half or more at the following time point (L. B. Turnbull, *pers. comm*).

The model was fit to data for three strains: Dd2 (a single replicate), HB3, and 3D7 (both with three replicates), with stage distribution and parasitemia calculated from blood smears at approximately eight hour intervals. We converted this data to times series of percentage of sample in the schizont stage, and percentage of the sample in the pre-schizont stages (i.e., rings and trophozoites). We used the Nelder-Mead algorithm (Lagarias *et al.*, 1998) to cycle through candidate parameter values for the shape parameter (n), the cycle length (α, where $\alpha = \alpha_1 + \alpha_2$), the proportion of the life stage spent in the schizont stage (used to calculate n_1, n_2, α_1 and α_2), the maximum invasion rate (p_{max}), and the interference coefficient (either q or m depending on the functional form of interference). The burst size (β) was specified as 17.52 and 14.83 for Dd2 and HB3 (Reilly *et al.*, 2007), and 15 for 3D7. We tried fits for both functional forms of interference (Eqns. 3.2-3.3) to locate the functional form and parameter values that would give the best fit according to weighted least squares (wls) criterion as appropriate for binomial data with a large but unknown denominator:

$$wls = \sum_{i=1}^{k} \frac{(I_{p,i} - \hat{I_{p,i}})^2}{\hat{I_{p,i}}(1 - \hat{I_{p,i}})} + \sum_{i=1}^{k} \frac{(S_{p,i} - \hat{S_{p,i}})^2}{\hat{S_{p,i}}(1 - \hat{S_{p,i}})} \tag{3.11}$$

for k observations where I_p and S_p are observed percentages of pre-schizont and schizont stage parasites (that is, the percentage of the entire sample, not the percentage of parasites), and $\hat{I}_p$ and $\hat{S}_p$ are the model-predicted values. The residuals are weighted by the variance of expected from a binomial distribution so that poor model fits at intermediate percentages—when the population variance would be

large—are less costly than poor fits at low percentages. We constrained the fit to only consider α values between one day and three days, and constrained candidate n values to vary between two (because one compartment is needed for pre-schizont and schizont dynamics) and 1000 (see Discussion). The invasion parameters, p_{max}, q and m, were constrained to be positive, and the proportion of the life cycle spent in the schizont stage was constrained to vary between zero and one. Model fits were performed USING the `optim` function in **R** (R Project for Statistical Computing, http://r-project.org/). Each strain was fit separately, but multiple replicates were fit simultaneously to increase the chances of being able to distinguish between different forms of density-dependent interference.

3.3.3 Invasion assays: experimental setup & analysis of blood smear images

We set up assays to follow a cohort of mature schizonts through bursting and reinvasion, for two of the three strains examined with detailed time series (Dd2 and HB3). Rather than recording only the number of red blood cells invaded, we also tracked how many parasites successfully invaded, so that we could assess whether interference occurs during invasion, post-invasion, or both. Detailed methods can be found in (Reilly *et al.*, 2007), but briefly, cultures were sorbitol synchronized and subsequently magnet synchronized to get a highly purified solution of schizonts estimated to represent a 10 hour-morphological window (L. B. Turnbull, *pers. comm.*). These schizonts were combined with washed red blood cells and culture medium to obtain a 1% parasitemia at 5% hematocrit. This 1% solution was then diluted to obtain 3mL cultures at four target parasitemias (still maintaining 5% hematocrit): 0.25%, 0.125%, 0.025%, and 0.0125%, with three replicates in for each concentration. To allow comparisons with previous invasion assays (Reilly *et al.*, 2007), we did not shake the cultures. The cultures were left in the incubator until they were expected to have burst, reinvaded, and formed into easily-identifiable ring-stage parasites. At that point, a monolayer of red blood cells was smeared over five slides for each replicate. The blood smears were fixed with methanol and stained with Giemsa (as described previously, Reilly *et al.*, 2007). Uninfected red blood cells and infected red blood cells were counted, with infected red blood cells

classified as rings, trophozoites, schizonts, representing the early, middle, and late stages of intra-erythrocytic development, respectively. Although rare under these artificial culture conditions, we occasionally observed transmission stages (gametocytes). Rings would be the result of successful invasion, while trophozoites and schizonts would represent bystanders, parasites that escaped synchronization and so did not burst on time to infect further red blood cells. Gametocytes were also classified as bystanders, because they take more than a week to develop (Lensen *et al.*, 1999). For multiply infected red blood cells, we counted the number of parasites that successfully invaded. These counts were either made on the microscope or from images of slides.

For slide images, at least 25 fields were captured for 0.25% starting concentration, at least 100 fields for 0.125% and 0.025% concentrations, and 200 fields for 0.0125% concentration. While an attempt was made to capture fields containing a moderate number of red blood cells in a monolayer and no artifacts (such as sediment from the Giemsa staining), fields were captured without bias to the infection status of the recorded cells. Given the large number of fields to sort, we developed a macro in ImageJ (Rasband, 2013) to automate red blood cell counts. While parasite counts were still performed by visual assessment of images, the automated red blood cell counts are especially useful when parasitemias are low, since most images are devoid of parasites and a large number of fields must be counted to obtain a reliable count. Further, this method of image processing allowed the images to be randomized prior to scoring (as was done for the HB3 images), and to track counts for individual fields, which were subsequently used to bootstrap confidence intervals for each replicate. The code for the macro can be found in Appendix B.2.

We compare two measures of invasion success: number of parasites invading successfully, and the excess invasions: the number of parasites invading already infected red blood cells. The counts for each replicate span a different number of red blood cells, so we make comparisons by calculating the expected number of schizonts present given the number of cells observed. The expected number of schizonts would be the ratio of schizonts to uninfected red blood cells from the initial dilutions multiplied by the number of red blood cells sampled. However, some of the sampled red blood cells contained bystanders (i.e., trophozoites, schizonts or gametocytes) that would not have participated in the wave of bursting

and invasion, but merely occupied red blood cells that would otherwise have been available for invasion. We therefore calculate the expected number of schizonts as the initial ratio of schizonts ($S(0)$) to uninfected red blood cells ($R(0)$) times the number of uninfected red blood cells that would have been available to parasites at the time of bursting, i.e., the sampled cells (j) minus bystander parasites (b):

$$E[S(t)] = \frac{S(0)}{R(0)}(j - b) \tag{3.12}$$

For each field, we calculated the expected schizonts, the number of merozoites that had invaded a red blood cell (whether that cell was already infected or not), and the number of merozoites that invaded a cell that was already infected. Since we had counts for each field, we subsampled the matrix of data for each replicate 5000 times to obtain bootstrapped 95% confidence intervals (`boot` package in **R**).

3.4 Results

3.4.1 Stage percentage data biases the estimated cycle length

Initial model simulations indicated that the apparent cycle length did not match up with the cycle length specified in the parameter values (α). The discrepancy highlights a bias in the way cycle length is typically estimated, as the period of time between peaks in the percentage of parasites in a particular life stage (e.g., Deharo *et al.*, 1994, 1996; Reilly *et al.*, 2007; Reilly Ayala *et al.*, 2010; O'Donnell *et al.*, 2011). Depending on whether the infection is growing or declining, the percentage of parasites in the schizont stage may under- or over-estimate the true cycle length (Fig. 3.2). The bias is exacerbated at higher intrinsic growth rates, and less pronounced—though not absent—when the variability in developmental rates is minimal (Fig. 3.3).

Greater variation in cycle length generates wide peaks in immature stage abundance, delaying the peak percentage of schizonts when infection is declining, or hastening the peak when infection is growing. Using only the percentage of parasites in the schizont stage ignores larger patterns of growth and decline in parasite numbers, and in each case, the peak abundance of schizont stage parasites yields a

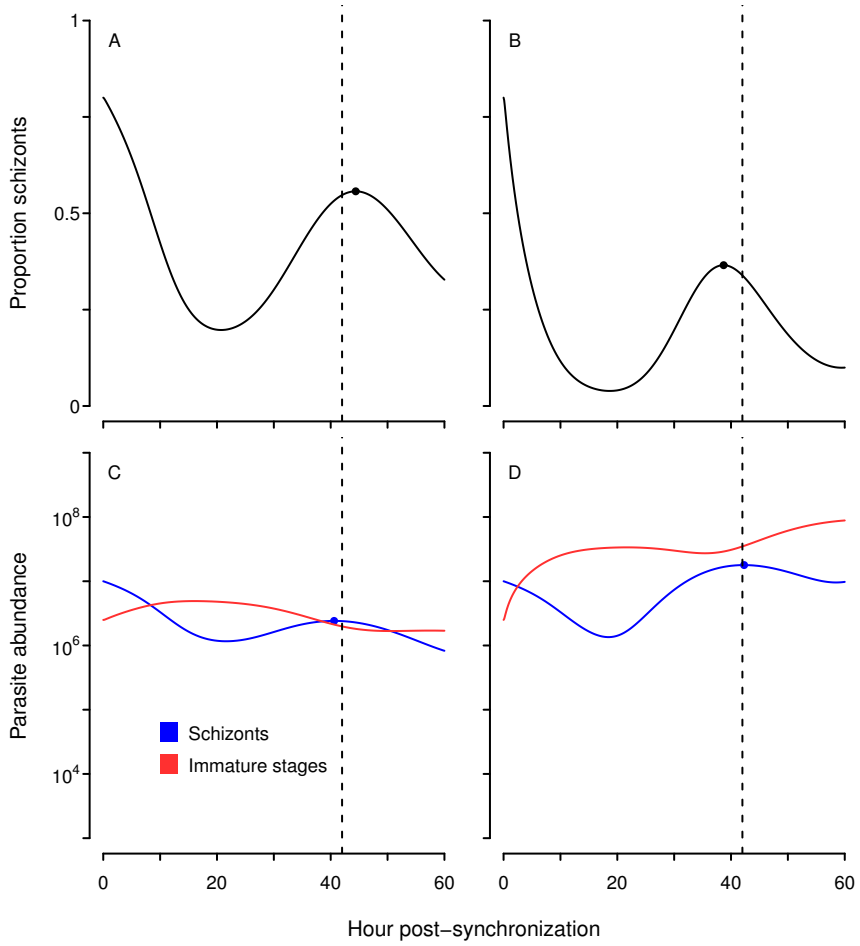

Figure 3.2. The period between peaks in the percentage of parasites in the mature schizont stage gives a biased estimate of the real cycle length, depending on whether the infection is declining (A,C) or growing (B,D). Simulations were run assuming hyperbolic interference ($q = 10$), a burst size of 16, and large variability in cycle length ($n = 30$, $CV = 0.18$). In each case, the true cycle length was set at 42 hours (dashed vertical line). In the left panels (A,C), the maximum invasion rate was set to 2×10^{-9}, while in the right panels, the maximum invasion rate was 2×10^{-8}, leading to growth.

more accurate estimate of cycle length. Unsurprisingly, simulations also show that quantifying the abundance of a short-lived life stage will yield better estimates of cycle length. In the simulations, progressing through the immature stages takes more than two-thirds of the life cycle on average (Fig. 3.2). The length of the life cycle could be estimated as the period between two peaks in the abundance of parasites in a particular life stage, but the long duration of immature stages generates plateaus rather than peaks in abundance. Without clear peaks, it is difficult to

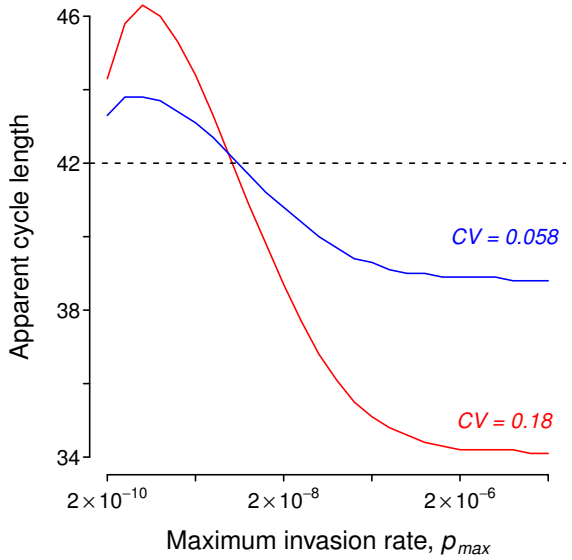

Figure 3.3. The maximum invasion rate can bias the apparent length of the life cycle, as estimated by the proportion of parasites in the schizont stage. The true cycle length (42 hours) is indicated by a dashed black line, while the red curve refers to simulations run with a high degree of developmental plasticity ($n = 30$) and the blue curve to simulations with little variability in life cycle length ($n = 300$). Other parameters as in Fig. 3.2.

decide which two points should be compared to arrive at an estimate of life cycle duration.

The proportion of parasites in the schizont stage undergoes damped oscillations through time as synchrony is lost (Fig. 3.2A,B). However, in the simulations shown, the variability in cycle length was kept the same, as were the initial conditions, so that the only difference was in the maximum invasion rate. In both scenarios, the proportion of parasites in the schizont stage was highest initially and rose to a shorter peak roughly one life cycle length later, with that peak being even shorter for a growing population because of the disproportionate increase in immature stages (Fig. 3.2B, C). If these simulated populations were sampled at 42 hours, for example, and the percentage of parasites in the schizont stage recorded, it might be concluded that the populations differ in the degree of synchronization, with the population in Fig. 3.2A being more highly synchronized because it has a greater proportion of parasites in a narrow morphological window. The model demonstrates that such apparent differences in synchrony could instead be caused

by expansion versus contraction of the parasite population.

3.4.2 Model fits to detailed time series data

Fitting the model to time series data for three *P. falciparum* strains, we find that hyperbolic interference (Eq. 3.2) yields the best fit overall (Fig. 3.4). When we re-ran the optimization for Dd2 assuming high starting numbers of red blood cells, we obtained better fits over all, but the hyperbolic form of interference still gave a better fit than parasitoid-like interference (Fig. B.5). Interestingly, the algorithm selected a much longer cycle length for Dd2 (52 hours, Table 3.1) than has been previously reported (44.1 hours, Reilly *et al.*, 2007). We plot the percentage of schizonts found in the present time series against two replicates of Dd2 from a previous experiment using similar methods (H. B. Reilly Ayala, *pers. comm*) for comparison.

Table 3.1. Fit parameters

Interference	Strain	CV	Cycle length	Schizont stage	Weighted least square error
Hyperbolic	Dd2	0.131	52.1 hours	15.7 hours	0.0731
Parasitoid	Dd2	0.302	72* hours	21.1 hours	0.147
Hyperbolic	HB3	0.302	72* hours	23.8 hours	0.297
Parasitoid	HB3	0.302	72* hours	27.0 hours	0.297
Hyperbolic	3D7	0.0579	53.4 hours	14.1 hours	0.0793
Parasitoid	3D7	0.289	57.3 hours	21.6 hours	0.165

*maximum allowable cycle length

The model also fit well to 3D7, again with hyperbolic interference giving a better fit, but both forms of interference converged on the same poor fit for HB3,

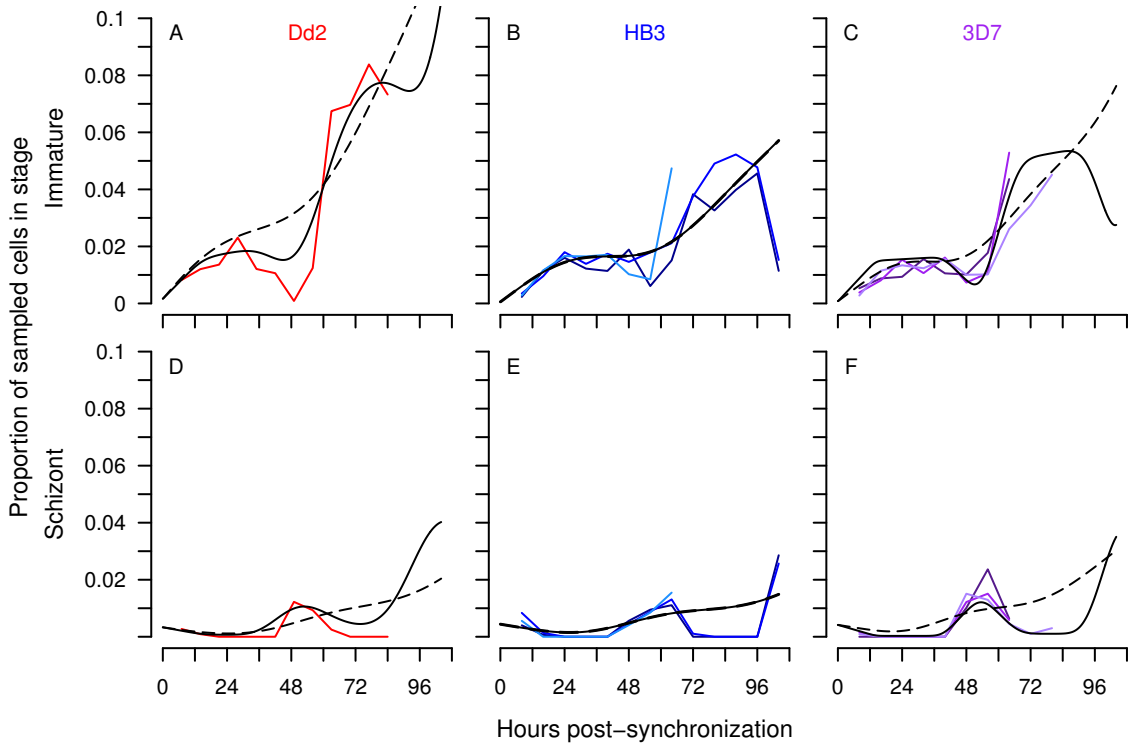

Figure 3.4. Model fits assuming hyperbolic interference (black solid curve, Eq. 3.2) or parasitoid-like interference (black broken curve, Eq. 3.3), with data is shown in colored lines. The black curves for each strain indicate a single best model fit to both the proportion of sampled red blood cells in the immature parasite stages (A-C) and in the schizont stage (D-F). Weighted least squares errors corresponding to each fit can be found in Table 3.1, along with the coefficient of variation in cycle length, cycle duration, and schizont stage length. The associated invasion parameters are listed in Table B.1.

with unrealistically long cycle lengths and large coefficients of variation in life cycle length, which has previously been characterized as having a life cycle closer to 50 hours and the capability to maintain a higher degree of synchrony than Dd2 (Reilly *et al.*, 2007). Again we can see differences in the dynamics comparing the present data to those collected previously (Fig. B.7).

3.4.3 Invasion assays: interference

We find no evidence that interference occurs as merozoites are invading red blood cells, which would appear as a nonlinear relationship between the number of successful invasions as the expected number of schizonts increases. Instead, the num-

ber of successful invasions increases approximately linearly with the expected number of schizonts (Fig. 3.5). With HB3 invasion success, the points fall below what would be expected from minimum burst sizes and 100% invasion success, but pattern is what would be expected given the short lifespan of merozoites. More surprising is the high invasion success of Dd2 merozoites. Given that some merozoites failed to invade (e.g., Fig. 3.1), the large number of invasion events suggests that Dd2 may have a larger burst size than has been previously appreciated, at least under certain conditions.

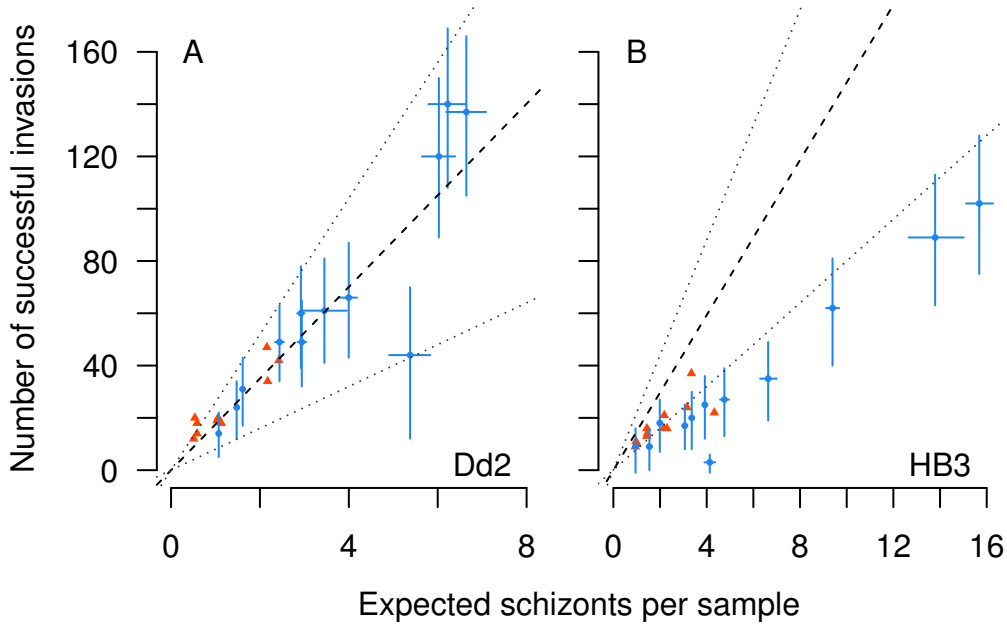

Figure 3.5. The number of merozoites successfully invading red blood cells as a function of the expected number of schizonts in the initial sample according to Eqn. 3.12 for Dd2 (A) and HB3 (B). Each blue dot represents a single replicate, with the blue lines indicated 95% confidence intervals obtained by bootstrapping the counts for individual fields. The dashed black line represents the expected number of invasions if each schizont contained the mean number of merozoites and each merozoite invaded, with dotted lines indicating the expectation if every schizont contained the maximum versus minimum number of merozoites reported (Reilly *et al.*, 2007). The orange triangles indicate counts done on a subset of the replicates by microscopy; thus these are not independent data points but are included here to allow comparison between estimates obtained from automated red blood cell counts and those derived from standard microscopy.

In contrast, we can see that many more merozoites are wasted—invading cells that have already been invaded—as the expected number of schizonts increases

(Fig. 3.6). As would be expected from the larger burst size of Dd2, the number of excess invasions increases much more rapidly as the expected number of schizonts increases, compared with HB3. Therefore the merozoite-wastage is dependent on starting parasite abundance, and we can see that for Dd2 the wastage becomes substantial at a lower schizont abundance than for HB3. Dd2 wastes a full schizont when the expected number of schizonts reaches approximately four, while HB3 shows no significant wastage until the expected number of schizonts nears seven.

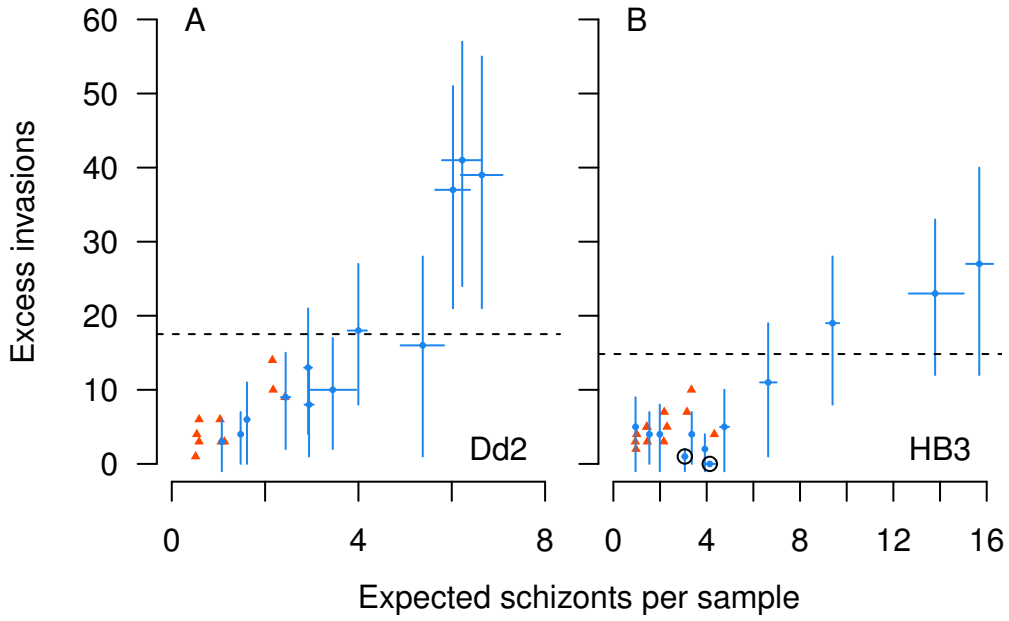

Figure 3.6. The excess number of merozoites invading (that is, the number of merozoites invading already-occupied red blood cells) as a function of the expected number of schizonts in the initial sample according to Eqn. 3.12 for Dd2 (A) and HB3 (B). Each blue dot represents a single replicate, with the blue lines indicated 95% confidence intervals obtained by bootstrapping the counts for individual fields. Two samples had too few invasions to construct reliable confidence intervals (B, black circles). As before, the orange triangles indicate counts done on a subset of the replicates by microscopy for comparison, and are not independent data points. The dashed line refers to the mean burst size for each strain.

3.5 Discussion

The dynamics of malaria parasites *in vitro* can inform our understanding of variability within and across strains, forming a basis for predicting how parasites will respond to the selective pressures. The length of the intraerythrocytic cycle and density-dependence in the rate of red blood cell invasion prove surprisingly difficult to quantify, for all that they are very basic aspects of malaria biology. A major part of the problem is that the stage distribution data commonly gathered (i.e., what fraction of parasites are in a particular life stage) tell only part of the story. We use a mechanistic model to show that whether an infection is growing or declining can give the appearance of differences in life cycle length and the degree of synchronization. We fit the model to time series for three strains to distinguish between different forms of interference competition, while providing estimates of life cycle length and the variability in developmental rates. To identify where in the life cycle competition is likely to occur, we performed invasion assays on two of the three strains, which suggest that the cost of interference likely manifests when parasite invasion is wasted on red blood cells that have already been infected.

Characterizing host-parasite interactions—especially the interplay between infection and host circadian rhythms (reviewed in Mideo *et al.*, 2013b)—requires accurate estimates of parasite life cycle length. The length of the erythrocytic cycle is typically calculated as the period between the peak percentages of a particular life stage (Deharo *et al.*, 1994, 1996; Reilly *et al.*, 2007; Reilly Ayala *et al.*, 2010; O'Donnell *et al.*, 2011). Though measuring mature schizont abundance might be ideal, mature stages often sequester in the capillaries, making it difficult to accurately assess cycle length from *in vivo* infections (MacPherson *et al.* 1985). The model results suggest that estimates of intraerythrocytic cycle length obtained using the percentage of a particular life stage may over- or under-estimate the true cycle length depending on whether the infection is growing or declining. The magnitude of the error is likely to increase with variation in developmental rate. Past work has estimated the life cycle length of two murine malaria strains, *P. yoelii* and *P. berghei*, finding cycle lengths shorter than 24 hours as estimated by stage percentage (Deharo *et al.*, 1994, 1996). For both strains, the parasites show little synchrony *in vivo*, and had to be artificially-synchronized prior to inoculation,

meaning that errors in estimating life cycle length could be substantial. Further, in at least one of the studies (Deharo *et al.*, 1994) and presumably the other (Deharo *et al.*, 1996), the infection was growing while sampling was taking place. Model simulations suggest that stage percentage data taken as the infection is expanding may underestimate the true life cycle length, so that the surprisingly short life cycle lengths reported (18 hours for *P. yoelii* and 21 hours for *P. berghei*, Deharo *et al.*, 1994, 1996, respectively) could actually be closer to the 24 hour life cycle reported for the highly-synchronized murine species *P. chabaudi* (O'Donnell *et al.*, 2011). Unfortunately, these issues spill over into the *in vitro* case, where strains are typically growing as cycle length is being assessed (Reilly *et al.*, 2007; Reilly Ayala *et al.*, 2010). These estimates of life cycle length may therefore tend to underestimate the true life cycle length, with the magnitude of the error varying with the intrinsic growth rate (Fig. 3.3). This bias could explain the observed negative correlation between cycle length and invasion efficiency (Reilly, 2007). Invasion efficiency is itself heritable (Reilly, 2007), that could further complicate efforts to quantify heritability in life cycle length.

This bias makes it difficult to compare previously reported cycle lengths to the values estimated by fitting the present model. Since Dd2 grows quickly, conventional methods are likely to underestimate the true cycle length, and that may be part of the reason the the best fit cycle length for Dd2 (52 hours) falls outside the range reported previously (39-48 hours, Reilly *et al.*, 2007). Aside from the bias introduced by intrinsic growth rates, the error in cycle length is likely to be increased for strains with greater heterogeneity in developmental rates (Fig. 3.3). Dd2 may have more variability in developmental rates than HB3, since it loses synchrony faster (Reilly *et al.*, 2007), and the cycle length estimates may therefore be more error prone. Unfortunately, we cannot get a good sense of the variation in developmental rates from the single replicate for which data was available. Comparing to a previous data set, for which only stage distribution data were available (H. B. Reilly Ayala, *pers. comm.*), we note clear differences in the time series themselves (Fig. B.6), suggesting that methodological differences might be partly responsible for the long estimated life cycle length for Dd2. For the other strains, HB3 and 3D7, data were taken for multiple replicates, which can give us a sense for the natural variation in the dynamics. We fit the model to all replicates simultaneously so

as to give the best chance of distinguishing between different forms of interference, but the model could also be fit to each replicate independently, yielding three different estimates of cycle lengths and developmental plasticity, and allowing us to make comparisons across strains and experiments.

The model suggests that stage distribution data give a similarly biased estimate of the degree of synchronization (Fig. 3.2). While changes in the distribution of parasite life stages might be expected to correlate with changes in the degree of synchronization (e.g., Deharo *et al.*, 1996), these simulations show that such changes could instead be merely the byproduct of population growth. In particular, the model suggests that, during periods of growth, the population of parasites is likely to be biased towards immature stages, as has been found in rodents infected with a poorly synchronized malaria strain (*P. berghei*, Khoury *et al.*, 2014). This bias makes estimates of synchrony challenging to interpret, even in the relatively well-controlled environment of artificial culture. Synchrony has been reported to decay more quickly when parasites are cultivated in static versus shaken cultures, since maturing parasites are more likely to experience different nutrient microenvironments in static culture and hence develop at rates that are more variable (Allen & Kirk, 2010). However, Allen & Kirk (2010) also report that shaking cultures great enhances the intrinsic growth rate of the population, consistent with their observation that fewer merozoites are wasted in multiple infections of red blood cells when cultures are shaken. Synchrony was assessed by observing the number of mature stage parasites appearing on alternate days, when only early stage parasites (rings) would be expected in a synchronous population. The shaken cultures appeared more synchronized because they had fewer mature stages compared with the slower-growing static cultures. While the logic is sound—that static cultures would promote variation in developmental rates—we would expect to see fewer mature stages present simply because the population expanding, and from the data it is not clear whether shaking cultures actually facilitates the maintenance of synchrony. Even more difficult to interpret are studies of human infections that rely on the stage distribution from a single time point (e.g., Touré-Ndouo *et al.*, 2009), so that we cannot assess whether parasite populations are growing or declining.

Quantifying how synchrony changes through time is challenging, with robust

methods still being developed and tested (Bjørnstad *et al., in revision*). The complex methods required to accurately quantify synchrony in simulated populations again suggest that the simpler approaches used to quantify synchrony in malaria parasites (e.g., using stage-distribution data, Deharo *et al.*, 1996) may be inadequate. In addition to the problem of accounting for the intrinsic growth rate of a population, the length of each morphological life stage is likely to be important. The ring stage of development lasts nearly half the life cycle in *P. falciparum* (Reilly *et al.*, 2007), so for example, finding all parasites in the ring stage would not give much information about the level of synchrony, while the percentage of parasites in a morphologically narrow window can provide better information. It can also be seen that the progression of the life stages should be incorporated into synchrony calculations. If parasites are evenly split between two adjacent life stages, that would represent a higher degree of synchrony that if parasites were divided between two life stages separated by a series of developmental steps. Therefore methods using only stage distribution data, without incorporating knowledge of the life cycle or parasite growth rates, are likely to give a skewed picture of the pattern of synchronization.

These issues highlight the problems associated with trying to quantify a portion of dynamics, such as cycle length or synchrony, in isolation. By fitting a mechanistic model to data, we can begin to tease apart how different processes contribute to the observed dynamics. One limitation of this approach is that distributed delay models can be computationally intensive (Crooks, 2008), and in the present case, the fitting algorithm was inclined to try larger and larger numbers of compartments for marginal gains in the weighted least squares error. We addressed this problem by constraining the number of compartments, so that the coefficient of variation in life cycle length could not be below a minimum value. As more time series data become available, it may be possible to clarify some the uncertainties that remain with respect to life cycle length, and to set reasonable bounds on the variability in developmental rates. Observing more replicates would be useful, as would observing the cultures for longer periods, provided detailed notes were kept on when and how many red blood cells were added to keep the culture from crashing. Still, the present work demonstrates that it is possible to tease apart complex processes—for example, obtaining estimated life cycle lengths while accounting for

the intrinsic growth of a population—by fitting a mechanistic model to time series data.

The growth rate of the population is itself complicated by the fact that the success of individual parasites is likely to be density dependent (Reilly *et al.*, 2007; Boyle *et al.*, 2010). A previous model showed that different forms of density-dependence interference among parasites could generate very different dynamics (Greischar *et al.*, 2014), so we used the present model to determine what form of density-dependence could best explain detailed time series data. In the two cases where good model fits were identified (for strains Dd2 and 3D7), the hyperbolic form of interference (Eqn. 3.2) gave a better fit as well as more reasonable estimates of cycle length and developmental plasticity (Table 3.1). This form of interference has the interesting property that it can damp extreme oscillations in parasite numbers—in effect keeping parasites from overexploiting resources and crashing—a characteristic that could have adaptive significance particularly for highly synchronized populations of parasites (Greischar *et al.*, 2014).

We also make use of *in vitro* assays to identify when in the life cycle interference is likely to take place: as parasites compete to infect red blood cells, during development within multiply-infected red blood cells, or both. These invasion assays were initialized with very low parasitemias, and it was necessary to observe a large sample of red blood cells to obtain a robust estimate of invasion success. Developing an image-processing algorithm that enabled us to sample a greater portion of the culture that would have been feasible with traditional microscopy counts. Capturing images was labor-intensive, but subsequent red blood cell counts could be done quickly, and with freely available software. The image processing algorithm also stores information about each field, and in combination with manual counts of parasite stages, we were able to use the variation across fields for each replicate to calculate 95% confidence intervals for each axis, which is not practical for counts done via microscopy. Critically, data points gathered using automated red blood cell counts gave qualitatively similar estimates as those obtained through traditional microscopy (blue dots versus orange triangles, Fig. 3.5).

Previous work reported invasion rates calculated from the percentage of red blood cells infected (Boyle *et al.*, 2010), implicitly assuming that parasites invading already-occupied cells are wasted. We find that per merozoite invasion success

is an approximately linear function of the number of schizonts present (Fig. 3.5), with no evidence that merozoites are less likely to invade at relatively high densities. However, the number of merozoites invading already-occupied red blood cells does increase with the initial number of schizonts. Taken together, there is no evidence that merozoites are more or less likely to invade cells that have already been infected, in accordance with previous observations of human infections (Simpson *et al.*, 1999). Previous work suggested that Dd2 invades at a high rate than HB3 regardless of whether multiply-infected red blood cells are counted as one invasion event or multiple invasions (Reilly *et al.*, 2007). We see the same qualitative pattern, and note that Dd2 accrues excess invasions much more rapidly than HB3 for the same starting number of schizonts (Fig. 3.6). The simplest explanation is that Dd2 has a larger burst size than HB3 (Reilly *et al.*, 2007), but the reported difference is not sufficient to explain fully explain the pattern: Dd2 would be expected to waste a full schizont's worth of merozoites on red blood cells that are already infected when only four schizonts are present in the initial sample, whereas HB3 does not waste a full schizont's worth of merozoites until seven or more schizonts are present. In light of the unusually high invasion success of Dd2 merozoites (Fig. 3.5), we cannot rule out that Dd2 has a much higher burst size than has been observed previously, and that could serve to explain why Dd2 experiences more severe merozoite wastage.

An alternative explanation would be that Dd2 is only able to infect a subset of the red blood cell population compared with HB3, and therefore tends to exhibit a greater number of multiple invasions, a phenomenon termed "selectivity" (Simpson *et al.*, 1999). A pattern consistent with "selective" parasites has been observed in human infections, where more multiply-infected cells were seen would be expected from a Poisson process, particularly when parasitemia was low (Simpson *et al.*, 1999). While we cannot rule out the possibility that Dd2 and HB3 infect different subpopulations of red blood cells, we find the opposite pattern to that reported by Simpson *et al.* (1999): that the number of multiply infected red blood cells increases when more schizonts are present initially (Fig. 3.6). Sampling *P. falciparum* infections in humans is complicated by the fact that mature parasite stages sequester out of circulation, behavior that means parasitemia may be a poor indicator of parasite biomass (reviewed in Cunnington *et al.*, 2013). Artificial cul-

ture avoids these sampling problems, potentially explaining why we see a different pattern.

We find that interference is likely to occur during the lengthy period when parasites are developing inside red blood cells rather than the transient period of invasion, so that the host has a long time window in which to intensify competition among parasites. One of the most important sources of parasite removal is the spleen, which acts as a filter to remove infected red blood cells based on their loss of surface area compared with uninfected red blood cells (Safeukui *et al.*, 2008, 2013). Although the spleen preferentially removes red blood cells containing mature parasites—the ostensible reason for parasite sequestration (reviewed in Cunnington *et al.*, 2013)—it also removes substantial numbers of immature ring-stage parasites (Safeukui *et al.*, 2008). Since multiply-invaded red blood cells would be expected to lose more surface area compared to singly-infected ones, the spleen has the potential to greatly intensify interference among parasites before they have a chance to sequester.

Since competitive interactions occur between individuals in a particular life stage, control measures—such as antimalarial drugs or immune defenses—could exacerbate or mitigate competition depending on which life stage is targeted. For example, removing merozoites could reduce the numbers of multiply-infected red blood cells, with negligible minimal reductions in parasite growth rates. Thus while there are immune components that target merozoites (including $\gamma\delta$ T cells, Costa *et al.*, 2011), there is no evidence from rodent malaria infections that merozoite clearance is associated with control of peak parasite numbers (Miller *et al.*, 2010). In contrast, by targeting misshapen red blood cells, the spleen would be expected to act synergistically with whatever interference occurs within red blood cells. Analogous issues have been identified in the control of an insect pest: a parasitoid has been found to reduce the adult abundance of an insect pest by targeting life-stages after major competitive interactions have occurred, while a virus does not exert effective control because it acts too early, removing individuals before they can engage in competition (Bjørnstad *et al.*, 2001). Antimalarial drugs also target certain parasite life stages (Geary *et al.*, 1989; ter Kuile *et al.*, 1993; Delves *et al.*, 2012), and timing drug treatment so as to maximize the effects of parasite competition could be important, especially with less aggressive drug therapy. Such

low-dose treatments have been suggested as a potential solution to the problem of minimizing selection pressure for drug resistance while maintaining host health (Read & Huijben, 2009; Huijben *et al.*, 2010a, 2011, 2013).

Finally, given the stage-specific action of antimalarial drugs, effective treatment requires good timing so that the majority of parasites are in a vulnerable life stage. Antimalarial drugs therefore represent a selective pressure not unlike that of artificial synchronization in culture. Accurately assessing the efficacy of drug treatment in patients requires knowledge of the synchronization of infection (White *et al.*, 1992), but the degree of synchronization is likely to be a complex function of the cycle length, developmental plasticity, and the underlying competitive interactions. The present model suggests that considering any of these factors independently is likely to give a skewed perspective of infection dynamics and the intra- and inter-strain variation in key traits. By considering these factors collectively, the model has the potential to characterize life history variation in cultured parasite strains. Although that variation is only a small fraction of the diversity present in natural infections, it can serve to elucidate what infection dynamics are parasite-driven, giving us a basis for understanding the complex interactions within the host.

3.6 Acknowledgements

I thank Dave Kennedy and Lauren Cator for helpful discussion, and Jennie Lavine for assistance with distributed-delay techniques.

3.7 Notes

This work was done in collaboration with Linsdsey B. Turnbull, Nestor Agbayani, Heather B. Reilly Ayala, Michael T. Ferdig, Ottar N. Bjørnstad, and Andrew F. Read, who will be co-authors when the manuscript is submitted for publication. In particular, Nestor Agbayani collected the time series data on Dd2, HB3, and 3D7, and I made use of data collected by Heather B. Reilly Ayala to develop a preliminary version of the distributed delay model. Lindsey B. Turnbull and I collaborated on the invasion assays: she took the lead on running the invasion assays, and provided the microscopy reads of the slides for the orange data points

shown in Figures 3.5 and 3.6. I captured images of blood smears, developed the Image J algorithm, recorded parasite counts from images, and ran the analysis.

Chapter 4

Predicting optimal transmission investment in malaria parasites

4.1 Abstract

Malaria parasites face a tradeoff between in-host replication and the production of transmission stages that can be passed onto mosquitoes, analogous to growth-reproduction tradeoffs in multicellular organisms. We use a fixed delay model to identify the optimal strategy for investing in transmission during acute infection. By allowing the level of investment to vary dynamically through time and maximizing the cumulative transmission potential, we show that plastic strategies can substantially out-perform fixed transmission investment. We find that host defenses, brief infections, and coinfecting malaria strains can select for in-host replication at the expense of transmission investment, especially early in infection. By competing time-varying investment strategies in coinfections, we show that coinfecting parasites might be expected to converge on a single optimal transmission investment strategy, because—in addition to potent competition—coinfecting strains also represent a source of mates. While we focus on tradeoffs in malaria life history, the approach for identifying optimal dynamic investing strategies is broadly applicable.

4.2 Introduction

Tradeoffs between reproduction and growth are ubiquitous, with tension arising between immediate fitness gains and potentially greater fitness gains in the uncertain future (e.g., Bell, 1980). The optimal balance depends on available resources and the probability of survival (reviewed in Clutton-Brock, 1984), density-dependent feedbacks and environmental variability (Metcalf *et al.*, 2008), and—for organisms capable of reproducing more than once—the reproductive effort expended previously (Charlesworth & Leon, 1976). Whenever successful reproduction requires finding a mate, good strategies may also require matching the timing of reproductive effort to that of conspecifics (i.e., reproductive synchrony, reviewed in Kelly & Sork, 2002). While the dilemma is often phrased in terms of macroorganisms (e.g., Bell, 1980; Clutton-Brock, 1984), malaria parasites provide a clear example of these conflicting selection pressures as they attempt to balance within-host replication and transmission to new hosts (reviewed in Taylor & Read, 1997). Parasites can serve as model systems for understanding the tradeoff between growth and reproduction (Reece *et al.*, 2009), and the theoretical approaches developed to identify optimal strategies in the complex landscape of infection could have applications well beyond malaria.

The fitness consequences of transmission investment emerge from malaria's complex life cycle: success within the vertebrate host depends strictly on replication (i.e., cycles of infection among red blood cells), but transmission to mosquitoes and new hosts requires sexual transmission stages. These gametocytes cannot invade red blood cells but instead differentiate into gametes upon ingestion by a mosquito, where successful fertilization is necessary to infect the vector (reviewed in Bousema & Drakeley, 2011). Upon infecting a red blood cell, a parasite can give rise to one gametocyte (either a male or female) or several asexual parasites capable of infecting new red blood cells (e.g., 4-10 in the murine *Plasmodium chabaudi*, 8-32 in the human malaria *P. falciparum*, Landau & Boulard, 1978; Garnham, 1966, respectively). The optimal balance between opposing selection pressures should change through time, and malaria parasites are predicted to vary their reproductive investment—denoted the "conversion rate"—in response to changing environmental conditions (Reece *et al.*, 2009; Pollitt *et al.*, 2011a; Carter *et al.*,

2013). In other organisms, reproductive investment has been shown to change with the probability of survival (Velando *et al.*, 2006) and the presence of competitors (Borg *et al.*, 2012). By analogy, malaria parasites would be expected to condition their level of reproductive investment based on the host immune response and the length of infection, as well as the presence of coinfecting parasites (Reece *et al.*, 2009).

Within the vertebrate host, success depends on parasite numbers, which can change by several orders of magnitude over the course of infection (Miller *et al.*, 1994). In-host replication is more rapid when larger numbers of parasites are inoculated (Timms *et al.*, 2001; Metcalf *et al.*, 2011), a pattern thought to be indicative of immune measures that—while efficient at removing small numbers of parasites—saturate as parasite numbers increase (Metcalf *et al.*, 2011). Since reproductive investment should limit within-host growth (Mideo & Day, 2008), gametocyte production should be especially costly early in infection, reducing parasite growth at a critical point and leaving parasites vulnerable to immune clearance. In contrast, when infection is drawing to a close, reproductive investment should increase (Pollitt *et al.*, 2011a), in analogy to the terminal investment predicted for animals near the end of life (reviewed in Clutton-Brock, 1984).

The addition of a competing strain can dramatically alter infection dynamics (e.g., Taylor *et al.*, 1997a,b, 1998; de Roode *et al.*, 2005; Wargo *et al.*, 2007). Models consistently predict that a coinfecting strain should select for reduced reproductive investment, because gametocyte production slows replication and allows the other strain to get a larger share of host resources either through direct competition (Mideo & Day, 2008) or apparent competition (i.e., mediated by the immune system, McKenzie & Bossert, 1998). Subsequent experimental infections of mice confirmed that malaria strains facultatively reduce their transmission investment in coinfections (Pollitt *et al.*, 2011b). Yet selection on reproductive investment is further complicated because coinfecting strains are not just competitors, but also potential mates, as evidenced by the observation that malaria parasites modify their sex ratios to take advantage of opportunities for outcrossing (Reece *et al.*, 2008).

Onward transmission to mosquitoes depends on whether a male and female gamete can find each other and complete fertilization within the mosquito gut

(reviewed in Bousema & Drakeley, 2011). When gametocytes are rare, a blood meal is unlikely to contain both a male and female gametocyte (mate-finding Allee effect in ecological parlance, Courchamp *et al.*, 2008). Modest increases in gametocyte numbers should then lead to disproportionate gains in transmission success, a pattern seen in human and rodent malarias (Huijben *et al.*, 2010a; Bell *et al.*, 2012, respectively). In contrast, when large numbers of gametocytes are present, the probability of infecting mosquitoes saturates, presumably because nearly all blood meals contain a sufficient number of gametocytes (Paul *et al.*, 2007; Huijben *et al.*, 2010a; Bell *et al.*, 2012). Thus increasing reproductive investment when few gametocytes are present may substantially increase the probability of onward transmission (and hence parasite fitness), while increasing investment when gametocytes are abundant yields diminishing returns.

Reproductive investment is possible throughout the lifespan of an infection, meaning that gametocytes can be produced and transmitted during the initial (acute) phase (Bell *et al.*, 2012) as well as from chronic infections with nearly-undetectable densities of parasites (Schneider *et al.*, 2007). Theory has been developed to understand optimal investment from chronic infections when reproductive effort trades off with survival (Pollitt *et al.*, 2011a), but further theory is needed to identify optimal strategies for early infection, when reproductive investment comes at the expense of in-host replication. The first peak in parasite numbers tends to be the largest (e.g., Miller *et al.*, 1994) and corresponds to the steepest drop in red blood cell numbers and host biomass (Huijben *et al.*, 2010a). Gametocytes produced during the acute phase can infect a large fraction of mosquitoes (Bell *et al.*, 2012), and the ability of parasites to survive long enough to cause chronic infections depends in part on the reproductive investment decisions made early in infection. Modifying reproductive investment during acute infection may therefore be expected to have a disproportionate impact on parasite fitness and host health.

Malaria parasites' strategies can evolve, because the selection imposed by culturing parasites can reduce or eliminate gametocyte production (reviewed in Bousema & Drakeley, 2011). The challenge is to determine how parasites should respond to conflicting selection pressures, and we model acute malaria infection to examine the factors that promote versus restrain transmission investment. Using a simulation-based approach, we compare optimal fixed and time-varying strate-

gies for reproductive investment. We consider the impact of infections of different length, immune defenses, and a competing malaria strain. Simulations suggest that parasites should often be able to enhance their overall transmission by delaying reproductive investment and by investing more heavily late in an infection. To explore the evolutionary response to competition, we compete flexible time-varying investment strategies against each other in simulated coinfections, showing that natural selection may converge on a single optimal strategy rather than diverse strategies conditioned on the competing strategy. While we focus on malaria infections, our approach could be extended to other parasite systems to identify optimal allocation strategies when selection acts on within-host success and between-host transmission (e.g., Gilchrist & Coombs, 2006) or within-population growth undermines metapopulation persistence (King *et al.*, 2009). More broadly, the approach could be used to identify the best plastic responses when life-history tradeoffs are expected to vary through time or space.

4.3 Model

We modify an existing model of infections by the rodent malaria *Plasmodium chabaudi*, allowing reproductive investment to remain constant or vary through time. The model framework was previously used to assess the fitness consequences of synchronous cycles of asexual growth in malaria parasites and so describes the sexual and asexual portions of the parasite life cycle as fixed time delays (Greischar *et al.*, 2014). In the context of reproductive investment, the model allows for realistic time lags between the decision to invest in gametocyte production, and the point at which mature gametocytes can contribute to transmission success. Parasites are implicitly assumed to have access to perfect information on when the infection will be terminated. Once optimal strategies are identified, we examine how optimal level of investment covaries with other state variables to determine what cues could serve as the best proxies for perfect information.

4.3.1 Single infections

In experimental infections, mice are typically inoculated with infected red blood cells (e.g., Reece *et al.*, 2008), which burst to release red blood cell-invasive forms called merozoites. The host replaces red blood cells lost to parasitism, but it may take a week or more for red blood cell abundance to return to initial values (e.g., Huijben *et al.*, 2010a). Merozoites are unlikely to persist very long outside of red blood cells, based on *in vitro* studies with *P. falciparum* (Boyle *et al.*, 2010). Following successful invasion, parasites may either replicate and burst open 24 hours later to release merozoites (O'Donnell *et al.*, 2011), or mature into gametocytes following a 48 hour developmental period (Gautret *et al.*, 1996). Infectious gametocytes usually persist less than a day for *P. chabaudi* (Gautret *et al.*, 1996; Reece *et al.*, 2003), and the probability of infecting mosquitoes is a sigmoidal function of gametocyte abundance according to an experimentally-derived curve for *P. chabaudi* (drug-sensitive clone, Bell *et al.*, 2012):

$$\tau(t) = \frac{\exp[-12.69 + 3.6 \log_{10} G(t)]}{1 + \exp[-12.69 + 3.6 \log_{10} G(t)]} \tag{4.1}$$

where $G(t)$ is the abundance of mature gametocytes. The mate-finding difficulties thought to be experienced by small numbers of gametocytes are implicit in the way τ accelerates when G increases from scarcity. The cumulative transmission potential at time ϵ would then be

$$f(\epsilon) = \int_0^{\epsilon} \tau(t) dt \tag{4.2}$$

The gametocyte numbers depend on the dynamics of red blood cells, asexual growth and reproductive investment, and survival through developmental periods. In the absence of infection and background mortality (μ), red blood cells (R) maintain stable numbers at a homeostatic equilibrium (K). When depleted, red blood cells are replenished in a logistic fashion, with realized replenishment rate approaching the maximum (λ) as red blood cell numbers move further from equilibrium:

$$\frac{dR}{dt} = \lambda \left(1 - \frac{R(t)}{K}\right) - \mu R(t) - pR(t)M(t) \tag{4.3}$$

where p is the rate at which merozoites (M) invade uninfected red blood cells given contact. At the point of invasion, infected red blood cells are either committed to developing into transmissible gametocytes or asexual merozoites. The proportion $c(t)$ recruited to sexual differentiation is the reproductive investment—by convention referred to as the "conversion rate" (Bruce *et al.*, 1990)—which is either left as a constant or defined as time-varying free spline (details of simulation and optimization in supplement). A proportion $1 - c(t)$ commit to asexual growth as infected red blood cells (I),

$$\begin{aligned} \frac{dI}{dt} &= (1 - c(t))pR(t)M(t) - \mu I(t) - \frac{a}{b + I(t)}I(t) \\ &\quad -(1 - c(t - \alpha))pR(t - \alpha)M(t - \alpha)S \end{aligned} \tag{4.4}$$

with infected red blood cells removed by saturating immunity at a maximum rate of a and a half-saturation constant of b. The delay between invasion and bursting is given by α (24 hours for *P. chabaudi*, Landau & Boulard, 1978), and survival through this period S is described by

$$S = \exp\left(-\int_{t-\alpha}^{t} \mu + \frac{a}{b + I(\omega)}d\omega\right) \tag{4.5}$$

The infected red blood cells that persist through the developmental period, α, will each burst to release β merozoites. Thus the overall change in the merozoite population is:

$$\frac{dM}{dt} = \beta(1 - c(t - \alpha))pR(t - \alpha)M(t - \alpha)S - \mu_z M(t) - pR(t)M(t) \tag{4.6}$$

A proportion of invaded red blood cells, $c(t)$, instead commit to sexual development in the I_G class of infected red blood cells:

$$\frac{dI_G}{dt} = c(t)pR(t)M(t) - \mu I_G(t) - (1 - c(t - \alpha_G))pR(t - \alpha_G)M(t - \alpha_G)S_G \tag{4.7}$$

where α_G represents the delay from invasion to maturation for developing game-

tocytes. Survival through this period is given by:

$$S_G = e^{-\mu\alpha_G} \tag{4.8}$$

Infected red blood cells that persist through the developmental period become mature gametocytes:

$$\frac{dG}{dt} = (1 - c(t - \alpha_G))pR(t - \alpha_G)M(t - \alpha_G)S_G - \mu_G G(t) \tag{4.9}$$

where μ_G describes the background mortality rate of gametocytes. We assume that gametocytes are not cleared by immunity, because gametocytes do not elicit a strong immune response (reviewed in Riley & Stewart, 2013). Thus, Eqn. 4.9 gives the abundance of mature gametocytes that can contribute to transmission potential as defined in Eqns. 4.1 and 4.2.

Note that Eqns. 4.5-4.6 are defined for $t > \alpha$, and Eqns. 4.7-4.9 for $t > \alpha_G$, and we must now describe the fate of initially inoculated parasites. We assume that no reproductive investment occurs until the simulation begins, or in other words, that all of the infected red blood cells inoculated at the beginning are asexual. Therefore, when $t \leq \alpha$:

$$\frac{dI}{dt} = (1 - c(t))pR(t)M(t) - \mu I(t) - \frac{a}{b + I(t)}I(t) - I_0 \text{Beta}(s_P, s_P)(t)S_0(t) \tag{4.10}$$

where I_0 is the number of parasites inoculated. The initial age structure of the population is given by a Beta distribution with shape parameter s_P; unless otherwise noted, we simulated asynchronous infections, which are initiated with parasites uniformly distributed throughout the asexual blood stages ($s_P = 1$). Survival until bursting is described by

$$S_0(t) = \exp\left(-\int_0^t \mu + \frac{a}{b + I(\omega)}d\omega\right) \tag{4.11}$$

so that the change in merozoite numbers follows

$$\frac{dM}{dt} = \beta I_0 \text{Beta}(s_P, s_P)(t)S_0(t) - \mu_z M(t) - pR(t)M(t) \tag{4.12}$$

Invaded red blood cells can be committed to sexual differentiation as soon as the simulation begins:

$$\frac{dI_G}{dt} = c(t)pR(t)M(t) - \mu I_G(t) \tag{4.13}$$

but since no developing gametocytes are inoculated, no mature gametocytes can be produced or transmission potential accrued while $t \leq \alpha_G$.

We simulate infection dynamics using the parameter values given in Table 3.1 and approximate the cumulative transmission potential (Eqn. 4.2) by summing $\tau(t)$ at each simulated time point and keeping the step size very small (0.01 days). To examine the effects of varying the duration of infection, we estimate the cumulative transmission potential for infections lasting 20, 30, 40, 45, and 50 days for a range of fixed conversion rates (i.e., constant reproductive investment). For comparison, the acute portion of infection is thought to last approximately two weeks in *P. chabaudi* (Bell *et al.*, 2006). We also examine the optimal plastic reproductive investment for 20-, 30- and 50-day infections. By comparing fixed with time-varying investment, we see when selection favors restrained versus increased reproductive investment. Singling out 20 day infections, we compare optimal reproductive investment (fixed and variable) in the face of saturating immune measures acting against infected red blood cells ($a = 150$, $b = 100$).

4.3.2 Coinfections

Coinfecting malaria strains are thought to interact via resource competition (Mideo & Day, 2008; Pollitt *et al.*, 2011b) but also have the potential to interact as mates, as suggested by recombination rates (e.g., Su *et al.* 1999; Mu *et al.* 2010, reviewed in McKenzie *et al.* 2008). Describing fitness in coinfections is therefore more complex. The probability of transmitting to a mosquito is given by Eqn. 4.1, with $G(t) = G_1(t) + G_2(t)$ where G_1 and G_2 represent the gametocyte abundance of each strain. The strain-specific fitness (f) is then defined as the probability of transmission weighted by its representation in the gametocyte pool, with $f(t)$ again summed at each time point over the course of the simulated infection:

$$f_1(t) \quad = \quad \tau(t)\frac{G_1(t)}{G_1(t) + G_2(t)} \tag{4.14}$$

$$f_2(t) = \tau(t)\frac{G_2(t)}{G_1(t)+G_2(t)} \tag{4.15}$$

These fitness functions epitomize the tension between selective forces: Each strain attempts to maximize its representation in the gametocyte pool even while benefitting from its competitor's reproductive investment in terms of overall infectivity to mosquitoes. In other words, when one strain increases its reproductive investment, the competing strain is free to reduce its investment without suffering from a lack of mates, thus reaping the benefits of 'piggy-backing' in a mate-limited world (the mosquito gut) and the benefits of enhancing competitive dominance by allocating to in-host replication. Nevertheless, the strain that has increased its gametocyte production improves its current representation in the mosquito vector, at the expense of the competing strain. The relative importance of these two fitness terms varies dynamically over the course of the infection.

We consider the simplest coinfection scenario: both strains infect the host simultaneously and with the same starting inoculum and both have identical characteristics, save for their reproductive investment. Both strains are therefore equally capable of infecting red blood cells and equally vulnerable to immune clearance. While this is an oversimplification, it allows us to examine the impact of differing levels of reproductive investment in the absence of any other differences. We simulate coinfections for 41^2 pairs of fixed conversion rates to identify the evolutionarily stable strategy (ESS) for this simple game—that is, the level of reproductive investment at which neither strain can increase their relative fitness by changing their fixed strategy.

Taking this ESS fixed strategy as a given, we find the optimal time-varying strategy in response. We then set the competitor's response to the best time-varying strategy and repeat the process. This approach is similar to a best response dynamics in that we take the competitor's strategy as a given (whether fixed or time-varying) for each optimization (Matsui, 1992), but with important differences: We find the optimal strategy assuming that the competing strategies begin at equal frequency, rather than finding the best response strategy for a small cluster of mutants within the population (Gilboa & Matsui, 1991). Though the competitor's strategy is set, the course of infection represents a dynamic interplay between

competing strategies, with both competitive and cooperative dynamics potentially favored by the payoff function (Eqn. 4.1).

We model coinfection dynamics by splitting the infected red blood cell, merozoite and gametocyte classes in two and setting the starting inoculum to $I_0/2$ for each strain. Thus Eqn. 4.5 becomes:

$$\begin{aligned}\frac{dI_1}{dt} &= (1-c_1(t))pR(t)M_1(t) - \mu I_1(t) - \frac{a}{b+I_1(t)+I_2(t)}I_1(t) \\ &\quad (1-c_1(t-\alpha))pR(t-\alpha)M_1(t-\alpha)S \end{aligned} \tag{4.16}$$

$$\begin{aligned}\frac{dI_2}{dt} &= (1-c_2(t))pR(t)M_2(t) - \mu I_2(t) - \frac{a}{b+I_1(t)+I_2(t)}I_2(t) \\ &\quad (1-c_2(t-\alpha))pR(t-\alpha)M_2(t-\alpha)S \end{aligned} \tag{4.17}$$

As before, a red blood cell may only be invaded once. The strength of immune clearance scales inversely with the total number of infected red blood cells, such that if one strain becomes abundant, both strains benefit from a reduced rate of immune removal. These dynamics are reflected in the survival through the developmental period α:

$$S = \exp\left(-\int_{t-\alpha}^{t} \mu + \frac{a}{b+I_1(\omega)+I_2(\omega)}d\omega\right). \tag{4.18}$$

Each strain likewise has its own merozoite class,

$$\begin{aligned}\frac{dM_1}{dt} &= \beta(1-c_1(t-\alpha))pR(t-\alpha)M_1(t-\alpha)S - \mu_z M_1(t) \\ &\quad -pR(t)M_1(t) \end{aligned} \tag{4.19}$$

$$\begin{aligned}\frac{dM_2}{dt} &= \beta(1-c_2(t-\alpha))pR(t-\alpha)M_2(t-\alpha)S - \mu_z M_2(t) \\ &\quad -pR(t)M_2(t) \end{aligned} \tag{4.20}$$

and each a separate class for infected red blood cells committed to developing into gametocytes,

$$\frac{dI_{G1}}{dt} = c_1(t)pR(t)M_1(t) - \mu I_{G1}(t) \tag{4.21}$$

$$\begin{aligned} & -c_1(t-\alpha_G)pR(t-\alpha_G)M_1(t-\alpha_G)S_G \\ \frac{dI_{G2}}{dt} &= c_2(t)pR(t)M_2(t) - \mu I_{G2}(t) \\ & -c_2(t-\alpha_G)pR(t-\alpha_G)M_2(t-\alpha_G)S_G \end{aligned} \tag{4.22}$$

and S_G as in Eqn. 4.8. The gametocyte abundance for each strain is defined by

$$\frac{dG_1}{dt} = c_1(t-\alpha_G)pR(t-\alpha_G)M_1(t-\alpha_G)S_G - \mu_G G_1(t) \tag{4.23}$$

$$\frac{dG_2}{dt} = c_2(t-\alpha_G)pR(t-\alpha_G)M_2(t-\alpha_G)S_G - \mu_G G_2(t) \tag{4.24}$$

As before, a separate set of equations describes the stage transitions for the initially-inoculated parasites. When $t \leq \alpha$,

$$\begin{aligned} \frac{dI_1}{dt} &= (1-c_1(t))pR(t)M_1(t) - \mu I_1(t) - \frac{a}{b+I_1(t)+I_2(t)}I_1(t) \\ & -(I_0/2)\text{Beta}(s_P, s_P)(t)S \end{aligned} \tag{4.25}$$

$$\begin{aligned} \frac{dI_2}{dt} &= (1-c_2(t))pR(t)M_2(t) - \mu I_2(t) - \frac{a}{b+I_1(t)+I_2(t)}I_2(t) \\ & -(I_0/2)\text{Beta}(s_P, s_P)(t)S \end{aligned} \tag{4.26}$$

with

$$S = \exp\left(-\int_0^t \mu + \frac{a}{b+I_1(\omega)+I_2(\omega)}d\omega\right). \tag{4.27}$$

Merozoite classes are therefore

$$\frac{dM_1}{dt} = \beta(I_0/2)\text{Beta}(s_P, s_P)(t)S - \mu_z M_1(t) - pR(t)M_1(t) \tag{4.28}$$

$$\frac{dM_2}{dt} = \beta(I_0/2)\text{Beta}(s_P, s_P)(t)S - \mu_z M_2(t) - pR(t)M_2(t) \tag{4.29}$$

and developing gametocytes follow

$$\frac{dI_{G1}}{dt} = c_1(t)pR(t)M_1(t) - \mu I_{G1}(t) \quad (4.30)$$

$$\frac{dI_{G2}}{dt} = c_2(t)pR(t)M_2(t) - \mu I_{G2}(t) \quad (4.31)$$

Again, no mature gametocytes can be produced while $t \leq \alpha_G$.

4.4 Results

4.4.1 Gametocyte investment delays infectivity

When the reproductive investment is fixed through time, increasing the level of investment delays the growth of infection and subsequent infectivity to mosquitoes (Fig. 4.1). In single infections, cumulative transmission investment is maximized when approximately 42% of infected red blood cells commit to sexual differentiation. Simulating across a range of conversion rates (i.e., levels of reproductive investment) shows that greater transmission investment delays the peak of infection and subsequent surge in gametocyte numbers (Fig. 4.1B). Because infectivity to mosquitoes is a sigmoidal function of gametocyte numbers (Bell *et al.*, 2012), maximizing gametocyte production does not necessarily maximize the cumulative transmission potential. The timing of gametocyte production is key: sub-optimal investment leads to an early peak in asexual and gametocyte abundance at the expense of gametocyte production, while super-optimal investment delays infectivity (Fig. 4.1B).

If the conversion rate is allowed to vary with time, the optimal strategy is to invest heavily in asexual growth early in infection and increase gametocyte investment later in infection (gray and black curves, Fig. 4.2A). Counterintuitively, shorter infections (20 versus 30 days) select for a longer period of purely asexual growth at the beginning, to increase parasite biomass prior to gametocyte investment. When the duration of infection is extended to 50 days, parasites benefit from investing in transmission throughout the infection, though conversion rates are still lower initially. Longer infections also select for lower variability in con-

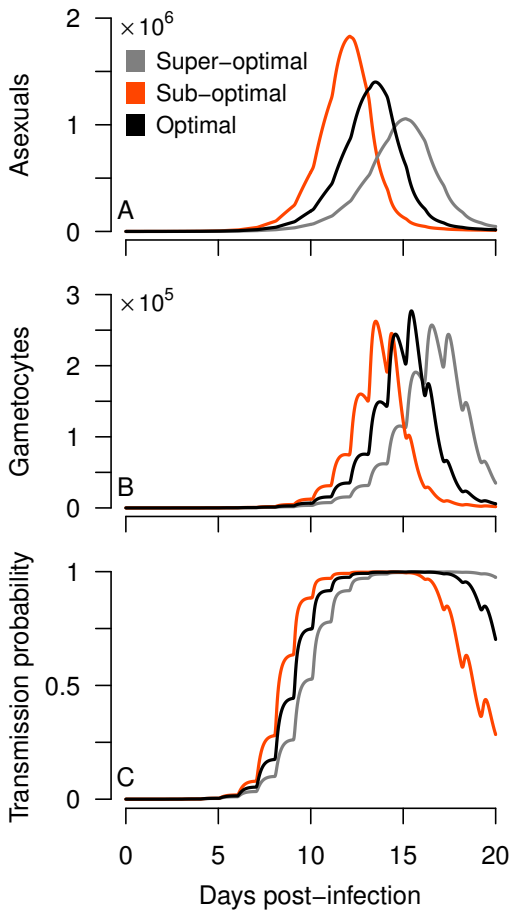

Figure 4.1. Reproductive investment limits asexual growth (A) and delays gametocyte production (B) and infectivity to mosquitoes (C). Infection was simulated assuming a fixed conversion rate and no immunity. Optimal investment (42.1%) gives the highest cumulative transmission potential (1078), while sub-optimal (35.1%) and super-optimal (48.1%) investment yield similar transmission potentials (1028).

version rates. Whereas the optimal 20-day strategy starts at zero conversion and ends at close to 100% investment, the 30- and 50-day strategies do not approach terminal investment.

The corresponding best fixed strategies for 20, 30 and 50 day infections are also shown (red lines, Fig. 4.2A), each representing an intermediate value of reproductive investment from the time-varying strategies. We find that when infections last longer than 20 days, there are two optimal levels of reproductive investment, one local and one global (Fig. C.1A). These optima correspond to fast and slow growth of the infection—low and high conversion rates, respectively—giving either two

peaks in the probability of transmission or one wide peak (Fig. C.1B & C). When infections last 30 days, it becomes possible to reduce reproductive investment and fit in two peaks in transmission potential, but the greatest cumulative transmission potential results from investing more into gametocytes, thereby generating a single drawn-out peak in the probability of transmission. When infections last longer, the fast growth/low reproductive investment strategy becomes favorable. As a result, the fitness-maximizing level of reproductive investment is substantially higher for 30 day infection compared with 20- and 50- day infections.

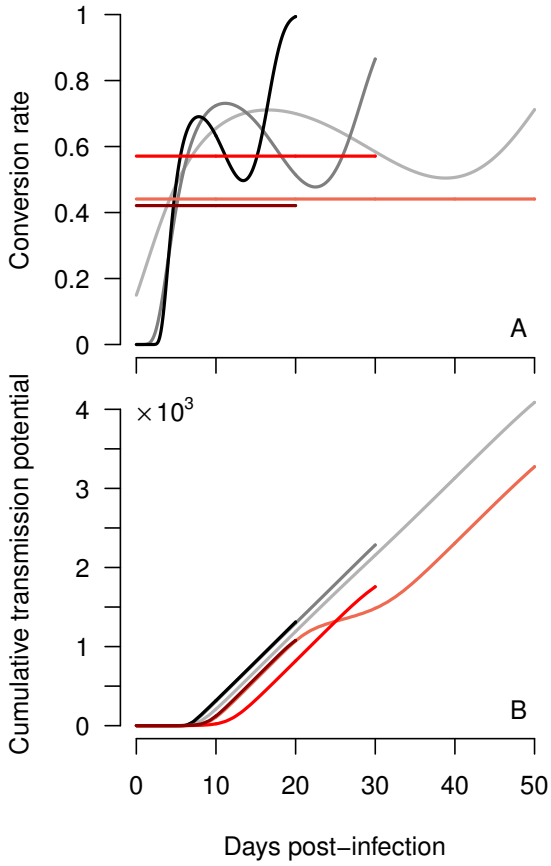

Figure 4.2. Optimal fixed (red) and free spline (gray/black) reproductive investment strategies (A) balance growth and transmission to maximize cumulative transmission potential over the course of the infection (B). The dark red and black lines ending at 20 days indicate outcomes for 20 day infections, with lighter curves and lightest curves showing the corresponding strategies and payoff for 30 and 50 days, respectively. Infection was simulated in the absence of host immunity, and the parameters defining each spline can be found in Table C.1.

These fixed strategies represent an imperfect balance between growth and reproductive investment, which incur a fitness cost compared with time-varying strategies (Fig. 4.2B). Strikingly, plastic reproductive investment allows parasites to begin accumulating transmission potential earlier than a fixed strategy, despite investing little into gametocyte production initially. The best fixed strategies require investing in transmission early, but that investment slows the growth of the infection. Thus early investment in gametocyte production is wasted, because gametocytes cannot be produced in large numbers until some degree of in-host replication has taken place.

Following an initial period of asexual growth, the time-varying investment strategies all accumulate transmission potential at similar rates. The approximately constant rate of increase in transmission potential (Fig. 4.2B) suggests that the plastic conversion rates can compensate for oscillations in parasite numbers (e.g., damped oscillations towards an equilibrium infection level as seen in Fig. 4.1). When investment is fixed, transmission potential will oscillate, as can be seen most clearly for the 50-day fixed strategy (Fig. 4.2B). The 20- and 30-day fixed strategies show fewer oscillations because they encompass only the first peak of infectivity.

4.4.2 Saturating immunity selects for reduced gametocyte investment

The optimal level of fixed reproductive investment rate is nearly halved in the presence of saturating immunity (Fig. 4.3, but the target of immune clearance (infected red blood cells versus short-lived merozoites) does not make a qualitative difference (Fig. C.2). In either case, immunity is most effective against the small number of parasites initiating infection. Parasites must invest in asexual growth—conversely dedicating less to transmission—to ensure that the infection grows fast enough to optimize the timing of gametocyte production. Investing in asexual growth reduces gametocyte production, so the cumulative transmission potential is necessarily lower in the presence of immune defenses.

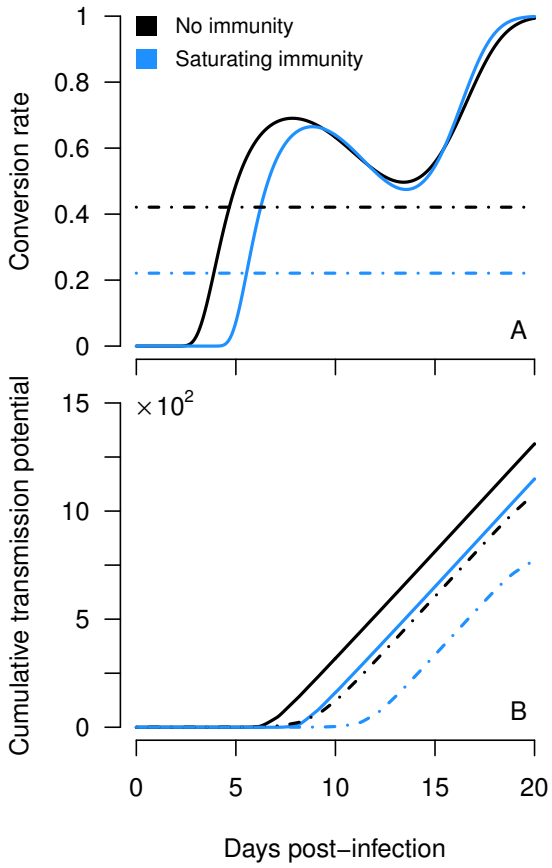

Figure 4.3. Saturating immunity favors reduced reproductive investment (A) despite the cost to cumulative transmission potential (B). If conversion rates are fixed (broken lines), the optimum gametocyte investment drops from 42.1% to 22.1%. When reproductive investment is allowed to vary through time (solid lines), immunity is predicted to select for delayed gametocyte investment early in infection. The parameters for the best spline strategies are in Table C.1.

4.4.3 Coinfection favors in-host replication

A competing malaria strain likewise benefits parasites that invest in replication. The evolutionarily stable strategy—assuming fixed reproductive investment—falls near 10% in the absence of immunity (Fig. 4.4A). Since we assume that strains do not interfere with each other, the selection pressure for reduced conversion must enter via direct competition for red blood cells. Apparent competition from immunity, which saturates as the total number of infected red blood cells increases, reduces the evolutionarily stable conversion rate even further (Fig. 4.4B).

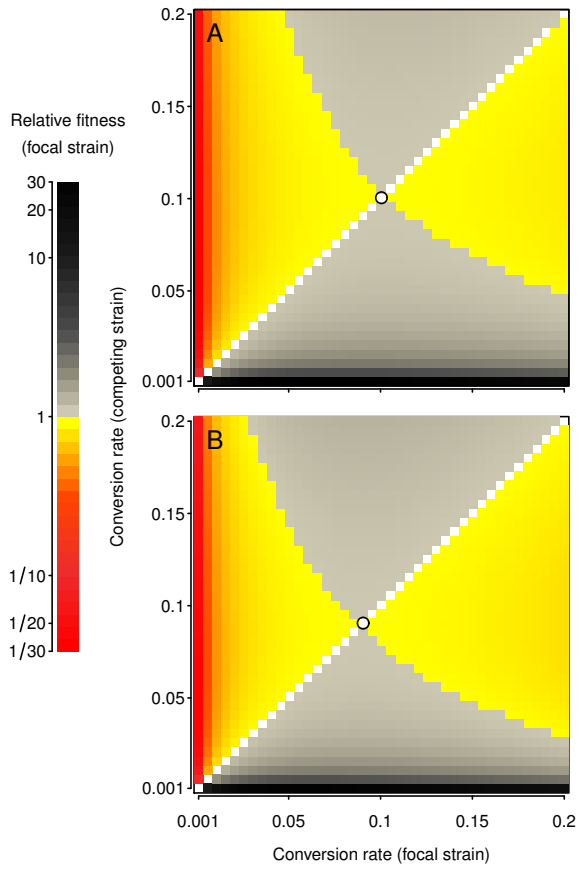

Figure 4.4. Coinfection reduces optimal reproductive investment. Relative fitness (transmission potential of focal/competing strain) is shown as both strains modify their conversion rates, either without immunity (A) or with saturating immunity removing infected red blood cells (B; $a = 150$, $b = 100$, $\sigma = 0$). Red regions indicate where the competing strain has higher relative fitness, while the gray area denotes where the focal strain has higher relative fitness. White boxes indicate that both strains have the same transmission potential (relative fitness of one). An open circle indicates the evolutionarily stable conversion rate.

We take the best conversion rates from Fig. 4.4 as a starting point to find an optimal time-varying strategy for a coinfecting strain. By iterating this process, each time retaining the strategy predicted to be optimal and competing it against a strain with plastic conversion rates subject to optimization, we can identify a candidate ESS (Fig. 4.5). The relative fitness of the time-varying strategy is 2.42 when competing against the best fixed strategy (Fig. 4.5A). As a frame of reference, the relative disadvantage of the best fixed strategy is comparable to the estimated

cost of drug resistance in *P. chabaudi* parasites (that is, in the absence of drugs, drug-sensitive parasites are predicted to infected 2-3 times as many mosquitoes as drug-resistant parasites, Huijben *et al.*, 2010a). The relative fitness of the best time varying strategy tends to decrease through successive optimizations (decreasing to 1.02 in Fig. 4.5B, 1.006 in C, 1.03 in D, and 1.007 in E), as would be expected if the competing strains were converging on an ESS. To further test whether diverse reproductive investment strategies should converge to a similar ESS, we identified the best free spline response to an investment strategy that decreases over time. We find that the best time-varying response is very close to the flexible strategies already identified (Fig. C.3), supporting the hypothesis that parasites should converge on a single optimal strategy in coinfections, rather than the best response varying with the competitor's strategy. Taken together, the optimal time-varying investment strategies suggest that parasites should leave transmission investment until later and invest less overall than they would in single infections.

Intriguingly, the combined transmission potential from the infection tends to increase as competing strains converge on similar strategies. While the best strategy from Fig. 4.5B is outcompeted in Fig. 4.5C, its transmission potential still increases from B to C (Fig. C.4), showing that a beneficial shift in strategy by one strain has the potential to benefit both strains. We also note that cumulative transmission potential is sensitive to the assumption that strains are capable of outcrossing freely (Eq. 4.16). For example, if we instead assumed the opposite extreme, that strains cannot outcross (as in Greischar *et al.*, 2014), the losing strategy in Fig. 4.5B (red) would have greater transmission potential than the winning strategy (purple) in a coinfection.

4.4.4 Optimal cues: how can parasites tell time?

We assume parasites have perfect knowledge of the age of the infection to find the ideal plastic conversion strategy, and identify cues that may serve as good proxies. Asexual abundance is predicted to be a very poor cue in single and coinfections (Fig. C.5, C.6, respectively) because different conversion rates correspond with the same number of parasites for nearly the entire course of infection. Since coinfections converge on a single optimal transmission strategy, competing strain abundance

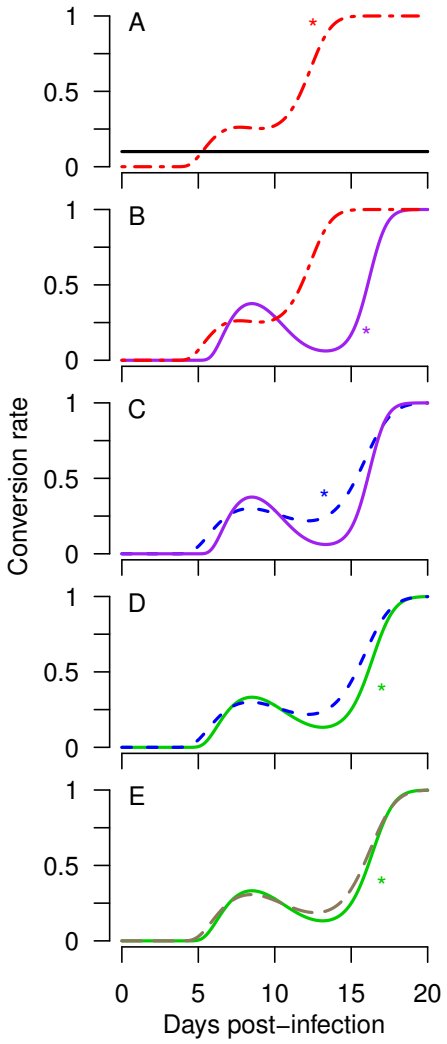

Figure 4.5. Dueling splines in successive optimizations: When two parasite strains infect the same host and differ only in their allocation to transmission, they should converge on an optimal strategy. In the first case (A), we assume the competitor uses the evolutionarily stable constant conversion rate identified in Fig. 4.4A (black line) and find the optimal free spline strategy. In B-E, we retain the optimal free spline strategy from the previous simulation and find the best free spline response. In each case the winning strategy is marked with an asterisk (fitness of each strategy in each iteration shown in Fig. C.4). For simplicity, we assume infection lasts 20 days, and that host immunity is absent. Spline parameters are given in Table C.1.

is an equally poor proxy for time. In contrast, red blood cell abundance could serve as an effective cue early in single infections (Fig. C.7), with each conversion rate corresponding to a single red blood cell abundance. In order for parasites to

utilize red blood cell numbers as a cue, they would need to be exquisitely sensitive to changes early in infection, when red blood cells are abundant, and insensitive late in infection, when red blood cells are limiting. In coinfections, red blood cell numbers might be an even easier cue to follow, at least until late in infection (Fig. C.8).

Parasite growth in the last 24 hours ($I(t)/I(t-\alpha)$) would be a poor cue early in infection, with the same growth rate corresponding to drastically different conversion rates (Fig. C.9). Late in single infections, asexual growth drops below replacement, and this corresponds to an increase in the optimal conversion rate. For coinfections, only very low growth rates (much lower than replacement) show a one-to-one correspondence with the optimal conversion rate (Fig. C.10). While no single cue appears to work for the entire duration of an infection, a good rule of thumb could be to respond to red blood cell numbers until parasite growth drops critically low.

4.4.5 Sensitivity to burst size, red blood cell replenishment, and synchrony

The optimal level of reproductive investment is likely to be influenced by parasites' maximum replication rate, by how quickly hosts can replenish resources, and by the level of synchronization of the infection. We therefore recalculate the optimal conversion rate when the burst size and maximum rate of erythropoiesis are increased versus decreased. Finally, we reexamine the role of immunity in depressing the conversion rates in synchronous infections. For simplicity, we examine the effects of these parameters in single infections assuming fixed conversion rates.

Malaria parasites can replicate into multiple asexual merozoites within a red blood cell or generate a single gametocyte. The cost of gametocyte investment should therefore depend on how many merozoites parasites can make within each infected red blood cell (the burst size). We find that the optimal fixed conversion rate increases with the burst size (β) in single infections (Fig. C.11). Thus, the relative cost of investing in gametocytes is much higher when burst size is lower, while strains with high burst sizes should be able to maintain robust asexual growth even while investing heavily in transmission.

The cost of gametocyte investment should also depend on how quickly the host can replenish red blood cells, or in other words, the cost of in-host replication should depend on the rate of erythropoiesis. If red blood cell replenishment is sluggish, investing too heavily in asexual growth may put parasites at risk of depleting the host of resources and reduce survival. A low rate of erythropoiesis may benefit strains that invest more in transmission. In contrast, if the host rapidly replaces red blood cells, red blood cell depletion may be unlikely, and parasites may benefit from investing more into growth and less into transmission. Accordingly, we find that increasing the maximum rate of erythropoiesis (λ) reduces gametocyte investment (Fig. C.12). We note that even dramatic changes in λ—in this case, 50% and 150% of the baseline λ—modify the optimal conversion rate by only a few percent, a change dwarfed by the effects of adding saturating immunity (Fig. 4.3) or a competing parasite strain (Fig. 4.4).

Synchronous development of gametocytes is predicted to help parasites overcome mating finding difficulties early in infection (Greischar *et al.*, 2014), so we might expect synchrony to alter the optimal conversion rate. However, we find a similar qualitative pattern for synchronous infections (Fig. C.13): the optimal conversion rate is identical to that of asynchronous infections in the absence of immunity, and adding saturating host defenses reduces the optimal conversion rate. We find that immunity targeting short-lived merozoites does not reduce the optimal conversion rate to nearly the same degree as in asynchronous infections. When the target of immunity is short-lived, synchronous bursting out of red blood cells should rapidly overwhelm host defenses (Greischar *et al.*, 2014), thereby mitigating the impact of immunity on the optimal conversion rate.

4.5 Discussion

The optimal balance between growth and reproduction is a complex function of the ecology of the system (e.g., Bell, 1980; Metcalf *et al.*, 2008). Malaria parasites must allocate to growth versus transmission in a rapidly changing environment. The model suggests that, counterintuitively, increased transmission investment delays infectivity by stunting the growth of the infection. We therefore predict that parasites will benefit from delaying their investment into transmission, at least

when infections are short, and that host defenses and coinfecting malaria strains will impose intense selection for in-host replication early in infection.

Malaria parasites have long been thought to employ reproductive restraint, investing very little into producing transmissible gametocytes (reviewed in Taylor & Read, 1997). Yet malaria parasites are highly successful at transmission, putting almost half of the world's population at risk of infection (Gething *et al.*, 2011). We use simulations to show that maximizing transmission potential requires restrained reproductive investment, at least early in infection, in direct analogy to adaptive delays in reproductive investment predicted for macroorganisms (e.g., Bell, 1980; Koons *et al.*, 2008). In chronic infections, fitness is predicted to be maximized by a u-shaped strategy that first declines—as parasites switch to investing in survival rather than reproduction—and then increases with deteriorating conditions within the host (Pollitt *et al.*, 2011a), we can rule that out as an optimal strategy in the acute phase of infection where growth trades off with transmission. Instead of producing gametocytes from the beginning, parasites would do better to attain a robust population size and then invest into transmission, in line with a general model of parasites with specialized transmission stages (Koella & Antia, 1995). Notably, the related intestinal parasite *Eimeria tenella* also delays production of specialized transmission stages until a couple of generations of asexual growth have taken place (Schmidt & Roberts, 1989). In keeping with this pattern, experimental infections of mice (Koella & Antia, 1995) and humans (*Plasmodium falciparum*, Taylor & Read, 1997; Collins & Jeffery, 2003) show increases in gametocyte abundance following periods of rapid asexual growth. Gametocyte numbers are expected to lag behind asexual parasitemia because sexual differentiation is a lengthy process, but gametocytes appear even later than expected given the lengthy period required for sexual differentiation (seven to eight days for the human malaria parasite *Plasmodium falciparum*, two days for the murine parasite *P. chabaudi*, Lensen *et al.*, 1999; Gautret *et al.*, 1996, respectively). Similarly, in experimentally-infected volunteers, asexual parasites rise to detectable levels before markers for early gametocyte differentiation can be detected (Schneider *et al.*, 2004).

Longer infections should erode the advantages of reproductive restraint, with shorter periods of purely asexual growth needed as parasites can count on more

time to grow and transmit. Malaria parasites may experience considerable variation in the duration of infection, from days to weeks (Daubersies *et al.*, 1996) up to hundreds of days (Miller *et al.*, 1994). Surprisingly, longer infections selected for reduced conversion rates at the end of infection (Fig. 4.2). In each case, the time-varying transmission investment strategies accrue transmission potential at very similar rates after an initial period of growth, suggesting that increasing the conversion rate to reach terminal levels would require an unacceptable decrease in the growth rate. We cannot rule out a discontinuous shift to terminal investment (such as the optimal strategy proposed by Koella & Antia, 1995) because the splines are constrained to be continuous, but evidence suggest that parasites may resist investing so much that they to preclude any future growth. *In vitro* assays did not detect terminal investment even when parasites were confronted with conditions far more crowded than they would typically experience *in vivo* (Bruce *et al.*, 1990). Much greater transmission potential is possible from longer infections (Fig. 4.2B), and that could shift the balance when parasites experience infections of varying length. While we considered infections of fixed duration, it makes sense that the transmission investment strategy should be weighted towards allowing continued transmission from longer infections when that possibility exists, especially given that parasites are unlikely to have perfect knowledge of when the infection will end. Terminal investment is likely to be selected against whenever there is a chance of a longer infection, potentially explaining why anti-malarial drugs—while increasing rates of gametocyte production—have not been shown to trigger conversion rates even close to terminal investment (Buckling *et al.*, 1999). While inducing terminal investment has been proposed as a possible means of treating malaria infections (Carter *et al.*, 2013), variability in the length of infection may impose strong counter-selection to keep parasites from investing everything into transmission.

Reproductive restraint has harsh implications for human health, since a malaria strain that invests more into transmission will tend to grow more slowly and to smaller population sizes (as shown in Fig. 4.1). High parasite biomass is a shared feature of severe malaria cases (reviewed in Cunnington *et al.*, 2013), and as gametocyte investment places limits on parasite replication, it has the potential to reduce virulence. There has been considerable interest in identifying the factors

that select for reduced conversion rates and, all else being equal, increased virulence to the host. Immunity triggered by large numbers of gametocytes has been suggested as a potential source of selection for reduced conversion rates (Taylor & Read, 1997). Evidence for such immune measures is limited, and low levels of gametocyte antibodies can actually enhance transmission (reviewed in Bousema & Drakeley, 2011). Subsequent modeling showed that if immunity penalizes increased gametocyte production, parasites could respond by altering either replication or conversion rates, so that immunity need not select on conversion rates per se (Mideo & Day, 2008). The present model predicts that saturating immunity against asexual stages will select for parasites that grow rapidly to greater numbers at the expense of gametocyte production. Thus reproductive restraint should be adaptive without the need to invoke intense immunity against gametocytes. Any immune measures that target asexual stages and lose efficacy with increasing numbers of targets—including platelets or $\gamma\delta$ T cells (McMorran *et al.*, 2009; Costa *et al.*, 2011, respectively)—should select for reproductive restraint and hence greater potential for host exploitation.

Previous models suggested that coinfecting parasite strains should select for reduced reproductive investment, as both strains jockey for a greater share of host resources (McKenzie & Bossert, 1998; Mideo & Day, 2008). The selection pressure of a competing strain should be extremely common in human malaria infections (e.g., Färnert *et al.*, 1999, 2008; Mideo *et al.*, 2013a). We confirm that coinfecting parasites select for reduced reproductive investment, and expand on previous theory to show that when transmission investment is allowed to vary through time, coinfection selects for a longer period of purely asexual growth at the beginning of infection. Critically, we predict that natural selection should converge on a single optimum strategy, rather than the rock-paper-scissors reproductive strategies that have evolved in other systems (Sinervo & Lively, 1996). The convergence to a single strategy is likely related to the fact that a coinfecting strain represents a source of potential mates. When mate-finding is a problem, reproductive success may require matching the timing of reproductive effort to that of conspecifics (e.g., through masting, Kelly & Sork, 2002), and this timing issue is encoded into the fitness function, with the probability of infecting a mosquito dependent on the total number of gametocytes present (Eq. 4.16). The convergence on a single strategy

is likely to be sensitive to the assumption that parasites are capable of outcrossing and suffer no fitness disadvantage from recombination, but there are reasons to expect that to be the case for malaria. Host immunity imposes negative-frequency dependent selection for rare variants in key virulence genes (Bull *et al.*, 1999) that could benefit strains which outcross (i.e., the Red Queen Hypothesis, Bell, 1982). Rodent malaria strains modify their sex ratios according to the diversity of the coinfection and in a way that should facilitate outcrossing in coinfections (Reece *et al.*, 2008). It follows that parasites may modulate their reproductive investment to match the timing of coinfecting strains and promote outcrossing, leading to convergence on a single optimal strategy.

The potential for evolution towards the optimal strategy depends on how well parasites can obtain reliable information from their environment. We find no single perfect cue among the state variables in the model. Rather simulations suggest that parasites should use red blood cell numbers to provision for transmission investment, at least early in an infection. The appropriate response to red blood cell numbers (and other environmental changes) may vary depending on how much longer the infection can be expected to persist. Parasites are thought to reduce reproductive investment to favor survival when host conditions deteriorate (Reece *et al.*, 2009; Pollitt *et al.*, 2011a). If the environment declines so far that parasite survival is unlikely, maximizing transmission may require dramatically increased reproductive investment (Pollitt *et al.*, 2011a), conceptually identical to the notion of terminal investment in multicellular organisms (e.g., Clutton-Brock, 1984). In line with these expectations, the present model shows that the optimal level of gametocyte investment may alternately increase or decrease with red blood cell numbers (Fig. C.7). Experimental rodent infections confirm that reproductive investment changes with red blood cell numbers, but whether the relationship is positive or negative remains controversial (Pollitt *et al.*, 2011b; Cameron *et al.*, 2012, respectively).

Late in infection, red blood cell numbers become a problematic cue, and per capita parasite growth could serve to indicate when parasites should switch to terminal investment. These results coincide with predictions from a previous model (Koella & Antia, 1995) suggesting that parasites should increase transmission investment when growth drops below replacement, analogous to the way macroor-

ganisms may intensify their reproductive investment when survival is doubtful (Velando *et al.*, 2006). Though increasing reproductive investment should maximize fitness near the end of infection, the optimal time to increase investment depends on the interplay between parasite growth rate, immune clearance, and virulence to the host (Koella & Antia, 1995), as well as whether parasites can make use of reliable cues in the rapidly changing environment of the host (reviewed in Carter *et al.*, 2013).

Identifying the optimal life-history allocation is a substantial challenge when there are dynamic feedbacks with resource availability, the difficulty of finding mates, and the allocation strategies of conspecifics. Here we present a means of incorporating ecological detail into a model and locating optimal strategies. The system need not be at any kind of equilibrium, and the fixed delay framework allows realistic time lags between modulating allocation and the fitness consequences. Such time lags are expected to determine when plastic strategies may be favored (Padilla & Adolph, 1996). Using free splines allows great flexibility in the shape of the candidate strategies, so that allocation can vary on whatever timescale or in response to whatever environmental gradient is deemed most relevant for the organism in question. The approach allows us to describe a dynamic tension in the selective forces acting on malaria parasites, and identify the factors that may select for replication—and host exploitation—over transmission investment.

4.6 Acknowledgements

I thank Dave Kennedy, Sarah Reece, and Laura Pollitt for useful discussion.

4.7 Notes

This chapter represents work done in collaboration with Nicole Mideo, Andrew F. Read, and Ottar N. Bjørnstad, who will be co-authors on when the manuscript is submitted for publication.

Chapter 5

Challenges in estimating transmission investment in malaria parasites

5.1 Abstract

Microparasites with specialized transmission stages face a tradeoff between replication within the host and spread between hosts, with malaria parasites serving as a notable example. To cope with changing conditions within the host, we may expect that parasites should employ plastic investment strategies, but testing that expectation requires methods that can rule out the null hypothesis: that parasites' transmission investment is fixed. Past experiments have focused on identifying how malaria parasites modify their allocation to transmission and growth through the course of infection. This transmission investment must typically be inferred rather than directly observed, and researchers arrive at qualitatively different conclusions depending on the inference method used. We test current methods against data simulated from a previously described mechanistic model, showing that all methods fail to recover the null hypothesis when it is true. Current methods instead generate spurious oscillations in transmission investment through time because the gametocytes produced by multiple cohorts of parasites are counted together. Even early markers of transmission investment can only overcome this problem under

special conditions. We describe a new method for inferring transmission investment for malaria parasites that works well on simulated data, whether the true transmission investment is fixed or time-varying. Therefore existing data can likely be used to better characterize transmission investment strategies in malaria parasites.

5.2 Quantifying transmission investment

Many parasites tradeoff between growth within a host and transmission to new hosts, and the optimal level of transmission investment is predicted to vary through the course of infection as parasites deplete resources and trigger immune defenses (e.g., Koella & Antia, 1995; Pollitt *et al.*, 2011a). Validating that theory—and characterizing the variation in this critical parasite life history trait—requires accurate assessment of transmission investment, a quantity that is often difficult to measure directly in real infections. Transmission investment is not unique in this regard; many important parasite traits must be inferred rather than measured, and models provide an ideal way to test out our ability to reconstruct unobserved processes. Simulated data was used to show that popular and intuitive methods for characterizing interactions between coinfecting macroparasite species can yield qualitatively wrong answers (Fenton *et al.*, 2010), and the methods prescribed for assessing transmission investment should be subject to the same scrutiny.

Malaria infections are a popular system in which to examine transmission investment, since mature sexual transmission stages (gametocytes) can be readily distinguished from asexual forms by molecular methods (Drew & Reece, 2007). Moreover, the tradeoff between within-host replication and transmission investment is obvious as an infecting parasite can develop into a single gametocyte or several asexual forms that can continue replication within the host (e.g., Garnham, 1966). There is evidence of plastic transmission investment in tightly-controlled *in vitro* experiments where it has been possible to measure investment directly (Bruce *et al.*, 1990). Previous experiments have provided curves to relate gametocyte numbers to fitness in terms of infectivity to mosquitoes (Huijben *et al.*, 2010a; Bell *et al.*, 2012), making it possible to infer the fitness consequences of varying levels of transmission investment. While understanding plasticity in transmission investment is interesting in its own right, it may also carry applied benefits.

The patterns found have the potential to improve malaria treatment strategies, for example by calling attention to cues that could trick parasites into employing suboptimal strategies (reviewed in Carter *et al.*, 2013).

Two recent studies highlight that important methodological and challenges remain: Using different inferential methods, researchers analyzed the same data set and came to opposing conclusions regarding how parasites' transmission investment varies with resource availability (Pollitt *et al.*, 2011b; Cameron *et al.*, 2012). Numerous methods are prescribed for inferring parasite reproductive investment (by convention the "conversion rate", Bruce *et al.*, 1990), each using a different set of simplifying assumptions about infection dynamics to back-calculate the proportion of parasite biomass committed to transmission stage production some time previously (Buckling *et al.*, 1999; Reece *et al.*, 2010; Carter *et al.*, 2013). These methods represent distinct but logical approaches to inferring plastic transmission investment; whether the logic stands up to the complex and nonlinear dynamics inherent to malaria infections is an open question.

The complexities of inferring conversion rates are most obvious *in vivo*, but it is worth mentioning that the only direct observations of transmission investment were obtained by fixing cells in a monolayer, making it possible to observe the causal chain between a cohort of parasites and subsequent development of gametocytes (Bruce *et al.*, 1990). Whenever parasites are free to move around, transmission investment must be inferred rather than observed, meaning that even *in vitro* studies cannot be assumed to accurately characterize conversion rates. Differential mortality rates between sexual and asexual forms are commonly thought to bias inferred conversion rates (e.g., Buckling *et al.*, 1999; Cameron *et al.*, 2012), especially *in vivo* where the innate immune response may preferentially target asexual stages (Riley & Stewart, 2013). The issue of differential mortality is less of a problem *in vitro* when immune measures can be excluded, but reconstructing the causal chain between a cohort of parasites and gametocytogenesis presupposes that parasites can be separated into discrete cohorts, a process that requires repeated artificial synchronization which can be lost rapidly (e.g., Trager & Jensen, 1976; Reilly *et al.*, 2007). A recent review concluded that transmission investment occurs continuously throughout the course of infection in malaria parasites (Morahan & Garcia-Bustos, 2014), in contrast to theory predicting that it would be optimal

to delay investment in transmission stages (Koella & Antia, 1995). Continuous transmission investment in malaria would make an interesting contrast to the life history of related parasites *Haemoproteus spp.* (Valkiunas, 2005) and *Eimeria tenella* (Schmidt & Roberts, 1989), both of which delay transmission investment to allow for within-host growth.

Given the existing data and inference methods, are we premature in drawing conclusions about transmission investment strategies in malaria parasites? We use simulated data—where the true transmission investment strategy is known—to characterize current methods for inferring conversion rates. To understand how transmission investment varies through time and in response to which cues, we must first be confident in our ability to rule out the null hypothesis: that parasites' transmission investment is fixed through time. Otherwise, systematic biases could undermine efforts to describe how parasites balance growth and transmission in a rapidly changing environment.

5.3 Transmission investment in malaria

Malaria parasites (*Plasmodium spp.*) grow asexually within the red blood cells of a vertebrate host, developing into mature stages called schizonts that burst to release merozoites capable of invading other red blood cells (Garnham, 1966). *In vitro* assays suggest that all of the merozoites emerging from a single schizont will be committed either to sexual differentiation—invading a red blood cell and developing into a sexual gametocyte that can be passed onto the vector in a blood meal—or to asexual growth, invading a red blood cell and maturing into another schizont (Bruce *et al.*, 1990). Gametocytes are specialized for transmission to the vector and cannot infect red blood cells (reviewed in Bousema & Drakeley, 2011), so that transmission investment should come at the cost of reduced within-host replication (Taylor & Read, 1997; Mideo & Day, 2008). Allocation to gametocyte production is thought to be subject to selection pressures analogous to those acting on reproductive effort in free-living species (Reece *et al.*, 2009; Pollitt *et al.*, 2011a). Making use of experimental malaria infections of mice, researchers have examined how the estimated transmission investment changes through time and in response to resource availability (red blood cell abundance, Pollitt *et al.*, 2011b; Cameron

et al., 2012), to anti-malarial drugs reducing the odds of survival (Buckling *et al.*, 1999; Reece *et al.*, 2010), and to competition from coinfecting malaria strains (Pollitt *et al.*, 2011b).

Transmission investment (i.e., reproductive effort) is defined as the fraction of a given cohort of parasites that commit to differentiation into gametocytes (Reece *et al.*, 2009). By convention, this fraction is referred to as the "conversion rate" (Bruce *et al.*, 1990). Implicit in this definition is the idea that parasites can be separated into identifiable cohorts. Many, but not all, malaria species exhibit synchronous cycles of blood stage infection, with cohorts of schizonts bursting in unison to release short-lived merozoites that will generate another cohort of infected red blood cells (reviewed in Mideo *et al.*, 2013b). Synchrony is helpful to quantifying reproductive effort because all parasites will be equally capable of committing to the sexual pathway. If commitment occurs in the schizont stage prior to invasion and gametocyte development as *in vitro* assays suggest (Bruce *et al.*, 1990; Eksi *et al.*, 2012), then younger parasites may not be capable of committing to sexual differentiation. In poorly synchronized infections, parasites of all age classes are present simultaneously, and estimating transmission investment is complicated by the fact that only a subset of the population is capable of committing one way or the other.

The rodent malaria species often used for experiments, *P. chabaudi*, appears to be well-synchronized (O'Donnell *et al.*, 2011), and PCR methods have been developed to quantify abundance for both asexual parasites and mature gametocytes beginning early in infection (Drew & Reece, 2007). Since only mature gametocytes can be differentiated from asexual forms, there is a time lag between when parasites commit to sexual differentiation and when researchers can detect that commitment. Early signals can be detected in the human malaria *P. falciparum* (Schneider *et al.*, 2004), including a marker expressed in mature schizonts and gametocyte development *in vitro* (Eksi *et al.*, 2012). However, both mature schizonts and immature gametocytes may sequester out of circulation where they cannot be easily sampled from the host (reviewed in Cunnington *et al.*, 2013; Bousema & Drakeley, 2011, respectively), so that even with early markers, there is likely to be a time lag between when the transmission investment is adjust and when result can be observed.

A variety of techniques have been developed to deal with this time lag. A recent study used linear mixed effects models to examine how transmission investment varied with resource use (Cameron *et al.*, 2012), while other studies attempt to estimate conversion rate explicitly, because direct estimates of transmission investment are conceptually appealing and easily incorporated into modeling efforts (e.g., Greischar *et al.*, 2014). Such direct estimates infer transmission investment c (i.e., the conversion rate) from time series of gametocyte abundance and total parasite numbers. The simplest method that accounts for the time lag between conversion and gametocyte maturity would be

$$c_t = \frac{G_{t+2}}{A_t}, \tag{5.1}$$

where A_t is the total number of red blood cells invaded, by either sexually- or asexually-committed merozoites. Thus c_t is the fraction of invaded cells that develop into mature gametocytes two days later (G_{t+2}), assuming no mortality during that two day window of development. This method is similar to ones commonly used *in vitro* (e.g., Reece *et al.*, 2010), where early stage gametocytes can be identified and neglecting mortality is likely to be a good approximation.

In vivo, neglecting mortality is thought to be too unrealistic an assumption, so methods attempt to correct the estimated conversion rate for mortality. A commonly used method (Buckling *et al.*, 1999) defines the conversion rate as

$$c_t = \frac{\frac{G_{t+2}}{A_t}}{\sqrt{\frac{A_{t+2}}{A_t}} + \frac{G_{t+2}}{A_t}} \tag{5.2}$$

making use of the fact that infected red blood cells take two days to develop into mature gametocytes (Gautret *et al.*, 1996). Buckling *et al.* derive this method by considering the conversion rate as a function of burst sizes (i.e., the number of merozoites emerging from a burst red blood cell) and mortality, both of which can be solved for in terms of A and G, yielding the squared terms. A subsequent review suggests that if asexual stages are counted on day one, and gametocytes do not mature until two days later, the time lag should be three days, making the

appropriate estimate

$$c_t = \frac{\frac{G_{t+3}}{A_t}}{\sqrt[3]{\frac{A_{t+3}}{A_t}} + \frac{G_{t+3}}{A_t}} \text{ (Carter } et \text{ } al.\text{, 2013)} \tag{5.3}$$

All three methods require synchronous rounds of bursting and invasion, because PCR counts developed for the rodent parasite *P. chabaudi* only yield reliable estimates of the number of infected red blood cells when parasite development is synchronized and sampling occurs prior to DNA replication (i.e., the ring stage, Cheesman *et al.*, 2003). Methods for inferring conversion rates are expected to be sensitive to the assumption of equal survival between gametocytes and asexual stages, which may fall apart due to differential immune clearance (Buckling *et al.*, 1999; Carter *et al.*, 2013), which is a concern since immunity predominately targets asexual parasites (Riley & Stewart, 2013).

5.4 How well can we estimate transmission investment from simulated data?

Simulated data provides a way to test different methods of detecting transmission investment by malaria parasites. Because the truth is known—that is, it is specified in the model—we can determine what methods give the most accurate estimate of transmission investment. We simulate dynamics in *P. chabaudi*-like infections of mice using a previously described model (Greischar *et al.*, 2014) that gives current methods the best possible chance of working, because we incorporate the key assumptions thought to yield reliable estimates of the conversion rate. Specifically, we assume a highly synchronized infection and, at least in initial simulations, no immune clearance. The model does, however, include a stylized version of homeostatic regulation of red blood cell abundance, as well as the capability to incorporate immune clearance of infected red blood cells. Critically, the model framework assumes that the duration of parasite development (both sexual and asexual) is fixed with no variation, so that a high degree of synchrony can be maintained through the course of the simulation (Greischar *et al.*, 2014). From high-resolution simulated data, we sample daily counts of total parasite numbers and gametocyte abundance,

assuming no sampling error, and initially assuming that sexually-committed but immature parasites cannot be distinguished from asexual stage parasites.

We expected that the lifespan of gametocytes could be a critical factor in how well Eqns. 5.1-5.3 perform, because as gametocytes die more quickly, fewer will be present at sampling, and the inferred value should underestimate the true conversion rate. Assuming that gametocytes die at a fixed rate (i.e., exponential distribution of survival times), model simulations confirm that short gametocyte lifespans causes all three inference methods to underestimate the conversion rate. Unfortunately, a longer lifespan causes a different problem. When gametocytes survive longer, it becomes more likely that some will survive through multiple sampling periods—in effect, blurring the synchronized waves of gametocyte production—causing gametocytes from different cohorts to be counted together (Fig. 5.1).

The model suggests two major challenges in obtaining accurate estimates of transmission investment: (1) sampling before substantial mortality has occurred, so as to avoid underestimating the conversion rate; (2) identifying parasites in a narrow morphological window, so that discrete cohorts can be distinguished. Current methods for inferring transmission investment must tradeoff between addressing these two challenges. Sampling a long-lived life stage would ameliorate the underestimation problem but worsen the chances of distinguishing between gametocytes produced by discrete cohorts. Conversely, when gametocytes have an unrealistically short lifespan (Fig. 5.1A, C), reproductive investment appears relatively constant through time, but the conversion rate is consistently and dramatically underestimated because most gametocytes have died at sampling. We suggest that systematic underestimation of conversion rates—while far from ideal—is not as serious a problem as the spurious oscillations in the inferred conversion rate seen in data simulated with realistic survival rates. The latter could seriously undermine our understanding of parasite life history, making it appear that parasites are responding to the changing environment within the host, even if they are not.

Identifying separate cohorts of gametocytes may be a greater challenge for certain malaria species. While mature gametocytes persist less than a day on average in *P. chabaudi* infections (Reece *et al.*, 2003), the human malaria *P. falciparum* produces gametocytes that can circulate for more than six days (reviewed

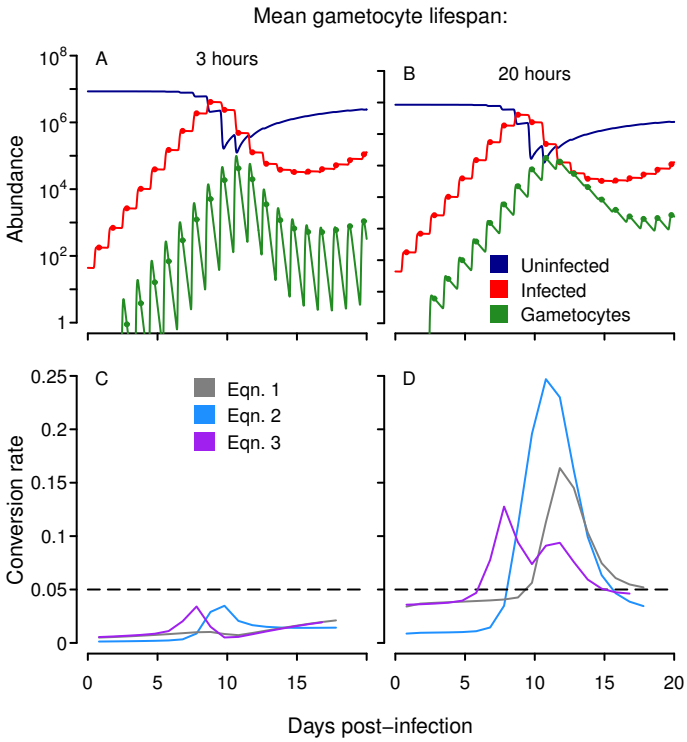

Figure 5.1. Longer gametocyte lifespan leads to spurious oscillations in the estimated conversion rate. Dynamics of uninfected and infected red blood cells (dark blue and red, respectively) and mature gametocytes (green) for short and long gametocyte lifespans (A and B, respectively). Estimates of conversion rate are shown below (C, D), with the actual conversion rate (5%) shown as a dashed line. We try an unrealistically short gametocyte lifespan (about 3 hours, A & C), and a more realistic longer lifespan as found by Reece *et al.* (2003) (half-life of 14 hours, equivalent to a mean lifespan of about 20 hours, B & D).

in Bousema & Drakeley, 2011), much longer than the two days required for the asexual life cycle. The long lifespan of *P. falciparum* gametocytes means that even in a highly-synchronized human infection, mature gametocytes from three cohorts could be present simultaneously, and methods analogous to Eqns. 5.1-5.3 would not yield reliable estimates of transmission investment.

Even if we can identify a narrow morphological window in gametocyte development, our ability to separate parasites into cohorts will depend on how strictly parasites maintain a synchronous rhythm through the course of the infection. The propensity of parasites to maintain synchronous cycles of infections has been observed to vary by parasite species (e.g., Kitchen, 1949; Garnham, 1966) and even

across strains (Reilly *et al.*, 2007). Synchrony may also change according to the immune status of the host and the age of the infection (Kitchen, 1949). Recording the age-structure of the observed parasite population may allow researchers to assess their ability to infer transmission investment from a given infection. If the synchrony of an infection declines (i.e., parasites spreading more evenly throughout developmental stages), the problem of estimating conversion becomes more complex, and the PCR counts themselves become unreliable (Cheesman *et al.*, 2003). The loss of synchrony is especially rapid *in vitro* (Trager & Jensen, 1976) and may decay faster or slower depending on the strain (Reilly *et al.*, 2007), meaning that error in conversion rates could likewise vary with the strain. As synchrony is lost, it may be necessary to correct conversion rates to account for the fact that a smaller portion of the population may be capable of committing to sexual differentiation at a given point in time.

5.5 Early markers for sexual differentiation

A great deal could happen in the time between commitment to gametocyte development and the appearance of mature gametocytes, so early markers for sexual differentiation should yield more reliable estimates of transmission investment. If we assume that sexual differentiation can be detected as soon as a committed merozoite invades a red blood cell, we see that early detection by itself does not ensure accurate estimates of conversion rates (Fig. D.1). While early detection avoids the problem of underestimating transmission investment, it lumps together developing gametocytes from two cohorts giving substantial errors as infected red blood cells and gametocytes fluctuate through the course of infection.

Therefore a marker of early gametocyte differentiation may yield spurious oscillations in conversion rates if it continues to be expressed throughout development during the course of multiple rounds of asexual growth, as would be the case for the *Pfdgv1* gene in *P. falciparum* (Eksi *et al.*, 2012). An early marker could still be very useful in conjunction with a marker for late sexual differentiation, so that sexually differentiating parasites that emerged from previous rounds of bursting and invasion can be excluded from calculations of conversion rates. We expand the model—adding age structure to sexual differentiation—to identify an ideal expres-

sion pattern from which accurate conversion rates can be obtained in *P. chabaudi* (Section D.1). We assume that an early marker is expressed immediately upon invasion and the beginning gametocyte development, and that other data (a later marker or morphological differences) can be used to distinguish between parasites undergoing the early versus later stages of sexual differentiation. Since sampling is performed daily, this early marker means that sexual differentiation can be detected the same day as the current cohort of infected red blood cells were invaded by merozoites and no time lag needs to be taken into account.

When we consider parasites in the first 12 hours of sexual differentiation, we see large daily oscillations in abundance due to the high degree of synchrony and the brevity of the stage (Fig. 5.2A), whereas if the stage lasted longer, the synchronized cycles would overlap, leading to less diurnal variation in abundance (Fig. 5.2C). If the early marker is expressed for too brief a period (Fig. 5.2A, B), then sampling at the same point in the life cycle becomes difficult following a very modest decline in synchrony. While the model assumes that the developmental periods are fixed, the lifespan of merozoites is exponentially-distributed rather than fixed, introducing variability in life cycle length (Greischar *et al.*, 2014). Since merozoites are extremely short-lived (on the order of minutes Boyle *et al.*, 2010) compared to the length of the period spent inside a red blood cell, the variation in life cycle length is very small, leading to a small but noticeable change in dynamics over time. With the added time spent as merozoites, the asexual cycle takes slightly longer than 24 hours, and the daily oscillations in abundance become slightly later during the 20 days simulated. This change can be seen in the abundance of parasites in the first 12 hours of sexual differentiation (Fig. 5.2A), where abundance is measured earlier and earlier in the cycle despite the fact that sampling occurs at the same time each day. This pattern suggests that markers expressed for too brief a period may be sensitive to very small changes in dynamics over the course of the infection, rendering them less than ideal for the purpose of estimating conversion. The difficulty in recovering the correct answer using existing methods is disappointing given that the simulations results represent an unrealistic extreme, because there is likely to be variation the length the parasite life cycle.

Critically, simulations suggest that the best expression profile for sexual differentiation would be one that mirrors the timing of asexual development exactly,

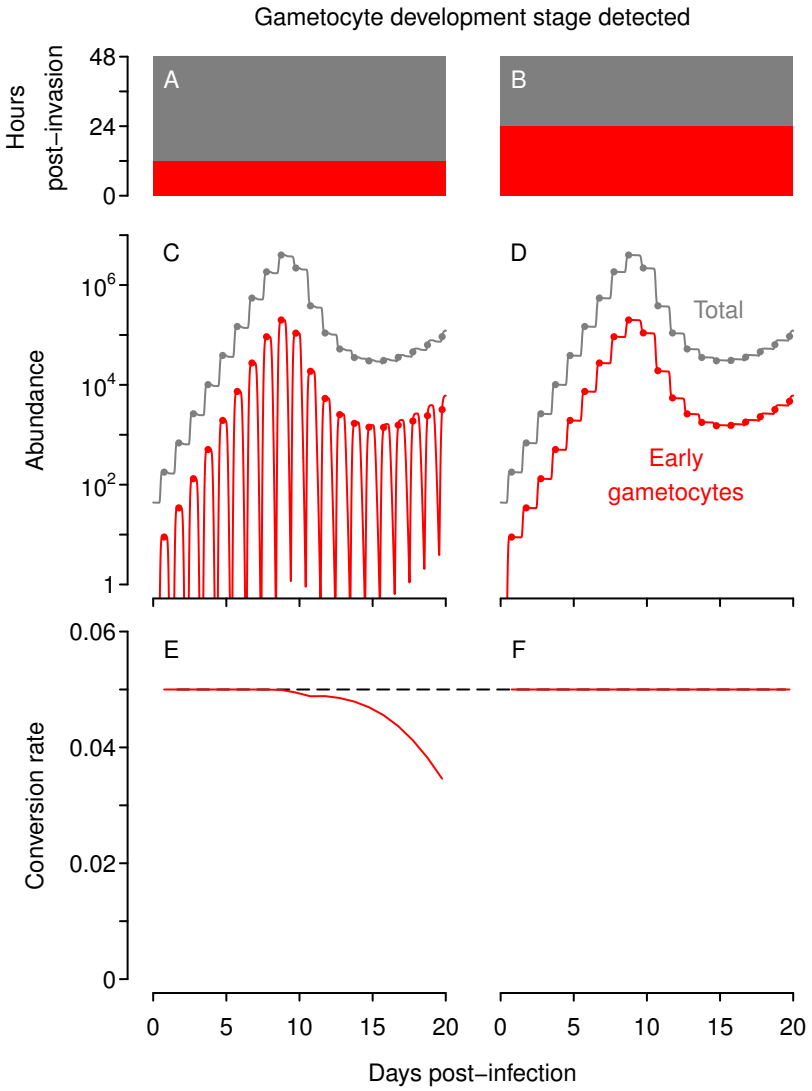

Figure 5.2. Hypothetical early markers for sexual differentiation can improve conversion rate estimates. The expression profile of the hypothetical marker is shown in red (A, B), the corresponding dynamics of the total abundance of cells (asexual and early sexual stage, gray) and early sexual parasites (red) is shown on a log scale with sampling given as dots (C, D), and the resulting estimates for conversion rate in the bottom panels (E, F). The actual conversion rate (5%) is shown as a dashed line, with conversion rates estimated as the fraction of early sexual stages divided by the total number of cells (asexual and early sexual). Mid- and late-stage sexual parasites, as well as mature gametocytes, were excluded from the calculations. We assume daily samples were taken six hours after peak-bursting and invasion.

meaning that it matches the mean duration and variation in duration experienced by parasites during asexual growth. If we assume that the first 24 hours of gametocyte development can be detected, and that that early developmental period is fixed in length, the slight change in dynamics affects early sexual stages and asexual stages in an identical manner, so that it does not generate errors in the conversion rate calculations. In contrast, using mature gametocytes to estimate conversion rates gives substantial errors (Fig. 5.1C, F), despite the fact that gametocytes survive nearly the length of the asexual life cycle on average. This error can be attributed to a difference in the variability in gametocyte lifespan, which is modeled as experiencing a constant mortality rate. The resulting exponentially-distributed lifespans are variable, with many gametocytes dying as soon as they mature and others persisting long after the mean lifespan of 20 hours. The Dirac-Delta distribution represents the opposite extreme of no variation about the mean. Even though the gametocytes and asexual stages have similar mean waiting times, the fact that the variances differ leads to substantial error over the course of infection (Fig. 5.1F).

To accurately recapitulate the conversion rate using existing methods, what is needed is the ability to detect the period of early sexual differentiation for the length of time required for the rest of the parasite cohort to develop through the asexual blood stages. For the *P. chabaudi* example modeled here, that means being able to detect the first 24 hours of sexual differentiation, while for *P. falciparum* it would be sufficient to detect the first 48 hours of gametocyte development period (Stage I gametocytes, Eksi *et al.*, 2012). *In vitro* experiments suggest that there is variability in the length of the asexual life cycle across and within *P. falciparum* strains (Reilly *et al.*, 2007; Reilly Ayala *et al.*, 2010), and if the length of time parasites spend as Stage I gametocytes varies in a different way, that could lead to increasing errors in estimating the conversion rate as synchrony decays.

Though our simulations mimic rodent infections, the problems we have identified here could equally apply to estimating conversion rates *in vitro*, even though mortality is minimal and all parasites are accessible to sampling. Since we are able to detect gametocytes in early stages of development, and estimating conversion from Stage II gametocyte abundance (i.e., Reece *et al.*, 2010; Eksi *et al.*, 2012) would be expected to work well, since Stage II is expected to last 48 hours, the

same as the length of the asexual life cycle in *P. falciparum* (Eksi *et al.*, 2012). The key problem *in vitro* is likely to be the rapid loss of synchrony, which may render unreliable any conversion rates estimated too long after artificial synchronization of the culture.

5.6 Interpreting plastic conversion rates *in vivo*

Current methods for calculating conversion rates can yield misleading results, even in situations where they would be expected to perform well (i.e., minimal mortality, no sampling error). Given this uncertainty, what can we conclude from previous studies about how parasites modify their transmission investment in response to their environment? We consider conflicting reports on how estimated conversion rates correlate with red blood cell availability (Pollitt *et al.*, 2011b; Cameron *et al.*, 2012), and the key finding that parasites should reduce their investment in transmission in response to a competing parasite strain (Pollitt *et al.*, 2011b), as predicted by theory McKenzie & Bossert (1998); Mideo & Day (2008).

One of the major barriers to accurately estimating conversion rates is double-counting gametocytes from different cohorts, which introduces time-varying errors depending on the number of gametocytes produced in the previous cohort (or cohorts, if gametocytes persist a long time). Therefore the errors in gametocyte counts are not independent, but rather depend on past gametocyte production. This dependence would be expected to introduce error even when researchers forgo estimating conversion rate directly to look for correlations between gametocyte production and other state variables (e.g., red blood cell numbers, Cameron *et al.*, 2012). Though we kept the conversion rate constant, gametocyte production—and the error introduced into gametocyte counts in the subsequent cycle—increases as asexual numbers increase, because there is a larger pool of parasites to differentiate into sexual forms. As asexual numbers increase, red blood cell numbers decline, and the inferred conversion rate appears to increase with decreasing numbers of red blood cells (Fig. 5.1). In other words, we can use the model to give the appearance that conversion rates are negatively correlated with red blood cell availability—the same pattern observed in recent experiments (Cameron *et al.*, 2012)—even when the real conversion rate is fixed.

Much harder to explain is a positive correlation between estimated conversion rates and red blood cell numbers, as found in previous work using Eqn. 5.2 (Pollitt *et al.*, 2011b). If this is a spurious correlation, it is in the opposite direction from what the model would predict, and tied to early infection dynamics since Pollitt *et al.* examine dynamics in the 5-12 days after infection. Setting aside the estimated conversion rate, the gametocytes themselves show strange dynamics with two peaks: a small peak preceding the peak in asexual parasite numbers, and the usual large peak in gametocyte abundance following peak infection (see Fig. 2 in Pollitt *et al.*, 2011b). A similar pattern can be found in other experiments with *P. chabaudi* (Buckling *et al.*, 1999; Mackinnon & Read, 2003), suggesting a gap in our understanding of transmission stage dynamics. Early immune defenses could certainly skew the observed numbers of asexual stages and gametocytes, since host defenses are directed mainly at asexual forms (Riley & Stewart, 2013).

Early immune clearance is thought to disproportionately remove small numbers of parasites and saturate as parasite biomass increases (Metcalf *et al.*, 2011), but such density-dependent mortality would skew the estimated conversion rate in the wrong direction (Fig. D.2), strengthening the appearance of a negative correlation between red blood cell availability and the apparent transmission investment. At least two other possibilities exist for explaining a positive correlation: (1) Immunity is altering gametocyte numbers directly and in a more complicated manner than simply saturating with large numbers of gametocytes. Saturating immunity would be expected to merely delay the gametocyte peak, and more complicated immune dynamics would be needed to give two peaks. (2) Parasites begin by investing too much into gametocytes and then scale back their conversion rates. Transmission investment is expected to increase as host conditions deteriorate (Pollitt *et al.*, 2011a), such as when red blood cell numbers are dropping precipitously (five to ten days post-infection, Cameron *et al.*, 2012). Thus a relatively high fraction of parasites may be committed to sexual differentiation when they are removed from donor mice five or ten days post-infection and inoculated into experimental mice (Mackinnon & Read, 1999). High levels of transmission investment are thought to be maladaptive early in infection (Koella & Antia, 1995), so parasites may restrain their transmission investment with improved host conditions. These two explanations are not mutually exclusive, and a combination of immunity and plastic

conversion rates may best explain gametocyte dynamics.

Despite conflicting results on how malaria parasites alter their transmission investment with changing resource availability, theory consistently suggest that transmission investment should be reduced when malaria strains coinfect the same host (McKenzie & Bossert, 1998; Mideo & Day, 2008). That prediction was subsequently confirmed in experimental *P. chabaudi* infections of mice (Pollitt *et al.*, 2011b). To test the strength of that finding, we simulate single infections with varying levels of transmission investment, finding that all three methods can detect a wholesale reduction in conversion rate (Fig. D.3). Thus, while current methods cannot necessarily describe how conversion rates vary through time, they may be capable of detecting overall changes in the conversion rate across infections. The finding that *P. chabaudi* strains reduce their transmission investment in coinfections may therefore be robust to errors in estimating conversion rates.

5.7 Alternative approach

We expand a recent statistical model of asexual growth in malaria parasites (Metcalf *et al.*, 2011) to attempt to correct for the problem of double-counting gametocytes. Asexual growth can be approximated by using linear regression to estimate the effective propagation number, $P_{e,t}$ at a given time step:

$$I_{t+1} = P_{e,t} I_t S_t \tag{5.4}$$

where I_t indicates the total number of infected red blood cells excluding any mature gametocytes, and S_t is the number of uninfected red blood cells. Thus I_t represents asexual parasites and immature sexual stages. Using linear regression as described by Metcalf *et al.* (2011), the time-varying growth $P_{e,t}$ can be estimated for each time step. If no gametocytes carried over into the next generation, we could approximate gametocyte dynamics as

$$G_{t+3} = c_t P_{e,t} I_t S_t \tag{5.5}$$

where c_t is again the conversion rate. Here the time lag is three days because the effective propagation number $P_{e,t}$ describes the invasion success of parasites sampled at time t. Those parasites will give rise to another generation of infected

red blood cells at time $t+1$, of which some fraction c_t will have begun the process of sexual differentiation that will be complete by time $t+3$. Since gametocytes are likely to carry over, we can add those terms:

$$G_{t+3} = c_t P_{e,t} I_t S_t + \epsilon G_{t+2} \tag{5.6}$$

with ϵ indicating the fraction of previously sampled gametocytes that persists to the current time point. While the number of gametocytes that persist is likely to vary through time, the fraction should be approximately constant. By analogy to susceptible reconstruction in epidemiology (e.g., Bjørnstad *et al.*, 2002) we may recast Eqn. 5.6 as a cumulative recursion in terms of infected and susceptible cells, as well as the gametocyte abundance at the time point when gametocytes could first be observed:

$$G_t = \left(\sum_{j=4}^{t} \epsilon^{t-j} c_{j-3} P_{e,j-3} I_{j-3} S_{j-3} \right) + \epsilon^{t-3} G_3 \tag{5.7}$$

In the simulated data, mature gametocytes are first observed at the third time point G_3, and this value would be used as a starting point for subsequent time steps. However, there is likely to be some error in the measured G_3 that could bias the fits to subsequent time points, so we instead fit G_3 as an additional parameter in the model.

Rather than fitting each c_t independently (which would be possible but extremely parameter-wasteful), we calculate the time-varying conversion rate as a smooth curve. Specifically, we calculate the spline basis functions for the sampled time points for five curves of increasing complexity, and then use AIC values to determine how much complexity is justified by our simulated data. We consider model fits assuming the conversion rate is (1) constant; (2) linear; (3) parabolic; (4) cubic; (5) or a cubic spline with one interior knot. For time-varying conversion rates, any polynomial up to a particular order can be described by a linear combination of the spline basis functions of the same order (e.g., de Boor, 2001). In **R** (R Project for Statistical Computing, http://r-project.org/), we obtain these basis functions using *bs* with the argument *intercept=TRUE*, which returns a matrix of coefficients describing these basis functions with one column for each degree,

one column for the intercept (and an additional column when an interior knot is used). We then need only fit a small number of parameters: one for each column of the basis matrix, the fraction of gametocytes persisting to the next sample, ϵ, and the initial number of gametocytes observed, G_3. For a given curve, the best fit parameters can be estimated by minimizing the sum squared error. Given that gametocyte abundance varies over several orders of magnitude, we calculate the sum of the squared error from the logged observed and predicted gametocyte abundance. We use the Nelder-Mead algorithm in the *optim* function, constraining G_3 and ϵ to be positive by estimating them on a log scale and c_t to vary between zero and one using a complementary log-log scale. While c_t of greater complexity should always be expected to fit better, we calculate the AIC values to compare across these models:

$$AIC = n * ln\left(\frac{sse}{n}\right) + 2p \tag{5.8}$$

where n is the number of observations used in the fitting, sse is the sum squared error of the best fit parameters, and p is the number of parameters used in the model. Code for the optimization can be found in the appendix.

Encouragingly, we find that this elaboration of the TSIR (Metcalf *et al.*, 2011) yields more reliable estimates of the time-varying conversion rate. When we simulate data assuming a fixed conversion rate, the spline method recapitulates the fixed conversion rate with a relatively modest bias (Fig. 5.3). The spline method consistently underestimates the true conversion rate because of the gametocytes that have died by the time the infection is sampled. When we correct the gametocyte abundances for this mortality, the estimate conversion rate is much closer to the true value (Fig. D.5). The estimated conversion rate tends to increase towards the end of infection, because sampling occurs slightly earlier in the diurnal cycle as the infection wears on due to the slightly-longer than 24 hour life cycle (Fig. 5.1, 5.2). Since this greater number of gametocytes cannot be accounted for in the effective propagation number, the spline method increases the estimated conversion rate to achieve a good fit to observed gametocyte abundance. This error is small and likely to be be negligible in reality, assuming that synchronized dynamics continue over the sampling period.

The spline method can also be used to characterize time-varying conversion rates. We apply the fitting algorithm to data simulated with a time-varying con-

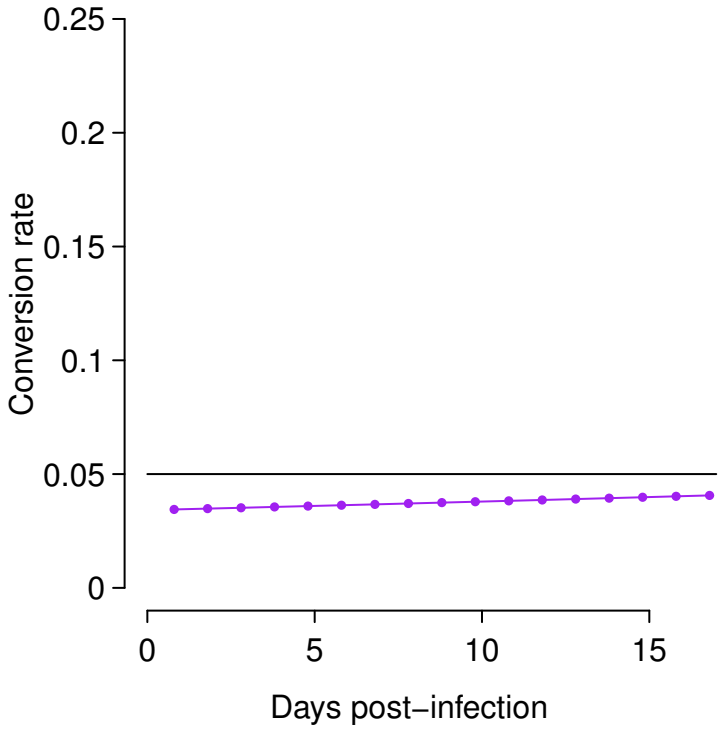

Figure 5.3. Conversion rates estimated from a spline fit to simulated data (purple dots and black lines, respectively) using two parameters (a slope and an intercept). This fitted conversion rate represents the best fit according to AIC values (AIC = −135), with the exception of a more complicated estimated conversion rate that gave a similar AIC value (AIC = −137). The other fitted conversion rates and AIC values can be found in Fig. D.4.

version rate (taken from Greischar *et al.*, manuscript) and find that the fitted conversion rate exhibits key features of the real conversion rate (Fig. 5.4A), including the time lag before transmission investment that has been predicted by theory (Koella & Antia 1995, Greischar *et al.* manuscript). The spline approach fails to capture the shape of the true conversion rate late in infection, mainly because conversion rates are so high that the effective propagation number is a poor estimate of asexual growth. Methods to estimate effective propagation were developed under the assumption that most infected red blood cells were asexuals, so that the error caused by those parasites developing into gametocytes would be minimal (Metcalf *et al.*, 2011). If we assume that developing sexual stages can be distinguished from asexual forms—for example, through early markers of gameto-

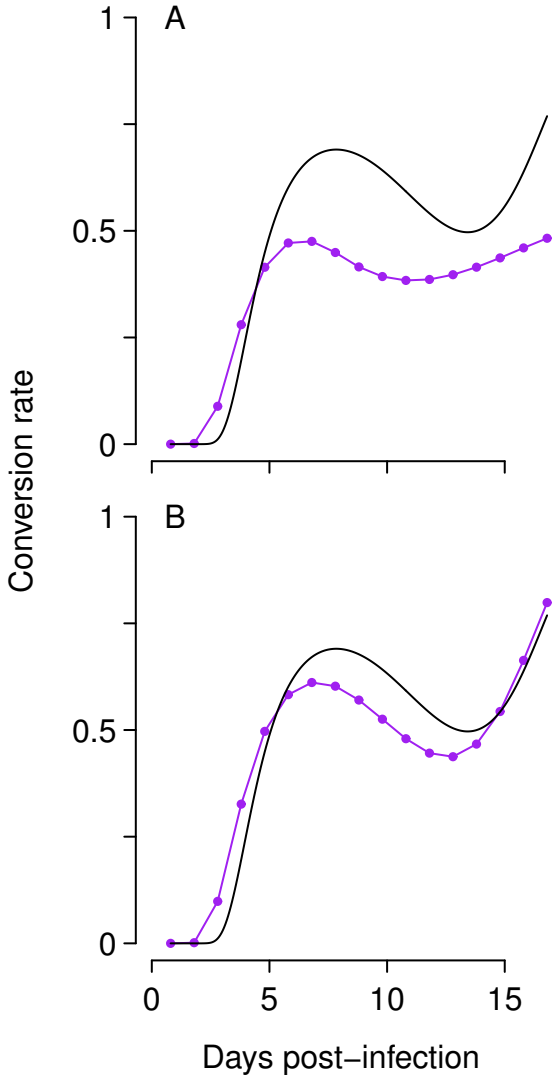

Figure 5.4. Conversion rates estimated from spline fits to simulated data (purple dots), with the real conversion rate shown in black. The time-varying conversion rate used to simulate the data was the predicted optimum strategy for single infections lasting 20 days in the absence of immunity (from Greischar *et al.*, manuscript). From those simulated data, the conversion rate was either estimated assuming that developing gametocytes cannot be distinguished from asexual parasites (A), or using a modified method assuming that the effective propagation number could be estimated from the abundance of asexual parasites only (B). Modified method replaces Eqn. 5.7 with details in appendix.

cyte differentiation—and the effective propagation number estimated accordingly, we can used a modified version of Eqn. 5.7 to obtain a much clearer picture of the

true conversion rate (Fig. 5.4B).

This alternative approach is subject to the same limitations that have always applied to estimated conversion rates: the inferred transmission investment will be biased whenever there is differential mortality of sexual and asexual stages. However, the effective propagation number, P_e has been used to identify when immunity is constraining asexual growth (Metcalf *et al.*, 2011), and P_e must be calculated to estimate the conversion rate via the spline method. Again making use of simulated data, now with immunity, we find that this approach is better able to cope with immune-mediated clearance of asexual parasites (Fig. D.6).

We use this approach on a published data set, with observations of mice infected with a drug-resistant *P. chabaudi* strain and not given any anti-malarial drugs (Huijben *et al.*, 2010a,b). The spline method was able to rule out the null hypothesis of fixed conversion rates in four out of six mice (Fig. 5.5). The lowest AIC value was always associated with a plastic conversion rates, but in two of the mice (A & B), the AIC values were not different enough to justify dismissing fixed conversion as a possibility (Sakamoto *et al.*, 1986). Though the same parasite strain was used for all six mice, we see a surprising amount of variation across hosts. Consistent with conversion rates estimated using different methods from another data set (Pollitt *et al.*, 2011b), we see that the estimated conversion tends to begin at a relatively high level before declining and then increasing after the peak of infection. For comparison, we plot the abundance of red blood cells, infected red blood cells, and gametocytes for all six mice (Fig. D.7).

5.8 Concluding remarks

Researchers are rarely able to measure transmission investment directly and then only under tightly controlled conditions. By fixing infected and uninfected red blood cells in a monolayer *in vitro*, Bruce *et al.* (1990) observed the fraction of parasites committing to sexual differentiation from a cohort, which varied from less than one percent to over 70%, depending on culture conditions. These experiments suggest considerable scope for adaptive plasticity in transmission investment. If that variability can be well-characterized, it may suggest means of manipulating conversion rates to reduce the malaria disease burden. However, in more realistic

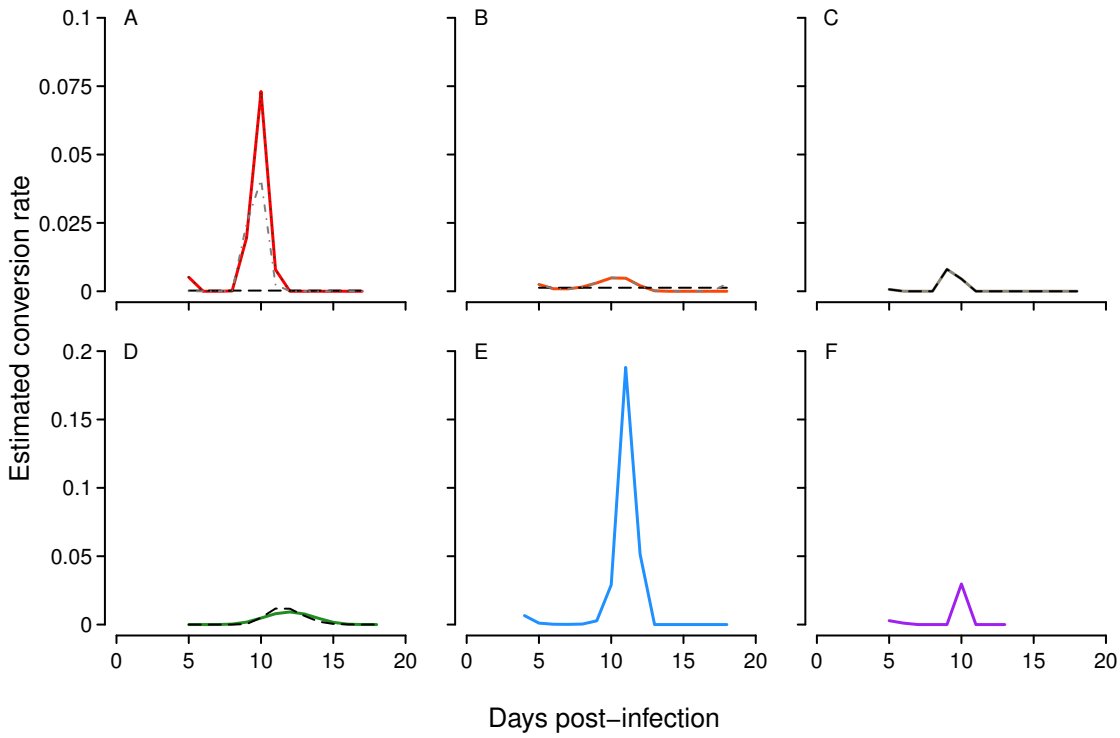

Figure 5.5. Conversion rates estimated from spline fits to real data for six mice. Solid lines indicate the fit giving the lowest AIC values. When other fits gave similar AIC values (i.e., within two units of the lowest AIC), those are also shown as broken black or gray lines.

settings—whether a living host or a flask of blood—transmission investment must be inferred rather than directly measured. Surprisingly, we found that the caveats often thought to hinder inference methods were only one part of the problem. While differential mortality between asexual and transmission stages can lead to over- or underestimation of conversion rates, the real problem is one of distinguishing gametocytes produced from separate cycles of synchronous infection.

Our simulations suggest that at least some of the observed patterns of variation in estimated conversion rates *in vivo* can be explained without needing to invoke plastic transmission investment. While researchers often worry about error introduced by unequal mortality of sexual and asexual forms (Cameron *et al.*, 2012), double-counting gametocytes can qualitatively alter results. Gametocytes may often survive longer than the length of the asexual cycle according to the mortality rates reported by Reece *et al.* (2003), so that gametocytes from different cohorts

of parasites may be counted as emerging from the same round of bursting and invasion. Hence the model suggests that gametocytes from different cohorts will tend to accumulate more as the number of asexual parasites increases (Fig. 5.1), giving the false impression that conversion rates are increasing as red blood cell number decline. Although *in vitro* work strongly suggests that conversion rates are plastic (Bruce *et al.*, 1990), current methods (Eqns. 5.1-5.3) cannot be relied upon to detect constant transmission investment.

Early markers of sexual differentiation cannot solve these problems, except under the special conditions. We propose an alternative statistical approach, building on the time-series methods of Metcalf *et al.* (2011). This method appears capable of distinguishing between fixed and time-varying investment with with relatively few parameters to fit to data. Further, it suggests that we can leverage the rich body of existing data to revisit the problem of how malaria parasites modify transmission investment in response to the changing within-host environment.

5.9 Acknowledgments

I thank Dave Kennedy and Elsa Hansen for valuable discussion.

5.10 Notes

This chapter represents a collaboration with Nicole Mideo, Andrew F. Read, and Ottar Bjørnstad, who will be coauthors on the eventual publication, planned as an opinion piece.

Chapter 6

Discussion

Malaria parasites display curious life history traits within the vertebrate host, among them synchronous infection dynamics—which should enhance competition for resources—and reproductive restraint, with parasites investing substantially less into the production of transmission stages than the presumed optimum. These traits should be costly, and the fact that they are frequently observed suggests a gap in our understanding. The objectives of this dissertation are to trace the transmission consequences of synchrony and reproductive restraint while assessing our ability to make inferences about the underlying processes from time series data of parasite dynamics.

The model shows that parasite fitness can be enhanced by synchrony (Chapter 2), analogous to the ways in which diverse free-living organisms employ synchronized reproduction to overwhelm natural enemies and overcome mate-finding difficulties (Kelly & Sork, 2002). In line with intuition, synchrony is predicted to exacerbate interference competition among merozoites, because the merozoites emerge in unison, but surprisingly, this effect can in fact increase transmission success if it damps extreme oscillations in parasite numbers. In Chapter 3, I examine intra-strain competition and the loss of synchrony *in vitro*. Invasion assays suggest that merozoite invasion rates *per se* are not density-dependent but rather merozoites are more likely to be wasted infecting already-invaded red blood cells when conditions are crowded. Fitting a distributed-delay *in vitro* model to detailed time series data, I find that the rate of viable new infections may vary with merozoites and uninfected red blood cell abundance, a form of density-dependence

that may often favor synchronous parasites. Since synchrony is also likely to be favored when transmission investment is low, I also examine the factors that should select for reproductive restraint by generalizing the fixed delay *in vivo* model from Chapter 2 to allow for time-varying transmission investment. Using an optimization algorithm, I identify strategies that should maximize the cumulative potential transmission to mosquitoes (Chapter 4). These optimal strategies suggest that reproductive restraint is beneficial early in infection and in the presence of saturating immune measures or a competing strain. Finally, I test current methods for inferring transmission investment on simulated data under conditions most likely to yield accurate estimates (Chapter 5). The methods cannot cope with fact that some gametocytes are likely to survive through multiple rounds of sampling and therefore confound the estimated transmission investment from distinct cohorts of parasites. I develop an alternative method that shows promise at identifying fixed and time-varying strategies from simulated and real time series data.

Synchrony is predicted to be advantageous when gametocytes are rare and the challenge of mate-finding would be expected to present a major barrier to infecting mosquitoes. Interestingly, the optimum level of transmission investment did not vary much depending on whether the infection was asynchronous or highly synchronized. In order for synchrony to make a difference, investment would need to vary on the same time scale as the oscillations in parasite abundance, that is, over the length of the asexual life cycle (a 24 hour period for *P. chabaudi*, Landau & Boulard, 1978). More importantly, if parasite populations can expand to large numbers and then invest in gametocyte production, we would expect gametocytes to emerge in large numbers over a very short time window, side-stepping the problem of mate-finding without the need to resort to synchrony. Therefore the selection pressures other than the challenge mate-finding may be needed to understand when synchrony should be favored, and competitive interactions are likely to strongly influence the transmission consequences of different temporal dynamics.

The dynamics of host exploitation vary considerably depending on the form of density-dependent competition. If interference takes a hyperbolic form (Eqn. 2.2), it has the effect of damping extreme oscillations in parasite abundance, which would otherwise be costly due to Jensen's inequality (Chapter 2). Because synchrony enhances the impact of interference competition, the damping is even more pro-

nounced in synchronous infections, and the model predicts those dynamics should favor synchrony over a large portion of the parameter space. This effect has no clear analogy in the masting literature, but modeling of RNA viruses suggests that pathogens can benefit from mutation rates so high they reduce the per capita growth rate and thereby keep the host alive long enough to transmit for longer periods (O'Fallon, 2011). While the present models do not consider the possibility of host death, it is entirely possible for parasites to overexploit red blood cell populations so that gametocyte production declines precipitously until erythropoiesis replenishes the pool of resources (Fig. 2.4). Thus faster within-host growth is not always favorable, even setting aside the cost of host mortality.

Subsequent analysis of parasite dynamics *in vitro* suggests that hyperbolic interference is a plausible scenario for the form of interference competition (Fig. 3.4). It is therefore possible that rather than suffering from competition, synchronous parasites may actually benefit from interference. Invasion assays suggest that interference does not change the rate of invasion, but instead occurs as two or more parasites attempt to develop within the same red blood cell (Chapter 3). Interestingly, multiple infections are far less common when cultures are shaken rather than static (Allen & Kirk, 2010), suggesting that some care must be taken in extrapolating the results of our static invasion assays to the relatively well-mixed environment within the host. However, particularly in patients with severe malaria, a large fraction of the parasite population may be sequestered out of circulation and not well-mixed (reviewed in Cunnington *et al.*, 2013). When a significant portion of the parasite population is sequestered, superinfection of red blood cells could be an important constraint on further population expansion.

Merozoite wastage—while far from ideal—could serve to prevent overexploitation of host resources. An alternative means of avoiding overexploitation of host resources would be adaptive modulation of burst sizes (N. Mideo, *pers. comm.*), such that parasites produce fewer merozoites per schizont in crowded conditions. Adaptive modulation of burst sizes would not have been possible in the invasion assays conducted for Chapter 3, since parasites were reared to the schizont stage in a stock culture prior to initiating the invasion assays. However, plastic burst sizes would not be expected to be advantageous unless producing a smaller number of merozoites would allow each one to be of higher quality, in terms of invasion ability

or longevity. While burst sizes are known to vary even within a single strain of *P. falciparum* (Reilly *et al.*, 2007), this variability does not appear to be adaptive. The fact that the *P. falciparum* strain Dd2 can make more merozoites faster, and maintain a higher intrinsic growth rate compared with the HB3 strain (Reilly *et al.*, 2007) calls into question whether tradeoffs exist between quality versus quantity of merozoites. When parasites have been reared at different parasitemias and fixed in a monolayer to follow commitment to sexual versus asexual development, the mean number of asexual parasites produced per schizont does not change in any consistent manner with the parasitemia of origin (Bruce *et al.*, 1990). While it might enhance parasite fitness, there is no evidence that burst sizes can be plastically modified in the same way as transmission investment. Reinvasion of occupied red blood cells does occur, though the frequency varies across parasite species and hosts (Garnham, 1966; Simpson *et al.*, 1999). Characterizing the dynamics of merozoite wastage across species could highlight different strategies of modulating host exploitation.

Regardless of the underlying mechanism, the advantages of restrained growth disappear in the presence of an imprudent competing strain, whether slower growth is due to synchrony (Fig. 2.6) or greater investment in gametocyte production (Fig. 4.4). Infections with multiple malaria strains are extremely common (e.g., Färnert *et al.*, 1997; Jafari-Guemouri *et al.*, 2006), but the fitness impact on transmission can be difficult to tease apart. A much-simplified version of the conflict between different levels of selection is described in Eqn. 4.16, suggesting that parasites can benefit from the overall increase in gametocyte numbers that follows having two strains investing in transmission simultaneously, but each strain is also under selection to maximize its representation in a mosquito's blood meal. The reality is made much more complicated by interactions with the immune system. Parasites likely pay a cost of coinfecting with other parasites; it appears that the host limits the total parasite density (Bruce & Day, 2002), such that each clone within a diverse infection cannot grow to densities as high as it would achieve in a single infection. In addition to the costs within the vertebrate host, infections with excessive numbers of gametocytes may compromise replication within the mosquito vector and reduce vector survival (Pollitt *et al.*, 2013), and coinfections may produce larger numbers of gametocytes (Taylor *et al.*, 1998).

The costs of apparent or direct competition among parasite clones are likely substantial, but there may be also be considerably greater opportunities for transmission from mixed infections. Individuals infected with *P. falciparum* maintained gametocytes three times as long if they had mixed versus single infections in an area of seasonal malaria transmission (Nassir *et al.*, 2005). The ability to persist through the dry season is necessary for the long-term persistence of a parasite lineage, and if coinfections give dramatically better odds for persistence, it could select for parasites that are capable of coexisting in multi-strain assemblages and place limits on the intensity of within-host competition. Nassir *et al.* (2005) also observed that infections with gametocytes were cleared an higher rate overall than infections where only asexual forms could be detecting, potentially pointing to the cost of gametocyte production in terms of per capita growth within the host. Yet the cost of gametocyte investment may be reduced by coinfection if strain diversity hinders efficient immune clearance. Accordingly, experimental rodent infections suggest a cost to the host of removing diverse parasites, since hosts with mixed-strain infections experienced more severe weight loss and anemia that could not be explained by differences in total parasite abundance (Taylor *et al.*, 1998).

Aside from prolonging the infectious period, multi-strain infections may also enhance infectiousness. The difficulty of clearing mixed infections may help explaining why more two coinfecting parasites strains would infect more mosquitoes than could be explained by their performance in single strain infections (Taylor *et al.*, 1997b). Even if coinfection drives down the asexual densities of each clone, the impact on transmission success far from obvious. Mosquitoes can reveal more parasite diversity than can be detected in the humans who supplied the blood meals, suggesting that rarity in the circulating parasite population need not be a barrier to transmission (Nwakanma *et al.*, 2008). The costs of competition could be further reduced by relatedness, and multi-strain infections can show a surprising degree of relatedness (Nkhoma *et al.*, 2012). In general, opposing selection pressures would be expected to act on individual strains versus the community of strains residing in a given host, but relatedness could align those selection pressures allow the collection of strains to move closer to the optimum level of host exploitation (reviewed in Chao *et al.*, 2000). The coinfection model utilized in Chapters 2 and 4 could be extended to determine whether the complex selection

pressures will ultimately reduce or enhance the virulence to the host.

The models developed to dissect the interplay between selective forces can also be useful for testing our ability to infer unobserved infection dynamics. Using these mechanistic models to generate simulated data sets can help to identify shortcomings in existing approaches. Analogously, simulated data of helminth coinfections has been used to critique common statistical methods for detecting interference versus facilitation among interacting species (Fenton *et al.*, 2010). The present model suggests that while a surprising amount of information can be gleaned from time series data, intuition often serves as a poor guide in the face of the complex and nonlinear processes. The distributed delay *in vitro* model shows that cycle length can be over- or underestimated depending on both the intrinsic growth rates and the developmental plasticity (Fig. 3.2). Similarly, simulated data on asexual and gametocyte abundance show that popular inference methods fail because errors are likely to depend on gametocyte abundance measured previously. It is perhaps not surprising that inference methods would fail in the complex and rapidly changing environment within the host, but analyzing parasite traits in the relatively simple environment of artificial blood culture also proves challenging. In both cases, errors vary depending on the rate of expansion in the parasite population, whether because growth alters the distribution of parasite life stages or because growth increases the number of gametocytes surviving through successive samples and fouling estimates of conversion rates. Thus inference methods perform better when they can account for the underlying growth or decline of the infection.

The malaria life cycle within the vertebrate host encapsulates tradeoffs conceptually identical to those facing diverse parasitic and free-living organisms: how to overcome natural enemies and find mates while minimizing the cost of competition, and how to balance growth and reproduction. The present collection of work uses mechanistic models of malaria infection to determine when synchrony and reproductive restraint should be viable solutions to those tradeoffs, predictions with broad relevance. The models also highlight the conceptual challenges associated with testing those predictions, thereby serving as a basis for further work examining the rich diversity in parasite life history.

Appendix A

Chapter 2 Supplemental Information

A.1 Description of Modeling Framework

A.1.1 Age-structured model

The age-structured model is identical to the single-strain model, except that the infected cells committed to the asexual cycle are split into young and mature classes (I_y and I_m, respectively), both with fixed development times (α_y and α_m, respectively). Saturating immunity targets only the mature infected red blood cells (I_m), so Eq. D.2 becomes

$$\begin{aligned}\frac{dI_y(t)}{dt} &= (1-c)p(t)R(t)M(t) - \mu I_y(t) \qquad \text{(A.1)}\\ &\quad -(1-c)p(t-\alpha_y)R(t-\alpha_y)M(t-\alpha_y)\exp(-\mu\alpha_y)\\ \frac{dI_m(t)}{dt} &= (1-c)p(t-\alpha_y)R(t-\alpha_y)M(t-\alpha_y)exp(-\mu\alpha_y) - \mu I_m(t)\\ &\quad -\frac{a}{b+I_m(t)}I_m(t) - (1-c)p(t-\alpha)R(t-\alpha)M(t-\alpha)S_m \qquad \text{(A.2)}\end{aligned}$$

where the survivorship is the mortality rates integrated over the respective developmental periods

$$S_m = \exp\left(-\int_{t-\alpha_y-\alpha_m}^{t-\alpha_m}\mu d\omega - \int_{t-\alpha_m}^{t}\mu + \frac{a}{b+I_m(\omega)}d\omega\right) \qquad \text{(A.3)}$$

A.1.2 Two strain model

The coinfection model tracks infected red blood cells (sexual and asexual), merozoites, and gametocytes for two strains in complete analogy to our single-strain model.

$$\begin{aligned}\frac{dR(t)}{dt} &= \lambda\left(1-\frac{R(t)}{K_{start}}\right) \\ &\quad -\mu R(t) - p(t)R(t)M_1(t) - p(t)R(t)M_2(t)\end{aligned} \tag{A.4}$$

where I_A indicates asexual infected red blood cells of both strains ($I_1 + I_2$).

$$\begin{aligned}\frac{dI_1(t)}{dt} &= (1-c)p(t)R(t)M_1(t) - \mu I_1(t) - \frac{a}{b+I_A(t)}I_1(t) \\ &\quad -(1-c)p(t-\alpha)R(t-\alpha)M_1(t-\alpha)S_A(t)\end{aligned} \tag{A.5}$$

$$\begin{aligned}\frac{dI_2(t)}{dt} &= (1-c)p(t)R(t)M_2(t) - \mu I_2(t) - \frac{a}{b+I_A(t)}I_2(t) \\ &\quad -(1-c)p(t-\alpha)R(t-\alpha)M_2(t-\alpha)S_A(t)\end{aligned} \tag{A.6}$$

$$\begin{aligned}\frac{dM_1(t)}{dt} &= \beta(1-c)p(t-\alpha)R(t-\alpha)M_1(t-\alpha)S_A(t) \\ &\quad -p(t)R(t)M_1(t) - \mu_Z M_1(t)\end{aligned} \tag{A.7}$$

$$\begin{aligned}\frac{dM_2(t)}{dt} &= \beta(1-c)p(t-\alpha)R(t-\alpha)M_2(t-\alpha)S_A(t) \\ &\quad -p(t)R(t)M_2(t) - \mu_Z M_2(t)\end{aligned} \tag{A.8}$$

$$\begin{aligned}\frac{dI_{G1}(t)}{dt} &= cp(t)R(t)M_1(t) - \mu I_{G1}(t) \\ &\quad -cp(t-\alpha_G)R(t-\alpha_G)M_1(t-\alpha_G)\exp\left(-\mu\alpha_G\right)\end{aligned} \tag{A.9}$$

$$\begin{aligned}\frac{dI_{G2}(t)}{dt} &= cp(t)R(t)M_2(t) - \mu I_{G2}(t) \\ &\quad -cp(t-\alpha_G)R(t-\alpha_G)M_2(t-\alpha_G)\exp\left(-\mu\alpha_G\right)\end{aligned} \tag{A.10}$$

$$\frac{dG_1(t)}{dt} = cp(t-\alpha_G)R(t-\alpha_G)M_1(t-\alpha_G)\exp\left(-\mu\alpha_G\right) - \mu_G G_1(t) \tag{A.11}$$

$$\frac{dG_2(t)}{dt} = cp(t-\alpha_G)R(t-\alpha_G)M_2(t-\alpha_G)\exp\left(-\mu\alpha_G\right) - \mu_G G_2(t) \tag{A.12}$$

with

$$S_A(t) = \exp\left(-\left[\int_{t-\alpha}^{t}\mu + \frac{a}{b+I_A(\omega)}d\omega\right]\right) \tag{A.13}$$

A.1.3 Annotated code for basic fixed delay model

The following is the code to run the basic fixed delay model described in Chapter 2. First, the delayed differential equation solver package must be loaded:

```
> library(PBSddesolve) # dde solver
```

I create the following function to set up the starting conditions assuming a Beta age distribution for the parasite inoculum:

```
> pulseBeta = function(initialI, shape, time){
+   res = rep(NA, length(time))
+   for (num in 1:length(time)){
+     res[num] = initialI*(dbeta(time[num], shape, shape))
+     }
+   return(res)
+   }
```

Note that the shape parameters are equal. I also define functions to allow for immune clearance (*satImm3*) and interference competition among merozoites (*pinf*):

```
> # Immunity with type II or III functional response
+     #(determined by betaValue parameter)
> satImm3 = function(aValue, bValue, betaValue, numI){
+   # note that when betaValue = 1, this function reduces
+       # to the type II
+   # functional response
+   # betaValue was set to 1 for all simulations shown in this thesis
+   return(aValue*(numI^(betaValue-1))/((bValue)+(numI^betaValue)))
+   }
> pinf = function(pVal, qVal, mero, rbc){
+   return(pVal/(1+qVal*(mero/rbc)))
+   }
```

Now I can define the basic delay function, which tracks red blood cells (R), infected red blood cells in asexual development (In), infected red blood cells developing

into gametocytes (InG), merozoites (M), and infectious gametocytes (G). 'Eta' serves to integrate the mortality rates, which makes it easy to calculate survival of different stages when mortality rates vary through time (e.g., with saturating immune clearance). I have four other state variables that serve as useful checks that the model is working but do not feed back into any equations, including infected red blood cell recruitment (asexual only, 'Irec'), merozoite recruitment ('Mrec'), the total number of infected red blood cells ('Itot'), and the gametocyte recruitment ('Grec').

After defining the parameters (including the initial conditions), and the state variables, the *pastvalue* function is called to define the delays. The function is split into three sets of code: (1) the model with delayed terms removed, so that the appropriate delayed terms can be added later; (2) the delayed terms for when time is greater than one full delay (α); (3) the delayed terms describing the transitions of the initial inoculum, which is the most conceptually challenging portion.

```
> # basic model with ratio-dependent invasion function (pinf)
> sis.delay = function (t, y, parms){
+         ## parameters--all units should be in terms of days
+         # RBC dynamics
+         mu = parms[1] # mortality rate of RBC
+         lambda = parms[2] # maximum replenishment rate of RBCs
+         K = parms[3] # carrying capacity of RBC population
+                 # without mortality
+         #infected RBC dynamics
+         p = parms[4] # rate of infection of RBC given contact
+                 # between RBC and merozoite
+   q = parms[5] # exponent of merozoite numbers, to induce
+                 # merozoite-competition when q<1
+         alpha = parms[6] # delay until infected RBC bursts
+                       # (committed to asexual cycle)
+   alphaG = parms[7] # delay until infected RBC bursts
+                 #(committed to sexual cycle)
+         a = parms[8] # limit in type II saturating immune
+                 # function: removes infected RBCs
```

```
+         b = parms[9] # days required to reach
+                # an immune-mediated removal
+                # rate of a/2 (half-saturation point)
+   betaI = parms[10]
+         # merozoites
+         beta = parms[11] # burst size of infected RBCs:
+                number of merozoites that emerge
+         muz = parms[12] # intrinsic mortality rate of
+                # free merozoites
+         # gametocytes
+         mug = parms[13] # intrinsic mortality rate of gametocytes
+         repro = parms[14] # proportion of infected RBCs committed
+                # to producing gametocytes
+         sigma = parms[15] # proportion of immune response acting
+                # against merozoites (modifies a)
+   ## Initial conditions
+   sP = parms[16] # shape parameter form beta distribution
+                # in starting values
+         R0 = parms[17] # initial number of uninfected RBCs
+         I0 = parms[18] # initial number of infected RBCs
+   IG0 = parms[19] # initial number of infected RBCs
+                # committed to making gametocytes
+         M0 = parms[20] # initial number of free merozoites
+         G0 = parms[21] # initial number of gametocytes
+
+         ## variables to keep track of (this is where R sets
+                # these equal to the initial values
+                # or updates them)
+         R = y[1] # red blood cells (RBCs)
+         In = y[2] # infected RBCs
+         InG = y[3] # infected RBCs committed to making gametocytes
+   M = y[4] # free merozoites (emerged from burst RBC)
+         G = y[5] # gametocytes (emerged from burst RBC)
```

```
+         Eta = y[6] # mortality rate of infected RBCs
+   # the following state variables assist in analyzing the model,
+                # but do not feedback into the model
+   Irec = y[7] # recruitment into infected class
+   Mrec = y[8] # recruitment into merozoite class
+   Itot = y[9] # total asexual pRBCs
+   Grec = y[10] # gametocyte recruitment
+
+         ## pastvalues
+         # delay
+         if(t>alpha){lag1=pastvalue(t-alpha)}
+   if(t>alphaG){lag2=pastvalue(t-alphaG)}
+
+   # Model without delayed terms
+         dRdt = - mu*R - pinf(p,q,M,R)*R*M + lambda*(1-((R)/K))
+                # no delay in this first equation
+         dIndt = (1-repro)*pinf(p,q,M,R)*R*M - mu*In
+                - satImm3((1 - sigma)*a, b, betaI, In)*In
+                 # plus delay
+                #(omitted in this portion of the code)
+         dInGdt = repro*pinf(p,q,M,R)*R*M - mu*InG # plus delay
+   dMdt = -pinf(p,q,M,R)*R*M - muz*M
+        - satImm3(sigma*a, b, betaI, M)*M
+                # plus delay (omitted in this portion of the code)
+         dGdt = - mug*G # plus delay
+                # (omitted in this portion of the code)
+
+         # Infected RBC survival through delay
+         S = exp(-Eta);if(t>alpha){S=exp(-Eta + lag1[6])}
+   SG = exp(-mu*t);if(t>alphaG){SG = exp(-mu*alphaG)}
+
+
+
```

```
+         # Adding in delayed terms
+         if(t>alpha){dIndt=dIndt
+           - (1-repro)*pinf(p,q,lag1[4],lag1[1])*lag1[1]*lag1[4]*S}
+   if(t>alphaG){dInGdt = dInGdt
+           - repro*pinf(p,q,lag2[4],lag2[1])*lag2[1]*lag2[4]*SG}
+
+         if(t>alpha){dMdt=dMdt
+         + (1-repro)*beta*pinf(p,q,lag1[4],lag1[1])*lag1[1]*lag1[4]*S}
+         if(t>alphaG){dGdt=dGdt
+        + repro*pinf(p,q,lag2[4],lag2[1])*lag2[1]*lag2[4]*SG}
+
+         # Track cells in initial cohort of infection
+         # (before the simulator has gone through a full delay)
+         if(t<=alpha){dIndt=dIndt - pulseBeta(I0, sP, t)*S}
+   if(t<=alphaG){dInGdt=dInGdt - pulseBeta(IG0, sP, t-1)*SG}
+
+         if(t<=alpha){dMdt=dMdt + beta*pulseBeta(I0, sP, t)*S}
+
+         if(t<=alphaG){dGdt=dGdt + pulseBeta(IG0, sP, t-1)*SG}
+
+         dEta = mu + satImm3((1 - sigma)*a, b, betaI, In)
+                # an infected RBC can die
+                # from intrinsic factors (mu) or from immunity
+
+   dIrec = (1-repro)*pinf(p,q,M,R)*R*M # asexual recruitment only
+
+   if(t<=alpha){dMrec = beta*pulseBeta(I0, sP, t)*S}
+                # number recruited
+                # into merozoite class per infected RBC
+                # (R will return cumulative value)
+   if(t>alpha){dMrec =
+        (1-repro)*beta*pinf(p,q,lag1[4],lag1[1])*lag1[1]*lag1[4]*S}
+
```

```
+   dItot = In
+         if(t<=alphaG){dGrec = pulseBeta(IG0, sP, t-1)*SG}
+         if(t>alphaG){dGrec =
+        + repro*pinf(p,q,lag2[4],lag2[1])*lag2[1]*lag2[4]*SG}
+
+         return(c(dRdt,dIndt,dInGdt,dMdt,dGdt,dEta,dIrec,
+                dMrec,dItot,dGrec))
+         } # end of SI function
```

The recruitment terms serve to allow me to back-calculate how many individuals entered the class at a particular time point, which cannot be gleaned from the abundance alone. The *sis.delay* function will return the cumulative recruitment at every point in the simulation. If I bind the vector of time points to the vector of cumulative recruitment and feed it to the function splinefun, it is straightforward to estimate the derivative of cumulative recruitment (i.e., the instantaneous recruitment) at any point simulated.

The parameter values are set as follows:

```
> # parameter values (convert values from data into
> # per microliter values)
> # calculate total number of RBCs in a healthy mouse
> RBCpermL = 8.5e9 # from Savill et al. 2009
> RBCsperuL = (RBCpermL/10e-3)*10e-6
> maxNewRBCspermL = 0.37e9 # from Savill et al. 2009
> maxNewRBCsperuL = (maxNewRBCspermL/10e-3)*10e-6
> # calculate starting number of parasites injected into a mouse
> weight = 2.4e-3 #24 g = 24e-3kg, avg for female CSI mice given
+        # in Riches et al. 1973
> mLperkg = 95 # again according to Riches et al. 1973
> # for female CSI mice
> mLperMouse = mLperkg*weight
> uLperMouse = mLperMouse*(10e3)
> IperuL = (10e4)/uLperMouse # assume 10e4 infectious
> # dose for each mouse
```

```
> cC = RBCsperuL # carrying capacity of RBCs
> # (with mortality, no infection)
> mu = 0.025 #(0.025/day cited in Miller et al. 2010 for mice)
> lambda = maxNewRBCsperuL # maximum number of new cells entering
+        # according to Savill et al. 2009 (see above)
> K = lambda*cC/(lambda-mu*cC) # carrying capacity of RBC population
+        # in the absence of mortality
> #infected RBC dynamics
> p = 4e-6 #2e-6 #2.5e-6 #3e-6 #plausible values based
+       # on Mideo et al. 2008:
+        # 1e-6  to 1.8e-5 (per day) given contact between
+        # RBC and merozoite
> alpha = 1 # delay until infected RBC bursts
> alphaG = 2 # delay until infected RBC committed
+        # to producing gametocytes bursts
> b = 100 #2000 #20 # speed of saturation (half-saturation point)
+        # in type II immune function
> betaI = 1 # when set to 1, immunity follows a type II response
> # merozoites
> beta = 10 # burst size of infected RBCs
+ # number of merozoites that emerge
> muz = 48 # intrinsic mortality rate of free merozoites
+       # (Gravenor et al. 1995
+        # estimate the mortality rate of free
+        # merozoites to be 72/day)
> # gametocytes
> mug = 4 # intrinsic mortality rate of gametocytes
+ # (=1/8, assumes they live 8 days)
> # Initial conditions
> R0 = cC # uninfected RBC carrying capacity
> I0 = IperuL # 30 # initial number of infected RBCs/microliter
+        # (effective inoculum dose
+        # estimated in Miller et al. 2010, p. 10)
```

```
> IG0 = 0 # initial number of infected RBCs committed
+        # to making gametocytes
+        # (assume to be zero)
> M0 = 0 # initial number of free merozoites
> G0 = 0 # initial number of gametocytes
> # one run
> days = 20 # length of time simulations are run
> h = 0.01 # resolution at which simulations are run
> a = 0 # no immunity
> sigma = 0
> # no merozoite interference
> q = 0
> repro = 0.001
> sP = 1 # asynchronous infection with this shape parameter
> parms=c(mu, lambda, K, p, q, alpha, alphaG, a, b, betaI, beta,
+ muz, mug, repro,sigma, sP, R0, I0, IG0, M0, G0)
> y.out = dde(y=c(R0,I0,IG0, M0,G0,0,0,0,0,0), times=seq(0,days,h),
+ dt = 0.1, func=sis.delay, parms=parms, tol = 1e-10, hbsize=1e7)
> head(y.out)

  time      y1       y2           y3       y4 y5      y6
1 0.00 8500000 43.85965 0.0000000000 0.000000  0 0.00000
2 0.01 8499999 43.98710 0.0005774749 2.992560  0 0.00025
3 0.02 8499998 44.80801 0.0018488845 4.309830  0 0.00050
4 0.03 8499997 45.93395 0.0034254163 4.889250  0 0.00075
5 0.04 8499995 47.19387 0.0051358251 5.143697  0 0.00100
6 0.05 8499993 48.51240 0.0069046893 5.255016  0 0.00125
         y7        y8        y9 y10
1 0.0000000  0.000000 0.0000000   0
2 0.5769486  4.385417 0.4383960   0
3 1.8473806  8.769737 0.8820028   0
4 3.4229904 13.152962 1.3355506   0
5 5.1327561 17.535091 1.8011186   0
6 6.9013543 21.916124 2.2796190   0
```

A.2 Supplemental figures

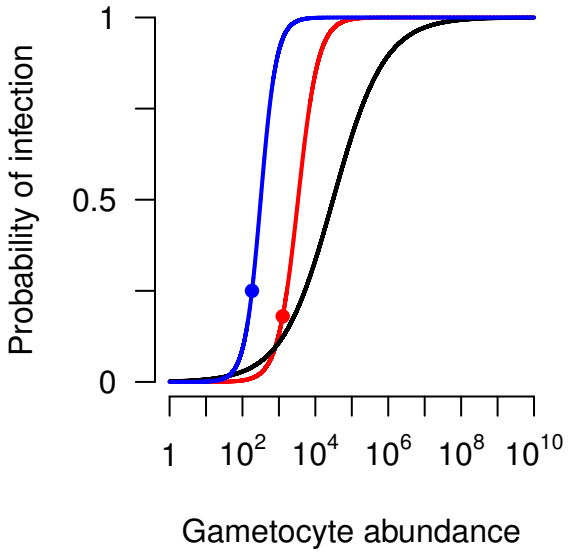

Figure A.1. Extremes in transmission biology: the probability of transmission is shown as a function of gametocyte abundance for drug-sensitive *P. chabaudi* (red, Eqn. 2.13), drug-resistant *P. chabaudi* (black, *probability of transmission* $= \exp(-6.37 + 1.42 \log_{10} G(t))/(1 + \exp(-6.37 + 1.42 \log_{10} G(t)))$, and *P. falciparum* (blue, *probability of transmission* $= 1 \times 10^{-5} G(t)^2/(1 + 1 \times 10^{-5} G(t)^2)$). Equations and parameter values from curves fit to data by Huijben *et al.* 2010a and Bell *et al.* 2012. Red and blue dots represent the inflection points for *P. chabaudi* (drug-sensitive) and *P. falciparum*, respectively, i.e., where the curve switches from accelerating to saturating. The drug-sensitive *P. chabaudi* curve was used for all simulations in the main text. Its inflection point falls below a 50% probability of infection—even though it is derived from a logistic regression—because it is a function of the $\log_{10}$ abundance of gametocytes and the chain rule applies. Note the absence of an inflection point on the drug-resistant *P. chabaudi* curve. Despite its appearance on a log scale, the black curve is saturating over the entire range.

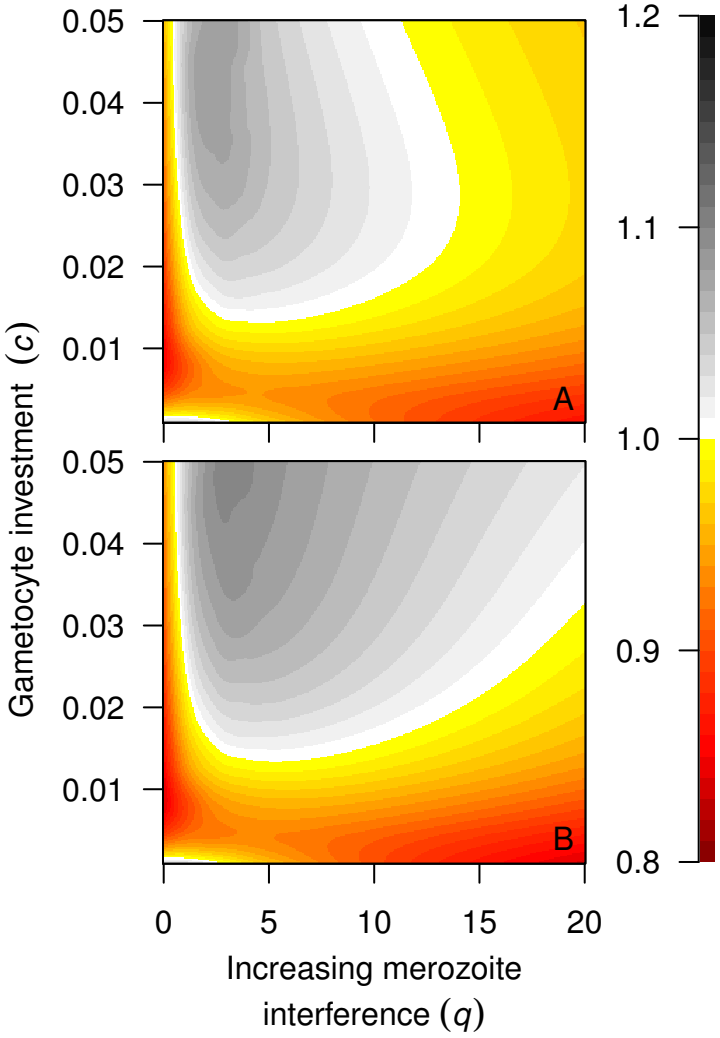

Figure A.2. Smoothed relative fitness of synchronous:asynchronous infections either for no immunity (A, $a = 0$) or for immunity targeting infected red blood cells in the last hour before bursting (B, $a = 1800$, $b = 100$). Younger infected red blood cells are not subject to immune clearance. Panel A is identical to Fig. 2.5A, and is placed here for comparison.

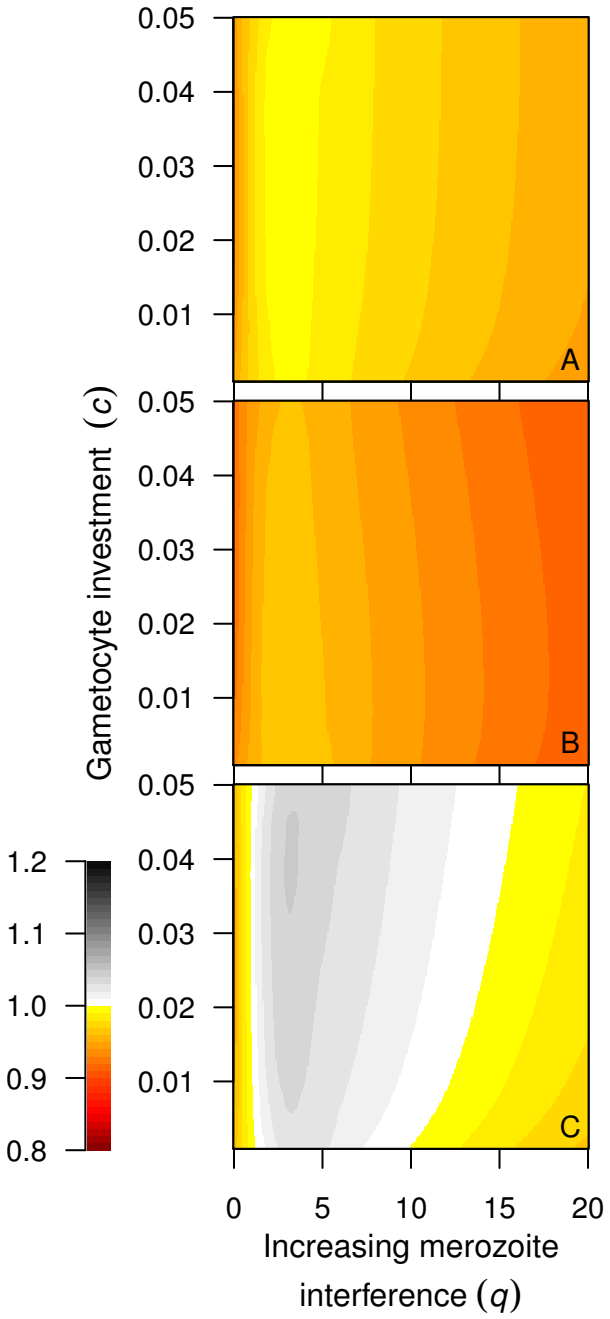

Figure A.3. Smoothed relative fitness in single infections (ratio of cumulative transmission for synchronous:asynchronous strain) calculated using the drug-resistant *P. chabaudi* transmission function (black curve in Fig. A.1). Otherwise, dynamics are identical to Fig. 2.5. Since the transmission function is entirely saturating, the relative fitness does not vary much with changes in gametocyte investment.

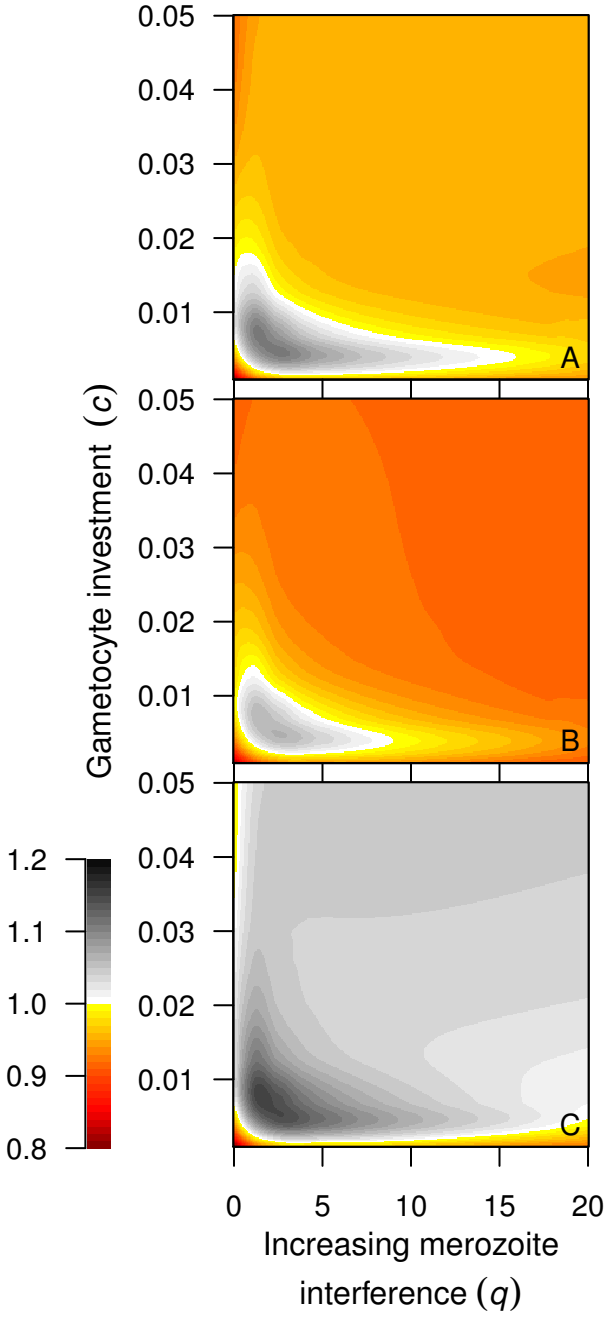

Figure A.4. Smoothed relative fitness in single infections (ratio of cumulative transmission for synchronous:asynchronous strain) calculated using the *P. falciparum* transmission function (blue curve in Fig. A.1). Save for the calculation of relative fitness, dynamics are identical to Fig. 2.5. Since the transmission function saturates earlier, a smaller region of the parameter space is favorable to synchronous parasites in the absence of immunity.

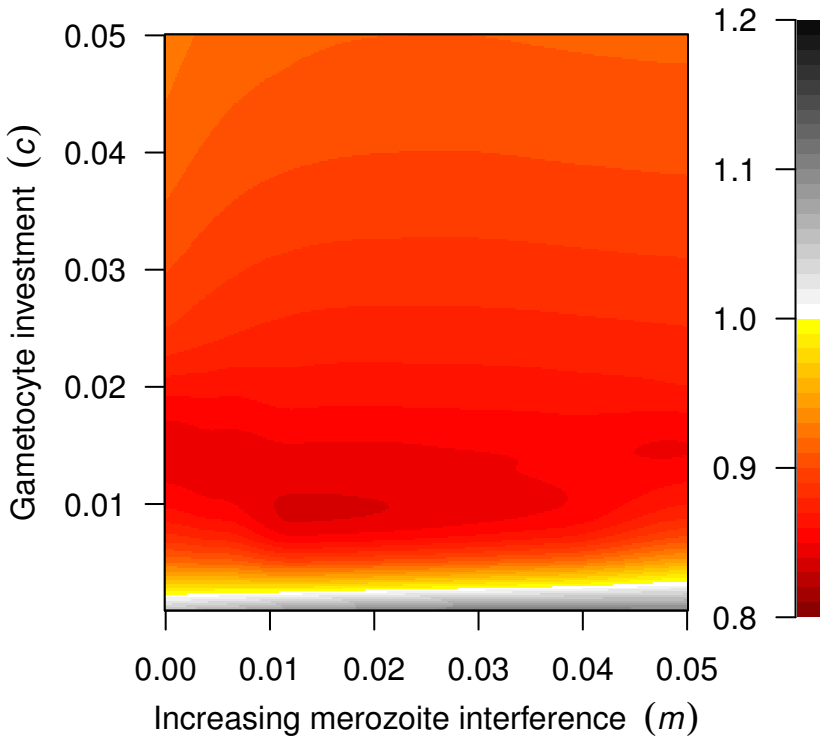

Figure A.5. Smoothed relative fitness in single infections (ratio of mean transmission for synchronous:asynchronous strain) using an alternate form of merozoite interference ($z(t)$, Eqn. 2.3). Parameters otherwise identical to Fig. 2.5 (i.e., relative fitness calculated with Eqn. 2.13).

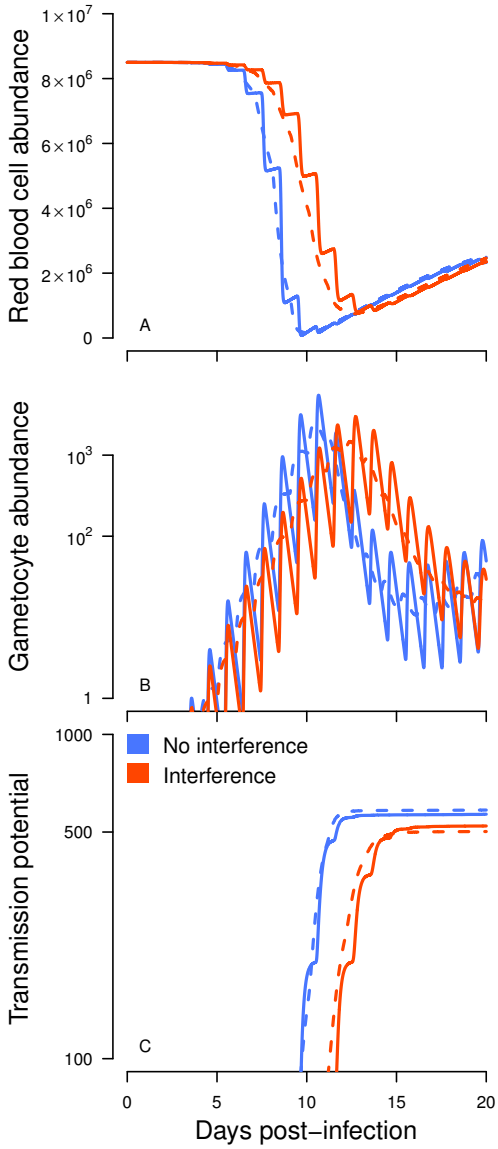

Figure A.6. Red blood cell abundance (A), gametocyte abundance (B), and transmission potential (C, cumulative probability of transmission) simulated for parasitoid-like merozoite interference (Eqn. 2.3), with $m = 0.05$ for orange curves. Synchronous dynamics are again shown in solid lines while asynchronous infections are denoted with dashed lines. Gametocyte investment was set low ($c = 0.002$), and immunity was absent ($a = 0$). Transmission potential was calculated using Eqn. 2.13. Synchronous strains can benefit from merozoite competition (C, orange lines), while the asynchronous infection would have transmitted better in the absence of competition (C, blue lines).

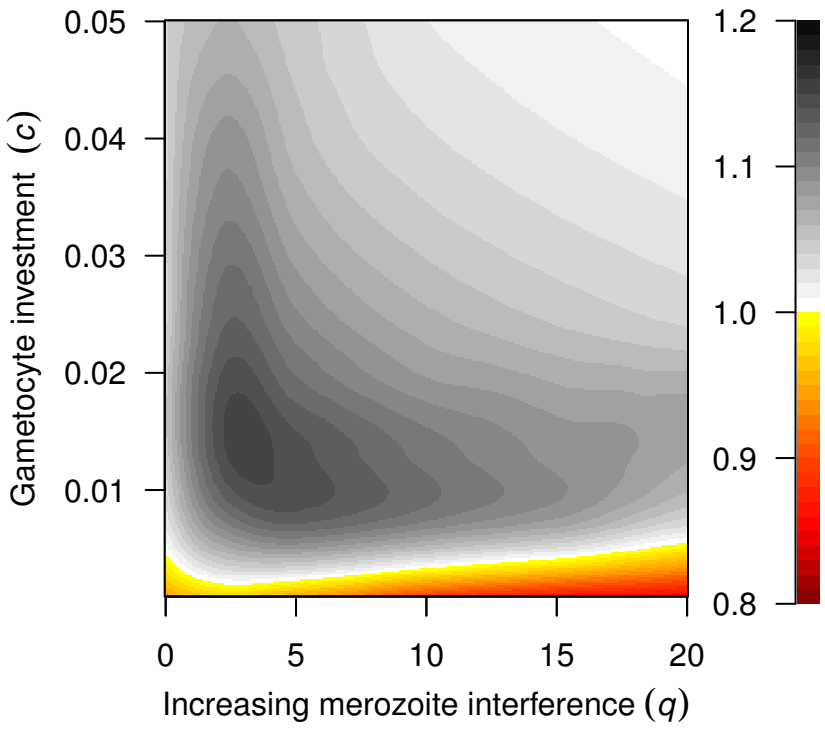

Figure A.7. Smoothed relative fitness of synchronous:asynchronous infections as shown in Fig. 2.5A, except that gametocytes have a mean infectious lifespan of approximately 20 hours (based on data in Reece *et al.* 2003) instead of six hours (from data in Gautret *et al.* 1996).

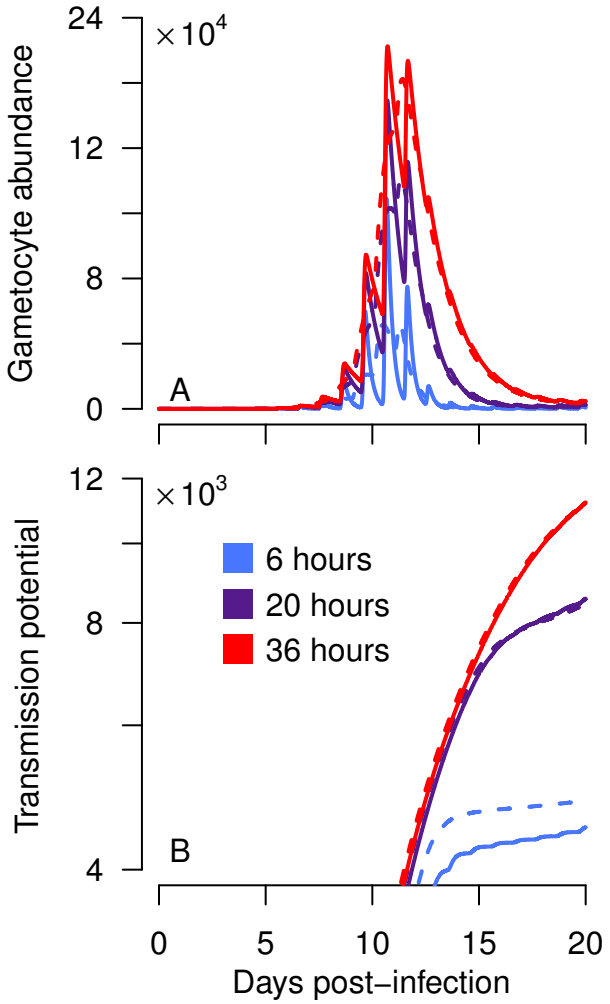

Figure A.8. Gametocyte abundance (A) and the transmission potential (i.e., the cumulative probability of transmission) (B) as gametocyte longevity increases. Asynchronous dynamics are given by dashed lines, and synchronized infections are shown with solid lines. Merozoite interference is absent ($q = 0$), and there is relatively high investment in gametocytes ($c = 0.05$). Increasing gametocyte longevity to 20 hours give synchronous strains an advantage, but increasing longevity still further—such that gametocytes outlive asexual forms—sharply reduces transmission differences between synchronous and asynchronous parasites.

Appendix B

Chapter 3 Supplemental Information

B.1 Annotated code for distributed delay model

This is the annotated code for the Gamma-distributed delay model, which represents a chain of ODEs. First we have to load the package to solve ODEs:

```
> # load required packages
> library(deSolve) # to solve ODEs
```

This model was run with a range of functional forms of interference, defined in this function, *pinfGeneral*:

```
> pinfGeneral = function(p,q,m,mero,RBC,fx){
+   # null hypothesis: Holling Type II, occurs for fx=1,2,3 & m=0
+   # hyperbolic interference (fx=4) does not reduce to the null model
+   if(fx==1){return(p/(1+q*RBC+m*(mero-1)))} # Beddington-DeAngelis
+   if(fx==2){return(p/((1+q*RBC)*(1+m*(mero-1))))} # Crowley-Martin
+   if(fx==3){return(p/(q*RBC+(mero^m)))} # Hassell-Varley
+   if(fx==4){return(p/(1+q*mero/RBC+0*m))} # hyperbolic
+   if(fx==5){return(p*((mero+1)^-m)+0*q*RBC)} # parasitoid-like
+   } # end of general interference function
```

Now we can code *gamma.ps*, the function to run the model simulation, for the equations given in Equations 3.4–3.9:

```
> # Distributed-delay model function
> gamma.ps = function (t, y, parms){ # gamma chain model for petri dish
+   # in contrast to si.petri, this model fits data for two life stages:
+        # schizonts and pre-schizonts
+         ## parameters--all units should be in terms of days
+         n1=parms[1] #shape parameter determining the number of
+                 # compartments for rings & trophozoites
+   n2=parms[2] #shape parameter determining the number of
+                   # compartments for schizonts
+         #RBC dynamics
+         mu = parms[3] # mortality rate of RBC
+         #infected RBC dynamics
+         alpha1 = parms[4] # mean delay until infected
+                                        #RBC becomes a schizont
+   alpha2 = parms[5] # mean delay until schizont bursts
+         # merozoites
+   fxform = parms[6] # parameter specifying functional form
+                                    # of interference
+   # fxform must be 1,2,3,4
+   p = parms[7] # 1st competition coefficient--maximum invasion rate
+   q = parms[8] # 2nd competition coefficient, meaning depends on
+                                    # functional form of interference
+   m = parms[9] # 3rd competition coefficient, meaning depends on
+                                    # functional form of interference
+   beta = parms[10] # burst size of infected RBCs, depends on strain
+         muz = parms[11] # intrinsic mortality rate of free merozoites
+   # muz may or may not depend on the strain in question
+
+         ## variables to keep track of (this is where R sets these
+                 # equal to the initial values or updates them)
+         R = y[1] # red blood cells (RBCs)
+         In = y[2:(n1+1)] # infected RBCs in the ring/trophozoite stages
+           S = y[(n1+2):(n1+n2+1)]
```

```
+         M = y[n1+n2+2] # free merozoites (emerged from burst RBC)
+
+         dR = - mu*R - pinfGeneral(p,q,m,M,R,fxform)*R*M
+         dIn = rep(0, n1)
+         dIn[1] = pinfGeneral(p,q,m,M,R,fxform)*R*M - mu*In[1]
+                - (n1/alpha1)*In[1]
+         if(n1>1){
+                 for(i in 2:n1){
+                         dIn[i] = (n1/alpha1)*In[i-1] - mu*In[i]
+                - (n1/alpha1)*In[i]
+                         }
+                 }
+
+   dS = rep(0, n2)
+   dS[1] = (n1/alpha1)*In[n1] - mu*S[1] - (n2/alpha2)*S[1]
+         if(n2>1){
+           for(i in 2:n2){
+             dS[i] = (n2/alpha2)*S[i-1] - mu*S[i] - (n2/alpha2)*S[i]
+             }
+           }
+
+   dM = beta*(n2/alpha2)*S[n2]
+ - pinfGeneral(p,q,m,M,R,fxform)*R*M - muz*M
+
+         res=c(dR, dIn, dS, dM)
+         list(res)
+         } # end two class petri dish model
```

The complicated part is getting the indexing of the state variables correct, so that the number of state variables varies with n_1 and n_2. **R** is flexible about allowing the state variable 'dIn' to be a vector. The parameters were defined as follows:

```
> # parameter values (red blood cell count, merozoite mortality)
> # Gonzales-Alonso et al. 2006 report means of 4.84x10^6 RBCs/mL
>         # and 4.64x10^6 RBCs/mL
> # for their controls, with 42.9% and 41.9%
> # hematocrit, respectively
> # assuming those hematocrits need to be diluted
>       # down to 5% in 5mL total
> # H. Reilly reports using 5mL cultures for invasion
> # and cycle length assays
> # using c1v1=c2v2 yields (with c1=0.429, v1 = ?, c2 = 0.05, v2 = 5mL)
> # but both Nester & H. Reilly would have assumed that
>         # the starting stock had 50% hematocrit
> rbc1=(0.05*5/0.5)*(4.84e6)
> rbc2=(0.05*5/0.5)*(4.64e6)
> cAmountHi = mean(c(rbc1,rbc2)) # rbcs/culture assuming 5% hematocrit
> startper = 0.005 # starting percentage schizonts for Nester's data
> cAmount = cAmountHi # assuming Nester's assays were run on 5mL
+ # cultures at 5% hematocrit
> initialpI0 = 0.2
> apers = 0.3
> n = 30
> alpha = 42/24
> fxform = 4
> q=10
> m=0
> n1 = round((1-apers)*n)
> n2 = round(apers*n)
> alpha1 = (1-apers)*alpha
> alpha2 = apers*alpha
> p = 2e-8
> beta = 16
> mu = 1/120 # according to Koury & Ponka 2004 the mean lifespan
>         # of an RBC is 120 days
```

```
>
> R0 = cAmount*(1-startper)
> I0 = cAmount*startper*initialpI0 # initial number of infected RBCs,
>         # pre-schizont stage
> S0 = cAmount*startper*(1-initialpI0) # initial number of schizonts
> M0 = 0 # initial number of free merozoites, here I assume good
>         # synchronization = no merozoites
> parms = c(n1, n2, mu, alpha1, alpha2, fxform, p, q, m, beta, muz)
> print(c(n,alpha,apers))

[1] 30.00  1.75  0.30

> syncI = rep(I0/n1, n1) # assume any rings are uniformly distributed
>         # through different age compartments
> syncS = rep(S0/n2, n2) # assume schizonts are uniformly distributed
>         # through the schizont stage
> start = c(R = R0, In = syncI, S = syncS, M = M0)
> days = 60/24
> h = 1/240
> y.new = as.data.frame(lsoda(start, times=seq(0/24,days,h),
+      func=gamma.ps, parms=parms))
> totalIn = apply(y.new[,3:(n1+2), drop = FALSE], 1, sum)
> totalS = apply(y.new[,(n1+3):(n+2), drop = FALSE], 1, sum)
> perS = totalS/(totalIn+totalS)
> perTotalS = totalS/(totalIn+totalS+y.new$R)
```

With the parameter values and initial conditions set, the model simulation is run as 'y.new', which is a rather wide data frame, consisting of $n + 3$ columns, including time. I then collate this large data frame into a single vector for the immature stages ('totalIn') and the mature schizonts ('totalS').

```
> head(cbind(y.new$time,y.new$R,totalIn,totalS,y.new$M))

                          totalIn   totalS
[1,] 0.000000000 2358150 2370.000 9480.000    0.000
```

```
[2,] 0.004166667 2358068 2361.967 9412.496 1090.945
[3,] 0.008333333 2357986 2354.127 9344.997 1983.925
[4,] 0.012500000 2357903 2346.445 9277.503 2714.854
[5,] 0.016666667 2357821 2338.890 9210.013 3313.136
[6,] 0.020833333 2357738 2331.439 9142.528 3802.836
```

B.2 Image processing

Image J is freely available image processing software (Rasband, 2013). The code for the macro is as follows:

```
dir = getDirectory("Choose Directory");
print(dir);
list = getFileList(dir);
newDir = dir + "ImageJOutput" + File.separator;
File.makeDirectory(newDir);
setBatchMode(true);
for(i=0; i<lengthOf(list); i++){
     print(list[i]);
     open(list[i]);
     name = getTitle();
     newTitle = substring(name, 0, lengthOf(name)-4)+"Count.jpg";
     newPath = newDir + newTitle;
     run("Options...", "iterations=1 count=1 black edm=Overwrite do=Nothing");
     run("Make Binary");
     run("Measure");
     run("Fill Holes");
     run("Watershed");
     run("Analyze Particles...", "size=2000-Infinity circularity=0.20-1.00
      show=Outlines display exclude summarize");
     selectWindow(list[i]);
     close();
     selectWindow("Drawing of "+list[i]);
     saveAs("jpeg", newPath);
     close();
     rIndex = i+1;
     resPath = newDir + "Results" + rIndex + ".txt";
     if(isOpen("Results")){
selectWindow("Results");
```

```
        saveAs("Results", resPath);
run("Close");
}
     }
sumPath = newDir + "Summary.txt";
if(isOpen("Summary")){
     selectWindow("Summary");
     saveAs("Text", sumPath);
     run("Close");
setBatchMode(false);
```

The code is saved as "CountRBCs.txt", and can be run by selecting Macros → Run... from the Plugins menu. A dialog box will open up allowing the user to select the appropriate code file, which then runs and allows the user to select the folder with the images to be counted. In the code shown, the setBatchMode is set so that the code will run faster (the user will not be able to view each image). The algorithm used to process each image is shown in Fig. B.1.

Comparing manual and digital counts. The counting macro will not give precisely the same number of red blood cells that would be counted by a person (nor would a person necessarily give identical counts from day to day), but it allows quantification of a much larger number of fields than would typically be feasible for a researcher at a microscope. The manual and digital counts line up well (Fig. B.2) though the algorithm may slightly overestimate red blood cell abundance at high density, as more and more RBCs overlap. Dramatic undercounts were detected and removed by excluding low counts (less than ten cells), which occurred when dark artifacts were present leading the algorithm to count the artifact as the only cell present. More subtle undercounts can occur when the algorithm cannot adequately divide a clump of red blood cells, which can be detected by scanning the meta-data in the "Results" files for cells greater than 2×10^4 pixels. Those images were removed. In general, the HB3 fields were much more crowded (the slides made subsequently for Dd2 were diluted further for that reason), and many more images had to be removed (Fig. B.3).

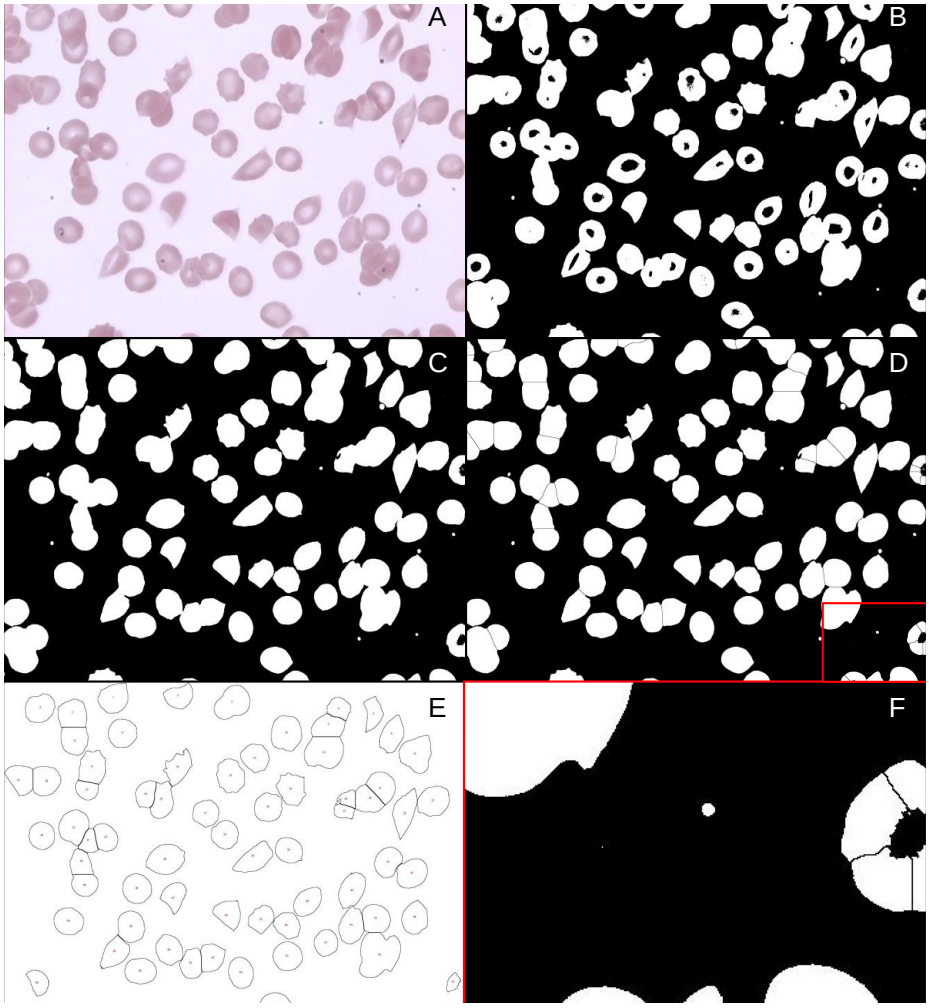

Figure B.1. Image processing. The original image (A) is converted to black and white (B, Process → Binary → Make Binary). The background must be set to be black prior to this step (with the dialog box in Process → Binary → Options...). The holes are filled in (C, Process → Binary → Fill Holes. The watershed command (Process → Binary → Watershed) subdivides shapes into individual red blood cells (or at least, ImageJ's best guess as to how many red blood cells comprise a clump of dots, D). ImageJ can now be directed to count to number of particles of a particular size and circularity (Analyze → Analyze Particles, with the size range set from 2000 to ∞ and the circularity range set from 0.2 to 1). ImageJ can be directed to show the outlines of the counted particles by selecting "Outlines" from the Show drop down menu in the Analyze Particles dialog box (E). The Fill Holes and Watershed commands run into errors at the edges of images (F), so ImageJ is directed omit particles touching the edges of the image by selecting the "Exclude on edges" option in the Analyze Particles dialog box.

B.3 Supplementary figures and tables

These parameters (along with those reported in Table 3.1) were obtained by initializing the optimization at $n = 200$, $\alpha = 2$, proportion of the life stage spent as

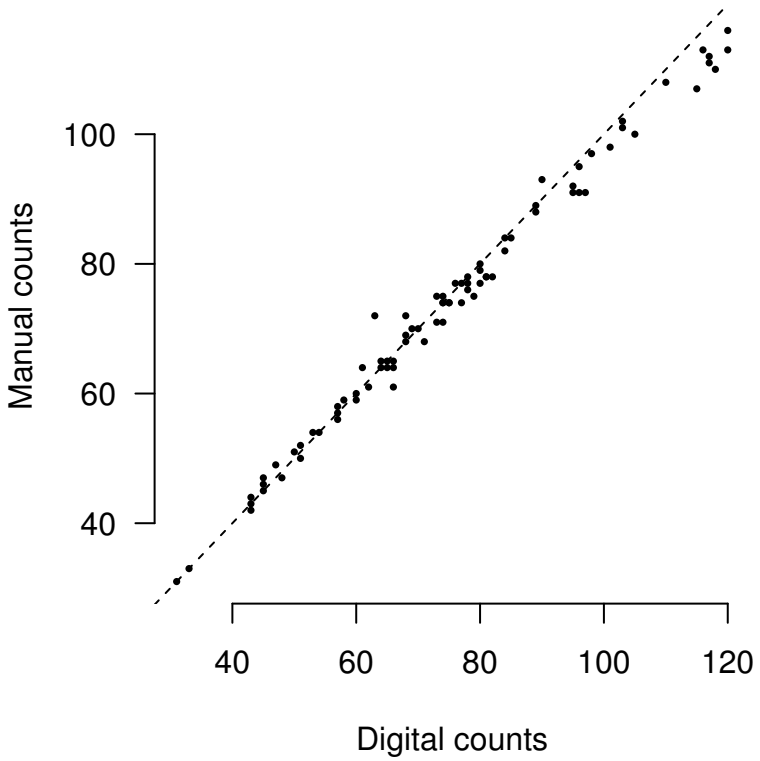

Figure B.2. Manual versus digital counts for Dd2 and HB3. Dashed line indicates the 1-to-1 line.

a schizont equal to 0.3, $p = 2 \times 10^{-6}$, $q = 0.5$ and $m = 0.3$.

Table B.1. Fit invasion parameters

Interference	Strain	Maximum invasion rate	Interference coefficient
Hyperbolic	Dd2	3.03×10^{-5}	0.770
Parasitoid-like	Dd2	2.38×10^{-4}	0.0504
Hyperbolic	HB3	3.37×10^{-5}	0.237
Parasitoid-like	HB3	3.42×10^{-5}	1.36
Hyperbolic	3D7	2.56×10^{-5}	0.181
Parasitoid-like	3D7	3.63×10^{-5}	66.9

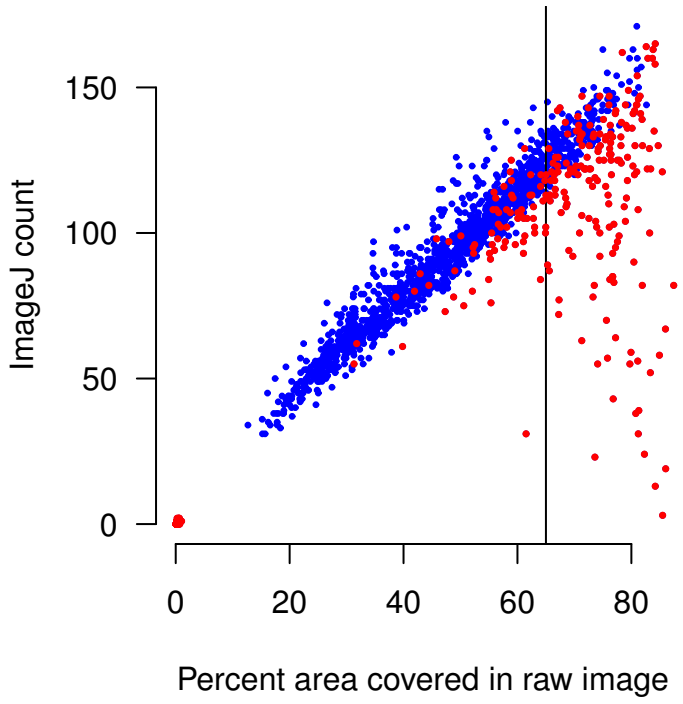

Figure B.3. Image J counts for HB3 as a function of area covered on the original image. The red points refer images that were excluded either because the count was improbably low, or because the maximum area of the particle detected was too high, indicating that the algorithm could not separate a large clump of red blood cells.

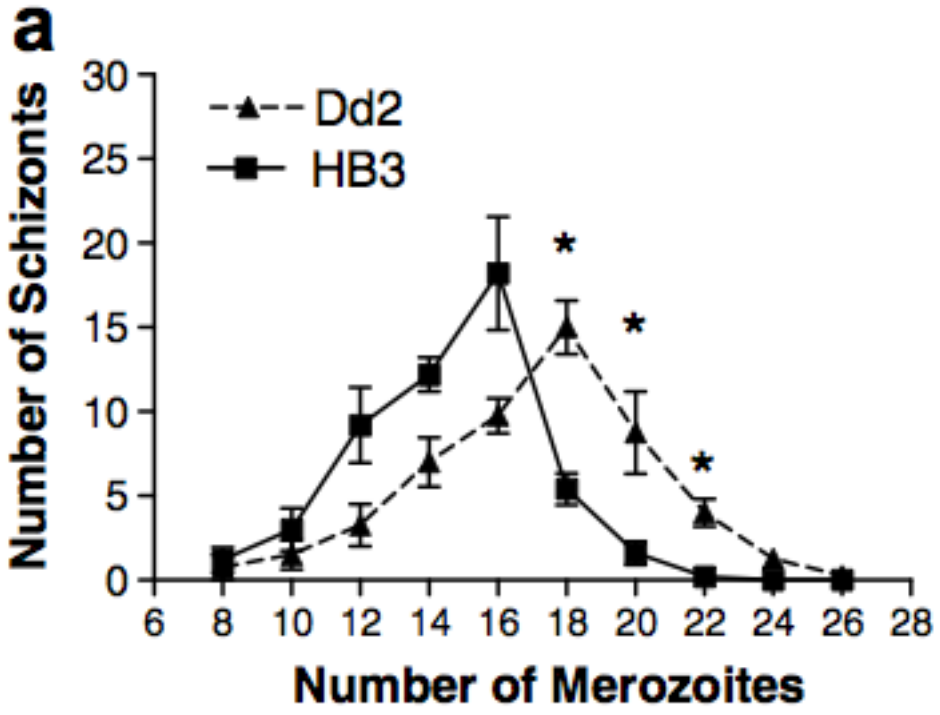

Figure B.4. Figure 3A from Reilly *et al.* (2007), reproduced here for illustrative purposes. The caption reads "Magnetically purified schizonts are viewed by light microscopy to determine the number of merozoites produced per schizont. Five replicates consisting of a minimum of 50 schizonts are counted. Error bars represent the SEM. Unpaired t-tests comparing merozoite numbers between Dd2 and HB3 give a $P < 0.05$ for 18, 20 and 22 merozoites per schizont."

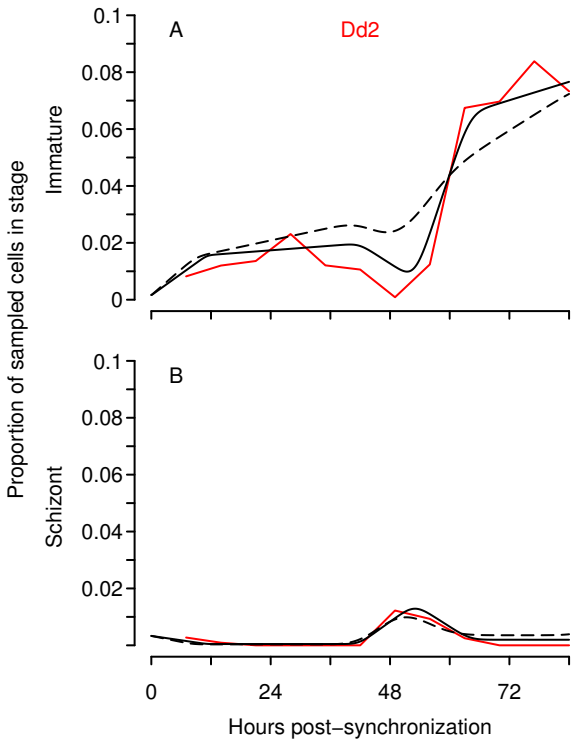

Figure B.5. Model fits assuming hyperbolic interference (black solid curve, Eq. 3.2) or parasitoid-like interference (black broken curve, Eq. 3.3), with data is shown in colored lines. The black curves for each strain indicate a single best model fit to both the proportion of sampled red blood cells in the immature parasite stages (A) and in the schizont stage (B). Weighted least squares errors are 0.03995 for hyperbolic interference, and 0.09685 for parasitoid-like interference.

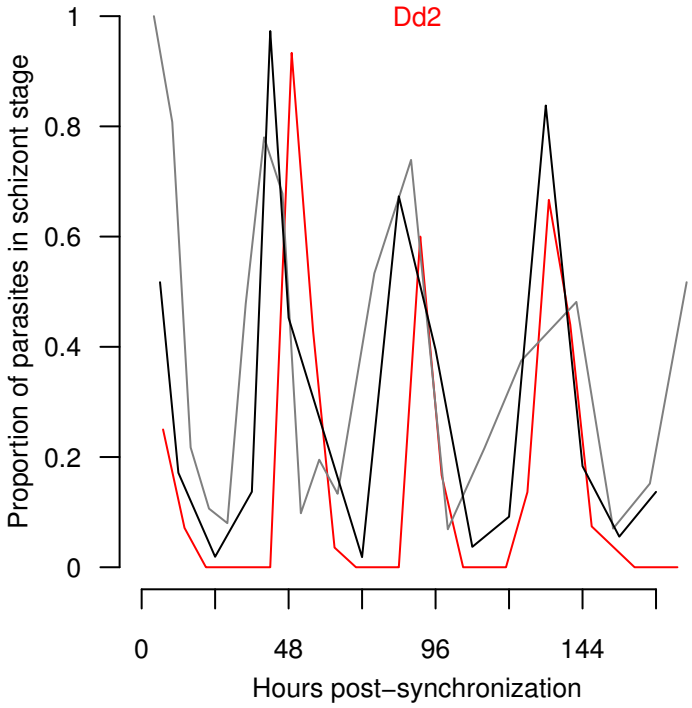

Figure B.6. Data collected by Nestor Agbayani (red) compared with data collected by Heather Reilly (gray and black curves). Initial parasitemia was 0.5% for the red curve, and 1% for the gray and black curves.

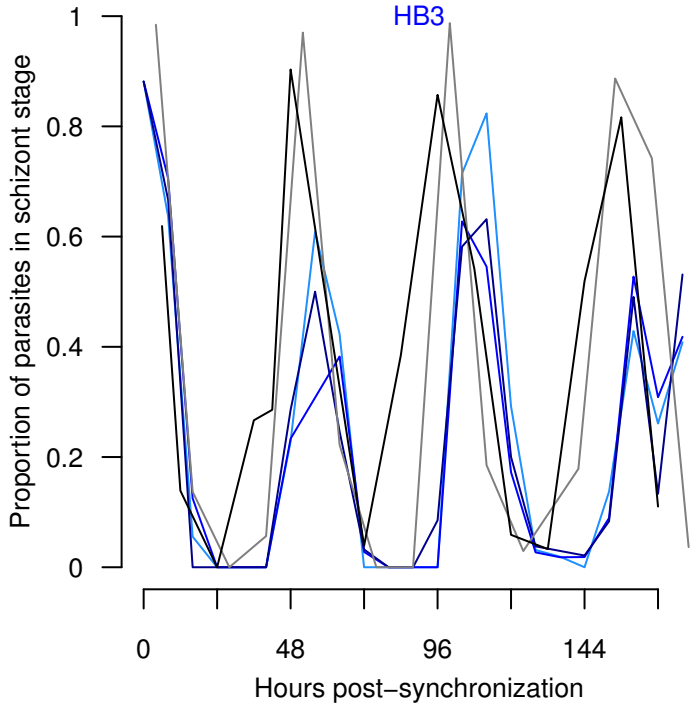

Figure B.7. Data collected by Nestor Agbayani (blue curves) compared with data collected by Heather Reilly (gray and black curves). Initial parasitemia was 0.5% for the red curve, and 1% for the gray and black curves.

Appendix C

Chapter 4 Supplemental Information

C.1 Supplemental methods: simulations and free spline investment

All simulations were run using the `PBSddesolve` package (developed by A. Couture-Beil, J. T. Schnute, and R. Haigh) in **R** versions 3.0.1 and 3.0.2 (R Project for Statistical Computing, http://r-project.org/).

To investigate optimal plastic reproductive investment under the assumption of perfect information, but with minimal assumptions, we formulate conversion rates to be a spline, a continuous, C^2 differentiable function of time (e.g., Härdle, 1990) that scales between zero and one. We code transmission investment as a B-spline object using the `splines` package (developed by Douglas M. Bates and William N. Venables). Specifying the investment strategy as a free spline allows great flexibility in the functional form; here we retain the defaults in **R** so that the spline is a cubic function with no interior knots:

$$c(t) = \exp\left(-\exp(jt^3 + kt^2 + lt + m)\right) \tag{C.1}$$

By taking the complimentary log-log of the spline, $c(t)$ is constrained to vary between zero and one, and the parameters j, k, l, and m are varied so as to optimize the cumulative transmission potential using the Nelder-Mead algorithm within the *optim* function. We arbitrarily set j, k, l, and m to 0.5 to initialize the optimization.

It is prohibitively computationally intensive for the algorithm to calculate $c(t)$ using the spline basis function at each time point within the delayed differential equation solver, so we calculate $c(t)$ for each thousandth of a day and fit a spline to those values using *splinefun*. This extra step allows **R** to calculate c as a function of time only, without regard to the basis function, which speeds up computation considerably (from one hour down to one minute to simulate an infection) and

makes the problem computationally tractable. Since $c(t)$ is an approximation, it occasionally becomes very slightly negative (most negative on the order of -1×10^{-154}).

C.2 Supplemental figures

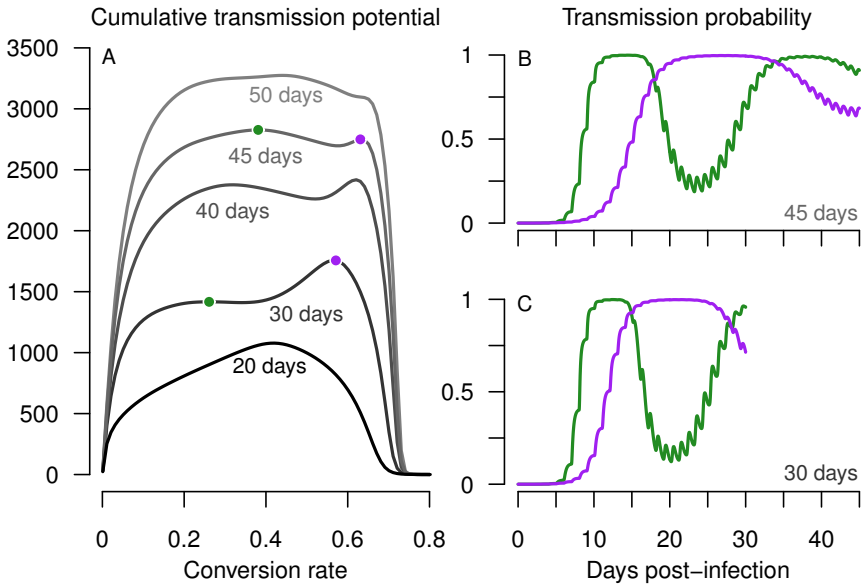

Figure C.1. The adaptive landscape shifts as infections last longer, with a single optimal conversion rate splitting into two optima (A). One optimum corresponds to relatively low conversion, generating rapid growth of the infection and allowing two peaks in transmission probability (green curves in B and C). The other optimum is a high conversion rate (purple curves), resulting in slow growth of the infection, and one drawn-out peak in the probability of transmission. The relative fitness of these two optima (i.e., which one is local and which one is global), depends on the length of the infection. As infections become longer, the fitness differences are less pronounced between intermediate conversion rates.

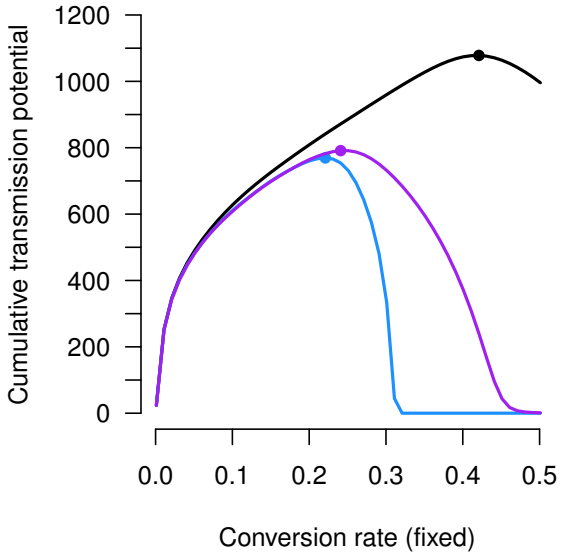

Figure C.2. In single, asynchronous infections, saturating immunity constrains the optimal fixed conversion rate (solid points). In the absence of immunity (black), the optimum transmission investment is 42.1% when infections last 20 days. With saturating immunity acting against infected red blood cells (blue, $a = 150$, $b = 100$) or merozoites (purple, $a = 7200$, $b = 100$), the optimal conversion rate is reduced to 22.1% and 24.4%, respectively. Except for the difference in x-axis range, the black curve shown here is identical to the black 20-day curve shown in Fig. C.1A.

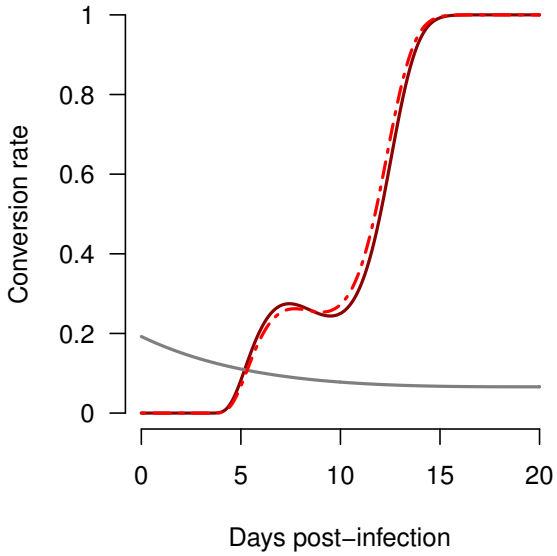

Figure C.3. Best free spline response to the gray strategy shown as the solid dark red line. For comparison, the best free spline response to fixed reproductive investment is shown as the red broken line (identical to the winning strategy shown in Fig. 4.5A).

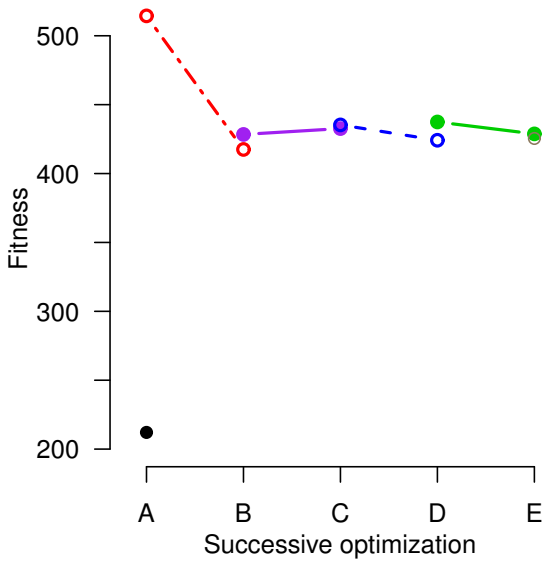

Figure C.4. Fitness of dueling splines in successive optimizations. X-axis labels correspond to panel letters in Fig. 4.5, with the colors and line styles chosen to match the dueling spline strategies in that figure.

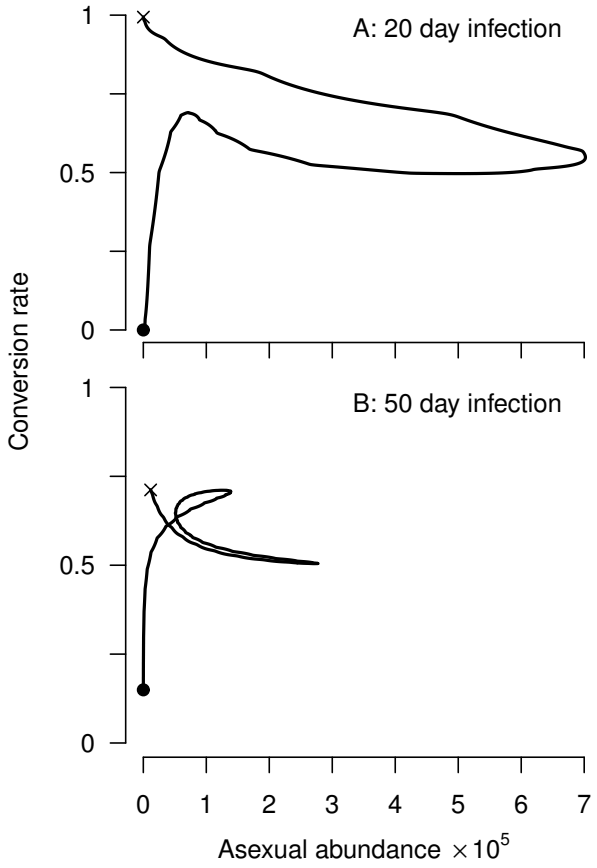

Figure C.5. Asexual abundance is a poor cue for the optimal conversion rate in single infections, because the same number of parasites corresponds to diverse conversion rates over nearly the entire range. The start of infection is indicated by a dot, and the end is marked with an 'x'.

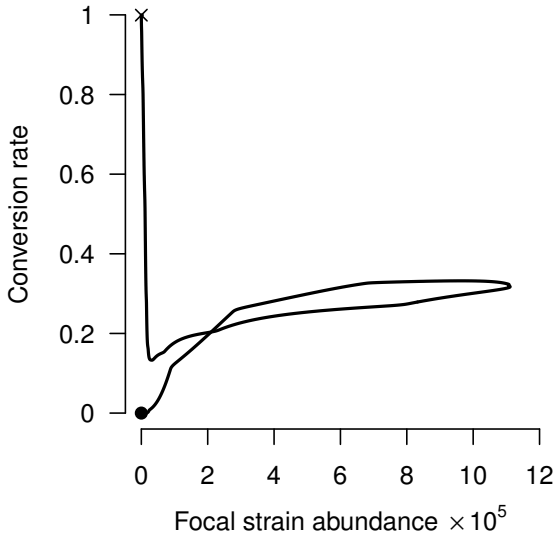

Figure C.6. Asexual abundance of the focal parasite strain is a poor cue for optimal conversion in coinfections. The start and end of infection are indicated by a dot or an 'x', respectively.

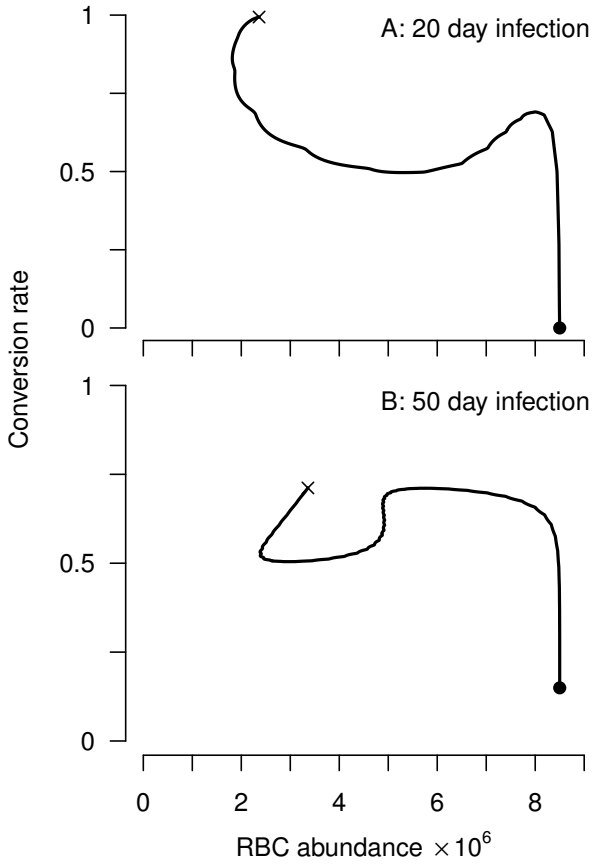

Figure C.7. Red blood cell abundance could help parasites determine when to begin investing in transmission, but not when to increase investment towards the end of infection. The start of infection is indicated by a dot, and the end is marked with an 'x'.

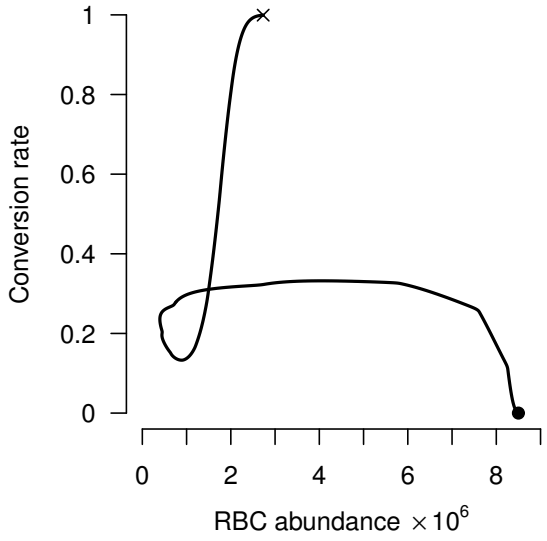

Figure C.8. Red blood cell abundance could serve as an effective cue in coinfections, at least until infection draws to a close. The start of infection is indicated by a dot, and the end is marked with an 'x'.

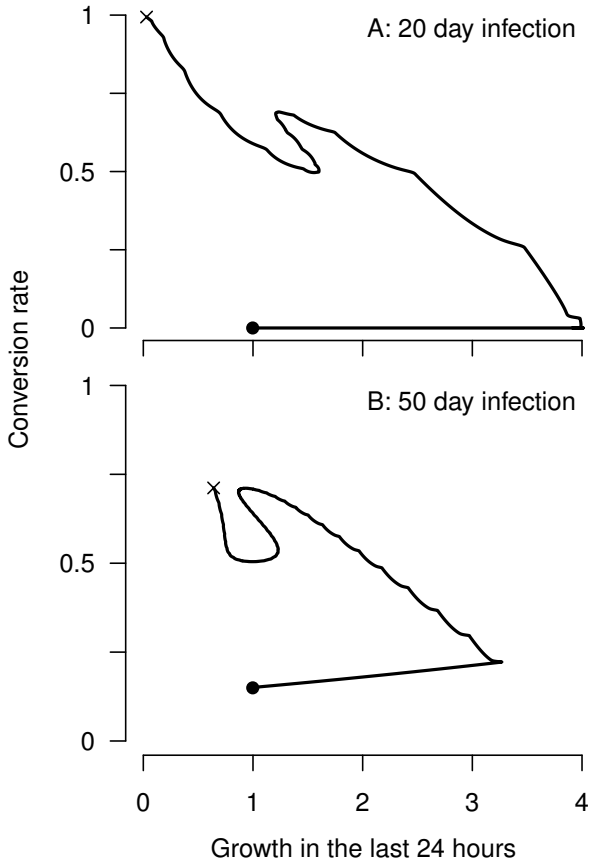

Figure C.9. In single infections, parasite growth in the last 24 hours is a poor indicator of when to turn on transmission investment, but could help parasites decide to increase investment towards the end of infection. The start of infection is indicated by a dot, and the end is marked with an 'x'.

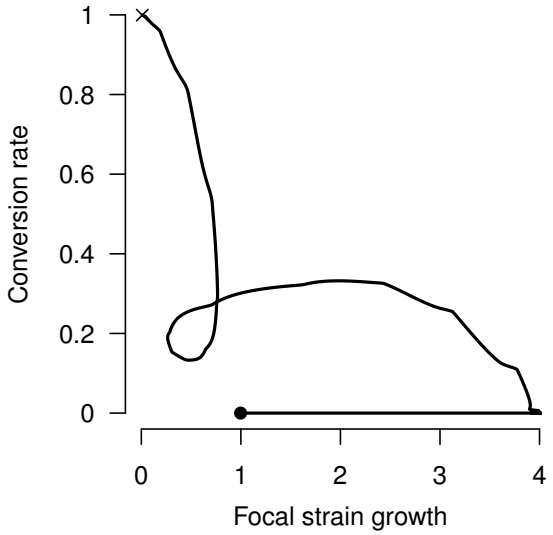

Figure C.10. In coinfections, growth of the focal strain in the last 24 hours is a poor proxy for time. The start of infection is indicated by a dot, and the end is marked with an 'x'.

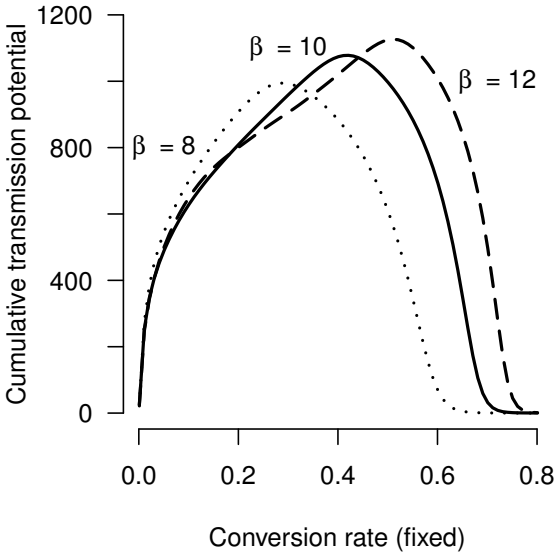

Figure C.11. The optimal conversion rate increases with the burst size (β) in single infections in the absence of immunity. Infections were simulated for 20 days for burst sizes of 8 (dotted), 10 (solid), and 12 (dashed).

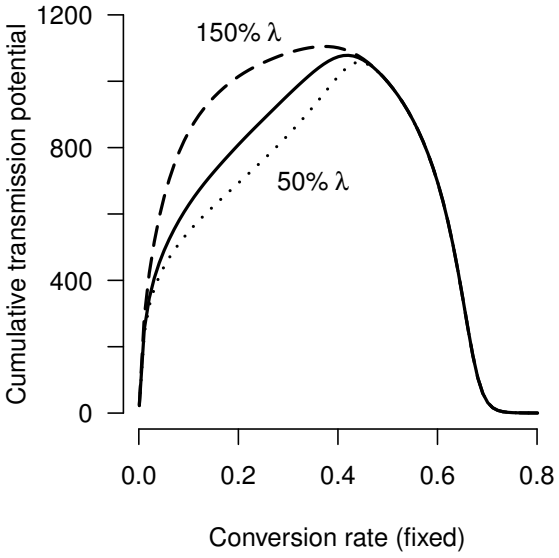

Figure C.12. The optimal conversion rate decreases slightly with the maximum rate of erythropoiesis (λ) in single infections in the absence of immunity. Infections were simulated for 20 days for $\lambda = 1.85 \times 10^5$ (dotted), $\lambda = 3.7 \times 10^5$ (solid), and $\lambda = 5.55 \times 10^5$ (dashed).

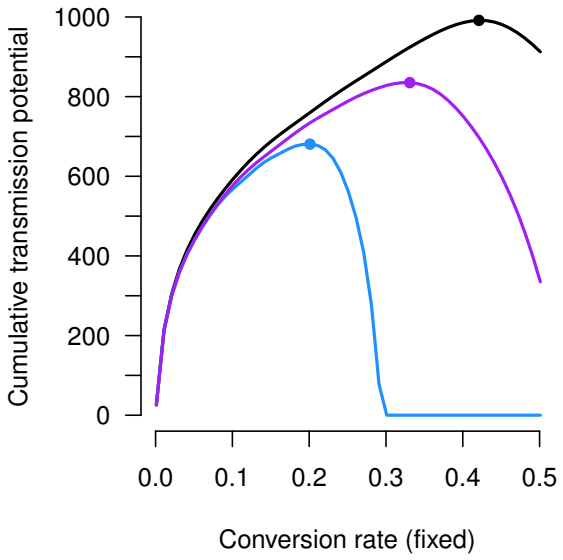

Figure C.13. Synchronous infections: the optimal conversion rate for single infections is still reduced in the presence of saturating immunity (blue), more so if immunity targets long-lived infected red blood cells. If immunity targets short-lived merozoites (purple), the optimal conversion rate is reduced to a lesser degree. In the absence of immunity, the optimal conversion rate is identical to that of asynchronous infections (black).

Table C.1. Parameters for optimal time-varying strategies

Spline	Parameters			
No immunity, single infection				
20 days	6.290962	-15.38119	0.3123698	-11.37115
30 days	2.986467	-8.900943	0.09278162	-4.920522
50 days	0.6422217	-4.034063	0.6273944	-1.720979
Immunity against parasites in				
I class, single infection				
20 days	13.45771	-27.66144	-3.624199	-20.24271
No immunity, coinfection, 20 days				
winner from Fig. 4.5A	11.91146	-28.05726	11.26698	-42.82205
winner from Fig. 4.5B	21.02123	-41.91842	-3.078478	-31.43425
winner from Fig. 4.5C	8.875516	-17.93721	0.2664415	-15.76727
winner from Fig. 4.5D	13.73466	-27.26571	-1.710064	-20.98166
loser from Fig. 4.5E	10.10987	-20.17194	-0.5457009	-16.53443
winner from Fig. C.3	11.95858	-28.40747	11.33155	-41.83195
loser from Fig. C.3	0.5	0.5	0.5	0.5

Appendix D

Chapter 5 Supplemental Information

D.1 Supplemental methods: Age-structured gametocyte development

Red blood cell dynamics are as in Greischar *et al.* (2014), keeping the merozoite invasion rate p constant:

$$\frac{dR(t)}{dt} = \lambda\left(1 - \frac{R(t)}{K_{start}}\right) - \mu R(t) - pR(t)M(t) \tag{D.1}$$

When red blood cells are depleted by infection or mortality (μ), they are replenished in a logistic fashion, where λ is the maximum rate of erythropoiesis and $K_{start} = \lambda R^*/(\lambda - \mu R^*)$. Once invaded by merozoites, most infected red blood cells can remain in the asexual part of the life cycle (I):

$$\frac{dI(t)}{dt} = (1-c)p(t)R(t)M(t) - \mu I(t) - \zeta(t) \tag{D.2}$$

where c is the conversion rate, the proportion of invaded red blood cells undergoing sexual differentiation. The null hypothesis would be a constant conversion rate, unaffected by environmental factors, so we leave c as a constant. While infected red blood cells are subject to background mortality, we assume no immune-killing. Infected red blood cells that survive through the life cycle are given by $\zeta(t)$:

$$\zeta(t) = \begin{cases} (1-c)pR(t-\alpha)M(t-\alpha)\exp(-\mu\alpha) & \text{if } t > \alpha \\ I_0 \text{Beta}(s_P, s_P)(t)\exp(-\mu t) & \text{if } t \leq \alpha \end{cases} \tag{D.3}$$

A highly synchronized infection is simulated by setting $s_P = 100$. Each infected red blood cell that survives for α days bursts to release β merozoites:

$$\frac{dM(t)}{dt} = \beta\zeta(t) - pR(t)M(t) - \mu_Z M(t) \tag{D.4}$$

Merozoites die at a high rate, μ_Z.

The previous model assumed a single developmental compartment for sexual differentiation I_G, and we split that into three to understand the consequences of detecting sexual differentiation early, mid-stage, or late. Early sexual differentiation is given by

$$\frac{dI_E(t)}{dt} = cpR(t)M(t) - \mu I_E(t) - \zeta_E(t) \tag{D.5}$$

where

$$\zeta_E(t) = \begin{cases} cpR(t-\alpha_E)M(t-\alpha_E)\exp(-\mu\alpha_E) & \text{if } t > \alpha_E \\ 0 & \text{if } t \leq \alpha_E \end{cases} \tag{D.6}$$

Mid-stage sexual differentiation is defined by

$$\frac{dI_M(t)}{dt} = \zeta_E(t) - \mu I_M(t) - \zeta_M(t) \tag{D.7}$$

Similarly,

$$\zeta_M(t) = \begin{cases} cpR(t-\alpha_E-\alpha_M)M(t-\alpha_E-\alpha_M)\exp(-\mu\alpha_E\alpha_M) & \text{if } t > \alpha_E+\alpha_M \\ 0 & \text{if } t \leq \alpha_E+\alpha_M \end{cases} \tag{D.8}$$

Progression through the final stages of gametocyte differentiation is described by

$$\frac{dI_L(t)}{dt} = \zeta_M(t) - \mu I_L(t) - \zeta_L(t) \tag{D.9}$$

Similarly,

$$\zeta_L(t) = \begin{cases} cpR(t-\alpha_G)M(t-\alpha_G)\exp(-\mu\alpha_G) & \text{if } t > \alpha_G \\ 0 & \text{if } t \leq \alpha_G \end{cases} \tag{D.10}$$

where $\alpha_G = \alpha_E + \alpha_M + \alpha_L$. After late-stage gametocyte differentiation, infected red blood cells become mature gametocytes (G):

$$\frac{dG(t)}{dt} = cp(t-\alpha)G)R(t-\alpha_G)M(t-\alpha_G)S_G - \mu_G G(t) \tag{D.11}$$

D.2 Description of spline method

We import simulated data assuming no immune-mediated mortality, an average gametocyte lifespan of 20 hours, and a fixed conversion rate of 5%, as plotted in Fig. 5.1C. We subsample the simulated data to obtain daily samples for uninfected red blood cell abundance ('rbc'), total parasite numbers (asexuals and early sexuals, labeled 'para' below), and gametocyte abundance ('gams'), assuming that the samples were taken eight hours after the peak of bursting and re-invasion of merozoites. We first estimate the effective propagation number (here denoted x) using the methods described by Metcalf *et al.* (2011):

```
> Itplus1 = para[2:length(para)]
> It = para[1:(length(para)-1)]
> St = rbc[1:(length(rbc)-1)]
> x = rep(NA, length(samplingTimes)-1)
> for (i in c(1:(length(samplingTimes)-1))){
+   fitA = lm(log(Itplus1[i])~offset(log(It[i])+log(St[i])))
+   x[i] = exp(fitA$coef[[1]])
+   } # end asex loop
```

To estimate the time-varying conversion rate assuming 3 degrees of freedom, we use the objective function `gobs`, which will be passed to *optim*. Aside from the spline parameters (a coefficient for each degree of the polynomial, plus an intercept), `gobs` also takes `epsilon` (the proportion of gametocytes surviving through the following sample), and `G3est`, the starting number of gametocytes.

```
> gobs <- function(parms,data){
+   cparms = parms[1:(length(parms)-2)]
+   cVal = exp(-exp(sVals%*%cparms))
+   epsilon = exp(parms[(length(parms)-1)])
+   G3est = exp(parms[(length(parms))])
+   rbcVals = data[,1]
+   paraVals = data[,2]
+   gamVals = data[,3]
+   Stminus3 = rbcVals[1:(length(rbcVals)-3)]
+   Itminus3 = paraVals[1:(length(paraVals)-3)]
+   Gt = gamVals[3:length(gamVals)]
+   GtPred = rep(NA, length(Gt))
+   GtPred[1] = G3est
+   for (k in c(4:20)){
+     futuret = k-3
+     j = c(4:k)
+     GtPred[(futuret+1)] = sum((epsilon^(k-j))*(cVal[(j-3)])
+          *xt[(j-3)]*Itminus3[(j-3)]*Stminus3[(j-3)])
+          +(epsilon^(futuret))*G3est
```

```
+     }
+   sse <- sum((log(GtPred)-log(Gt))^2)
+   } # end gobs fx
```

Note that all parameters are constrained to be positive, and the conversion rate (`cVal`) is constrained to vary between zero and one. Since gametocyte abundance varies over orders of magnitude, we log-transform the observed (`Gt`) and predicted (`GtPred`) abundances so that *optim* will fit to the whole time series and not just the peak. To fit the polynomial describing the conversion rate, we trim the time points to `tVals` and the effective propagation numbers to `xt`. We define the expected mortality rate of gametocytes to give a good guess for the starting parameters to pass to *optim*. The algorithm will loop over the vector `degrees` to find the best polynomial conversion rate with the corresponding degree. The matrix `bestFit` will hold the best parameters for each degree, and the vectors `sseVals` and `aicVals` will store the sum squared error and Akaike Information Criterion for the best fit parameters. Finally, the data are bound together into `simData`.

```
> # sexual bit
> tvals = times[1:(length(times)-3)]
> xt = x[1:(length(x)-2)]
> mug = (log(2)/14)*24
> degrees = c(1,2,3,4)
> bestFit = matrix(NA, ncol = max(degrees)+3, nrow = length(degrees))
> sseVals = rep(NA, length(degrees))
> aicVals = rep(NA, length(degrees))
> simData = cbind(rbc,para,gams)
```

Before running the following code, the package *splines* needs to be loaded. The fitting algorithm sometimes returns local rather than global optimal due to the starting values given, so we try a number of random starting values (`tries=10`) uniformly distributed between -10 and 10 and find the parameters that give the lower sum squared error. Starting from many different points increases the chances that the fitting algorithm will locate a global optimum. Higher degree c_t functions should always improve the fit (i.e., lead to lower sum squared error) over lower degree functions, and checking that can provide one way of testing whether the fitting algorithm has located a global optimum. If higher degree functions are not yielding lower sum squared error, it is worth rerunning the algorithm with a larger number of iterations if Nelder-Mead frequently fails to converge (specified using the *maxit* argument to *control* within *optim*), or with a larger number of starting parameter values. Each of the resulting best fit parameters will be recorded in the `bestFit` matrix, along with the sum squared error, so that we can take the best parameters located by the algorithm for a wide range of starting values.

```
> for (val in c(1:length(degrees))){
+   dg=degrees[val]
```

```
+   print(dg)
+   sVals = bs(tvals,degree=dg,intercept=TRUE)
+
+   tries = 10
+   parms0 = c(rep(0.5,ncol(sVals)),-mug,log(gams[3]))
+   parmTries = matrix(NA, nrow = tries, ncol = length(parms0)+1)
+   for (take in c(1:tries)){
+     dummy=1
+     while(dummy!=0){
+       convFit <- optim(parms0, gobs, data=simData,
+               control=c(maxit=5000))
+       dummy=convFit$convergence
+       parms0 = c(runif(length(parms0),min=-10,max=10))
+       sseVal = gobs(convFit$par, data=simData)
+       } # end while loop to get convergence
+     parmTries[take,] = c(convFit$par,sseVal)
+     } # end loop to get multiple convergent tries
+
+   bestrow = parmTries[which.min(parmTries[,(length(parms0)+1)]),
+       1:length(parms0)]
+   parms = bestrow
+   sse <- gobs(parms, data=simData)
+   bestFit[val,1:length(convFit$par)] = parms
+   sseVals[val] = sse
+   nobs = length(c(3:20))
+   aic <- 2*length(convFit$par)+nobs*log(sse/nobs)
+   aicVals[val] = aic
+
+   } # end degree loop

[1] 1
[1] 2
[1] 3
[1] 4
```

For this example the best fit parameters shown below, with their corresponding sum squared errors and AIC values:

```
> print(bestFit)

         [,1]     [,2]      [,3]       [,4]      [,5]
[1,] 1.195420 1.142468 -1.198908  1.8034851        NA
[2,] 1.197015 1.164670  1.143554 -1.2013532  1.802941
[3,] 1.197493 1.174908  1.160085  1.1411749 -1.202107
[4,] 1.293598 0.803580  1.629363  0.8910278  1.150988
          [,6]     [,7]
```

```
[1,]         NA       NA
[2,]         NA       NA
[3,]  1.803066       NA
[4,] -1.187292 2.033757

> print(sseVals)

[1] 0.0007056737 0.0005882090 0.0006777972 0.2457135256

> print(aicVals)

[1] -174.64113 -175.91840 -171.36661  -63.29129
```

In this example, we limit ourselves to ten tries for each degree `dg`, so that the code can be run quickly. Ten tries was not sufficient for the algorithm to find the global optima, since the sum squared error should be lower whenever more parameters are used to fit the conversion rate. For Figures 5.3, D.6, and D.5, we use 500 tries for each degree. For all cases when the true conversion rate was fixed, the parameters in `bestFit` were well-within the bounds we placed on the selection of starting parameters (-10,10). When the true conversion rate was time-varying, the free spline parameters returned in `bestFit` parameters were outside those bounds (up to approx. 28), so we re-ran the optimization after resetting the random uniformly-distributed starting parameters to vary between -30 and 30, increasing the `tries` to 1000 (Fig. 5.4A) or 5000 (Fig. 5.4B) to better cover the increased parameter space. In each case, we increased the number of tries until the fits for increasingly complex splines gave lower sum squared error.

For fits to experimental data, we ran the optimization algorithm for 10,000 starting values to ensure that more complex candidate conversion rates would give lower sum squared errors. We constrained the starting guesses for the spline coefficients to vary uniformly from -45 to 85, and the starting guesses for the other parameters to vary uniformly between negative eight and $-\mu_G/2$. While zero gametocyte abundance was not an issue in the simulated data, in experiments gametocytes are not always detected. To cope with the zero values we added one to the observed and predicted gametocyte abundances before log-transforming them and calculating the sum squared error.

D.3 Description of modified spline method, assuming early markers for gametocyte differentiation

If markers can be used to differentiate parasites in the early stages of gametocyte differentiation from asexual forms, then the effective propagation number can be estimated more exactly as:

$$I_{t+1} = x_t I_t S_t \tag{D.12}$$

where $x_t = (1 - c_t)P_{e,t}$, and x_t is the quantity estimated by the regression methods described by Metcalf *et al.* (2011). Therefore,

$$P_{e,t} = \frac{x_t}{1 - c_t} \tag{D.13}$$

As before, if we assume that no gametocytes persist through more than one time point, then combining Eqns. 5.5 and D.13 yields:

$$G_{t+3} = c_t \frac{x_t}{1 - c_t} I_t S_t \tag{D.14}$$

Eqn. 5.7 can then be rewritten as

$$G_t = \left(\sum_{j=4}^{t} \epsilon^{t-j} c_{j-3} c_t \frac{x_t}{1 - c_t} I_{j-3} S_{j-3} \right) + \epsilon^{t-3} G_3 \tag{D.15}$$

D.4 Supplementary figures

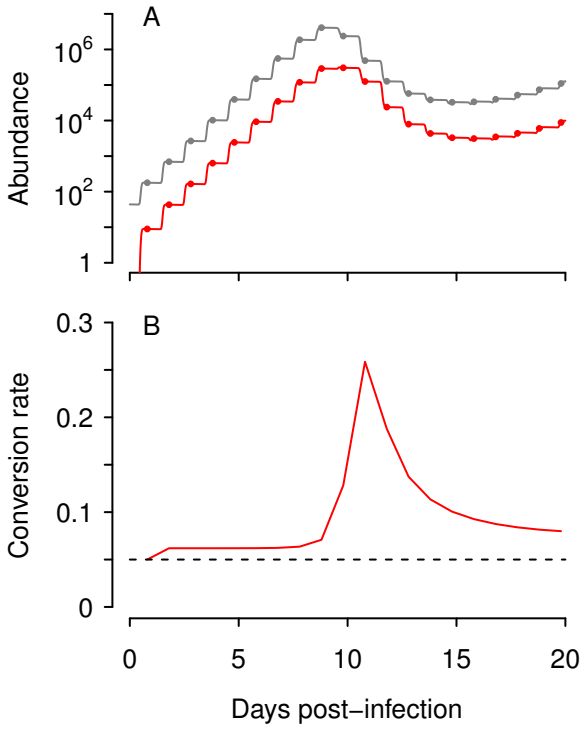

Figure D.1. Early detection *per se* does not ensure that conversion rates will be correctly estimated. Here we assume that sexual differentiation can be detected as soon as a red blood cell is invaded, and the resulting abundance of infected red blood cells undergoing sexual differentiation (red) is compared with the total number of infected red blood cells (gray, A). Sampled time points are indicated by dots. The inferred conversion rate is shown below (B), taken as the fraction of the total number of infected red blood cells that are undergoing sexual differentiation. The true conversion rate (5%) is shown as a dashed black line.

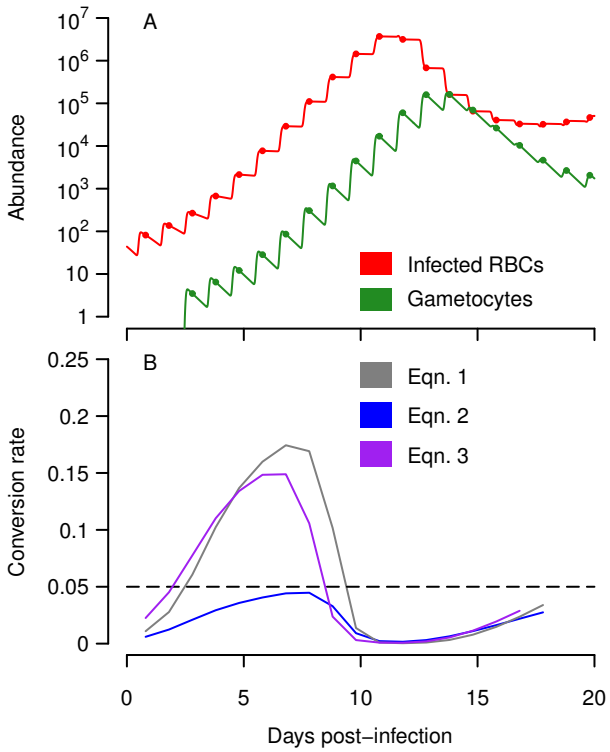

Figure D.2. Immune-mediated mortality of asexual parasites causes overestimation of the conversion rate early in infection. Dynamics of infected red blood cells (red) and mature gametocytes (green) assuming that immunity targets (and saturates as a function of) red blood cells infected with asexual parasites (A, maximum per capita clearance, $a = 150$, half-saturation constant, $b = 100$). The corresponding estimates of conversion rate are shown below (B), again with the actual conversion rate (5%) shown as a dashed line.

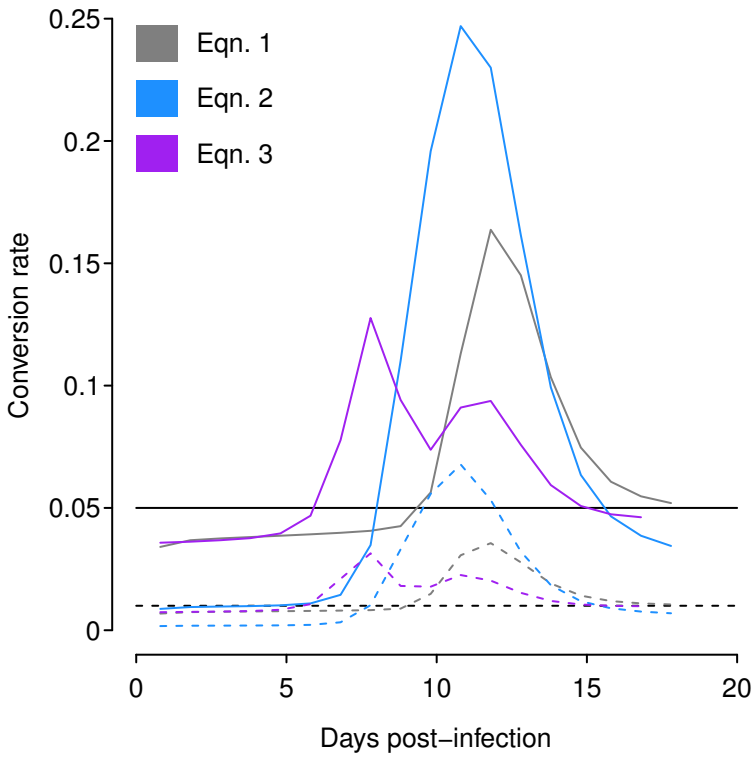

Figure D.3. All three methods for inferring transmission investment are capable of detecting a wholesale decrease in conversion rates. Here the proportion of parasites differentiating into sexual forms was set at 5% (solid lines) or 1%, for single infections assuming no immunity.

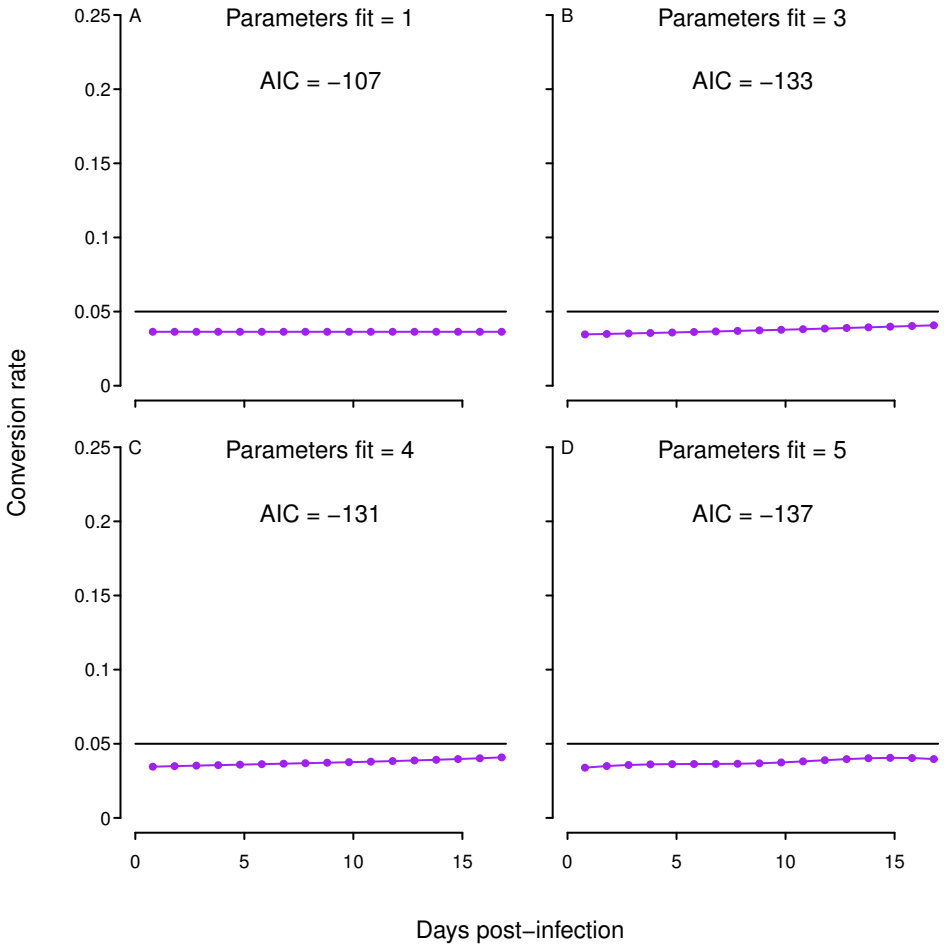

Figure D.4. Conversion rates estimated from spline fits to simulated data (purple dots), with the true conversion rate shown in black. The estimated conversion rate was assumed to be a curve of increasing complexity, with each panel showing the AIC value corresponding to the predicted versus observed gametocyte abundance, as well as the number of parameters fit to obtain the spline. Note that even as the fitted conversion rates assume more degrees of freedom, the predicted conversion rate stays approximately fixed, close to the true conversion rate.

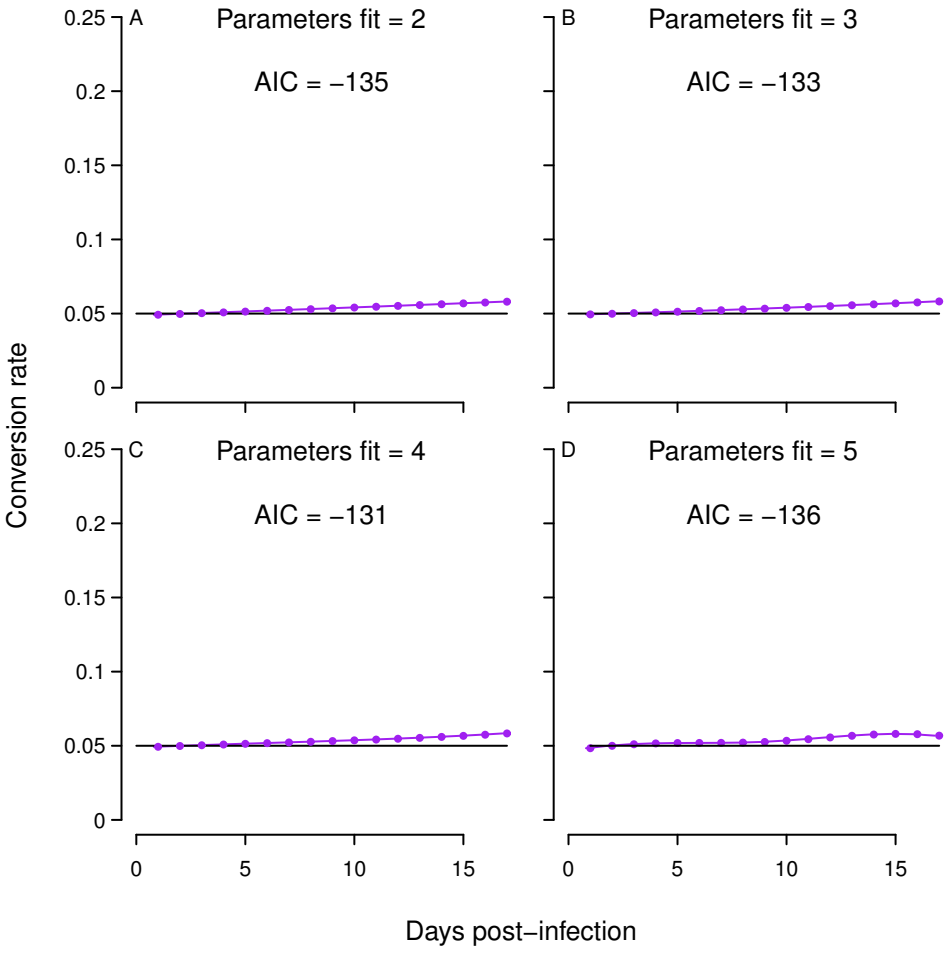

Figure D.5. The estimated conversion rate is closer to the true value when we correct for gametocyte mortality by dividing gametocyte abundance by $exp(-\mu_g * 0.3$, where μ_g is the mortality rate for gametocytes, and 0.3 represents the time lag between synchronous bursting events and sampling. Conversion rates estimated from spline fits to simulated data (purple dots), with the true conversion rate shown in black. We fit splines of increasing complexity as in Figures 5.3 and D.4. Fitting a constant conversion (one parameter) rate gave a less negative AIC and is not shown here.

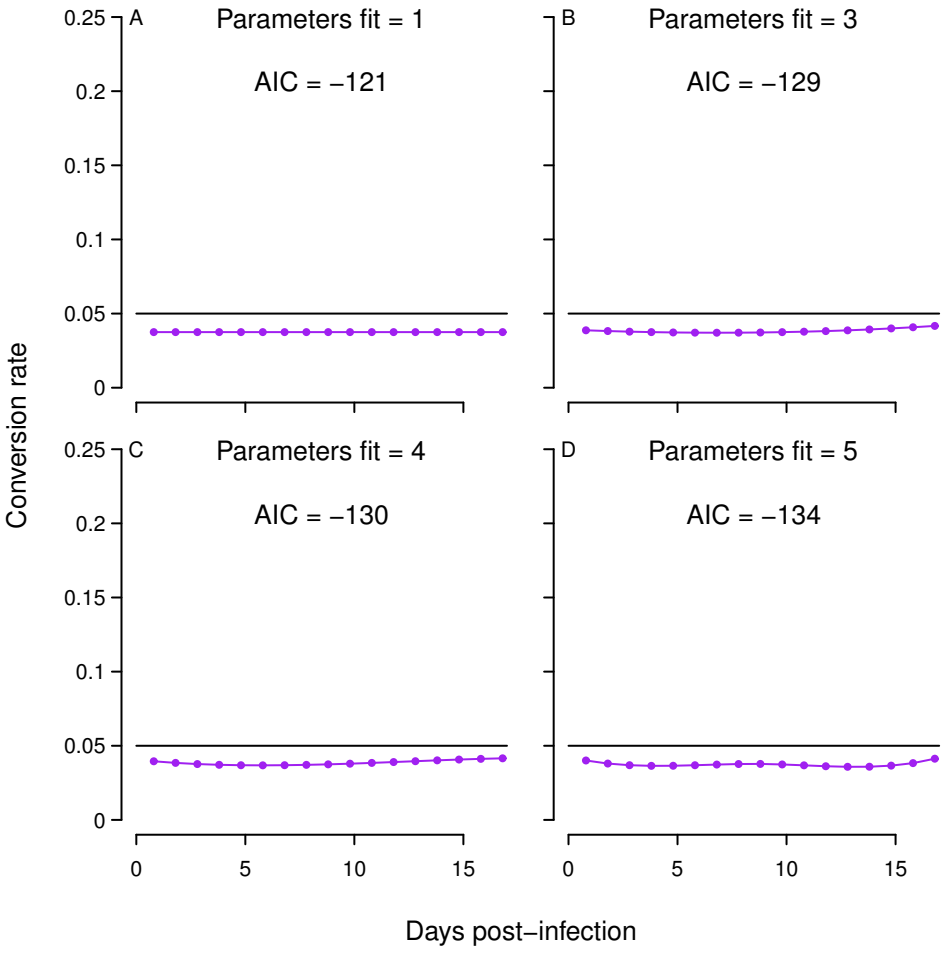

Figure D.6. Estimated conversion rate in the presence of immunity (purple dots), with the true conversion rate shown in black. As before, conversion rates of increasing complexity were fit to the data, with the number of parameters for the conversion rate and the corresponding AIC shown in each panel. The fit with two parameters had the largest AIC value (-120) and is not shown here. The "data" at each time point were simulated assuming that asexual parasites infecting red blood cells were cleared more efficiently at lower densities ($a = 150$, $b = 100$).

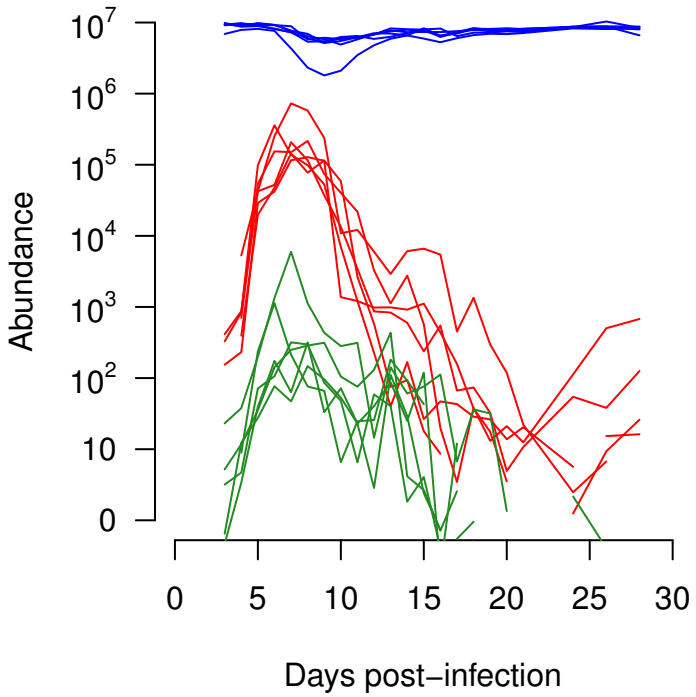

Figure D.7. Abundance of red blood cells, infected red blood cells and gametocytes for the six mice used to estimate conversion rates. Data from infections with drug-resistant *P. chabaudi* parasites (Huijben *et al.*, 2010a,b).

Bibliography

Allen, R. J. W. & Kirk, K. (2010). *Plasmodium falciparum* culture: the benefits of shaking. *Molecular and Biochemical Parasitology*, 169, 63–65.

Antia, R. & Koella, J. C. (1994). A model of non-specific immunity. *Journal of Theoretical Biology*, 168, 141–150.

Arnot, D. & Gull, K. (1998). The *Plasmodium* cell cycle: facts and questions. *Annals of Tropical Medicine and Parasitology*, 92, 361–365.

Bell, A. S., de Roode, J. C., Sim, D. & Read, A. F. (2006). Within-host competition in genetically diverse malaria infections: parasite virulence and competitive success. *Evolution*, 60, 1358–1371.

Bell, A. S., Huijben, S., Paaijmans, K. P., Sim, D. G., Chan, B. H. K., Nelson, W. A. & Read, A. F. (2012). Enhanced transmission of drug-resistant parasites to mosquitoes following drug treatment in rodent malaria. *PLoS ONE*, 7, e37172.

Bell, G. (1980). The costs of reproduction and their consequences. *American Naturalist*, 116, 45–76.

Bell, G. (1982). The Red Queen. In: *The Masterpiece of Nature*. Croom Helm, Ltd., London, pp. 143–157.

Bjørnstad, O. N., Finkenstädt, B. F. & Grenfell, B. T. (2002). Dynamics of measles epidemics: estimating scaling of transmission rates using a time series SIR model. *Ecological Monographs*, 72, 169–184.

Bjørnstad, O. N., Sait, S. M., Stenseth, N. C., Thompson, D. J. & Begon, M. (2001). The impact of specialized enemies on the dimensionality of host dynamics. *Nature*, 409, 1001–1006.

Borg, Å. A., Åsmul, T., Bolstad, G. H., Viken, Å., Berglund, A. & Rosenqvist, G. (2012). Interactions among female guppies (*Poecilia reticulata*) affect growth and reproduction. *Ethology*, 118, 752–765.

Bousema, T. & Drakeley, C. (2011). Epidemiology and infectivity of *Plasmodium falciparum* and *Plasmodium vivax* gametocytes in relation to malaria control and elimination. *Clinical Microbiology Reviews*, 24, 377–410.

Boyle, M. J., Wilson, D. W., Richards, J. S., Riglar, D. T., Tetteh, K. K. A., Conway, D. J., Ralph, S. A., Baum, J. & Beeson, J. G. (2010). Isolation of viable *Plasmodium falciparum* merozoites to define erythrocyte invasion events and advance vaccine and drug development. *Proceedings of the National Academy of Sciences of the USA*, 107, 14378–14383.

Bray, R. S., McCrae, A. W. R., Smalley, M. E. & Gambia, T. (1976). Lack of a circadian rhythm in the ability of the gametocytes of *Plasmodium falciparum* to infect *Anopheles gambiae*. *International Journal for Parasitology*, 6, 399–401.

Bruce, M. C., Alano, P., Duthie, S. & Carter, R. (1990). Commitment of the malaria parasite *Plasmodium falciparum* to sexual and asexual development. *Parasitology*, 100, 191–200.

Bruce, M. C. & Day, K. P. (2002). Cross-species regulation of malaria parasitaemia in the human host. *Current Opinion in Microbiology*, 5, 431–437.

Bruce, M. C., Donnelly, C. A., Alpers, M. P., Galinski, M. R., Barnwell, J. W., Walliker, D. & Day, K. P. (2000a). Cross-species interactions between malaria parasites in humans. *Science*, 287, 845–848.

Bruce, M. C., Donnelly, C. A., Packer, M., Lagog, M., Gibson, N., Narara, A., Walliker, D., Alpers, M. P. & Day, K. P. (2000b). Age- and species-specific duration of infection in asymptomatic malaria infections in Papua New Guinea. *Parasitology*, 121, 247–256.

Buckling, A., Crooks, L. & Read, A. F. (1999). *Plasmodium chabaudi*: effect of antimalarial drugs on gametocytogenesis. *Experimental Parasitology*, 93, 45–54.

Bull, P. C., Lowe, B. S., Kortok, M. & Marsh, K. (1999). Antibody recognition of *Plasmodium falciparum* erythrocyte surface antigens in Kenya: evidence for rare and prevalent variants. *Infection and Immunity*, 67, 733–739.

Cameron, A., Reece, S. E., Drew, D. R., Haydon, D. T. & Yates, A. J. (2012). Plasticity in transmission strategies of the malaria parasite, *Plasmodium chabaudi*: environmental and genetic effects. *Evolutionary Applications*, 1–12.

Carter, L. M., Kafsack, B. F. C., Llinás, M., Mideo, N., Pollitt, L. C. & Reece, S. E. (2013). Stress and sex in malaria parasites: Why does commitment vary? *Evolution, Medicine, and Public Health*, 2013, 135–147.

Chao, L., Hanley, K. A., Burch, C. L., Dahlberg, C. & Turner, P. E. (2000). Kin selection and parasite evolution: higher and lower virulence with hard and soft selection. *Quarterly Review of Biology*, 75, 261–275.

Charlesworth, B. & Leon, J. (1976). The relation of reproductive effort to age. *American Naturalist*, 110, 449–459.

Cheesman, S. J., de Roode, J. C., Read, A. F. & Carter, R. (2003). Real-time quantitative PCR for analysis of genetically mixed infections of malaria parasites: technique validation and applications. *Molecular and Biochemical Parasitology*, 131, 83–91.

Chimanuka, B., Francois, G., Timperman, G., Vanden Driessche, T. & Plaizier-Vercammen, J. (1997). Chronobiology of *Plasmodium chabaudi chabaudi*: analysis of hourly recorded total and differential parasitaemia during a schizogonic cycle. *Parasite*, 4, 319–323.

Clutton-Brock, T. H. (1984). Reproductive effort and terminal investment in iteroparous animals. *American Naturalist*, 123, 212–229.

Collins, W. E. & Jeffery, G. M. (2003). A retrospective examination of mosquito infection on humans infected with *Plasmodium falciparum*. *The American Journal of Tropical Medicine and Hygiene*, 68, 366–71.

Costa, G., Loizon, S., Guenot, M., Mocan, I., Halary, F., de Saint-Basile, G., Pitard, V., Déchanet-Merville, J., Moreau, J.-F., Troye-Blomberg, M., Mercereau-Puijalon, O. & Behr, C. (2011). Control of *Plasmodium falciparum* erythrocytic cycle: $\gamma\delta$ T cells target the red blood cell-invasive merozoites. *Blood*, 118, 6952–6962.

Courchamp, F., Berec, L. & Gascoigne, J. (2008). Reproductive mechanisms. In: *Allee Effects in Ecology and Conservation*, 1st edn., chap. 2. Oxford University Press, Inc., New York, pp. 20–34.

Crooks, L. (2008). Problems with continuous-time malaria models in describing gametocytogenesis. *Parasitology*, 135, 881–896.

Cunnington, A. J., Riley, E. M. & Walther, M. (2013). Stuck in a rut? Reconsidering the role of parasite sequestration in severe malaria syndromes. *Trends in Parasitology*, 29, 585–592.

Daubersies, P., Sallenave-Sales, S., Magne, S., Trape, J.-F., Contamin, H., Fandeur, T., Rogier, C., Mercereau-Puijalon, O. & Druilhe, P. (1996). Rapid turnover of *Plasmodium falciparum* populations in asymptomatic individuals living in a high transmission area. *American Journal of Tropical Medicine and Hygiene*, 54, 18–26.

de Boor, C. (2001). *A practical guide to splines*. Springer-Verlag New York Inc., New York.

de Roode, J., Helinski, M., Anwar, M. & Read, A. (2005). Dynamics of multiple infection and within-host competition in genetically diverse malaria infections. *American Naturalist*, 166, 531–542.

Deharo, E., Coquelin, F., Chabaud, a. G. & Landau, I. (1996). The erythrocytic schizogony of two synchronized strains of *Plasmodium berghei*, NK65 and ANKA, in normocytes and reticulocytes. *Parasitology Research*, 82, 178–182.

Deharo, E., Gautret, P., Ginsburg, H., Chabaud, A. G. & Landau, I. (1994). Synchronization of *Plasmodium yoelii nigeriensis* and *P. y. killicki* infection in the mouse by means of Percoll-glucose gradient stage fractionation: determination of the duration of the schizogonic cycle. *Parasitology Research*, 80, 159–164.

Delves, M., Plouffe, D., Scheurer, C., Meister, S., Wittlin, S., Winzeler, E. A., Sinden, R. E. & Leroy, D. (2012). The activities of current antimalarial drugs on the life cycle stages of *Plasmodium*: A comparative study with human and rodent parasites. *PLoS Medicine*, 9, e1001169.

Dhar, R., Zhang, K., Talwar, G. P., Garg, S. & Kumar, N. (1998). Inhibition of the growth and development of asexual and sexual stages of drug-sensitive and resistant strains of the human malaria parasite *Plasmodium falciparum* by Neem (*Azadirachta indica*) fractions. *Journal of Ethnopharmacology*, 61, 31–39.

Dobaño, C., Rogerson, S. J., Taylor, T. E., McBride, J. S. & Molyneux, M. E. (2007). Expression of merozoite surface protein markers by *Plasmodium falciparum*-infected erythrocytes in peripheral blood and tissues of children with fatal malaria. *Infection and Immunity*, 75, 643–652.

Drakeley, C., Sutherland, C., Bousema, J. T., Sauerwein, R. W. & Targett, G. A. T. (2006). The epidemiology of *Plasmodium falciparum* gametocytes: weapons of mass dispersion. *Trends in Parasitology*, 22, 424–430.

Drew, D. R. & Reece, S. E. (2007). Development of reverse-transcription PCR techniques to analyse the density and sex ratio of gametocytes in genetically diverse *Plasmodium chabaudi* infections. *Molecular and Biochemical Parasitology*, 156, 199–209.

Eksi, S., Morahan, B. J., Haile, Y., Furuya, T., Jiang, H., Ali, O., Xu, H., Kiattibutr, K., Suri, A., Czesny, B., Adeyemo, A., Myers, T. G., Sattabongkot, J., Su, X.-z. & Williamson, K. C. (2012). *Plasmodium falciparum* gametocyte development 1 (*Pfgdv1*) and gametocytogenesis early gene identification and commitment to sexual development. *PLoS Pathogens*, 8, e1002964.

Elliott, D. A., McIntosh, M. T., Hosgood, H. D., Chen, S., Zhang, G., Baevova, P. & Joiner, K. A. (2008). Four distinct pathways of hemoglobin uptake in the malaria parasite *Plasmodium falciparum*. *Proceedings of the National Academy of the Sciences of the USA*, 105, 2463–2468.

Elliott, S. R., Spurck, T. P., Dodin, J. M., Maier, A. G., Voss, T. S., Yosaatmadja, F., Payne, P. D., McFadden, G. I., Cowman, A. F., Rogerson, S. J., Schofield, L. & Brown, G. V. (2007). Inhibition of dendritic cell maturation by malaria is dose dependent and does not require *Plasmodium falciparum* erythrocyte membrane protein 1. *Infection and Immunity*, 75, 3621–3632.

Etablissement Français du Sang. (2012). Cultured red blood cells: life span in vivo study. URL `http://clinicaltrials.gov/ct2/show/NCT00929266`.

Färnert, A., Lebbad, M., Faraja, L. & Rooth, I. (2008). Extensive dynamics of *Plasmodium falciparum* densities, stages and genotyping profiles. *Malaria Journal*, 7, 241–245.

Färnert, A., Rooth, I., Svensson, Å., Snounou, G., Björkman, A., Farnert, A. & Svensson, A. (1999). Complexity of *Plasmodium falciparum* infections is consistent over time and protects against clinical disease in Tanzanian children. *Journal of Infectious Diseases*, 179, 989–995.

Färnert, A., Snounou, G., Rooth, I. & Bjorkman, A. (1997). Daily dynamics of *Plasmodium falciparum* subpopulations in asymptomatic children in a holoendemic area. *American Journal of Tropical Medicine and Hygiene*, 56, 538–547.

Feng, Z., Xu, D. & Zhao, H. (2007). Epidemiological models with non-exponentially distributed disease stages and applications to disease control. *Bulletin of Mathematical Biology*, 69, 1511–36.

Fenton, A., Viney, M. E. & Lello, J. (2010). Detecting interspecific macroparasite interactions from ecological data: patterns and process. *Ecology Letters*, 13, 606–615.

Garnham, P. C. C. (1966). *Malaria Parasites And Other Haemosporidia*. 1st edn. Blackwell Scientific Publications, Oxford.

Gautret, P., Miltgen, F., Gantier, J. C., Chabaud, A. G. & Landau, I. (1996). Enhanced gametocyte formation by *Plasmodium chabaudi* in immature erythrocytes: pattern of production, sequestration, and infectivity to mosquitoes. *Journal of Parasitology*, 82, 900–906.

Gautret, P., Voza, T., Chabaud, A. & Landau, I. (2001). Short-term effect of chloroquine on the infectivity to *Plasmodium chabaudi* gametocytes. *Parasite*, 33, 363–367.

Geary, T. G., Divo, A. A. & Jensen, J. B. (1989). Stage specific actions of antimalarial drugs on *Plasmodium falciparum* in culture. *American Journal of Tropical Medicine and Hygiene*, 40, 240–244.

Gething, P. W., Patil, A. P., Smith, D. L., Guerra, C. A., Elyazar, I. R. F., Johnston, G. L., Tatem, A. J. & Hay, S. I. (2011). A new world malaria map: *Plasmodium falciparum* endemicity in 2010. *Malaria Journal*, 10, 378–393.

Gilboa, I. & Matsui, A. (1991). Social stability and equilibrium. *Econometrica: Journal of the Econometric Society*, 59, 859–867.

Gilchrist, M. A. & Coombs, D. (2006). Evolution of virulence: interdependence, constraints, and selection using nested models. *Theoretical Population Biology*, 69, 145–53.

Githeko, A. K., Brandling-Bennett, A. D., Beier, M., Mbogo, C. M., Atieli, F. K., Owaga, M. L., Juma, F. & Collins, F. H. (1993). Confirmation that *Plasmodium falciparum* has aperiodic infectivity to Anopheles gambiae. *Medical and Veterinary Entomology*, 7, 373–376.

Gonzalez-Alonso, J., Mortensen, S. P., Dawson, E. A., Secher, N. H. & Damsgaard, R. (2006). Erythrocyte and the regulation of human skeletal muscle blood flow and oxygen delivery: Role of erythrocyte count and oxygenation state of hemoglobin. *The Journal of Physiology*, 1, 295–305.

Gravenor, M. B. & Kwiatkowski, D. (1998). An analysis of the temperature effects of fever on the intra-host population dynamics of *Plasmodium falciparum*. *Parasitology*, 117, 97–105.

Gravenor, M. B. & Lloyd, A. L. (1998). Reply to: Models for the in-host dynamics of malaria revisited: errors in some basic models lead to large over-estimates of growth rates. *Parasitology*, 117, 409–410.

Greischar, M. A., Read, A. F. & Bjørnstad, O. N. (2014). Synchrony in malaria infections: how intensifying within-host competition can be adaptive. *American Naturalist*, 183, E36–E48.

Härdle, W. (1990). Spline smoothing. In: *Applied nonparametric regression*, chap. 3. Cambridge University Press, New York, pp. 56–57.

Hassell, M. P. (2000). *The Spatial and Temporal Dynamics of Host-Parasitoid Interactions*. Oxford University Press, New York.

Hawking, F. (1970). The clock of the malaria parasite. *Scientific American*, 222, 123–131.

Hawking, F., Worms, M. J. & Gammage, K. (1968). 24- and 48-hour cycles of malaria parasites in the blood; their purpose, production and control. *Transactions of the Royal Society of Tropical Medicine and Hygiene*, 62, 731–760.

Haydon, D. T., Matthews, L., Timms, R. & Colegrave, N. (2003). Top-down or bottom-up regulation of intra-host blood-stage malaria: do malaria parasites most resemble the dynamics of prey or predator? *Proceedings of the Royal Society of London B*, 270, 289–298.

Hellriegel, B. (1992). Modelling the immune response to malaria with ecological concepts: short-term behaviour against long-term equilibrium. *Proceedings of the Royal Society of London B*, 250, 249–56.

Hetzel, C. & Anderson, R. M. (1996). The within-host cellular dynamics of blood-stage malaria: theoretical and experimental studies. *Parasitology*, 113, 25–38.

Hogh, B., Thompson, R., Hetzel, C., Fleck, S., Kruse, N., Jones, I., Dgedge, M., Barreto, J. & Sinden, R. E. (1995). Specific and nonspecific responses to *Plasmodium falciparum* blood-stage parasites and observations on the gametocytemia in schoolchildren living in a malaria-endemic area of Mozambique. *American Journal of Tropical Medicine and Hygiene*, 52, 50–59.

Hoshen, M. B., Heinrich, R., Stein, W. D. & Ginsburg, H. (2000). Mathematical modelling of the within-host dynamics of *Plasmodium falciparum*. *Parasitology*, 121, 227–235.

Huijben, S., Bell, A. S., Sim, D. G., Tomasello, D., Mideo, N., Day, T. & Read, A. F. (2013). Aggressive chemotherapy and the selection of drug resistant pathogens. *PLoS pathogens*, 9, e1003578.

Huijben, S., Nelson, W. A., Wargo, A. R., Sim, D. G., Drew, D. R. & Read, A. F. (2010a). Chemotherapy, within-host ecology and the fitness of drug-resistant malaria parasites. *Evolution*, 64, 2952–2968.

Huijben, S., Nelson, W. A., Wargo, A. R., Sim, D. G., Drew, D. R. & Read, A. F. (2010b). Data from: Chemotherapy, within-host ecology and the fitness of drug-resistant malaria parasites. URL `http://datadryad.org/resource/doi:10.5061/dryad.4h0g0`.

Huijben, S., Sim, D. G., Nelson, W. A. & Read, A. F. (2011). The fitness of drug-resistant malaria parasites in a rodent model: multiplicity of infection. *Journal of Evolutionary Biology*, 24, 2410–22.

Ims, R. A. (1990). The ecology and evolution of reproductive synchrony. *Trends in Ecology & Evolution*, 5, 135–140.

Jafari-Guemouri, S., Boudin, C., Fievet, N., Ndiaye, P. & Deloron, P. (2006). *Plasmodium falciparum* genotype population dynamics in asymptomatic children from Senegal. *Microbes and Infection*, 8, 1663–1670.

Janzen, D. H. (1976). Why bamboos wait so long to flower. *Annual Review of Ecology and Systematics*, 7, 347–391.

Kelly, D. & Sork, V. L. (2002). Mast seeding in perennial plants: Why, how, where? *Annual Review of Ecology and Systematics*, 33, 427–447.

Khoury, D. S., Cromer, D., Best, S. E., James, K. R., Kim, P. S., Engwerda, C. R., Haque, A. & Davenport, M. P. (2014). Effect of mature blood-stage *Plasmodium* parasite sequestration on pathogen biomass in mathematical and in vivo models of malaria. *Infection and immunity*, 82, 212–20.

King, A. A., Shrestha, S., Harvill, E. T. & Bjørnstad, O. N. (2009). Evolution of acute infections and the invasion-persistence trade-off. *American Naturalist*, 173, 446–455.

Kitchen, S. F. (1949). Symptomatology: General Considerations. In: *Malariology– A Comprehensive Survey of All Aspects of this Group of Diseases From a Global Standpoint, Vol. 2* (ed. Boyd, M. F.), chap. 40. W.B. Saunders Company, Philadelphia, pp. 966–994.

Koella, J. C. & Antia, R. (1995). Optimal pattern of replication and transmission for parasites with two stages in their life cycle. *Theoretical Population Biology*, 47, 277–291.

Koons, D. N., Metcalf, C. J. E. & Tuljapurkar, S. (2008). Evolution of delayed reproduction in uncertain environments: a life-history perspective. *American Naturalist*, 172, 797–805.

Koury, M. J. & Ponka, P. (2004). New insights into erythropoiesis: the roles of folate, vitamin B12, and iron. *Annual Review of Nutrition*, 24, 105–131.

Kwiatkowski, D. (1989). Febrile temperatures can synchronize the growth of *Plasmodium falciparum in vitro*. *The Journal of Experimental Medicine*, 169, 357–361.

Kwiatkowski, D. & Nowak, M. (1991). Periodic and chaotic host-parasite interactions in human malaria. *Proceedings of the National Academy of the Sciences of the USA*, 88, 5111–5113.

Lagarias, J. C., Reeds, J. A., Wright, M. H. & Wright, P. E. (1998). Convergence properties of the Nelder–Mead Simplex Method in low dimensions. *SIAM Journal on Optimization*, 9, 112–147.

Lambros, C. & Vanderberg, J. P. (1979). Synchronization of *Plasmodium falciparum* erythrocytic stages in culture. *Journal of Parasitology*, 65, 418–420.

Landau, I. & Boulard, C. (1978). Life Cycles and Morphology. In: *Rodent Malaria* (eds. Killick-Kendrick, R. & Peters, W.), chap. 2. Academic Press Inc., New York, pp. 53–84.

Landau, I., Chabaud, A., Cambie, G. & Ginsburg, H. (1991). Chronotherapy of malaria: an approach to malaria chemotherapy. *Parasitology Today*, 7, 350–352.

Lavine, J. S., King, A. a. & Bjørnstad, O. N. (2011). Natural immune boosting in pertussis dynamics and the potential for long-term vaccine failure. *Proceedings of the National Academy of Sciences of the USA*, 108, 7259–64.

Lensen, A., Bril, A., van de Vegte, M., van Gemert, G. J., Eling, W. & Sauerwein, R. (1999). *Plasmodium falciparum*: infectivity of cultured, synchronized gametocytes to mosquitoes. *Experimental Parasitology*, 91, 101–103.

Lloyd, A. L. (2001). Realistic distributions of infectious periods in epidemic models: changing patterns of persistence and dynamics. *Theoretical Population Biology*, 60, 59–71.

Mackinnon, M. J. & Read, A. F. (1999). Selection for high and low virulence in the malaria parasite *Plasmodium chabaudi*. *Proceedings of the Royal Society of London B*, 266, 741–748.

Mackinnon, M. J. & Read, A. F. (2003). The effects of host immunity on virulence-transmissibility relationships in the rodent malaria parasite *Plasmodium chabaudi*. *Parasitology*, 126, 103–112.

MacPherson, G. G., Warrell, M. J., White, N. J., Looareesuwan, S. & Warrell, D. A. (1985). Human cerebral malaria A quantitative ultrastructural analysis of parasitized erythrocyte sequestration. *American Journal of Pathology*, 119, 385–401.

Magesa, S. M., Mdira, Y. K., Akida, J. A., Bygbjerg, I. C. & Jakobsen, P. H. (2000). Observations on the periodicity of *Plasmodium falciparum* gametocytes in natural human infections. *Acta Tropica*, 76, 239–246.

Mata-Cantero, L., Lafuente, M. J., Sanz, L. & Rodriguez, M. S. (2014). Magnetic isolation of *Plasmodium falciparum* schizonts iRBCs to generate a high parasitaemia and synchronized *in vitro* culture. *Malaria Journal*, 13, 112.

Matsui, A. (1992). Best response dynamics and socially stable strategies. *Journal of Economic Theory*, 57, 343–362.

McKenzie, F. E. & Bossert, W. H. (1998). The optimal production of gametocytes by *Plasmodium falciparum*. *Journal of Theoretical Biology*, 193, 419–428.

McKenzie, F. E., Smith, D. L., O'Meara, W. P. & Riley, E. M. (2008). Strain theory of malaria: the first 50 years. *Advances in Parasitology*, 66, 1–46.

McMorran, B. J., Marshall, V. M., de Graaf, C., Drysdale, K. E., Shabbar, M., Smyth, G. K., Corbin, J. E., Alexander, W. S. & Foote, S. J. (2009). Platelets kill intraerythrocytic malarial parasites and mediate survival to infection. *Science*, 323, 797–800.

McQueen, P. G. & McKenzie, F. E. (2008). Host control of malaria infections: constraints on immune and erythropoeitic response kinetics. *PLoS Computational Biology*, 4, e1000149.

Meshnick, S. R., Taylor, T. E. & Kamchonwongpaisan, S. (1996). Artemisinin and the antimalarial endoperoxides: from herbal remedy to targeted chemotherapy. *Microbiological Reviews*, 60, 301–315.

Metcalf, C. J. E., Graham, A. L., Huijben, S., Barclay, V. C., Long, G. H., Grenfell, B. T., Read, A. F. & Bjørnstad, O. N. (2011). Partitioning regulatory mechanisms of within-host malaria dynamics using the effective propagation number. *Science*, 333, 984–988.

Metcalf, C. J. E., Rose, K. E., Childs, D. Z., Sheppard, A. W., Grubb, P. J. & Rees, M. (2008). Evolution of flowering decisions in a stochastic, density-dependent environment. *Proceedings of the National Academy of Sciences of the USA*, 105, 10466–10470.

Mideo, N., Barclay, V. C., Chan, B. H. K., Savill, N. J., Read, A. F. & Day, T. (2008). Understanding and predicting strain-specific patterns of pathogenesis in the rodent malaria *Plasmodium chabaudi*. *American Naturalist*, 172, 214–238.

Mideo, N. & Day, T. (2008). On the evolution of reproductive restraint in malaria. *Proceedings of The Royal Society B: Biological Sciences*, 275, 1217–1224.

Mideo, N., Kennedy, D. A., Carlton, J. M., Bailey, J. A., Juliano, J. J. & Read, A. F. (2013a). Ahead of the curve: next generation estimators of drug resistance in malaria infections. *Trends in Parasitology*, 29, 321–328.

Mideo, N., Reece, S. E., Smith, A. L. & Metcalf, C. J. E. (2013b). The Cinderella Syndrome: Why do malaria-infected cells burst at midnight? *Trends in Parasitology*, 29, 10–16.

Mideo, N., Savill, N. J., Chadwick, W., Schneider, P., Read, A. F., Day, T. & Reece, S. E. (2011). Causes of variation in malaria infection dynamics: insights from theory and data. *American Naturalist*, 178, E174–E188.

Miller, L. H., Good, M. F. & Milon, G. (1994). Malaria pathogenesis. *Science*, 264, 1878–1883.

Miller, M. R., Råberg, L., Read, A. F. & Savill, N. J. (2010). Quantitative analysis of immune response and erythropoiesis during rodent malarial infection. *PLoS Computational Biology*, 6, e1000946.

Morahan, B. & Garcia-Bustos, J. (2014). Kinase signalling in *Plasmodium* sexual stages and interventions to stop malaria transmission. *Molecular and Biochemical Parasitology*, 1–10.

Mu, J., Myers, R. A., Jiang, H., Liu, S., Ricklefs, S., Waisberg, M., Chotivanich, K., Wilairatana, P., Krudsood, S., White, N. J., Udomsangpetch, R., Cui, L., Ho, M., Ou, F., Li, H., Song, J., Li, G., Wang, X., Seila, S., Sokunthea, S., Socheat, D., Sturdevant, D. E., Porcella, S. F., Fairhurst, R. M., Wellems, T. E., Awadalla, P. & Su, X.-z. (2010). *Plasmodium falciparum* genome-wide scans for positive selection, recombination hot spots and resistance to antimalarial drugs. *Nature Genetics*, 42, 268–271.

Nardin, E. H. & Nussenzweig, R. S. (1993). T cell responses to pre-erythrocytic stages of malaria: role in protection and vaccine development against pre-erythrocytic stages. *Annual Review of Immunology*, 11, 687–727.

Nassir, E., Abdel-Muhsin, A.-M. A., Suliaman, S., Kenyon, F., Kheir, A., Geha, H., Ferguson, H. M., Walliker, D. & Babiker, H. A. (2005). Impact of genetic complexity on longevity and gametocytogenesis of *Plasmodium falciparum* during the dry and transmission-free season of eastern Sudan. *International Journal for Parasitology*, 35, 49–55.

Nkhoma, S. C., Nair, S., Cheeseman, I. H., Rohr-Allegrini, C., Singlam, S., Nosten, F. & Anderson, T. J. C. (2012). Close kinship within multiple-genotype malaria parasite infections. *Proceedings of The Royal Society B-Biological Sciences*, 279, 2589–2598.

Nwakanma, D., Kheir, A., Sowa, M., Dunyo, S., Jawara, M., Pinder, M., Milligan, P., Walliker, D. & Babiker, H. A. (2008). High gametocyte complexity and mosquito infectivity of *Plasmodium falciparum* in the Gambia. *International Journal for Parasitology*, 38, 219–227.

O'Donnell, A. J., Schneider, P., McWatters, H. G. & Reece, S. E. (2011). Fitness costs of disrupting circadian rhythms in malaria parasites. *Proceedings of The Royal Society B: Biological Sciences*, 278, 2429–2436.

O'Fallon, B. (2011). Two optimal mutation rates in obligate pathogens subject to deleterious mutation. *Journal of Theoretical Biology*, 276, 150–158.

Padilla, D. & Adolph, S. (1996). Plastic inducible morphologies are not always adaptive: the importance of time delays in a stochastic environment. *Evolutionary Ecology*, 10, 105–117.

Paul, R. E. L., Bonnet, S., Boudin, C., Tchuinkam, T. & Robert, V. (2007). Aggregation in malaria parasites places limits on mosquito infection rates. *Infection, Genetics and Evolution*, 7, 577–586.

Perkins, S. L. & Schall, J. J. (2010). A molecular phylogeny of malarial parasites recovered from cytochrome *b* gene sequences. *Journal of Parasitology*, 88, 972–978.

Pollitt, L. C., Churcher, T. S., Dawes, E. J., Khan, S. M., Sajid, M., Basáñez, M.-G., Colegrave, N. & Reece, S. E. (2013). Costs of crowding for the transmission of malaria parasites. *Evolutionary Applications*, 6, 617–629.

Pollitt, L. C., MacGregor, P., Matthews, K. & Reece, S. E. (2011a). Malaria and trypanosome transmission: different parasites, same rules? *Trends in Parasitology*, 27, 197–203.

Pollitt, L. C., Mideo, N., Drew, D. R., Schneider, P., Colegrave, N. & Reece, S. E. (2011b). Competition and the evolution of reproductive restraint in malaria parasites. *American Naturalist*, 177, 358–367.

Rasband, W. (2013). Image J. URL `http://imagej.nih.gov/ij`.

Read, A. F. & Huijben, S. (2009). Evolutionary biology and the avoidance of antimicrobial resistance. *Evolutionary Applications*, 2, 40–51.

Reece, S. E., Ali, E., Schneider, P. & Babiker, H. A. (2010). Stress, drugs and the evolution of reproductive restraint in malaria parasites. *Proceedings of The Royal Society B: Biological Sciences*, 277, 3123–9.

Reece, S. E., Drew, D. R. & Gardner, A. (2008). Sex ratio adjustment and kin discrimination in malaria parasites. *Nature*, 453, 609–614.

Reece, S. E., Duncan, A. B., West, S. A. & Read, A. F. (2003). Sex ratios in the rodent malaria parasite, *Plasmodium chabaudi*. *Parasitology*, 127, 419–425.

Reece, S. E., Ramiro, R. S. & Nussey, D. H. (2009). Plastic parasites: sophisticated strategies for survival and reproduction? *Evolutionary Applications*, 2, 11–23.

Rees, M., Kelly, D. & Bjørnstad, O. N. (2002). Snow tussocks, chaos, and the evolution of mast seeding. *American Naturalist*, 160, 44–59.

Reilly, H. B. (2007). *The genetic dissection of differential growth in Plasmodium falciparum and its relationship to chloroquine drug selection*. Ph.D. thesis, Notre Dame, Indiana.

Reilly, H. B., Wang, H., Steuter, J. A., Marx, A. M. & Ferdig, M. T. (2007). Quantitative dissection of clone-specific growth rates in cultured malaria parasites. *International Journal for Parasitology*, 37, 1599–1607.

Reilly Ayala, H. B., Wacker, M. A., Siwo, G. & Ferdig, M. T. (2010). Quantitative trait loci mapping reveals candidate pathways regulating cell cycle duration in *Plasmodium falciparum*. *BMC Genomics*, 11, 577–590.

Riley, E. M. & Stewart, V. A. (2013). Immune mechanisms in malaria: new insights in vaccine development. *Nature Medicine*, 19, 168–78.

Rouzine, I. M. & McKenzie, F. E. (2003). Link between immune response and parasite synchronization in malaria. *Proceedings of the National Academy of the Sciences of the USA*, 100, 3473–3478.

Ruel, J. J. & Ayres, M. P. (1999). Jensen's inequality predicts effects of environmental variation. *Trends in Ecology & Evolution*, 14, 361–366.

Safeukui, I., Buffet, P. A., Perrot, S., Sauvanet, A., Aussilhou, B., Dokmak, S., Couvelard, A., Hatem, D. C., Mohandas, N., David, P. H., Mercereau-Puijalon, O. & Milon, G. (2013). Surface area loss and increased sphericity account for the splenic entrapment of subpopulations of *Plasmodium falciparum* ring-infected erythrocytes. *PloS One*, 8, e60150.

Safeukui, I., Correas, J. M., Brousse, V., Hirt, D., Deplaine, G., Mulé, S., Lesurtel, M., Goasguen, N., Sauvanet, A., Couvelard, A., Kerneis, S., Khun, H., Vigan-Womas, I., Ottone, C., Molina, T. J., Tréluyer, J.-M., Mercereau-Puijalon, O., Milon, G., David, P. H. & Buffet, P. A. (2008). Retention of *Plasmodium falciparum* ring-infected erythrocytes in the slow, open microcirculation of the human spleen. *Blood*, 112, 2520–2528.

Sakamoto, Y., Ishiguro, M. & Kitagawa, G. (1986). *Akaike Information Criterion Statistics*. KTK Scientific Publishers, Boston.

Saul, A. (1998). Models for the in-host dynamics of malaria revisited: errors in some basic models lead to large over-estimates of growth rates. *Parasitology*, 117, 405–407.

Savill, N. J., Chadwick, W. & Reece, S. E. (2009). Quantitative analysis of mechanisms that govern red blood cell age structure and dynamics during anaemia. *PLoS Computational Biology*, 5, e1000416.

Schmidt, G. & Roberts, L. (1989). *Foundations of Parasitology*. 4th edn. Times Mirror/Mosby College Publishing, St. Louis.

Schneider, P., Bousema, J. T., Gouagna, L. C., Otieno, S., van de Vegte-Bolmer, M., Omar, S. A. & Sauerwein, R. W. (2007). Submicroscopic *Plasmodium falciparum* gametocyte densities frequently result in mosquito infection. *The American Journal of Tropical Medicine and Hygiene*, 76, 470–474.

Schneider, P., Schoone, G., Schallig, H., Verhage, D., Telgt, D., Eling, W. & Sauerwein, R. (2004). Quantification of *Plasmodium falciparum* gametocytes in differential stages of development by quantitative nucleic acid sequence-based amplification. *Molecular and Biochemical Parasitology*, 137, 35–41.

Simpson, J. A., Aarons, L., Collins, W. E., Jeffery, G. M. & White, N. J. (2002). Population dynamics of untreated *Plasmodium falciparum* malaria within the adult human host during the expansion phase of the infection. *Parasitology*, 124, 247–263.

Simpson, J. A., Silamut, K., Chotivanich, K., Pukrittayakamee, S. & White, N. J. (1999). Red cell selectivity in malaria: a study of multiple-infected erythrocytes. *Transactions of the Royal Society of Tropical Medicine and Hygiene*, 93, 165–168.

Sinervo, B. & Lively, C. (1996). The rock-paper-scissors game and the evolution of alternative male strategies. *Nature*, 380, 240–243.

Skalski, G. T. & Gilliam, J. F. (2001). Functional Responses with Predator Interference: Viable Alternatives to the Holling Type II Model. *Ecology*, 82, 3083–3092.

Slater, A. F. G. & Cerami, A. (1992). Inhibition by chloroquine of a novel haem polymerase enzyme activity in malaria trophozoites. *Nature*, 355, 167–169.

Smalley, M. E. & Sinden, R. E. (1977). *Plasmodium falciparum* gametocytes: their longevity and infectivity. *Parasitology*, 74, 1–8.

Sturm, A., Amino, R., van de Sand, C., Regen, T., Retzlaff, S., Rennenberg, A., Krueger, A., Pollok, J.-M., Menard, R. & Heussler, V. T. (2006). Manipulation of host hepatocytes by the malaria parasite for delivery into liver sinusoids. *Science*, 313, 1287–1290.

Su, X.-z., Ferdig, M. T., Huang, Y., Huynh, C. Q., Liu, A., You, J., Wootton, J. C. & Wellems, T. E. (1999). A genetic map and recombination parameters of the human malaria parasite. *Science*, 286, 1351–1353.

Taylor, L. H., Mackinnon, M. J. & Read, A. F. (1998). Virulence of mixed-clone and single-clone infections of the rodent malaria *Plasmodium chabaudi*. *Evolution*, 52, 583–591.

Taylor, L. H. & Read, A. F. (1997). Why so few transmission stages? Reproductive restraint by malaria parasites. *Parasitology Today*, 13, 135–140.

Taylor, L. H., Walliker, D. & Read, A. F. (1997a). Mixed-genotype infections of malaria parasites: within-host dynamics and transmission success of competing clones. *Proceedings of the Royal Society of London B*, 264, 927–935.

Taylor, L. H., Walliker, D. & Read, A. F. (1997b). Mixed-genotype infections of the rodent malaria *Plasmodium chabaudi* are more infectious to mosquitoes than single-genotype infections. *Parasitology*, 115, 121–132.

ter Kuile, F., White, N. J., Holloway, P., Pasvol, G. & Krishna, S. (1993). *Plasmodium falciparum: in vitro* studies of the pharmacodynamic properties of drugs used for the treatment of severe malaria. *Experimental Parasitology*, 76, 85–95.

Timms, R., Colegrave, N., Chan, B. H. & Read, A. F. (2001). The effect of parasite dose on disease severity in the rodent malaria *Plasmodium chabaudi*. *Parasitology*, 123, 1–11.

Touré-Ndouo, F. S., Zang-Edou, E. S., Bisvigou, U. & Mezui-Me-Ndong, J. (2009). Relationship between *in vivo* synchronicity of *Plasmodium falciparum* and allelic diversity. *Parasitology International*, 58, 390–393.

Trager, W. & Jensen, J. B. (1976). Human malaria parasites in continuous culture. *Science*, 193, 673–675.

Valkiunas, G. (2005). *Avian malaria parasites and other Haemosporidia*. CRC Press, New York.

Velando, A., Drummond, H. & Torres, R. (2006). Senescent birds redouble reproductive effort when ill: confirmation of the terminal investment hypothesis. *Proceedings of The Royal Society B: Biological Sciences*, 273, 1443–1448.

Wargo, A. R., de Roode, J. C., Huijben, S., Drew, D. R. & Read, A. F. (2007). Transmission stage investment of malaria parasites in response to in-host competition. *Proceedings of The Royal Society B: Biological Sciences*, 274, 2629–2638.

Wearing, H. J., Rohani, P. & Keeling, M. J. (2005). Appropriate models for the management of infectious diseases. *PLoS medicine*, 2, e174.

White, N. J., Chapman, D. & Watt, G. (1992). The effects of multiplication and synchronicity on the vascular distribution of parasites in falciparum malaria. *Transactions of the Royal Society of Tropical Medicine and Hygiene*, 86, 590–597.

Williams, K. S., Smith, K. G. & Stephen, F. M. (1993). Emergence of 13-Yr periodical cicadas (Cicadidae: *Magicicada*): phenology, mortality, and predators satiation. *Ecology*, 74, 1143–1152.

Yayon, A., Vande Waa, J. A., Yayon, M., Geary, T. G. & Jensen, J. B. (1983). Stage-dependent effects of chloroquine on *Plasmodium falciparum in vitro*. *Journal of Protozoology*, 30, 642–647.

Vita

Megan A. Greischar

Education

The Pennsylvania State University State College, Pennsylvania 2009–2014

Ph.D. in Entomology, August 2014

Indiana University Bloomington, IN 2002–2007

B.S. in Biology, B.A. in Mathematics

Research Experience

Doctoral Research The Pennsylvania State University 2009–2014

Dissertation Advisors: Prof. Ottar N. Bjørnstad & Prof. Andrew F. Read

Research to identify the transmission consequences of malaria life history within the vertebrate host.

Undergraduate Research Indiana University 2004–2007

Research Advisors: Prof. Curtis M. Lively & Britt Koskella

Research to synthesize work on parasite local adaptation and model how parasites alter host population dynamics.

Undergraduate Research Indiana University 2002-2004

Research Advisors: Prof. Miriam Zolan

Research examining meiosis and DNA repair defects in the fungus *Coprinus cinereus*.

Teaching Experience

Co-Instructor for Intro to Population Dynamics Penn State University 2013

Ran labs designed to teach students how to implement population dynamics models in **R**.

Teaching Assistant for Introduction to Entomology Penn State University 2011

Taught laboratory sessions on insect physiology and taxonomy.

Teaching for The Insect Connection Penn State University 2010

Gave a lecture on insect-vectored disease and critiqued student papers.

Selected Awards and Honors

President and Co-founder of CIDD Graduate Student Association 2011-2012

University Graduate Fellowship, The Pennsylvania State University 2009-2010

Publications

Greischar, M.A., A.F. Read, and O.N. Bjørnstad. (2014). Synchrony in malaria infections: How intensifying within-host competition can be adaptive. *American Naturalist*, 183(2). E-article.

Greischar, M.A. and C.M. Lively. (2011). Parasites can simplify host population dynamics and reduce the risk of extinction. *Evolutionary Ecology Research*, 13: 557-569.

Acharya, S., A.M. Many, A. Schroeder, F. Kennedy, O.P. Savytskyy, J. Grubb, J. Vincent, E. Friedle, M. Celerin, D. Maillet, H.J. Palmerini, **M.A. Greischar**, G. Moncalian, R.S. Williams, J.A. Tainer, M.E. Zolan. (2008). *Coprinus cinereus rad50* mutants reveal an essential structural role for Rad50 in axial element and synaptonemal complex formation, homolog pairing, and meiotic recombination. *Genetics*, 180: 1889-1907.

Greischar, M.A. and B. Koskella. (2007). A synthesis of experimental work on parasite local adaptation. *Ecology Letters*, 10: 418-434.